Glycosphingolipidomic Investigations of Gangliosides and Glycosphingolipids in Development and Disease

Joanna Pamela Alexis Cappell, BSc, MRes

Submitted in fulfilment of the requirements for the Degree of Doctor of Philosophy, Institute of Infection, Inflammation and Immunity

College of Medical, Veterinary & Life Sciences

University of Glasgow

August 2014

I dedicate this work to my granddad, Dr David James Bruce, 07.11.1928 – 19.08.1998. To an academic who lived for knowledge, joy and family. You were often in my thoughts; it would have been amazing to share the doctorate experience with you.

Declaration

I declare that, except where explicit reference is made to the contribution of others, that this dissertation is the result of my own work and has not been submitted for any other degree at the University of Glasgow or any other institution.

Signature _____

Printed name _____

Abstract

Gangliosides, complex sialic acid-containing glycolipids, and other glycosphingolipids are active physiological membrane components with an array of functions in development and disease. Altered profiles are found in many disorders including those of neurological and cancerous aetiologies. Glycosphingolipids are also important for lateral membrane organization, cell communication and as binding sites for extra-cellular components. These lipids have long been implicated as targets in autoimmune diseases such as Guillain-Barré Syndrome (GBS) and Multifocal Motor Neuropathy. In GBS, auto-antibodies bind native membrane gangliosides signalling immune-mediated breakdown of nerves causing acute flaccid paralysis. While the fundamental pathology is understood, differences in clinical presentation, and preference for motor over sensory nerves, have yet to be explained. Understanding the precise nature of native gangliosides, including low abundance species and modifications, is an important first step. Meanwhile genetically engineered mouse models are under development that should increase our understanding of disease pathogenesis. To be truly functional it is essential these models contain a full range of complex and simple glycosphingolipids in the neurological tissue.

Mass spectrometry has recently been applied with great effect to lipidomics; the comprehensive profiling of all lipids involved in a system. However, heavily glycosylated, low abundance and chemically unusual lipids such as the gangliosides tend to be neglected in otherwise thorough lipidomic studies. It was the aim here to optimise separation and mass spectrometry methodologies for ganglioside analysis. Workflows were developed for high performance thin layer chromatography (HPTLC) combined with direct imaging mass spectrometry (IMS) detection and identification, and for high performance liquid chromatography (HPLC) with online high resolution mass spectrometry detection and identification with dissociation to confirm structures (MSMS). A range of lipid standards were analysed using this second method to build a database of characteristic ionization behaviour,

retention times, and product ion spectra to aid the analysis of unknowns in complex mixtures. Methods were then applied to molecular phenotyping in novel mouse models of GBS, and to glycosphingolipidomics in peripheral sensory and motor nerves. Finally the recently developed technique of imaging mass spectrometry, using matrix assisted laser desorption ionisation (MALDI) and secondary ion mass spectrometry (SIMS) ion sources, was investigated for its capability for direct ganglioside analysis in brain and spinal cord tissue sections.

Results are presented below demonstrating the significant benefits of the mass spectrometry-based workflows over more conventional profiling methods as well as comparing and contrasting the two techniques developed here. Limitations and potential areas for future development are debated. Findings from profiling knockout and rescue mouse models and from single nerve glycosphingolipidomics are discussed along with further experiments and directions for these studies. The discovery of a full range of complex gangliosides in neurological tissue from rescue mice, albeit at low levels compared to the wild type, confirmed their molecular usefulness for modelling neurological autoimmune diseases. The sensitivity and reproducibility of the mass spectrometry technique enabled relative quantitation, revealing details into the abundance of different ganglioside species and inclusion of ceramide structures in each mouse type. The ability to detect very low abundance lipids with an additional dimension of structural description also suggested that O-acetylation of the second sialic acid on native disialylated lipids is more prevalent than previously thought. Finally imaging mass spectrometry results are presented. Although sensitivity was limited, both simple and complex gangliosides were detected in spinal cord sections; the first known IMS detection of these lipids outside of the brain. Results also demonstrate the abundance of parallel lipidomic information that can be obtained using these methods. Possible solutions to increasing the sensitivity limit are discussed that may increase IMS usefulness to glycosphingolipid studies in future.

Contents

List of Figures

List of Tables

Abbreviations

(2OH)	Hydroxyl group on the sn-2 position
9-AA	9-aminoacridine
ACN	Acetonitrile
ATS4	Automatic TLC Sampler 4
Cer	Ceramide
CGE	Commercial ganglioside extract
CHCA	α-cyano-4-hydroxycinnaminic acid
Chol	Cholesterol
CID	Collision induced dissociation
CL	Cardiolipin
Da	Dalton
DGDG	Digalactosyldiacylglycerol
DHAP	2,5-dihydroxyacetophenone
DHB	2,5-dihydroxybenzoic acid
ESI	Electrospray ionization
Fuc	Fucose
Gal	Galactose
GalC	Galactocerbroside
GalNAc	N-acetyl galactose
GalNAcT	N-acetly galastosamine transferase
GBS	Guillain-Barré Syndrome
GD1a	NeuAcα2-3Galβ1-3GalNAcβ1-4Gal(3-2αNeuAc) β1-4Glcβ1-1Cer
GD1b	Galβ1-3GalNAcβ1-4Gal(3-2αNeuAc8-2αNeuAc)β1-4Glcβ1-1Cer
GD3	NeuAcα2-8NeuAcα2-3Galβ1-4Glcβ1-1Cer
Glc	Glucose
GlcNAc	N-acetyl glucose
GM1	Galβ1-3GalNAcβ1-4Gal(3-2αNeuAc)β1-4Glcβ1-1Cer
GM2	GalNAcβ1-4Gal(3-2αNeuAc)β1-4Glcβ1-1Cer
GM3	NeuAcα2-3Galβ1-4Glcβ1-1Cer
GT1b	NeuAcα2-3Galβ1-3GalNAcβ1-4Gal(α3-2NeuAcα2-8NeuAc)β1-4Glcβ1-1Cer
HCD	High energy collision induced dissociation
HPLC	High performance liquid chromatography
HPTLC	High performance thin layer chromatography
IMS	Imaging mass spectrometry
ITO	Indium-tin oxide
Lac	Lactose (Galβ1-4Glu)
m/z	Mass to charge ratio
MALDI	Matrix assisted laser desorption ionization
MeOH	Methanol
MFS	Miller Fisher Syndrome
MGDG	Monogalactosyldiacylglycerol
MMN	Multifocal motor neuropathy
MS	Mass spectrometry
MSMS	Tandem mass spectrometry
NFL	Neurofilament light (ref: promoter)
NL	Neutral loss
OAc-	O-acetyl
OAS	Overall average spectra
PA	Phosphatidic acid
PC	Glycerophosphocholine
PE	Glycerophosphoethanolamine
PG	Glycerophosphoglycerol

PI	Glycerophosphoinositol
PLP	Proteolipid protein (ref: promoter)
PS	Glycerophosphoserine
RT	Retention time
SIMS	Secondary ion mass spectrometry
SM	Sphingomyelin
ST(I,II,III)	Sialyl transferase
Sulf	Sulfatide
TIC	Total ion chromatogram
TOF	Time of flight
XIC	Extracted ion chromatogram

Publications

Yao, D., McGonigal, R., Barrie, J. A., Cappell, J., Cunningham, M. E., Meehan, G. R., Fewou, S. N., Edgar, J. M., Rowan, E., Ohmi, Y., Furukawa, K., Furukawa, K., Brophy, P. J., and Willison, H. J. (2014). Neuronal Expression of GalNAc Transferase Is Sufficient to Prevent the Age-Related Neurodegenerative Phenotype of Complex Ganglioside-Deficient Mice. The Journal of Neuroscience, 34(3), 880–91.

Rupp, A., Galban-Horcajo, F., Bianchi, E., Dondi, M., Penderis, J., Cappell, J., Burgess, K., Matiasek, K., McGonigal, R., Willison, H. J. (2013) Anti-GM2 ganglioside antibodies are a biomarker for acute canine polyradiculoneuritis. Journal of the Peripheral Nervous System, 18(1), 75-88.

Chapter 1. Begin at the Beginning…

1.1 Introduction

Lipids are ubiquitous throughout biological systems. A wide variety of functions have been identified and each new finding suggests yet more active and complex roles for these fascinating molecules. These roles can be arbitrarily categorised into energy storage, lipid signalling and lipid membrane functions. The most established is energy storage. Reservoirs of neutral lipids accumulate as anhydrous intracellular lipid droplets in the cytoplasm. Originally thought to serve as passive fat deposits, it is now known that lipid droplets are actively associated with the regulation of intracellular lipid metabolism, inflammatory responses and metabolic disorders (Martin & Parton, 2006; Walther & Farese, 2012). They are also intricately involved in the biogenesis of, and are therefore metabolic mediators of, precursors for lipid signalling.

Other lipids act as signalling molecules within and between cells. These tend to be smaller species such as lyso-phospholipids; arachidonic acid-derived eicosanoids, mediating numerous pathways in inflammation, immunity and the central nervous system; or simple amino alcohols such as sphingosine and sphingosine-1-phosphate, which are involved in signalling diverse cell processes including cell fate and apoptosis (Harizi, Corcuff, & Gualde, 2008; Pyne & Pyne, 2000; Spiegel & Milstien, 2003). Larger lipids such as phosphoinositides, reversibly phosphorylated inositol-containing membrane phospholipids, are also recognized primary and secondary messengers. The associated signalling pathways include, but are not limited to; recruitment of cytoskeletal proteins, vesicle trafficking, endo- and exocytosis, and classical signal transduction via membrane protein by the recruitment of effectors for cell proliferation, migration, differentiation and survival pathways (Di Paolo & De Camilli, 2006; Downes, Gray, & Lucocq, 2005).

Many signalling lipids act from a membrane embedded anchorage so there is overlap between signalling molecules and those defined as 'membrane lipids'. However, membrane lipids

exclude most of the smaller signalling lipids (although may include their larger metabolic precursors). Instead the term refers to a wide variety of larger diacyl species that function in a fundamental manner for cellular life alongside fulfilling a number of diverse, subtle and active roles. It is with these membrane lipids that this project is primarily concerned and, in particular, large acidic glycosylated species that interact with extracellular components.

1.2 <u>Membrane Lipids and the Lipid bilayer</u>

The definition of a membrane lipid is partially structural. Membrane lipids are characteristically amphipathic; containing both hydrophilic and hydrophobic moieties (Figure 1a). As a result of this distinctive polarity they will spontaneously self-assemble in aqueous media in order to shield the hydrophobic portion. The most common structures are micelles, bilayers and vesicles. Micelles are formed exclusively by lipids with single fatty esters; membrane lipids, which tend to be diacyl, form bilayers and vesicles (illustrated in Figure 1) due to the larger volume of the hydrophobic moiety. The theoretical energetics of these processes are explained in detail by Israelachvili *et al*. (Israelachvili, Mitchell, & Ninham, 1976). The monolayers of a bilayer are known as 'leaflets'. The physicochemical properties of each leaflet and the bilayer as a whole are dependent upon the lipid composition. A couple of examples of how lipid composition can affect the membrane structure are illustrated in Figure 1d & e. This composition, on the nanoscale, is not fixed; fluidity is observed throughout the bilayer. Lipids rapidly move laterally and, under certain conditions, 'flip-flop' from one leaflet to the other creating compositional asymmetry that is often observed in nature. Transient lateral interactions occur as well as lipid clustering which can affect localised phase behaviour, permeability, electrostatic potential or membrane curvature. These processes, which are simply and clearly described by Heimburg (Heimburg, 2009), and many others require fluidity.

Lipid bilayers are essential for cellular life as we know it. They form the foundation of the cell membrane and act as a physical barrier to the external environment. By controlling the
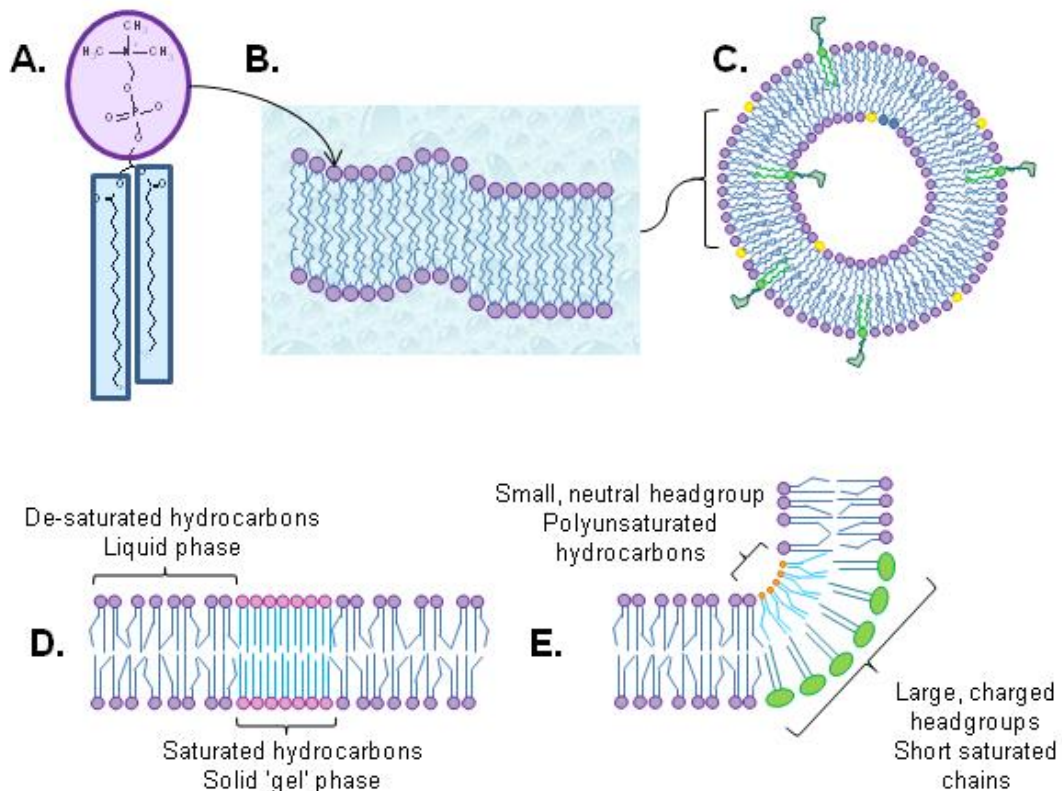
Figure 1. Lipid Structure, Bilayer Formation and Membrane Properties. Membrane lipids like glycerophosphocholine **(A)** are amphipathic with hydrophobic (blue, fatty esters) and hydrophilic (purple, choline head-group) moieties. In aqueous media they spontaneously self-assemble into bilayers **(B)** and ultimately vesicles **(C)** to shield the hydrophobic region. These form the foundation of biological cell and organelle membranes. Membrane properties such as phase behaviour **(D)** and curvature **(E)** depend upon the lipid composition. Desaturations in the fatty ester cause kinks so chains cannot pack as closely as saturated chains influencing membrane fluidity and permeability. Saturated sphingomyelin and cholesterol co-localise to form solid 'gel' phase microdomains known as lipid rafts. The clustering of small, neutral head-groups with polyunsaturated chains can result in negative membrane curvature while co-localised large, sometimes charged head-groups can result in positive curvature.

diffusion of molecules and ions in to and out of the cell, the membrane enables the creation

and maintenance of an ideal intracellular environment. Organelle membranes made up of lipid

bilayers allow the internal segregation of materials and creation of conditions within the cell.

Aside from their barrier functions membranes also provide structural support and a physical

location for many metabolic processes. This often occurs through the association of intrinsic,

extrinsic and associated membrane proteins as described by the Fluid Mosaic Model proposed

in 1972 (Singer & Nicolson, 1972). This remains the most widely accepted model of membrane

organisation and structure. The physical makeup of biomembranes is highly heterogeneous

including phospholipids, glycolipids, cholesterol, membrane proteins and ion channels. This

heterogeneous composition varies significantly between species, cell and tissue type, developmental stage, and between organelles, cell membrane and membrane leaflets.

The function of individual membrane lipids was once thought to be limited to the formation of an inert physical barrier and support structure. Bilayer composition, when considered, was assumed to be a passive serendipitous process. Both these assumptions are now known to be false. Many cell processes involve membrane lipid activity and these functions are vital and lipid-specific. Compositional heterogeneity is also tightly regulated and dynamic. This occurs via multiple mechanisms. Initially this is through the biosynthesis of new lipids which is the result of an intricate balance of multiple metabolomic pathways, genetic transcription, enzyme activation, precursor abundance and self-mediated feedback mechanisms. Intracellular vesicle trafficking, also thought to be partially lipid-mediated, is intrinsically linked to regulating composition via the delivery and removal of specific lipids.

Regulation also occurs at the membrane itself. Metabolic proteins have been isolated from plasma membranes that construct, break down, and modify membrane lipids. On the micro-scale certain species associate into cholesterol-rich domains known as lipid "rafts" which affect local membrane composition and properties. Lipids may also undergo other lateral interactions which may confer alternative functions. Many proteins are recruited and regulated by lipid binding and may in turn modify the local composition via catabolic activity or leaflet re-orientation by 'flippase' activity. A host of proteins have been shown to associate with lipids. Some, such as ATPases/synthases, require this association to activate and function (van Meer, Voelker, & Feigenson, 2008; Zhou et al., 2011). Other proteins may cluster with charged lipids during the production of calveolae, blebs and vesicles in order to alter the membrane curvature (Ewers & Helenius, 2011; McMahon & Gallop, 2005). Meanwhile membrane lipids with large head groups projecting into the extracellular space act more directly, physically interacting with extracellular components such as antibodies, viruses and bacterial toxins.

1.3 <u>Membrane Lipid Classification, Structure and Nomenclature</u>

There are hundreds of membrane lipids with distinct chemical formulae; thousands if all the structural variants of head-group, fatty ester constitution and bond configuration are considered. Nomenclature and classification is understandably complex. This is augmented by the regular and continued use of multiple names for the same lipid or lipid group. For example glycerophosphocholine can be found referred to in the literature as; 'lecithin', the substance it was originally identified from in 1846 (Gobley, 1846); phosphocholine, the most common reference; glycerophosphocholine, the official LIPID MAPS reference (E Fahy et al., 2005); and PC, the most abundant abbreviation. New tools and instrumentation have also resulted in the description of a large number of novel configurations, or more specific description of existing structures, since nomenclature was last systematically addressed in 1978 (IUPAC-IUB, 1978). More recently the LIPID Metabolites and Pathways Strategy (LIPID MAPS, available at: http://www.lipidmaps.org/) infrastructure has made one of the largest efforts to date to standardise classification and nomenclature, adapted from and building upon the 1978 effort (Fahy et al. 2005; Fahy et al. 2009). However despite the integration of the LIPID MAPS classification and nomenclature system into many informatics tools and databases, many publications ignore or only partially use this system. It is therefore useful to describe and define the classification and nomenclature system, including defining structural characteristics and all shorthand used.

The initial categorisation of lipids into classes and subclasses usually concerns large molecular features. According to the LIPID MAPS system there are eight major categories; fatty acyls; glycerolipids; glycerophospholipids; sphingolipids; sterol lipids; prenol lipids; saccharolipids; and polyketides. For a full description of each see Fahy *et al.* 2005. The membrane lipids of interest to this thesis are encompassed in the glycerophopholipid and spingolipid categories which are discussed below. Cholesterol, a ubiquitous biomembrane component belonging to the sterol group, is also discussed.

1.3.1   Sterol Lipids

Sterol lipids contain a fused four-ring structure indicated in Figure 2 which illustrates the structures of cholesterol, a metabolic intermediate lanosterol, and 7-dehydrocholesterol, a cholesterol precursor which is also converted to vitamin D_3 in the skin. Each shows the conserved four-ring structure. There are seven classes of sterol lipid categorised mostly by function. Sub-classes are devised by biological source and/or the number of carbons in the core structure. Common structural modifications found within these sub-classes include the addition of hydroepoxy, epoxy, hydroxyl and keto groups, and fatty ester derivatisation. Cholesterol and cholesterol ester derivatives (Figure 2) are the only mammalian membrane-associated sterol of interest here. Other sterol groups, such as steroids and bile acids, have important roles that are less tightly associated with the membrane. Here they act from the interior of the bilayers to influence fatty ester packing and phase behaviour. Their importance in altering the properties of biological membranes is significant. However their investigation

Figure 2. Chemical Structure of Sterols.

Cholesterol, cholest-5-en-3β-ol

Lanosterol, lanosta-8,24-dien-3β-ol

Dehydrocholesterol, cholestan-3β-ol
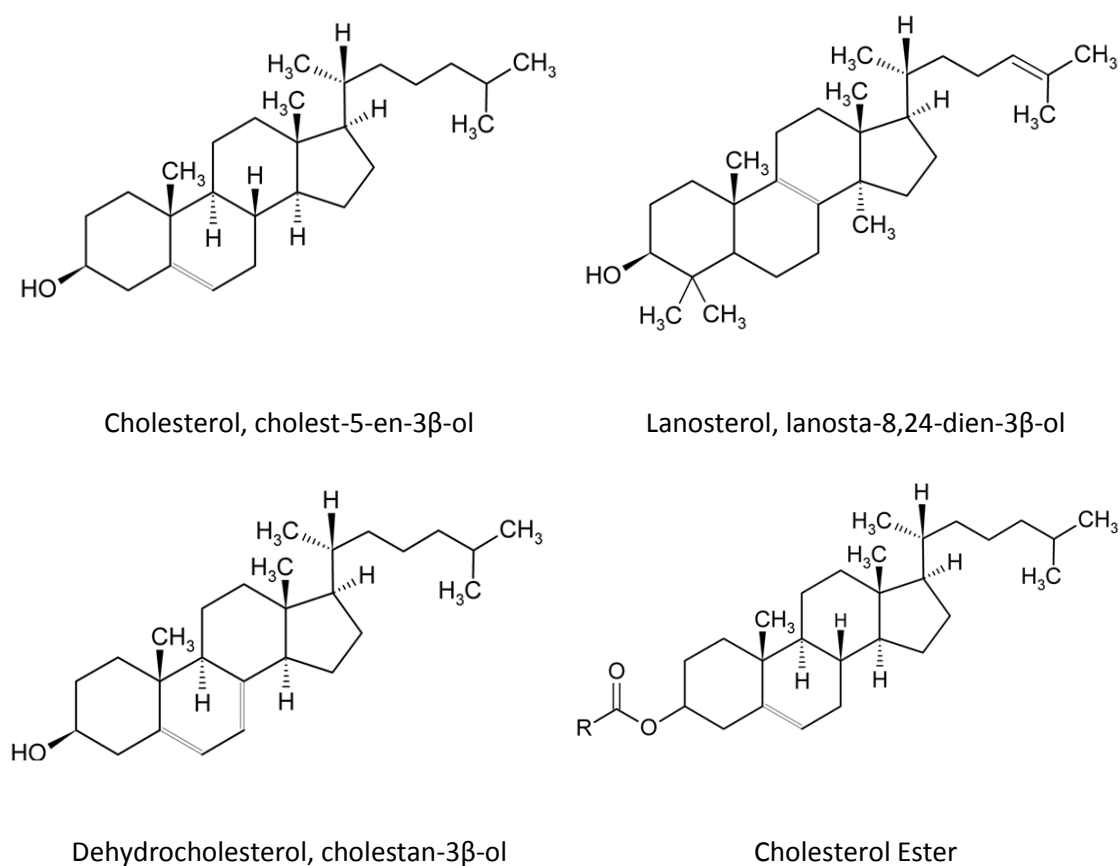
Cholesterol Ester

requires quite distinct instrumentation to the membrane lipids of interest here. They are mentioned in order to define the structure(s) referred to by the term 'cholesterol' when used.

1.3.2 <u>Glycerophospholipids</u>

Glycerophospholipids are the core component of cell membranes with the exception of the cells of the central and peripheral nervous system. Phospholipids characteristically contain a glycerol molecule (blue); a phosphate linked polar head-group generally in the *sn*-3 (stereospecific numbering) position (yellow); and one or two fatty esters (red), shown in a typical phospholipid configuration in Figure 3. Phospholipid classes are based on the polar head-group. There are seven major classes in eukaryotes. These are commonly known and referred to here as; glycerophosphocholine (PC), glycerophosphoethanolamine (PE), glycerophosphoglycerol (PG), glycerophosphoinositol (PI), glycerophosphoserine (PS), and cardiolipin (CL). The structure of each head-group is illustrated in Figure 3. The phosphoinositol head-group can readily be modified on the 3, 4 and 5 carbon by inositol phosphorylases to form phosphoinositol phosphate (PIP), bisphosphate (PIP_2) and trisphosphate (PIP_3).

Fatty ester chain lengths are defined as short (<10 carbons) or long (>10 carbons) (IUPAC-IUB, 1978). Membrane lipids almost exclusively contain long chain fatty esters that can be saturated, monounsaturated or polyunsaturated. Details of the hydrophobic constituents are affixed in several ways through shorthand terms and systematic naming. The prefix 'mono-' or 'di-' indicates one or two fatty acids with -acyl, alkyl or alkenyl, to indicate an ester (most common), ether and vinyl ether glycerol linkage. Stereospecific numbering (sn-) position on the glycerol is often included. The term 'lyso-' is occasionally used to denote a phospholipid with a single fatty ester although this strictly speaking implies the removal of an acyl derivative by hydrolysis. A higher degree of specificity can be provided with the trivial or systematic fatty ester name(s) (illustrated in Table 1). If the fatty ester is unsaturated bond position and *cis-* or *trans-* configuration can be included. More simply, the chain length(s) and number of double bonds can also be indicated numerically after the head-group classification, often in brackets,

with or without the bond position or geometry. If this shorthand is used it is assumed that the

fatty ester linkage is via a standard ester bond unless specified.

1.3.3   Sphingolipids

The sphingolipid category includes many important membrane lipids. These are characterised

by the presence of a sphingoid base in place of the glycerol and one of the fatty esters. In

mammals this sphingoid base can be 16 to 20 carbons long. The most abundant, sphingosine,

has 18 carbons and a single double bond in position 4 in the *trans* configuration (Figure 4).

Figure 3. Phospholipid Structures and Headgroups.

Glycerophosphatidic acid   Glycerophosphoinositol

Glycerophosphocholine

Generic Phospholipid Structure

Glycerophosphoethanolamine   Glycerophosphoserine

Glycerophosphoglycerol
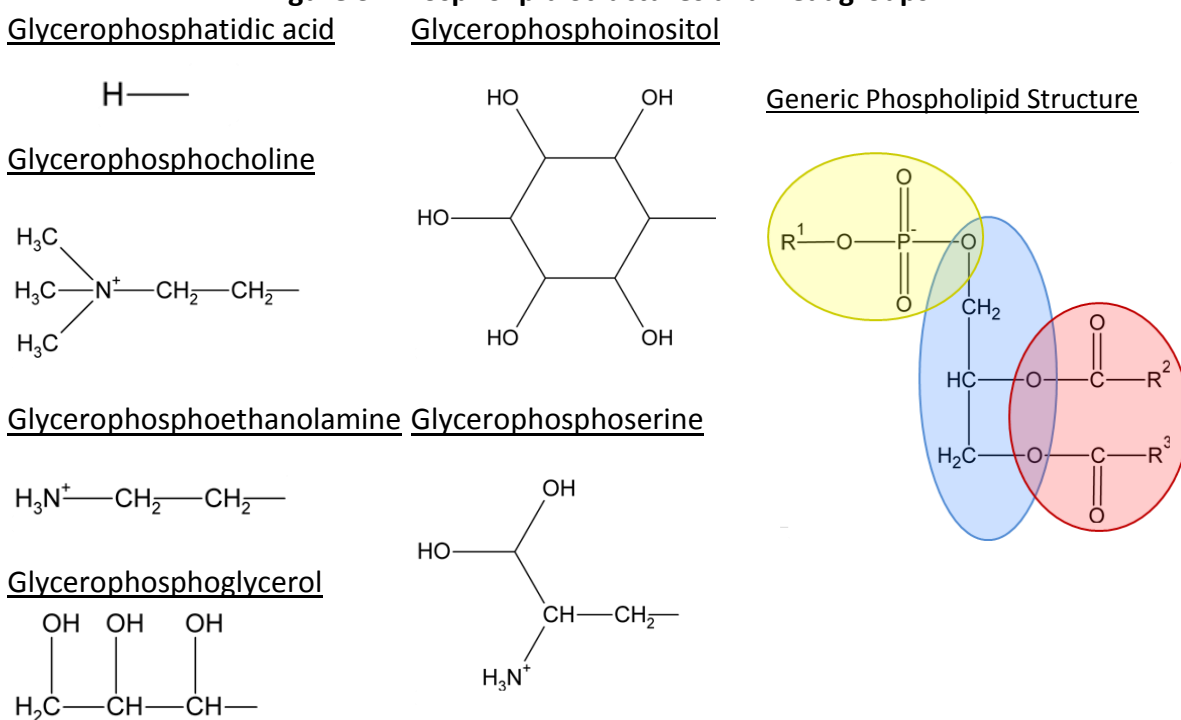
Table 1. Nomenclature for Mammalian Long Chain Fatty Acids.			
Systematic	Trivial	Carbon number	Double bonds
Decanoic acid	Capric acid	10	0
Dodecanoic acid	Lauric acid	12	0
Tetradecanoic acid	Myristic acid	14	0
Hexadecanoic acid	Palmitic acid	16	0
Octadecanoic acid	Stearic acid	18	0
c-9-octadecanoic acid	Oleic acid	18	1
c-9,12-octadecadienoic acid	Linoleic acid	18	2
Eicosanoic acid	Arachidic acid	20	0
c-5,8,11,14-eicosanoic acid	Arachidonic acid	20	4
c-15-tetracosanoic acid	Nervonic acid	24	1

Sphingosine can also be found referred to as (2*S*,3*R*,4*E*)-2-aminooctadec-4-ene-1,3-diol, D-*erythro*-sphingosine and sphing-4-enine. Other sphingoid bases have been identified including dihydrosphingosine, also known as sphinganine, and phytosphingosine (also shown in Figure 4). The 16 – 20 carbon forms have been identified at low levels in mammals. The chain length is indicated by prefixing the base name with the systematic terms applied to fatty acids of the same chain length (see Table 1), for example by adding 'eicosa' to sphingosine for the 20-carbon analogue. Shorthand can also be used similarly to fatty acids by denoting the carbon number and number of double bonds after the lipid class. The di- and trihydroxy bases (sphingosine and phytosphingosine) are designated by the prefix 'd' or 't' respectively.

Sphingolipids are sub-divided into ten classes that include ceramides, phosphosphingolipids, neutral glycosphingolipids and acidic glycosphingolipids. These four cover the major membrane sphingolipids. Ceramides are identified by the amide-linked sphingoid base and fatty acid (Figure 4, shown with stearic fatty ester). Fatty acids are typically 14 to 26 carbons and can be modified with a hydroxyl group in the *sn*-2 position, denoted in the shorthand by (2OH). Ceramides are the biosynthetic precursors of other classes of sphingolipid. For example phosphosphingolipids are the ceramide analogues of the glycerophospholipids. By far the most abundant membrane phosphosphingolipid is ceramide glycerophosphocholine, or 'sphingomyelin' (Figure 4). Neutral glycosphingolipids are based on a ceramide backbone modified with uncharged sugars such as glucose (Glc), galactose (Gal), N-acetylgalactosamine (GalNAc) and fucose (Fuc) (structures and shorthand terms given in Figure 5).

Sub-classes, or series', are defined by the number, order and configuration of the sugar subunits of which several consistent combinations have been isolated from natural systems. Simple glycosylceramides, more commonly known as hexosylceramides, are the most straightforward. This subclass includes important membrane lipids, and precursors to more complex glycosphingolipids, such as galactosyceramide and lactosylceramide.

Sphingosine
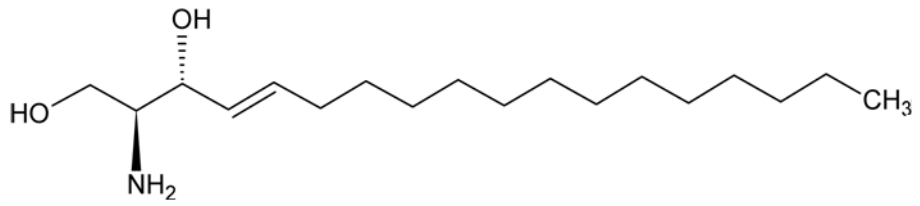
Sphingenine
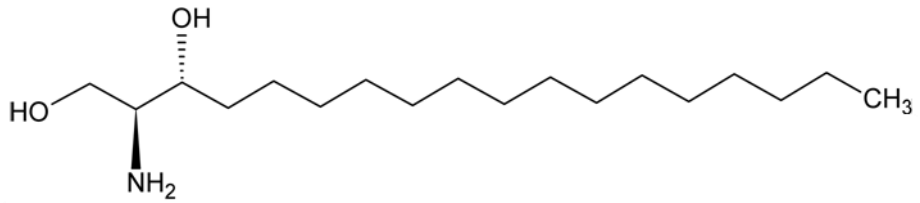
Phytosphinganine
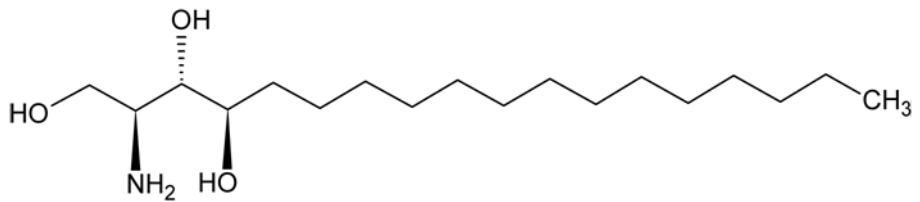
Ceramide
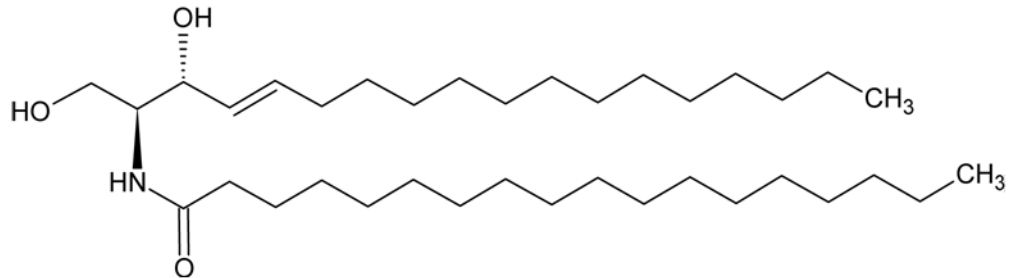
Sphingomyelin
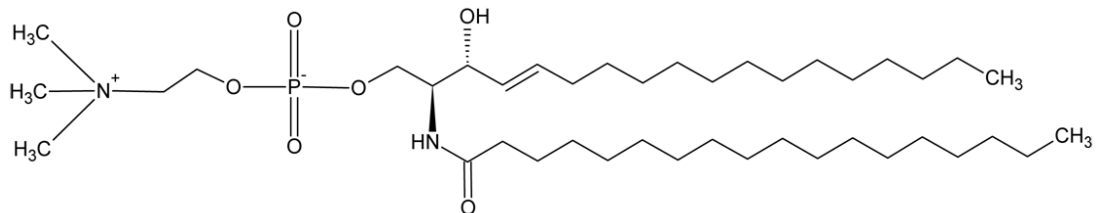
Figure 4. Sphingolipid Structures.

Glucose (Glu)
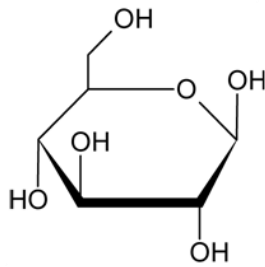
N-acetylglucosamine (GluNAc)
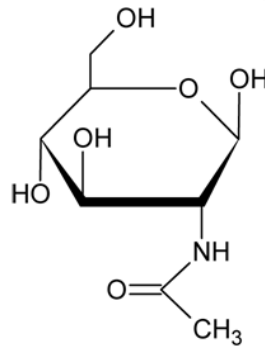
Lactose (Lac)

Galactose (Gal)

N-acetylgalactoseamine (GalNAc)

N-acetylneuraminic acid (5-N-acetyl sialic acid, Neu5Ac)
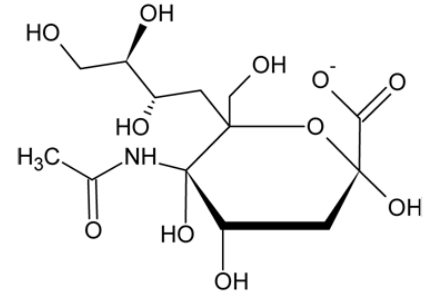
Fucose (Fuc)
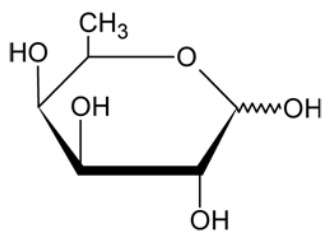
Figure 5. Glycosphingolipid Sugar Structures, Nomenclature and Shorthand.

The acidic glycosphingolipid class contains glycosphingolipids modified with ionised groups. Sulfglycosphingolipids, usually referred to as 'sulfatides', are characterised by the presence of an ionised sulphate group on a glycosphingolipid, most commonly galactosylceramide. Another subclass, the gangliosides, are characterised by the presence of one or more *N*-substituted neuraminic acid residues on a conserved Galβ1-3GalNAcβ1-4Galβ1-4Glc-ceramide sequence, (although not all of these hexose units must be present). In mammals the most common neuraminic acid is N-acetyl neuraminic acid; or 'sialic acid', abbreviated to Neu5Ac although other modifications such as N-glycolyl neuraminic acid (Neu5Glc) are occasionally found. In humans the ganglioside neuraminic acid is exclusively Neu5Ac. Gangliosides have

been identified that contain from one to five sialic acids in various configurations. Ganglioside

structures can be represented using a systematic nomenclature that details sugar sequence,

bond number and configuration. However a simplified system was suggested by Lars

Svennerholm, a pioneer in early ganglioside research, that is still popular today (L

Svennerholm, 1980). This shorthand is described in Table 2 below, and is used throughout.

Table 2. Shorthand Nomenclature of Common Mammalian Gangliosides (L Svennerholm, 1980).	
Svennerholm Shorthand	**Glycan Sequence**
GM1	Galβ1-3GalNAcβ1-4Gal(3-2αNeuAc)β1-4Glcβ1-1Cer
GM2	GalNAcβ1-4Gal(3-2αNeuAc)β1-4Glcβ1-1Cer
GM3	NeuAcα2-3Galβ1-4Glcβ1-1Cer
GM4	NeuAcα2-3Galβ1-1Cer
GD1a	NeuAcα2-3Galβ1-3GalNAcβ1-4Gal(3-2αNeuAc) β1-4Glcβ1-1Cer
GD1b	Galβ1-3GalNAcβ1-4Gal(3-2αNeuAc8-2αNeuAc)β1-4Glcβ1-1Cer
GD2	GalNAcβ1-4Gal(α2-3NeuAcα2-8NeuAc)β1-4 Glcβ1-1Cer
GD3	NeuAcα2-8NeuAcα2-3Galβ1-4Glcβ1-1Cer
GT1a	NeuAcα2-8NeuAcα2-3Galβ1-3 GalNAcβ1-4Gal(α3-2NeuAc)β1-4Glcβ1-1Cer
GT1b	NeuAcα2-3Galβ1-3GalNAcβ1-4Gal(α3-2NeuAcα2-8NeuAc)β1-4Glcβ1-1Cer
GT3	NeuAcα2-8NeuAcα2-8NeuAcα2-3Galβ1-4Glcβ1-1Cer
GQ1b	NeuAcα2-8NeuAcα2-3Galβ1-3GalNAcβ1-4Gal(α3-2NeuAcα2-8NeuAc)β1-4Glcβ1-1Cer

1.4 Ganglioside Biology

Gangliosides, with large complex head-groups projecting into the extracellular space, comprise

one of the most interesting groups of membrane lipids. An overview is provided below

summarising key findings in their discovery and description, abundance and function, synthesis and their association with diseases, in particular their involvement in autoimmune neuropathies. Although their relative abundance is low compared to other membrane lipids their biological significance, as understood by cell culture, tissue profiling or genetically engineered animal modelling, cannot be underestimated.

1.4.1   A Brief History of Gangliosides

Ernst Klenk isolated and identified the first gangliosides in 1942 while studying sugar-containing lipidoses associated with amaurotic infantile idiocy and Niemann-Pick's disease (Klenk, 1942). Originally named 'substance X' he later changed this to 'ganglioside' for their abundance in the ganglions of the human brain. Klenk used methanolysis to fragment a "hexosamine-free polyhydroxy-amino acid with 9 or 10 carbon atoms" from gangliosides which he named "neuraminic acid", now known to be the un-substituted precursor of sialic acid. He would later link this structure with viral reception of the mumps-influenza group Paramyxovirus (Herrler, Hausmann, & Klenk, 1995). Ahead of growing interest Klenk was the first to identify the remaining structural constituents; sphingosine, fatty acid, hexose and hexosamines. Alternative N-acetylated and O-substituted neuraminic acids were soon isolated by Werner and Odin in 1952 (Werner & Odin, 1952). N-glycolylneuraminic acid was also found on mammalian gangliosides, although rarely in humans.

The aforementioned glycan sequence was revealed in 1958 by Samuel Bogoch who went on to associate gangliosides with influenza virus and with schizophrenia (Bogoch 1958; Bogoch 1957a; Bogoch 1957b). Lars Svennerholm first suggested carbohydrate moieties containing an incomplete hexose sequence, and a higher degree of sialisation (L Svennerholm, 1956). In the 1960s Klenk returned his attention to gangliosides to extensively describe the molecular arrangement of both the sphingosine and the oligosaccharide. He observed most structural variation in the sugar, confirming Svennerholm's suggestion of heterogenic carbohydrate moieties. Over 200 different species of ganglioside have now been identified from both

prokaryotic and eukaryotic cells (Yu, Yanagisama and Ariga 2007).

1.4.2   Metabolism

Gangliosides are the product of a complex biosynthetic network. Neobiosynthesis in vertebrates begins at the cytostolic interface of the endoplasmic reticulum with the formation of the precursor ceramide. The surrounding networks and synthetic pathways associated with the anabolism of ceramide are described in Figure 6. Ceramide for galactosylation or sulfatide synthesis remains in the ER on the luminal side where it is modified by ceramide galactotransferase, a type I membrane protein, before transferring to the luminal leaflet of the Golgi stack. Neo-synthesised ceramide determined for ganglioside production moves to the cis-face of the Golgi stack by an unknown mechanism and is inserted into the outer leaflet. Nucleotide-activated sugars are added stepwise by a series of co-localised membrane-bound glycosyltransferase enzymes. Ceramide glucosyltransferase, a type III membrane protein, starts this process at the cytostolic face of the Golgi body. Some monoglycosylsphingolipids are transferred at this point to the plasma membrane via non-vesicular transport. The mechanisms governing this precise intracellular localisation of early precursor glycosphingolipids are not yet understood.

Subsequent glycosylations occur on the luminal face of the golgi body presumably after the action of an unknown flippase enzyme. Galactosyltransferase I catalyzes the addition of galactose to glucosylceramide (GluCer) to form lactosylceramide (LacCer), the common precursor of all known vertebrate gangliosides (with the exception of GM4) (Huwiler, Kolter, Pfeilschifter, & Sandhoff, 2000). Sialytransferases I, II and III (STI, II and III) catalyse the stepwise addition of one, two or three sialic acid residues to the *sn*-3-position of the inner galactose forming simple gangliosides GM3, GD3 and GD4. Complex species are synthesised from these precursors along assembly lines known as the 0-, a-, b- and c- series' (Figure 7). Additional glycosylations are regulated across the series' by β-1,4-N-acetylgalactosaminyl-transferase (GalNAc transferase), β-1,3-galactosyltransferase II and sialyltransferases IV, V and
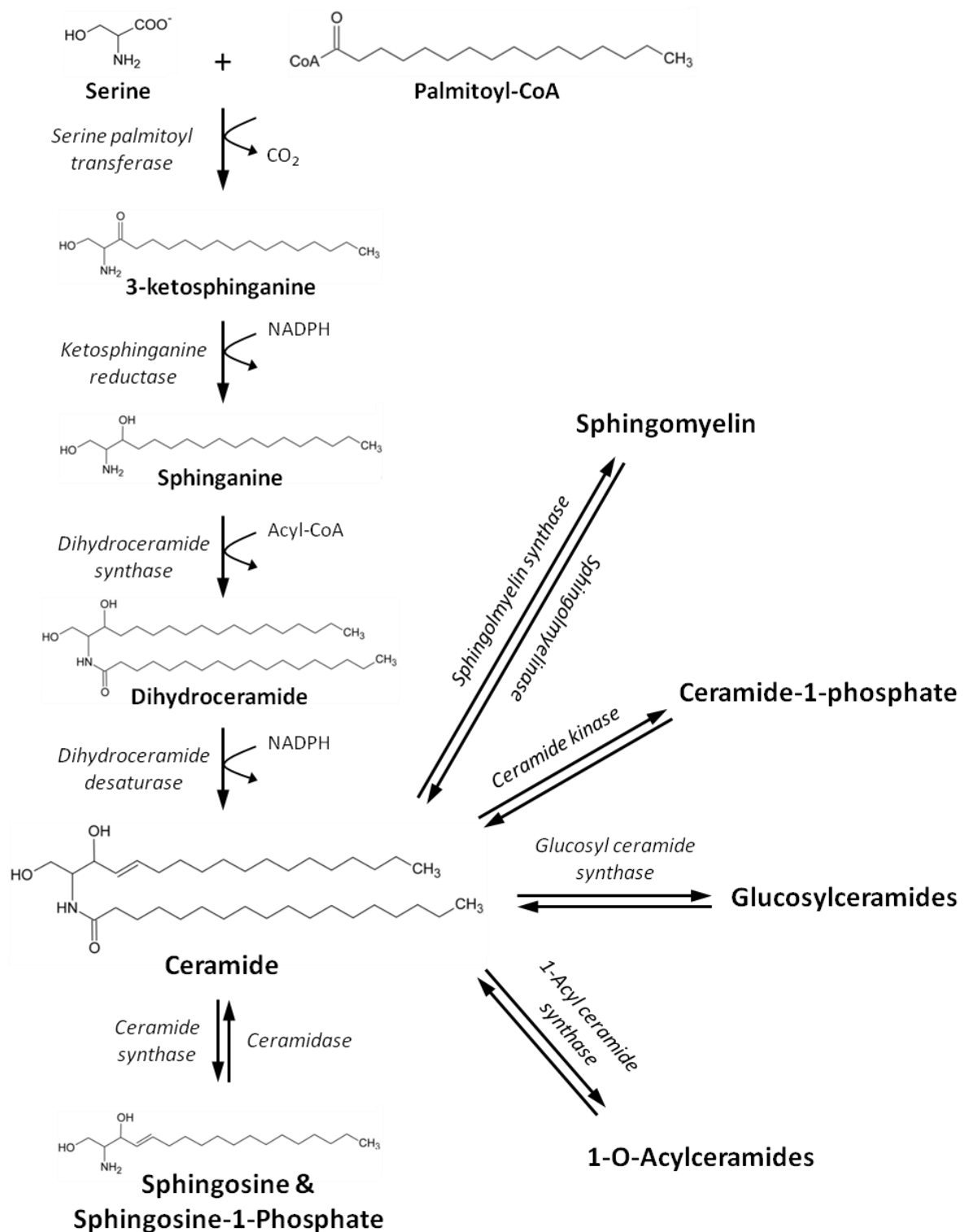
Figure 6. Ceramide Metabolism. Ceramide is the biosynthetic precursor for many sphingolipids. *De novo* synthesis begins at the endoplasmic reticulum with the condensation of serine and palmitoyl-coA. Ceramide then feeds into multiple metabolic pathways including sphingosine-1-phosphate, an important extracellular signalling lipid, and sphingomyelin. Ceramide can also be produced via the catabolism of any of these other pathways.

VII which may be organised in functional complexes for each gangliosides. Relative amounts of

ganglioside species appear to be a function of the steady state ratio of the four precursors.

Trace amounts of the c- series are found in humans and the 0- series have only been observed

in vivo in mutant mouse models. The lesser known alpha series has also been identified only as

a minor component of brain gangliosides in cows and rodents (Furuya et al., 1994).

Gangliosides are then transported via carrier protein-modulated vesicles to the plasma

membrane. Synthesis in the lumen of the ER drives their enrichment on the outer leaflet of

these vesicles and consequent fusion with the plasma membrane results in asymmetric

distribution in the outer leaflet [For reviews see (Daniotti & Iglesias-Bartolomé, 2011; Kolter,

Proia, & Sandhoff, 2002)].
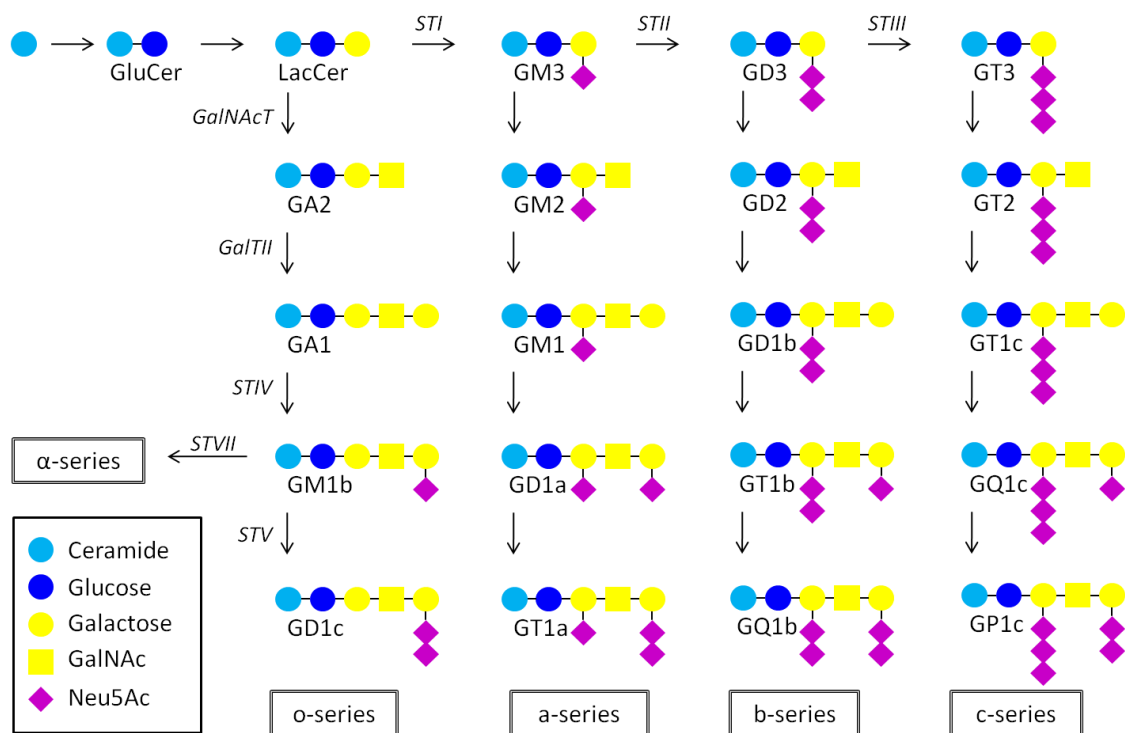
Figure 7. Ganglioside Biosynthesis. Lactosyl ceramide (LacCer) is the common precursor of gangliosides except GM4 (not shown, sialylated GalCer). Sialyltransferases I, II and III (STI, STII and STIII) catalyse the addition of sialic acid to form simple gangliosides GM3, GD3 and GT3 which, with LacCer, form the precusor constructs for the o-, a-, b- and c-series gangliosides. Low specificity enzymes N-acetylgalactose transferase (GalNAcT), galactosyl transferase II (GalTII), and sialyltransferase IV, V and VII (STIV, STV, STVII) regulate synthesis of the complex gangliosides across the four series.

Endocytosis occurs from the plasma membrane. Gangliosides can be recycled back to the plasma membrane from early or recycling endosomes or return to the golgi complex in late endosomes for reglycosylation or degradation in the lysosome. Lysosomal catabolism of gangliosides occurs in a similarly stepwise manner to anabolism. This is covered in detail elsewhere (K. Sandhoff & Harzer, 2013; K. Sandhoff & Kolter, 2003; Tettamanti, 2004). Briefly, gangliosides exposed to the lysosomal matrix are degraded by various soluble glycohydrolases via the sequential removal of sugar residues from the non-reducing terminal to form lactosylceramide. This is degraded by β-galactosidase and β-glucosidase to form ceramide which is broken down in to fatty acid and sphingosine components ceramidases. Degradation products (monosaccharides, long chain bases, fatty acids) may return to the cytosol for further metabolic processing via a number of salvage mechanisms (Tettamanti, Bassi, Viani, & Riboni, 2003). Alternative lysosomal pathways include the separation of ceramide and oligosaccharide by a ceramide glyconase and removal of the fatty acid by sphingolipid ceramide N-deacylases to form lyso-derivatives (Basu, Kelly, Girzadas, Li, & Basu, 2000; Furusato et al., 2002; Imokawa, 2009).

Cell membrane-bound enzymes have been identified that may also mediate ganglioside synthesis at the cell surface. Mammalian synaptosomal membranes have been shown to carry both sialidase and sialyltransferase enzymes with ganglioside specificity (Prinetti, Chigorno, Mauri, Loberto, & Sonnino, 2007) and a ganglioside-specific myelin-associated sialidase has been described (Yohe, Jacobson, & Yu, 1983). Sialyltransferase and GM3 glycosylhydrolase activity have been demonstrated at the membrane surface of epithelial and melanoma cells and human fibroblasts (Crespo, Demichelis, & Daniotti, 2010; Valaperta et al., 2006) and a sialytransferase enzyme has been described from brain (Preti, Fiorilli, Lombardo, Caimi, & Tettamanti, 1980). Despite this ganglioside and glycosphingolipid composition appears to be primarily regulated by a combination of genomic and epigenetic mechanisms. Dynamic transcription of glycosyltransferase and activator protein genes has been directly linked to changes in composition, suggesting minimal post-translational delay (Henion, Zhou, Wolfer,

Jungalwala, & Hennet, 2001; Ngamukote, Yanagisawa, Ariga, Ando, & Yu, 2007; R. K. Yu, Bieberich, Xia, & Zeng, 2004). Epigenetic controls such as pH (Iber, van Echten, Klein, & Sandhoff, 1990), enzyme phosphorylation (R. Yu & Bieberich, 2001) and feedback control from immediate and downstream reaction products (Furukawa et al. 2008) have been identified.

1.4.3 Abundance and Function

Gangliosides and other glycosphingolipids have complex functions throughout the body, most noticeably in the central and peripheral nervous system. Here they are vital for the development, function and repair of nerves and neurological tissue. This has been investigated at a molecular, cellular and systemic level. Genetically engineered animal models have been particularly important in understanding ganglioside function on a systemic scale. In the membrane they are thought to instil lateral organization to other lipids, glycans and proteins, assist and regulate signalling molecules, and act as recognition and binding sights. Via these mechanisms gangliosides are known to influence cell cycle and differentiation, and regulate cell interactions. The composition of the ganglioside fraction has been shown to vary significantly between species, cell type and developmental stage and profile changes have been observed in various diseases including cancer. Several human metabolic diseases are associated with the genetic interruption of ganglioside catabolism. The functions assigned to gangliosides can apply to conserved glycan motifs while others are very species-specific. Further functions may be conferred by lateral and heterodimeric interactions within the membrane. The following chapter is an overview of the abundance and function of cell membrane gangliosides as they stand with a focus on the mammalian nervous system.

1.4.3.1 Abundance

Gangliosides are asymmetrically distributed in the outer leaflet of the plasma membrane in most animal tissues at low levels (1-2% total lipid content). They are highly enriched in the brain where they can constitute 10-12% of the total lipid content and 20-25% of the content from the outer membrane leaflet. Early profiling studies found that the composition of

individual gangliosides is highly specific to species, organ and developmental stage. For example GM4, a negligible component in human and mouse gangliosides, is a major component in primate and chicken brain gangliosides (Ando, Chang, & Yu, 1978). In mouse brain tissue the total amount of gangliosides increases after birth and switches from predominantly simple precursors GM3 and GD3 to complex gangliosides such as GM1, GD1a/b and GT1b. Profiles in the white matter and cerebral cortex are similar at birth but differentiate via a steep rise in GM1 content and drop in di- and trisialylated species in the white matter (L Svennerholm et al., 1989). Total gangliosides in mouse brain drop again just before senescence (Ohsawa, 1989). This sharp rise and late fall in total brain gangliosides has also been observed in teleost fish although age-specific changes in composition are quite different (Seybold & Rahmann, 1985).

In human brain lipids sialic acid concentration also increases in the cerebral cortex in early development up to the age of approximately two years where concentrations plateaux at adult levels. In the white matter, where gangliosides occur at lower concentration to the grey matter, this rise peaks at 3 months before falling to adult levels (Vanier, Holm, Öhman, & Svennerholm, 1971). Relative ganglioside composition however appears to remain fairly consistent in the brain comprising mostly GM1, GD1a, GD1b and GT1b with minor components including GM2, GM3, GD3 and GQ1b although c-series gangliosides, rarely observed in adult brain, have been observed by immunohistochemistry in early embryonic brain (Kracun et al., 1991). A post-birth age-related switch from a-series to b-series gangliosides has also been observed in the frontal lobe (L Svennerholm et al., 1989). Human spinal cord contains about half the ganglioside content of cerebral white matter, and one-tenth that of cerebral grey matter. Unlike brain gangliosides, the composition is not dominated by complex species, instead comprising comparable amounts of simple gangliosides GM4, GM3 and GD3 and complex gangliosides GM1 and GD1b (Ueno, Ando, & Yu, 1978). Similar changes in composition are observed in peripheral nerves where GD1a, GD1b, GT1b and the monosialylated lacto-series ganglioside LM1 dominate the profiles of both sensory and motor

nerves in human. More lacto-series gangliosides have been identified from peripheral nerve myelin as well as GD3, GM3 and GD1b (Ogawa-Goto & Abe, 1998). Although no consistent differences in head-group composition have been identified between motor and sensory nerves the ceramide moieties are thought to differ significantly (Ogawa-Goto, Funamoto, Abe, & Nagashima, 1990). Unexpectedly this may significantly influence antibody binding affinities (Ohta, 1994).

1.4.3.2 <u>Functions (So Far)</u>

The essential nature of gangliosides was originally explored by *in vitro* cell studies. Exogenously applied gangliosides invoked recognisable responses in cell cultures associated with differentiation, proliferation and function. Specific gangliosides have been shown to encourage neuronal sprouting and neuritogenesis in mouse neuroblastoma cells (Tsuji *et al.* 1988), induce differentiation in keratinocytes, murine stem cells (Paller *et al.* 1995), and in leukemic cell lines (Nojiri *et al.* 1986) and activate microglia, the macrophages of the brain (Pyo *et al.* 1999). They have induced apoptosis in T-cells (Das *et al.* 2008) and dendritic cells (Bennaceur *et al.* 2010) and autophagic cell death in astrocytes (Hwang *et al.* 2010) and are known to regulate cell recognition and cell-cell interactions as both membrane antigens and signalling modulators.

Their important functions within cell membranes have been indicated in cell, *in vitro* and immunostaining studies, and supported bilayers. Lateral interactions with attenuating or enhancing activity have been proposed between gangliosides and membrane receptors after associations have been shown via cross-linking and fluorescence microscopy. Notable proteins include insulin receptors, epithelial growth factor receptors and integrins, as well as with cytoplasmic signal transducers like small G-proteins and the Src-family kinases (Kabayama et al., 2007; Miljan et al., 2002; Todeschini, Dos Santos, Handa, & Hakomori, 2007). This may occur in conjunction with the formation of distinct liquid-ordered phase micro-domains where ganglioside epitopes can co-localise with proteins. These micro-domains may have far-

reaching consequences but are difficult to study due to their small size and transient nature. There is no space to cover the full complexities of the structure and function of these rafts here. However the area is fascinating and discussed in several comprehensive review articles (Michel & Bakovic, 2007; Schengrund, 2010; Simons & Toomre, 2000) and specifically in relation to gangliosides (Sandro Sonnino, Mauri, Chigorno, & Prinetti, 2007).

Many exogenous and endogenous ganglioside lectins have been identified that interact with the projecting glycan head-group in the extracellular space. Endotoxins from *Vibrio Cholera, Escherichia coli*, *Clostridium tetani*, and *Shigella dysenteriae,* among others, recognise specific gangliosides with varying affinity. Cellular invasion follows after glycosphingolipid mediated endocytosis of the toxin targeted to the golgi body and ER where the toxins are activated (Angström, Teneberg, & Karlsson, 1994). More than a dozen sialic-acid binding animal lectins known as "siglec" (Sialic-acid binding Immunoglobulin-like) proteins have been identified in humans. These trans-membrane proteins bind various glycan-bound sialic acid structures in gangliosides to regulate cell behaviour. For example Siglec 7 which preferentially binds the disialic NeuAcα2-8NeuAc motif on *b*-series gangliosides, acts as an inhibitory receptor on natural killer (NK) cells (Crocker, Paulson, & Varki, 2007). Over-expression of GD3, a *b*-series ganglioside bearing the motif, was found to modulate natural killer cell cytotoxicity in a Siglec-7 dependent manner (Nicoll et al., 2003). This interaction has been fruitfully investigated using protein co-crystallization with a synthetic GT1b analogue (Yamaji, Teranishi, & Alphey, 2002). Further evidence has linked ganglioside binding with E-selectins presented on circulating macrophages during infection and injury (Nimrichter et al., 2008), and adhesion-modulating galectins (Elola, Wolfenstein-Todel, Troncoso, Vasta, & Rabinovich, 2007).

Genetically engineered animals have been essential in understanding the systemic roles of gangliosides and other glycosphingolipids. As the enzymes involved in sphingolipid metabolism were described, it became possible to knock out the genes responsible. Various mice have been produced that are incapable of synthesising certain branches of the metabolic pathway.

One of the earliest mice, the UDP-GluCer synthase gene (Ugcg) knock-out mouse which is unable to synthesise glucoylceramide, the precursor of most glycosphingolipids, demonstrated their vital nature in development. Ceramide accumulation caused an apoptotic process at gastrulation resulting in universal embryonic lethality. Some ill-characterised tissue differentiation into endoderm, mesoderm and ectoderm was observed, but severely retarded, suggesting that glycosphingolipids are essential for tissue differentiation during development (Yamashita et al., 1999). A study of neural-tissue specific Ugcg -/- mice observed structural and functional abnormalities in the cerebellum tissue and mortality within three weeks of birth (Jennemann et al., 2005). Galactosylceramide synthase knockout mice, unable to synthesise galactosyl-ceramide glycosphingolipids specifically, developed normally but exhibited sterility and early hind limb weakness, ataxia and neurodegeneration (Coetzee et al., 1996). Similarly hexosylceramide sulfotransferase (Cst, *Gal3STI* gene) knockout mice exhibited sterility and hind-limb weakness, tremors and progressive ataxia within the first year, suggesting the essential nature of sulfatides in myelin function and spermatogenesis (Honke et al., 2002).

Mutant mice lacking the synthetic enzymes for complex gangliosides specifically have also been generated. These knockouts are indicated for a-series (purple) and b-series (red) by crosses in Figure 8. Age related reduction in nerve conductance, stability and integrity were observed in GalNAcT -/- mice (also called GM2/GD2 synthase knockouts, *B4GalNT* gene, red cross), demonstrating the dependence of axon-myelin interactions and the maintenance of healthy, functional axons on complex gangliosides (Takamiya, 1996). Mice reached adulthood but displayed impaired motor function and loss of hind-limb mobility within the first year. This was due to significant axon demyelination and degeneration in central and peripheral nervous systems, loss of nodal axo-glial junction adhesion, and poorly structured myelin attachments (Chiavegatto, Sun, Nelson, & Schnaar, 2000; Susuki et al., 2007). Myelin is the multilamellar membrane that sheaths vertebrate axons and is essential for axonal protection, stability and for electrical conductance. Interestingly mice lacking *b*-series gangliosides (GD3 synthase -/-,

GD3S gene, purple cross) did not show the same impaired phenotype, exhibiting only poorability to repair peripheral nerves (H. Kawai et al., 2001; Okada, Itoh Mi, et al., 2002a). This supports the theory that there is some functional redundancy between glycan structures. Schnaar suggests more specifically that this was because both models were still able to synthesise gangliosides containing a terminal NeuAcα2–3Galβ1–3GalNAc sequence; a preferential binding site of myelin-associated glycoprotein (MAG), otherwise known as Siglec 4, which stabilises axon-myelin interactions (Schnaar, 2004, 2010). Double knockouts meanwhile are limited to GM3 synthesis

Figure 8. Genetic Knockouts in Ganglioside Metabolism. GalNAcT knockouts (red) cannot synthesise complex gangliosides while STII knockouts (purple) cannot synthesise b-series gangliosides, helping unravel the systemic roles of specific species.

only. These mice have exhibited varied neurodegenerative phenotypes including lethal audiogenic seizures (H. Kawai et al., 2001), early neuronal degeneration resulting in motor, sensory and emotional dysfunctions (Tajima et al., 2009) and peripheral nerve degeneration and reduced sensory function at the skin (Inoue et al., 2002).

1.4.4   Gangliosides in Human Disease and Disorders

As may be expected from their ubiquitous nature gangliosides are a factor in many human diseases. As may be expected from their functional complexity, rarely are their roles in said diseases well understood. A build-up of ganglioside or glycosphingolipid precursors has been observed in several inherited lysosomal storage disorders (LSD). Genetic mutations relating to

31

the inactivation of key hydrolase enzymes in the ganglioside catabolic pathway have been identified in GM1 gangliosidosis, GM2 gangliosidosis, Tay-Sachs disease and Sandhoff disease. Less clear is the cause of secondary accumulation of gangliosides in LSD where primary defects in ganglioside degradation have not been identified such as Niemann-Pick, Gaucher disease and galactosialidosis (Walkley, 2004). Many LSD-associated symptoms are neurodegenerative reflecting the vital nature of ganglioside metabolism in the central and peripheral nervous system.

Compositional changes in ganglioside profile have also been closely linked to cancer and identified as lipid biomarkers or prognosis indicators. The mechanisms and significance of these changes are often not understood. Abnormal profiles have been found in breast, gastrointestinal, and brain tumours (Birklé, Zeng, Gao, Yu, & Aubry, 2003). Simple gangliosides like GM3, GD2 and GD3 were found to be highly expressed in human melanomas (K Furukawa, Hamamura, & Nakashima, 2008). The complexity of these associations is twofold. Different ganglioside species can enhance or inhibit oncogenic behaviour in one cancer while single species can enhance or inhibit oncogenic behaviour in different tumour types. For example high levels of GM3 have been shown to reduce proliferation and enhance apoptosis in astrocytes (Nakatsuji & Miller, 2001) and inhibit angiogenesis in brain cancer (Seyfried & Purna, 2010) suggesting a cancer inhibitory effect. However GM3 is also an alleged oncogenic promoter in breast cancer and suggested target for immunotherapy. Mammary cancer tumour cell migration and invasion were enhanced in mice by over-expression of GM3-synthase and inhibited by GM3-synthase silencing (Y. Gu et al., 2008). A vaccine that induces anti-GM3 antibodies has shown sufficient activity to reach phase III clinical trials (Labrada et al., 2009).

Altered metabolism and a host of other intriguing interactions have also been identified in well-known neurological disease pathologies. For example great importance is placed on ganglioside metabolism in Alzheimer's disease. Alzheimer's is characterised by 'senile plaques', rich in aggregated amyloid β-protein (Aβ), in the brain. *In vitro* the addition of GM1-rich lipid

vesicles to soluble random coil Aβ promoted a transition to the aggregated Aβ structure found in these plaques (Choo-Smith, Garzon-Rodriguez, Glabe, & Surewicz, 1997). GM1 and Aβ have also been observed to co-localise in the membrane by fluorescent confocal microscopy (Wakabayashi, Okada, Kozutsumi, & Matsuzaki, 2005). Lipid rafts rich in sphingomyelin, cholesterol and GM1 are now generally considered to be the processing platforms of amyloid precursor protein to normal and toxic Aβ (Ariga, McDonald, & Yu, 2008). Additionally the cleavage products of amyloid precursor protein (APP); Aβ and APP intracellular domain (AICD), have been shown to regulate the activity of GD3-synthase by binding the substrate GM3 and by down regulating transcription of GD3 synthase. In turn GM3 decreased Aβ production while GD3 increased production (Grimm et al., 2012). These interactions are known to depend heavily on the glycan moiety and play a critical role in Alzheimer's pathogenesis. It is thought that ganglioside interactions may have similar importance in the pathogenesis of Parkinson's disease, where administration of ganglioside GM1 is thought to confer a clinical benefit to patients, and Huntington's disease (Desplats et al., 2007; Schneider, Sendek, Daskalakis, & Cambi, 2010). However the multi-factorial nature of these diseases means that the precise mechanisms of ganglioside involvement are not yet known.

1.5 Glycosphingolipid-Associated Autoimmune Neuropathies

Aside from the complex associations mentioned above, gangliosides are intricately involved in the development of a distinct grouping of human diseases. A growing number of autoimmune neuropathies affecting the central and peripheral nervous systems have been associated with increased titres of anti-ganglioside antibodies in patient serum. While the finer details of antibody specificity are not well understood it is known that antibody binding to native gangliosides may trigger B-cell mediated immunodegradation in nerves, sometimes in conjunction with T-cell mediated responses. The most studied of these is Guillain-Barré Syndrome. Work is underway to understand this hetergeneous disease, particularly the roles of these anti-ganglioside antibodies and ganglioside-specificity, and the many controversies

and unknowns associated with them. It is possible that research findings may shed light on associated syndromes and diseases.

1.5.1 Guillain-Barré Syndrome

The earliest clinical description of Guillain-Barré syndrome (GBS), formerly referred to as Landry's Ascending Paralysis, is credited to the French physician Jean Landry in 1859 (Landry, 1859). It was however named for George Guillain and Jean Alexandre Barré who defined the characteristic feature of the disease - elevated protein levels in the cerebrospinal fluid with normal cell counts - with André Strohl in 1916 from two acutely ill World War I soldiers presenting motor weakness, paresthesias and muscular pain (Guillain, Barré, & Strohl, 1916). GBS was recognised as a radiculoneuropathy several years later by Walter, then Haymaker and Kernohan, who found primary lesions in fatal GBS cases at the junction between motor and sensory roots and the spinal cord (Haymaker & Kernohan, 1949; Walter, 1919). Subsequent reports emerged and, in 1927, the term 'Guillain-Barre Syndrome' was coined (Draganesco & Claudian, 1927). Diagnostic criteria were defined and clarified in 1978 by the National Institute of Neurological and Communicative Disorders and Stroke (NINCDS) and updated by Asbury (Asbury & Cornblath, 1990; Asbury, 1981; NINCDS, 1978). These criteria are still largely used in clinical diagnosis today.

1.5.1.1 Clinical Syndrome and Variants

Guillain-Barré Syndrome is an acute-phase peripheral neuropathy characterised by rapid onset of symmetrical, flaccid paralysis and areflexia. A number of different axonal and demyelinating subtypes have been identified that occur with regional specificity. Key features of the major subtypes; acute motor axonal neuropathy (AMAN), acute motor and sensory axonal neuropathy (AMSAN), acute inflammatory demyelinating polyneuropathy (AIDP), and Miller-Fisher syndrome (MFS), are summarised in Table 3. Although rare (1-2 cases per 100,000) GBS causes severe disturbances. One in five patients experience lasting nerve damage or paralysis after the acute phase (Buzby, Allos, & Roberts, 1997). During the acute phase 90% of patients

Table 3. Clinical Guillain-Barré Syndrome Variants.		
Subtype (Acronym)	Principal clinical features	Associated antibodies
Acute motor axonal neuropathy (AMAN)	Direct axonal damage by invading macrophages; motor nerves only; affects limbs and respiration.	GM1, GM1b, GD1a, GalNAc-GD1a
Acute motor and sensory axonal neuropathy (AMSAN)	Direct axonal damage by invading macrophages; motor and sensory nerves; affects limbs and respiration.	GM1, GM1b, GD1a
Acute inflammatory demyelin-ating polyneuropathy (AIDP)	Segmental demyelination; collateral axonal injury; autonomic involvement.	Unknown
Miller-Fisher Syndrome (MFS)	Ophthalmoplegia, ataxia and areflexia triad; facial and lower cranial nerve involvement.	GT1a, GQ1b

lose ambulatory motility, 30% require mechanical ventilation and more than half suffer autonomic disruptions (T. Burns, 2008). The onset of paralysis is rapid (<4 weeks) and commonly occurs 10 to 14 days after an unremarkable preceding bacterial or viral infection commonly by cytomegalovirus (13%), Epstein-Barr virus (10%), *Mycoplasma pneumoniae* (5%) or *Campylobacter jejuni* (30%) (Jacobs et al., 1998). Other pathogens, surgery, vaccination and parturition have all also been associated with GBS.

1.5.1.2 Pathogenesis and Pathophysiology

GBS pathophysiology results from the interruption or blocking of action potential conduction in peripheral nerve axons after direct or collateral degradation. This process is known to be immune-mediated although two distinct pathologies have been observed in GBS variants (Figure 9). In AIDP an as yet unidentified antibody target activates a complement-mediated demyelinating attack on the Schwann cells. During the resulting segmental demyelination axons suffer secondary or 'bystander' degradation as a result of the inflammatory environment and infiltration of scavenging macrophages. In AMAN and AMSAN however macrophages target the axons themselves leaving myelin intact. Auto-antibodies bind to gangliosides which are enriched at the nodes of Ranvier such as GM1 and GD1a. This results in the complement-mediated detachment of the paranodal myelin and loss of voltage gated
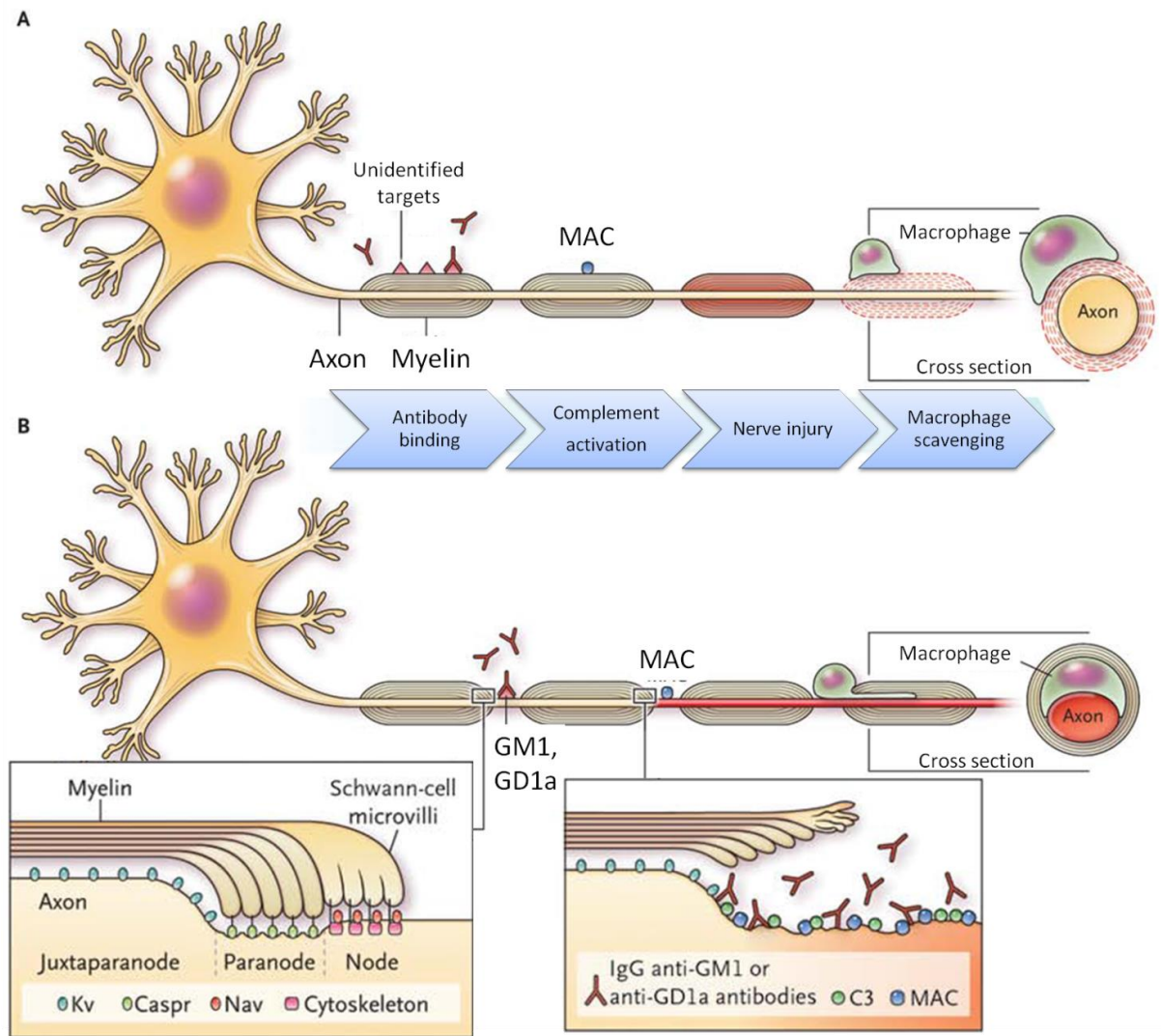
Figure 9. Models of Immunopathogenesis in Guillain-Barre Syndrome Variants. Copied with permission from (Nobuhiro Yuki & Hartung, 2012), Copyright Massachusetts Medical Society. While GBS is understood to be an immune-mediated, distinct immunopathologies are observed in the major variants variants. Panel A shows the current model for AIDP where activating antibodies bind as yet unknown targets on the Schwann cells to trigger complement-mediated degradation of the Schwann cell myelin via the assembly of membrane-attack complex (MAC). Axons may undergo 'bystander' degradation as a consequence of the inflammatory environment and scavenger macrophages. Panel B shows the current model of immunopathogenesis of AMAN and AMSAN variants. Myelinated axons consist of four regions (shown below); internodes, juxtaparanodes, paranodes and nodes of Ranvier. Gangliosides GM1 and GD1a are enriched at the nodes where voltage gated sodium (Nav) channels localise. Voltage-gated potassium channels (Kv) and contactin associated protein (Caspr) are present at the juxtaparanodes and paranodes respectively. Antibody binding to gangliosides and consequent MAC formation results in the loss of Nav clusters and detachment of paranodal myelin. This causes nerve-conduction failure. Macrophages subsequently invade the myelin-axon junction to scavenge the injured axon.

sodium channel (Nav) clusters, causing conduction failure and muscle weakness. Macrophages subsequently infiltrate the myelin-axon junction to scavenge injured axons via the nodes of Ranvier and/or nerve terminals; both of which are noticeably susceptible to injury in AMAN (Lehmann & Sheikh, 2008). It is now widely accepted that this follows cross reactive antibodies binding native glycosphingolipid epitopes, most commonly gangliosides, resulting in pathogenic complement deposition and macrophage activation in axonal subtypes. There is also increasing evidence that, while T-cell mediation plays a part in the recruitment of macrophages, autoimmune antibodies also play a significant role in the genesis of demyelinating subtypes.

1.5.1.3 <u>Antibody Targets, Ganglioside Mimicry and Heterodimeric Complexes</u>

Autoantibody targets in GBS were first implied in 1976 when Nagai *et al.* revealed that experimental allergic neuritis (EAN), the benchmark animal model at the time, could be induced in rabbits immunised only with certain ganglioside species or total extract (Nagai, Momoi, Saito, Mitsuzawa, & Ohtani, 1976; Saida et al., 1979). Since then patient sera have been heavily screened for antibody reactivity profiles using thin layer chromatography overlays, enzyme-linked immunosorbent assays (ELISA) and lipid arrays. A number of different ganglioside targets have been identified. Some relate to particular glycan motifs while others target explicit gangliosides with high affinity. Specific affinity-profiles have now been correlated with various subtypes (Table 3), symptoms or syndrome severity.

During the acute phase anti-ganglioside antibodies are identified in the sera of ~60% of patients. This figure is now thought to be an underestimate after the identification of heterodimeric ganglioside complex-specific antibodies in 2004. During a routine TLC-overlay a seroreactive band was observed at the overlap between GD1a and GD1b. This band disappeared when GD1a and GD1b were separated completely during a repeat overlay. This observation was the first published sighting of complex-reactive antibodies in GBS patient serum (Kaida et al., 2004). Further research identified antibodies to GD1a/GD1b, GD1a/GM1,

GD1b/GT1b and GM1/GT1b complexes then isolated GSC antibodies in 17% of 234 GBS patients and correlated severe disability with anti-GD1a/GD1b and anti-GD1b/GT1b specificity. Binding affinities were highest using 1:1 ratios and antigens of more than two GSLs appeared to inhibit anti-GSC antibody activity suggesting natural heterodimeric structures (Kaida et al., 2007). Most recently intense study using high-throughput 'combinatorial glycoarrays' has observed ganglioside complexes to exert one of three influences on lectin binding; "complex attenuated", "complex independent" and "complex enhanced" (Rinaldi et al., 2009). Further *in vivo* work has shown attenuation of anti-GM1 IgG binding at live neuromuscular junctions through *cis*-masking of GM1 head groups by GD1a. This effect could be reversed with neuraminidase treatment which cleaves GD1a to GM1 (Greenshields et al., 2009).

Insight into a potential source for these cross-reactive antibodies was discovered in 1993 when a molecular mimic of the GM1 glycan moiety was identified in the lipopolysaccharide (LPS) of *Campylobacter jejuni* (Yuki *et al.* 1993). Mimics of human GM2, GD1a, GD3 and GT1a were identified soon afterwards and analogues have since been identified on *Campylobacter jejuni, Mycoplasma pneumoniae, Haemophilus influenzae* and Cytomegalovirus (Blank, Barzilai and Schoenfield 2007). The theory that cross-reactive antibodies are induced by bacterial mimics is supported by animal experiments demonstrating the induction of cross-reactive anti-ganglioside antibodies after immunization with pathogen LPS (Goodyear *et al.* 1999, Wirguin *et al.* 1997).

1.5.1.4 **Animal Modelling**

While fundamental pathology is relatively well understood there are many unresolved questions surrounding the specifics of GBS. For instance during the generation of EAN symptoms have often been heterogeneous and inconsistent. Using *C.jejuni* as a model infection, in some animal studies LPS has failed to even trigger a noticeable antibody response (Kawashima, Nakamura, & Tai, 1992). This is reflected in humans where only a small minority of *C.jejuni* infected individuals develop post-infectious GBS while no trigger can be identified in

nearly a third of GBS cases. Subtypes, patient to patient differences in clinical presentation and severity, and immune preference for motor or sensory nerves are not understood. Consistent correlations between serotype and GBS phenotype are difficult to identify and few syndromes are consistently linked to antibody specificity. One exception to this is Miller Fisher syndrome (MFS) where anti-GQ1b antibodies with GT1b cross reactivity are present in >90% of Miller Fisher cases and are a recognised serum marker (A Chiba, Kusunoki, Shimizu, & Kanazawa, 1992). Correlations between serological specificity, site of activity and disease pathology other than this are weak and inexplicably inconsistent. For example anti-GM1 antibodies are associated exclusively with motor neuropathy syndromes yet GM1 is evenly distributed between the sensory and motor nerves. Meanwhile other studies have found poor correlation between anti-GM1 antibodies and axonal motor neuropathies (Rees, Gregson, & Hughes, 1995; Vriesendorp, Mishu, Blaser, & Koski, 1993).

In order to investigate, researchers have turned to mouse models. EAN, the first animal model of Guillain-Barré Syndrome, was devised in 1955 by injecting peripheral nerve homogenate into rabbits to induce a demyelinating neuropathy with Guillain-Barré Syndrome-like symptoms (Waksman & Adams, 1955). Investigations of EAN induced in rabbits, rats and mice have shed light on the roles of myelin activated T-cells, macrophages and inflammatory cytokines in cell-mediated demyelinating neuropathies. In 1976 a second model was developed, the so-called galactocerebroside-neuritis (GCN) model, after an EAN-like syndrome was induced in rabbits sensitised with galactocerebroside only (Nagai et al., 1976; Saida et al., 1979). GCN models highlighted the importance of the antibody and inflammatory responses in the development of a similar neuropathy (Powell et al, 1987; Saida et al, 1981; Sumner, 1981). This shift in focus to the humoral response corresponded with the dawning realisation of gangliosides as pathogenic autoantigens in human neuropathies (Freddo et al., 1986).

As mentioned, however, animal responses in these models have not been consistent. Often inoculation with purified gangliosides is followed by no observable increase in antibody titres.

This supports the theory that the immune system contains a degree of self-tolerance to native cell membrane antigens like gangliosides (Bowes, Wagner, & Boffey, 2002). This initial difficulty in raising anti-ganglioside antibodies in wild type mice was solved genetically, by knocking out essential enzymes in complex ganglioside biosynthesis (Takamiya et al., 1996). The lack of systemic gangliosides enables the induction of a strong antibody response on inoculation with appropriate lipid species. A range of anti-ganglioside antibodies have now been raised and cloned from these mice which can be injected into wild type mice to induce disease. The next step has been to engineer mice with the same enzymes knocked out but replaced under transcriptional control of promoters that are exclusively active in nerve tissues, either in axons ("NFL rescue") or myelin ("PLP rescue") (Yao et al., 2014). Enzyme function assays show <5% enzyme functionality compared to wild type mice which appears to be sufficient to rescue a healthy phenotype in certain models. The concept behind these models is that anti-ganglioside antibodies can be raised but still have ganglioside targets in the peripheral nerves in order to induce an autoimmune-mediated neuropathy similar to Guillain-Barré Syndrome.

1.5.2   **Multifocal Motor Neuropathy**

Multifocal motor neuropathy (MMN) is a chronic motor neuropathy originally described in 1988 in five patients presenting multifocal weakness and muscular atrophy without sensory involvement or distal motor neuron features typical of motor neuron disease (Parry & Clarke, 1988). Patient's presented gradual or step-wise asymmetric distal weakness associated with specific peripheral nerve territories. Conduction block is often observed in motor nerves but is not required, making diagnosis particularly difficult. Key diagnostic features include lack of muscle wastage or inclusion of sensory loss or symptoms (Pakiam & Parry, 1998). Patchy demyelination is often observed in MMN patients as well as onion bulb formations resulting from repeated demyelination and remyelination. It has not been distinguished however whether disruption of nerve myelin is a primary pathology or secondary to damage to the axon

at the axolemma (Muley & Parry, 2012).

What is acknowledged is that MMN is probably autoimmune-mediated. MMN is associated with the presence of anti-gangliosides in patient serum and immunological therapies are often successful treating the disease. Serum antibodies against GM1, first identified in MMN in 1988, have since been identified in 30-80% of MMN patients by ELISA (Nobile-Orazio, 2001; Pestronk et al., 1988). Why this value is so inconsistent is not known, although centre to centre variability in ELISA procedure has been suggested (van Schaik, Bossuyt, Brand, & Vermeulen, 1995). This variability has prevented a clinical GM1-assay from having much diagnostic value except in rare cases. Less frequently, antibodies against asialo-GM1, GD1a and GM2 have also been identified (Cavanna et al., 1999; Krarup, Stewart, Sumner, Pestronk, & Lipton, 1990; Pestronk et al., 1990). Recently a study using a combinatorial glycoarray to screen for specificity against single and dimeric glycosphingolipid epitopes strongly correlated anti-GM1:GalC complex antibodies with MMN. Anti-GA1 and GM2 antibodies were also detected. Interestingly detection intensities of antibody binding were enhanced by the presence of GM1, GM2 and GA1 in complex with GalC. Sensitivity values were therefore significantly higher for the heterodimer (100%) than for GM1 alone (58%) while specificity values were comparable (Galban-Horcajo et al., 2013). Although further investigation will be necessary this new study may indicate a clinical usefulness for immunoassays for anti-GM1:GalC complex antibodies in MMN diagnosis.

1.5.3 Amyotrophic Lateral Sclerosis, Multiple Sclerosis and Systemic Lupus Erythematosus

Amyotrophic lateral sclerosis (ALS), Multiple Sclerosis and Systemic Lupus Erythematosus (Lupus) are not exclusively neuropathological diseases. ALS is a debilitating neuromuscular disease characterised by the death of upper and lower motor neurons in the central nervous system. Multiple sclerosis is a chronic progressive inflammatory disease that presents with a multitude of autonomic, visual, motor and sensory problems. Lupus is a chronic systemic autoimmune disorder that can affect nearly any organ system, most commonly the

mucocutaneous, musculoskeletal, renal and central nervous systems. The pathogenesis of all of these is thus far unknown although each is thought to contain at least a partial autoimmune element. A wide variety of associated genetic, proteinaceous and infectious risk factors have been established in each and it is in no way the intention here to review their highly complex pathophysiology. These extremely unpleasant disorders are mentioned only because, although not necessarily the cause of their primary pathology, anti-ganglioside antibodies have been associated with all three.

In multiple sclerosis, alongside T-cell autoreactivity for myelin proteins, gangliosides have been repeatedly highlighted as potential autoantigens. Antibody reactivity for GM1 and GM4 and to a lesser extent GM2 was indicated in multiple sclerosis serum samples in 1980 by the lysis of ganglioside containing-vesicles by serum antibodies (Arnon et al., 1980). Anti-GM3 antibodies have since been associated with primary and secondary progressive multiple sclerosis, (Sadatipour, Greer, & Pender, 1998) and increased T-cell reactivity to GM3 and GQ1b with primary progressive multiple sclerosis (Pender et al., 2003). Increased neurological disability has also been correlated with anti-GD2 autoantibodies (Marconi et al., 2006). Evidence of complement deposition in active multiple sclerosis lesions suggests these autoantibodies may be active in multiple sclerosis pathogenesis rather than a secondary feature from the release and circulation of myelin glycosphingolipids (Lucchinetti et al., 2000). In ALS correlations have been observed with higher serum and cerebrospinal fluid titres of autoantibodies against GM1 and asialo-GM1, (Niebroj-Dobosz, Jamrozik, Janik, Hausmanowa-Petrusewicz, & Kwieciński, 1999) GalNAc-GD1a, (Yamazaki et al., 2008) and GM1 and GD1a (Pestronk et al., 1989). Serum antibodies with GM2 and GD2 reactivity have also been identified in a single case of sporadic ALS (Mizutani et al., 2003). The situation is even more complex in Lupus which apparently has more associated autoantibodies than any other human autoimmune disease. These include ganglioside antigens such as asialo-GM1, which correlated with neuropsychiatric manifestations, GM1, GD1a, GD1b and GT1b (Sherer, Gorstein, Fritzler, & Shoenfeld, 2004).

Persistent detection of anti-ganglioside antibodies in autoimmune neuropathies, encompassing differential affinities for heterodimeric complexes, suggests that gangliosides fulfil vital but complex roles in disease pathogenesis, pathology, severity, clinical presentation and/or time course. A vital connection to discern will be between the presence of these autoantibodies and the distribution of very specific ganglioside species and glycan epitopes in different nerve tissues. Large scale profiling has been done before in brain and nervous tissue. However considering the subtly of some of these antibody-glycan interactions, more sensitive, specific profiling methods are necessary. An overview of traditional methodologies and the application of mass spectrometry to ganglioside and lipid profiling will now be covered.

1.6 Lipid Profiling Technologies

1.6.1 Traditional Profiling Methodologies

Lipid profiling, like most profiling of complex mixtures, fundamentally involves three steps; separation, detection and identification. Table 4 describes the main conventional techniques for lipid separation with available avenues of detection/identification and key features for each. All of these require the prior preparation of a purified lipid fraction to remove contaminants. In the study of very low abundance lipids such as gangliosides this is often combined with further steps to enrich the lipid(s) of interest. High performance thin layer chromatography (HPTLC) is one of the most ubiquitous techniques for lipid separation (and preparation). Mixed samples are immobilised on a solid hydrophilic HPTLC plate, often silica, and separated by the wicking of a hydrophobic solvent system. Both solid phase and solvent system must be tailored to the lipids of interest so this method is not appropriate for global analysis. Lipids are separated based on their hydrophobic/hydrophilic characteristics into head-group 'bands' or zones. Optimal HPTLC conditions for ganglioside separation have been investigated previously (Scandroglio et al., 2009). Bands can be detected using various stains and dyes. For gangliosides the sialic acid stain resorcinol, involving the spraying and heating of concentrated hydrochloric acid, is most commonly used (El-Rassi, 2002).

Table 4. Key Characteristics of Conventional Lipid Profiling Techniques.

Separation	Detection	Identification	Key Features
High performance thin layer chromatography	Stains and dyes Immunostaining	Reference standards On/off-plate chemistry Offline MS Immunostaining	HPTLC itself is cheap, easy to set up and run with minimal equipment and training. Versatile and tolerant to contaminants. Compatible with stains and dyes. Not universal. Low resolution and sensitivity. Low automation and reproducibility.
Gas chromatography	Flame ionisation Electron capture Mass spectrometry	Reference standards Offline chemistry Reference standards Offline chemistry Mass spectrometry	Quantitative and versatile. High resolution and sensitivity. Requires chemical separation or modification such as methylesterification masking native structures.
High performance liquid chromatography	UV spectroscopy	Reference standards Offline chemistry	High resolution and sensitivty. Seperates whole underivatised lipids. Expensive to set up and run, requires training.

HPTLC has been applied to profiling many different membrane lipids including phospholipids, sphingolipids, gangliosides and glycerolipids in different tissues, species or diseases with great success. Much of the early profiling of gangliosides in human development was done using HPTLC and ganglioside profiles in the genetically engineered mouse models mentioned earlier are routinely characterised by HPTLC. The method itself is cheap and easy to set up and run without specialist training and many samples may be separated quickly in parallel on a single plate. The chance for contamination is low as a new stationary phase is used each time and the method is relatively tolerant to salts and contaminants. Densitometry measurements have also been used for relative quantitation within datasets (Ando et al., 1978; Muthing, 1998). That said several properties including the targeted nature and poor reproducibility of HPTLC

have limited its usefulness in untargeted lipid studies. The open system means that environmental factors such as temperature and humidity can significantly affect separation. Identification of unknown lipid bands on HPTLC plate is also restricted by the availability of high quality reference standards and sensitive, specific antibodies. No information is obtained on the fatty ester portion from HPTLC without excision of bands of interest, re-extraction and analysis by mass spectrometry. These limitations are increasingly problematic as novel species are described with increasing structural detail, sometimes with very low native abundance.

Gas or gas-liquid chromatography (GC) has also been used for lipid profiling for many years. Samples are vaporised and injected via an inert carrier gas the composition of which is defined by the detector in use. In the gas phase lipids travel through a packed column containing a thin layer of liquid immobilised on an inert packing material of which there are several structures. This column is heated to the mid-point boiling range of the sample ('isothermal') or varied through the separation to maintain this temperature ('temperature program'). Lipids are separated based on their interactions with the gas and liquid phases, which can be tailored to target certain characteristics. A number of different detection and identification methods can be used. Most of these are again dependent on the availability of reference standards to run in parallel limiting the usefulness of GC for global analysis of unknowns. However GC coupled to mass spectrometry has all but replaced other detectors for lipid analysis due to its combined detection and identification capabilities. GC-MS is free from the dependency on standards.

Appropriately set up, GC can be fast, sensitive, high resolution and quantitative. The technique has been used to profile free ceramides from human platelets (Krivit & Hammarström, 1972), ceramide constituents from bovine brain hexosylceramides (Hammarstrom, 1970), and the glycan moieties of several very minor gangliosides (Hirabayashi et al., 1990, 1992; T. Kawai, Kato, Higashi, Kato, & Naiki, 1991). However GC-MS is only suitable for volatile, non-polar molecules. Ceramides must therefore be removed from glycans prior to GC-MS. The loss of this link between ceramide structure, which may have an active role in functionality, and

head-group means that distinct species-specific distributions cannot be studied (Christie, 1989). Furthermore for GC-MS analysis of the glycan moieties themselves chemical treatment is required, such as methanolysis, N-acetylation and trimethylsilylation, resulting in the masking or loss of native modifications. As these may have also profound importance in immunological reactions, GC-MS is not an ideal method for glycosphingolipid profiling when the intact molecule is of interest.

High performance liquid chromatography (HPLC) has in many cases taken over from GC for lipid profiling. Large, thermally labile and polar lipids can all be analysed by HPLC . Samples no longer need to be volatile or chemically modified for vaporisation in the gas phase but are injected in a liquid phase that is often highly compatible with lipid solubility. This makes HPLC a versatile technique for the separation of a wide range of intact lipids. An abundance of column chemistries are available enabling separation tweaked for specific structural features, such as chirality, or whole molecule chemistry. The technique can be fast, highly resolved, and sensitive. The closed system means that external factors have minimal influence on separation while the high level of automation means that reproducibility and robustness are higher than for HPTLC Relative quantitation by HPLC is routine and several techniques for absolute quantification of lipids have been published (Grizard, Sion, Bauchart, & Boucher, 2000; Norlén, Nicander, Lundsjö, Cronholm, & Forslind, 1998; Silversand & Haux, 1997). However the requirement for an automated system means that set up and run costs are high and that HPLC users will require specialist training. Detection methods such as UV spectroscopy cannot distinguish co-eluting species and identifications are still dependent on the availability of reference standards or offline chemistry. One way to solve this is to couple HPLC with mass spectrometry which is popular in lipid analysis. This can distinguish co-eluting species (assuming their mass to charge ratio differs) and identify by accurate mass without standards. A major drawback of this detector is the further high costs associated with setting up and running a mass spectrometer.

1.6.2   Mass Spectrometry; Fundamentals

Mass spectrometry (MS) is an analytical technique that separates gas-phase ions in a vacuum based on their mass (m)-to-charge (z) ratios (m/z). Separated ions are detected and summarised into mass spectral read out of m/z on the x-axis and ion intensity on the y-axis. When interpreted carefully, mass spectra can be used to elucidate chemical formula and identify components in heterogeneous mixtures. Simply put, instrumentation consists of an ion source, a mass analyser and a detector. The ion source generates gas phase ions from molecules in a sample through the addition or removal of a charge. Molecules may be natively charged or have a predisposition to form either positive ($[M+H]^+$, $[M+Na]^+$, etc) or negative ($[M-H]^-$, $[M+Cl]^-$, etc) ions. An analyst must therefore choose which polarity best suits their needs. Gangliosides are traditionally analysed in negative ion mode due to the presence of the sialic acid(s) which carries a negative charge at neutral pH. Separation, or resolution, of ions by m/z occurs under high vacuum in the mass analyser(s) which has an integrated detector. Various configurations are available that combine the ionising capabilities of different sources with one or more mass analysers of diverse resolving power, mass accuracy, sensitivity, scan time and dynamic range. These parameters define the appropriateness of the configuration to different applications and the capabilities of the technique. Soft ionisation techniques and tandem mass spectrometry, which are described in detail in the following paragraphs, have been key developments in applying MS to life sciences.

MS was first applied to glycosphingolipids in answer to the shortcomings of the analytical techniques available at the time. Identification after chromatographic separation was not possible without a large bank of reference standards or fraction collection and traditional offline chemistry. Other limitations included the inability to distinguish co-eluting species and to resolve intramolecular linkage positions and isomeric stereochemistry within the glycan moiety. Proof-of-concept MS analyses were performed in 1969 by several groups who analysed derivatised glycosphingolipids by GC-MS (Karlsson, Samuelsson, & Steen, 1969;

Samuelsson & Samuelsson, 1969; Sweeley & Dawson, 1969). These yielded information on the molecular composition of the sphingolipid, saccharide, sialic acid and the relative amount of fatty acid. GC-MS was soon routinely applied to analysing the sugar sequence, branching patterns, the presence of labile structures, glycosidic linkage sites, and to the conformation of sugar rings. These experiments demonstrated the sensitivity and mass accuracy of the technology establishing MS as a useful tool in early structural elucidation.

1.6.2.1 Tandem Mass Spectrometry and Lipid Dissociation

As mass spectrometry developed it was recognised that fragmentation as a result of high-energy ionisation or post-source decay of metastable ions could provide additional intramolecular data. However this passive fragmentation yielded low, non-specific signals disguised by buffer adducts, contamination and heterodimers. This was solved by the arrangement of high-performance mass analysers in series separated by a cell for active dissociation, termed 'tandem MS' (MSMS) (McLafferty, 1981). MSMS hinges on the induced dissociation of a selected precursor ion after a first round of mass analysis by an external energy source. A second round of analysis yields mass information on product ions pertaining to the precursor ion; careful interpretation can reveal structures within the parent (Figure 10). Employing one or more (MS^n) rounds of ion dissociation allows a multitude of experimental designs including single and multiple reaction monitoring, precursor and product ion scans and constant neutral loss scans.

During early applications analysers were spatially separated by a field free collision cell containing inert gas molecules such as nitrogen or helium. This is known as collision induced dissociation or CID. In 1988 Domon and Costello analysed a number of ceramides and gangliosides structures from pure samples using fast atom bombardment (FAB)-CID MSMS on a multiple sector instrument in positive and negative ion mode (Domon & Costello 1988). They identified conserved degradation patterns in the glycan across multiple samples, in both modes, and defined a novel definition of fragment shorthand (Domon & Costello 1988). Using
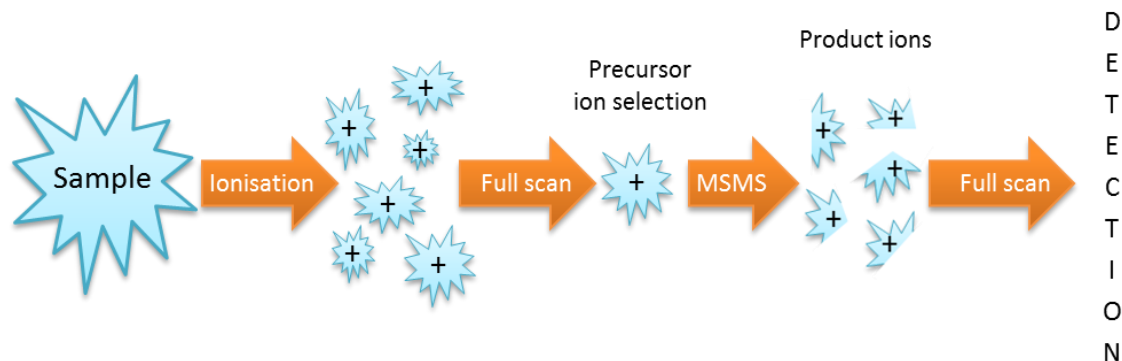
Figure 10. Principles of Tandem Mass Spectrometry. Tandem mass spectrometry enables the active dissociation of a selected precursor m/z of interest that has been detected during an initial full scan. This precursor ion is isolated and fragmented in a collision cell to form product ions. A second full scan then detects the m/z of these product ions generating a spectrum which, with careful interpretation, can reveal structures contained within the precursor ion.

high and low energy CID has revealed different dissociation patterns in derivatised glucocerebrosides enabling identification of both saturation and hydroxyl positions in the ceramides (Duh & Her, 1992). Commercial instruments are now available that employ collision, surface, photon, thermal and electron induced dissociation. Each source can be used to reveal complementary information about bonds and structures.

1.6.2.2 <u>Soft Ionisation; Matrix Assisted Laser Desorption Ionisation</u>

Another key development in the application of MS to life sciences was the development of 'soft' ionisation techniques. Matrix assisted laser desorption/ionisation (MALDI) (Hillenkamp, Karas, Beavis, & Chait, 1991) and electrospray ionisation (ESI) (Fenn, Mann, Meng, Wong, & Whitehouse, 1989) enabled the direct injection of large polar macromolecules into the mass analyser with negligible fragmentation or loss of labile structures. While earlier ionisation techniques such as fast atom bombardment (FAB) have been successfully applied to lipids in the past, the higher energies involved resulted in significant dissociation and loss of signal from the molecular ion. Lipids were often therefore ionised pure, after separation, and recognised as much by their dissociation fingerprint as by their mass. For a detailed description see (Ashcroft, 1997). Briefly described MALDI, illustrated in Figure 11, employs a light
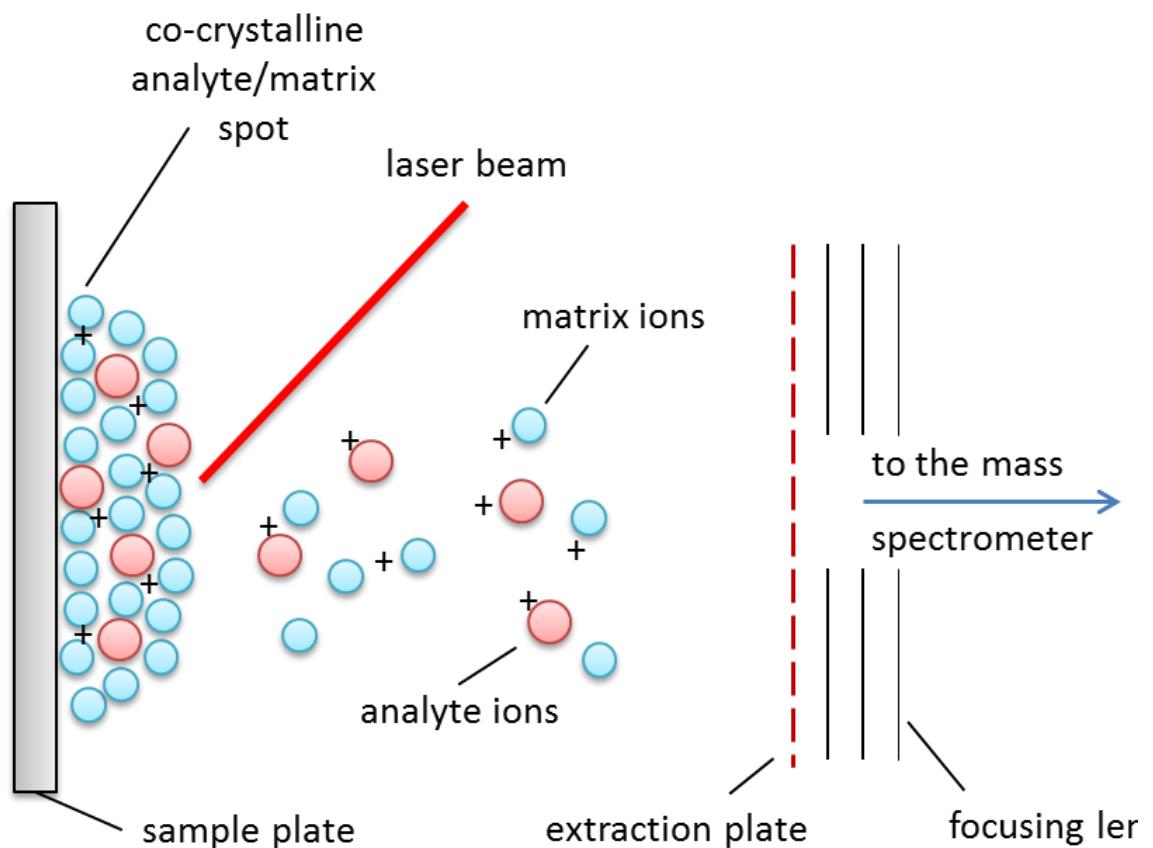
Figure 11. Principles of Matrix Assisted Laser Desorption Ionisation. Analyte is spotted on a sample plate with a light absorbing matrix to co-crystallise. A pulsed laser beam is fired at the spot, desorbing both matrix and analyte molecules in to the gas phase, alongside charges contained within the crystalline structure which transfer onto both matrix and analyte. Positive charges are illustrated; negative can also be generated using different matrices and conditions. The extraction plate then accelerates these ions using an opposing voltage pulse towards the focusing lens which guides them into the mass spectrometer. MALDI is often but not exclusively coupled with time-of-flight (TOF) mass analysers.

absorbing organic matrix co-crystallised with a sample of interest and pulsed laser beam to generate sample ions. Energy from the laser beam causing rapid vibrational excitement of the matrix resulting in ablation of the matrix/sample molecules into the gas phase. The matrix functions to separate (prevent clustering of) the analyte during crystallisation, shield the biomolecules from direct application of the laser energy and absorb and transfer the laser energy, facilitating charge exchange to the analyte. A suitable choice of matrix based on laser, matrix and analyte properties is paramount to successful ionisation. Thus far lipid analysis using MALDI has almost exclusively employed a 377 nm wavelength N_2 laser and UV-absorbing

organic matrices. Several matrices have been trialled for lipid analysis, however 2,3-dihydroxybenzoic acid (DHB) has emerged as most appropriate and commonly cited (Fuchs, SuB, & Schiller, 2010; J Schiller et al., 2004).

While MALDI has been applied to qualitative and quantitative analysis of phospholipids (Harvey, 1995; Petkovic et al., 2001) and sphingolipids (Fujiwaki, Tasaka, & Yamaguchi, 2008; Ma et al., 2007) it has so far been of limited use to ganglioside mixtures. This is due to the easy fragmentation of the labile sialic acid group(s) during MALDI. Chemical modification has been used to stabilise this bond, however as discussed this could mask native modifications in these lipids. There is an emerging field that may increase the usefulness of MALDI for ganglioside analysis; that is the direct combination of HPTLC separation with MALDI-MS detection and identification. First published for peptide analysis in 1995 (Gusev, Vasseur, Proctor, Sharkey, & Hercules, 1995) HPTLC-MALDI-MS involve the direct introduction of the whole HPTLC plate into the MALDI source. The laser is directed towards bands that have been pre-located by staining of parallel reference lanes or using MALDI-compatible dyes such as primulin. Spectra are collected and bands can be identified by mass. This is discussed further in Chapter 4.

TLC-MALDI-MS applied to glycosphingolipids was first published by Guittard, Hronowski and Costello (Guittard, Hronowski, & Costello, 1999). Native GSLs were developed on TLC plates, heat transferred to polymer membranes and analysed by MALDI-TOF MS with a detection limit of 5-50 pmols. The uneven surface of the membrane limited resolution and mass accuracy, and was only partially compensated for using delayed extraction. This was addressed by Dreisewerd *et al.* using an orthogonal TOF (oTOF) analyser 'decoupled' from the MALDI source to analyse the composition of a native GM3 ganglioside mixture (Dreisewerd et al., 2005). Mass accuracy and resolution was similar to regular MALDI preparations. Other groups have employed fourier transform ion cyclotron resonance (FTICR) (VB Ivleva, Elkin, & Budnik, 2004) and quadrupole ion trap (QIT)-TOF (Nakamura, Suzuki, Goto-Inoue, Yoshida-Noro, & Suzuki, 2006) mass spectrometers to eliminate mass accuracy and resolution problems associated

with the uneven surface of TLC plates. However the uneven surface of membranes and TLC plates continues to limit resolution and mass accuracy on the more common 'axial' TOF analyser configuration. That said the preparative separation of different mono-, di- and trisialylated gangliosides means that sialic acid fragmentation is no longer limiting and the sensitivity, specificity and/or simplicity of HPTLC-MS is often higher than traditional detection and identification methods.

1.6.2.3 <u>Soft Ionisation; Electrospray Ionisation</u>

Electrospray ionisation (Dole, 1968) now dominates lipid research as the MS ionisation method of choice. It is capable of the introduction of intact charged lipids including thermally labile and non-volatile species into a mass analyser with negligible fragmentation. The volatile organic solvents used to solvate lipids are well-matched with ESI. With its compatibility with online HPLC, which will be discussed later, ESI-MS is now one of the most comprehensive tools in lipid analysis. The process is summarised in Figure 12. Samples are introduced in solution with a steady flow rate along the electrospray needle, which receives a high voltage in respect to the counter electrode. This forces the nebulisation of charged droplets from the tip with the same charge polarity as the electrospray needle. These are electrically repulsed towards the source sampling cone on the counter electrode, sometimes aided by a sheathing gas.

Although the exact mechanism is not known it is thought that the solvent evaporates throughout this trajectory, increasing charge density on the droplets (assisted by a heated capillary or auxillary gas; so-called heated-ESI or HESI) until electrostatic repulsion overcomes surface tension and they experience coulombic fission resulting in smaller droplets. These undergo similar rounds of evaporation and fission until the charge is transferred directly to the analyte molecules. These are then introduced into the mass analyser as charged ions (Dewald, 1999; Griffiths, Jonsson, Liu, Rai, & Wang, 2001). This model is based upon Iribarne and Thompson's ion evaporation theory (Iribarne & Thompson, 1976). ESI can be used in positive or negative ion mode to generate positive and negative ions and adducts with single and
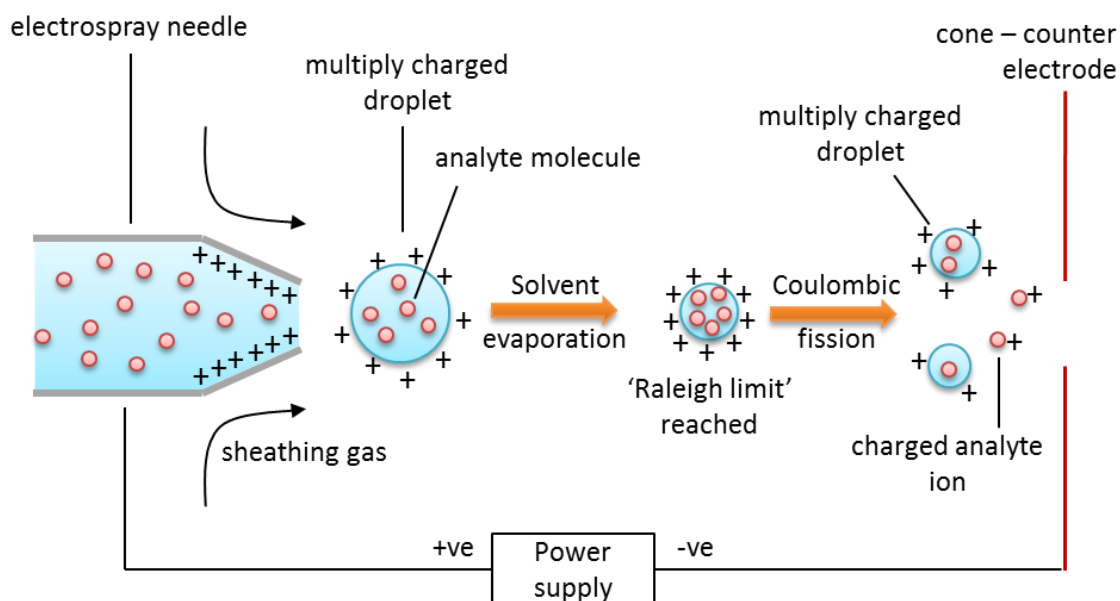
Figure 12. Principles of Electrospray Ionisation. Based upon Ion Evaporation theory (Iribane & Thompson, 1976).Samples are introduced in solution along a fine electrospray needle at a steady flow rate. The needle receives a high voltage in respect to the counter electrode, producing a spray of charged droplets of the same polarity as the tip. These are repulsed towards the counter electrode, sometimes aided by an inert sheathing gas. As the solvent evaporates the charge density on the surface increases until the Raleigh limit is reached. Smaller charged droplets are formed and undergo rounds of solvent evaporation until charges are transferred onto the analyte molecules to form ions which are introduced into the mass spectrometer.

multiple charges. Although not relevant to the lipid mass range the production of these multiply charged ions is another advantage of ESI as it greatly increases the upper mass limit in biomolecular analysis.

As mentioned, ESI is extremely versatile in lipid analysis. The technique has been applied to the ionisation of many important lipid groups including but not limited to; phospholipids, (Koivusalo, Haimi, Heikinheimo, Kostiainen, & Somerharju, 2001) sterols, (Liebisch et al., 2006) sphingolipids, (M. Gu, Kerwin, Watts, & Aebersold, 1997; Merrill, Sullards, Allegood, Kelly, & Wang, 2005) and non-volatiles including free fatty acids and eicosanoids (R. C. Murphy, Fiedler, & Hevko, 2001). For a well written and comprehensive review on phospholipid analysis see (Pulfer & Murphy, 2003). Hsu et al. have also written a series of clear articles on ESI and MSMS analysis of lipids including triacylglycerols, (F. F. Hsu & Turk, 1999) phospholipids, (F. Hsu & Turk, 2000; F.-F. Hsu & Turk, 2003, 2009) cardiolipins, (F.-F. Hsu et al., 2005) sulfatides,

(F.-F. Hsu & Turk, 2004) glycosphingolipids as lithiated adducts (F. F. Hsu & Turk, 2001) and sphingomyelins (F. F. Hsu & Turk, 2000). Several publications have also focused on the methodological aspects of electrospray ionisation of gangliosides (Ii, Ohashi, & Nagai, 1995; Tsui, Chen, Thomas, Samuel, & Cui, 2005). Unlike MALDI, ESI enables the introduction of intact, underivatised gangliosides without fragmentation of the labile sialic acids and maintaining native modifications such as O-acetylations on the sialic acid.

It must be mentioned that the ionisation efficiency of ESI is closely linked to the electrical propensity of an analyte to lose or gain a charge in an electrical field. For acidic and basic lipids with anionic or cationic groups that carry an inherent charge at pH 7, ionisation efficiency is higher than for neutral lipids such as triacylglycerols. Equally lipids without an inherent charge but carrying a dipole potential can be induced to form charged adducts relatively easily. Fortunately this accounts for many of the membrane lipids which are polar by nature. However it is important to keep this in mind when referring to MS peak intensity as a measure of quantitation between lipid species that differ significantly in their physicochemical properties.

1.6.3   Mass Spectrometry and Lipidomics

Lipidomics refers to the systems level study of the 'lipidome', the total lipids of a given system, in order to understand the fluctuations and interactions of the pathways and networks involved. This can refer to mapping the lipidome of specific systems (organism, tissue, cell) or detecting changes in the lipidome in response to certain stimuli (heavy exercise, pathogenic attack, heat stress). Lipidomics is technically contained within the field of metabolomics, lipids forming one the major molecular groups of metabolic systems. However lipidomics shifts the focus solely onto the thousands of different lipid components. Although lipidomics can and does employ traditional lab-based techniques, microscopy and spectroscopies such as nuclear magnetic resonance (NMR), it has benefitted immensely from the complementary application of mass spectrometry. The historical benefits of MS to lipid research have already been

discussed; lipidomics takes advantage of these to comprehensively separate, detect and identify lipids from extremely complex extracts with minimal preparation. Bioinformatics is usually an essential part of lipidomics in order to make sense of the data obtained and integrate it into previously existing systems knowledge.

There are two main paradigms in current lipidomic mass spectrometry pertaining to the method of separation. These are shotgun lipidomics, which employs an interesting ESI intrasource separation invented specifically for this purpose, and HPLC-MS, which uses an online HPLC system directly attached to the ESI source for lipid separation. Thus far lipidomics is rarely performed by MALDI-MS (although HPTLC-MALDI-MS may open the technique up for ganglioside lipidomics). For a short paper on why this may be, see (Jurgen Schiller et al., 2007). Shotgun lipidomics has been developed over the previous decade by Xiaolin Han and Richard Gross. It is an ESI-MS method that employs the differing physical and chemical properties of lipids to facilitate high-throughput, direct injection lipidomic analysis without previous (online) chromatographic separation. Several platforms have emerged that enable rapid fingerprinting of crude lipid mixtures with over 90% coverage of lipid mass. For a more detailed explanation see (Xianlin Han & Gross, 2005). While shotgun lipidomics is extremely quick for the analysis of most major species, it is less suitable for minor species, or those of particularly unique physicochemical properties such as gangliosides. Indeed there are few publications on shotgun lipidomics even mentioning hexosylceramides of more than one saccharide; for an example see Kjellberg *et al.* 2014.

High performance liquid chromatography coupled to mass spectrometry (HPLC-MS) is now ubiquitously used in lipidomics. It is one of few methods truly capable of near global separation and analysis of lipid mixtures. Due to the compatibility of HPLC with direct coupling to an ESI source, this set up is most common. HPLC enables a first dimension of separation by physicochemical characteristics before the elutate is directly introduced at a constant flow rate into the mass spectrometer for a second degree of separation by m/z. This enables extremely

complex mixtures to be analysed with minimal preparation, although HPLC-MS is more sensitive to salts and contamination than for example HPTLC or MALDI-MS. Chromatographic retention times supply an additional level of identification to accurate mass. Tandem mass spectrometry is often applied throughout an HPLC-MS run for another additional layer of information although instruments with a high scan rate are required for this. For lipids MSMS acquisition is most commonly data dependent; precursor ions are selected based on prerequisite conditions such as the *n* most intense peaks from the full scan.

One of the beneficial yet problematic features of HPLC-MSMS is the amount of data produced in a single run. Bioinformatics is an essential part of the workflow both to extract the maximum amount of meaningful information from datasets and to integrate this with other systems data from alternate sources. This is currently an area of intense development for lipidomics where tools are not yet up to the standards of those available for genomics or proteomics. Classical tools designed for the peak picking and building chromatograms in metabolomics datasets, such as XCMS, mzMine and mzMatch, (Pluskal, Castillo, Villar-Briones, & Oresic, 2010; Scheltema, Jankevics, Jansen, Swertz, & Breitling, 2011; Smith, Want, O'Maille, Abagyan, & Siuzdak, 2006) can be applied here. These supply a mass list that can be manually fed into databases such as the LipidMAPS structural database (LMSD) or LipidBank in Japan. Alternatively metabolomic databases such as the Scripps METLIN: metabolite and tandem MS database or Human Metabolome Database (Wishart et al., 2007) can be used although results will contain both lipid and metabolite identifications. This does not make the most of the intensity levels, also provided by the software, which may be used to track comparative changes between datasets. Several new tools such as LipidXplorer (Herzog et al., 2012) and LipidBlast (Kind et al., 2013) have been released that combine peak picking, chromatogram building, inbuilt integration with databases and informatics tools for comparative profiling.

The applications of HPLC-MS lipidomics are too numerous to discuss here. Some excellent review articles have been published on lipidomics in health, disease and nutrition, (S. A.

Murphy & Nicolaou, 2013) biomarker discovery, (Hu et al., 2009) and brain injuries and disease (Adibhatla, Hatcher, & Dempsey, 2006). One of the positive features of these papers is that lipidomics is usually performed in a highly collaborative environment. Samples are often sourced from the clinical environment allowing the interpretation of results to answer useful biological questions. Translatable results may take some time to emerge, and require the future combination of targeted classical techniques, clinical data and further mass spectrometry. Still lipidomics has the capacity to contribute a vast amount to the molecular understanding of many human conditions. An noteworthy characteristic however is that lipidomic papers rarely mention gangliosides. Extraction technique are widely used that segregate lipids away from contamination in two-phase systems based on their hydrophobic nature. This however results in the loss of the particularly hydrophilic lipids such as the gangliosides from the sample.

1.6.4 Imaging Mass Spectrometry in Tissue Sections

Imaging mass spectrometry (IMS) is the final mass spectrometry technology to be discussed here. This technique aims to combine the advantages of mass spectrometry with traditional imaging in order to visualise the spatial distribution of molecules in tissue sections. Although IMS has been around for some time, it has also recently benefitted immensely in the biological sciences from the development of soft ionisation sources such as MALDI. Other ionisation sources currently used or under development for biological IMS include secondary ion mass spectrometry (SIMS), desorption electrospray ionisation (DESI), liquid extraction surface analysis (LESA) and laser ablation electrospray ionisation (LAESI). The key features of each relating to IMS such as spatial resolution are summarised in Table 5.

The technique involves the introduction of carefully prepared whole tissue sections, typically between 10-100 µm, into the ionisation source on specially adapted platforms. The ion source, typically a laser or ion beam, is then moved in an automated and stepwise manner across the section, collecting spectra from each 'pixel'. Each spectrum contains molecular ions and

Table 5. Key Features of IMS-Compatible Ion Sources.

Ion source	Spatial resolution	Environment	Sample preparation	Typical mass range
Matrix assisted laser desorption ionisation	5 μm	High vacuum	Cryosectioning, matrix	100-500,000
Desorption electro-spray ionisation	>150 μm	Ambient	None	100-500,000
Laser ablation electro-spray ionisation	300-400 μm	Ambient	Water rich targets needed	100-500,000
Liquid extraction surface analysis	1 mm	Ambient	None	100-500,000
Secondary ion mass spectrometry	~1 μm	High vacuum	Cryosectioning, can use gold coating or matrix	0-700

adducts separated and identified by their m/z as usual in mass spectrometry. The novelty of IMS is that the intensity of each ion is obtained at recorded points across the tissue and can be combined to form an ion 'map'. Tissue samples are not homogenised and molecules of interest do not have to be extracted prior to MS analysis. Because, with careful preparation, anatomical features are maintained within the tissue, the enrichment or localisation of ions to particular areas can be observed in specially designed software. IMS is also compatible with traditional histology or immunostaining, either on the same or immediately adjacent tissue sections, enabling conventional images to be overlaid with these ions maps to confirm features and/or identifications. IMS with MSMS has also been used to fragment and confirm identifications.

IMS has been applied to a host of biomolecules. These include proteins and peptides, being compatible with on-tissue tryptic digestion prior to analysis, drug distribution and metabolism for PKPD studies and metabolites including lipids. Careful sample preparation is paramount to a successful experiment. Tissue collection must be carefully thought through to avoid deformation or delocalisation and degradation of molecules of interest, which has been shown to occur within minutes of dissection (Goodwin, Dungworth, Cobb, & Pitt, 2008). These should be stored at ultralow temperatures (<-70 °C) and avoid repeated cycles of thawing and freezing. Tissue sectioning is another area where thought is needed as traditional embedding

and mounting media contain polymers that can interfere with mass spectrometry (Schwartz, Reyzer, & Caprioli, 2003). This is usually performed in a cryomicrotome ensuring the tissue is kept at -20 °C or below. Section thickness is also something that will vary depending upon the tissue and ionisation method. Various preparative and derivatisation methods can be used such as washing to avoid contaminants. However these also increase the opportunity for lateral diffusion. With MALDI, as with regular MALDI-MS, the choice of matrix is important. Application is also crucial for extracting and co-crystallising analytes of interest with homogenous crystal sizes while limiting lateral diffusion. For a more comprehensive review of the traps and pitfalls of IMS sample preparation refer to (Goodwin, 2012).

While IMS is still in the early stages of development for lipid imaging (methodological optimisations accompany most studies and consistent methods have not yet been established) some interesting data on lipid distribution has been collected. MALDI-IMS has been used to map certain lipids to hypoxic, necrotic and viable regions in breast tumour xenograft models (Chughtai et al, 2012) and show abnormal ceramide metabolism in human skin in Dorfman-Chanarin syndrome, in which the skins barrier function is affected (Goto-Inoue et al., 2012). Principal component analysis (PCA) has been useful for determining hidden variables in IMS datasets, distinguishing white matter from grey matter, and grey matter from the hippocampus and cerebellar cortex based on principal components in MALDI-IMS data from rat brain. Meanwhile DESI-IMS has been used to identify potential phospholipid biomarkers distinguishing benign and invasive ductal carcinomas, and healthy tissue based on distribution (Wiseman et al, 2005), LAESI-IMS to simultaneously image metabolites and lipids in rat brain tissue (Nemes, Woods, & Vertes, 2010) and imaging-SIMS to image cholesterol and PC based on characteristic fragments in single cells (D. Touboul, Laprévote, & Brunelle, 2011). SIMS is currently the only IMS technique capable of cellular resolution but sacrifices the capability to ionise whole molecular ions. All IMS techniques however exhibit a trade-off between sensitivity and spatial resolution (Benabdellah et al., 2010). IMS in the context of ganglioside imaging is discussed further in Chapter 8.

1.7 <u>Conclusions</u>

Lipids are increasingly important molecules in the understanding of living biological systems. In a reflection of their vast number of functions and activities, a large number of different lipid structures and subtypes have and continue to be described. Of these the membrane lipids, and especially large acidic gangliosides, are a particularly diverse and dynamic group with essential roles in cellular life. The fundamental roles of these gangliosides, as well as other glycosphingolipids such as hexosylceramides and sulfatides, have been demonstrated repeatedly, especially in the neurological system where they're enriched, by cell studies, tissue culture, genetically engineered animal models and the study of human disease biology. Of particular and growing interest is the subject of anti-ganglioside antibodies in neuropathies with a proven or suspected autoimmune basis. These range from the principally understood, such as Guillain-Barré Syndrome and Multifocal Motor Neuropathy, where auto antibodies remain after infection by pathogens carrying ganglioside mimics and trigger damage where the targets are most enriched, to the largely enigmatic, such as Multiple Sclerosis, where antibodies are detected without knowing whether they are part of the multifaceted primary pathology of the disease or what roles they may fulfil.

It is here where novel technology, or the novel application of old technology, will make a significant contribution. Understanding the roles of gangliosides and anti-ganglioside interactions will be closely linked to understanding the distribution of very specific gangliosides, glycan groups and modifications, within and around affected tissues, with high sensitivity and specificity. While traditional profiling techniques have been adequate thus far for separating and identifying the major ganglioside head-groups, it is becoming increasingly clear that the fatty ester moiety, or extremely minor modifications, may have significant influence on their activity. Mass spectrometry is an analytical technique that is well established in the structural description of lipid structures, and identification of unknown lipids through offline coupling with traditional profiling methods. Developments in hardware have

greatly facilitated the use of MS in the life and lipid sciences; namely the development of softer ionisation sources that can introduce whole non-volatile lipids into the MS, and tandem mass spectrometry, which enables the dissociation of whole ions and recognition of internal structures such as the loss of a head-group or sugar. Online coupling of mass spectrometry to lipid profiling methods such as high performance thin layer or liquid chromatography, as well as the reduced requirement for reference standards through combined detection and identification by mass, has increased the relevancy of MS even further.

However while MS is now a regular feature in many lipids studies, the group we are most interested in, the gangliosides, are often excluded from large scale lipid profiling. This is for several reasons including their very low native abundance leading to signal suppression by more abundant lipids, their large mass, odd chemistry (acidic, polar), and the presence of multiple labile sugars, which make them difficult to include in regular lipid studies. It appears that all but the predominant species are also excluded from most lipid databases.

1.7.1   Aims

The aim of this thesis is to develop and apply methods of chromatography and mass spectrometry analysis to gangliosides and other glycosphingolipids. Once developed, these techniques can be applied to useful biological questions relating to glycosphingolipid profiles in various tissues, and to understanding changes in metabolism in response to genetic alterations. In the first instance this will involve traditional high performance thin layer chromatography that is already well optimised for ganglioside separation. This will be coupled however to a novel MS method for detecting and identifying separated lipid bands. This direct coupling will be simplified compared to current reports of similar techniques and optimised to create a functional workflow for sample preparation and analysis. As much of the process as possible will be automated to maximise reproducibility and all equipment used for this technique will be commercially available and un-modified.

A second method will be developed for separating, detecting and identifying ganglioside using

high performance liquid chromatography (HPLC) combined with online detection on an LTQ orbitrap mass spectrometer capable of accurate mass detection. Data dependent dissociation will be adapted to gain additional information from structural dissociations. Although well-established in the field of lipidomics HPLC of gangliosides is rarely included in otherwise comprehensive studies. The few published methods specifically for ganglioside separation report different conditions, solvents and variable result qualities. HPLC conditions including solvents and phase will therefore be optimised first using commercial standards. Mass spectrometry settings will be adapted that extract maximum information from these separations. Because in-depth ganglioside dissociation has not been fully investigated since initial description by FAB-MSMS, this will be investigated on this instrumental setup using all available lipids standards; ganglioside and other groups. Once product ion spectra have been collected and described they can be utilised to aid ganglioside identification in complex unknown mixtures from biological sources.

Once optimised, the above methods can be applied to answering biological questions on ganglioside metabolism. This will initially involve their application to what might be considered a proof-of-principle cohort. HPTLC-MS and HPLC-MS will be utilised to confirm the ganglioside profiles in wild type mice and a genetically modified knockout, GalNAcT -/-, the profiles of both of which are published. If both methods can be used to accurately profile gangliosides they will be utilised to describe the ganglioside phenotypes of several novel mouse models of Guillain-Barré Syndrome that have not previously undergone molecular description. It is important for the relevancy of these models to discover whether or not synthesis of complex gangliosides occurs in the nervous tissue of these mice and, if so, to what degree this resembles ganglioside metabolism in the wild type.

A second study will investigate ganglioside profiles in motor and sensory nerves from mice. In GBS and other autoimmune diseases, and the associated animal models, antibodies show preference for either sensory or motor nerves, although it is thought that ganglioside

distribution is similar in both. One of the principle motivations of this project is to harness the high sensitivity of mass spectrometry to ganglioside analysis. Assuming this sensitivity is maintained, the more sensitive method will be applied to analysing nerves in more detail than previously possible. Novel or low abundance modifications may be observed that are not detected or separated by traditional HPTLC and staining that may shed light on antibody propensity.

A final aim is to assess the applicability of imaging mass spectrometry (IMS), a relatively young technology, to ganglioside analysis in tissue sections. IMS combines the specificity and multiplicity of mass spectrometry with the spatial resolution of imaging. There is however a trade-off between sensitivity and resolution. Considering the low abundance gangliosides it will be investigated whether IMS techniques can detect these lipids outside of the brain. Matrix assisted laser desorption ionisation-IMS, optimised in brain tissue sections where gangliosides have been detected before, will be used to investigate gangliosides in the spinal cord. Sections from wild type and GalNAcT -/- mice can be used to confirm the method before sections from a rescue mouse will be imaged for the presence of complex gangliosides. High resolution secondary ion imaging mass spectrometry will also be applied to peripheral nerve cross sections in response to observations made during immunohistochemistry investigations in peripheral nerves that are described in detail in Chapter 7.

The overall aim of this thesis is to adapt mass spectrometry analysis, in various forms, specifically to ganglioside profiling and to demonstrate the benefits of these methods in studies of biological interest to autoimmune neuropathological diseases.

Chapter 2. Materials and Methods

2.1 Reagents, Lipid Shorthand and Suppliers

All chemicals and solvents were obtained from Sigma Aldrich (UK) at analytical (lipid extractions and cleaning) or HPLC grade (for HPLC and mass spectrometry analysis). Lipid standards (phospholipids – glycerophosphocholine (PC), glycerophosphoethanolamine (PE), glycerophosphoglycerol (PG), glycerophosphoserine (PS), cardiolipin (CL); sphingolipids – ceramide (cer), galactocerebrosides (galC), sulfatide (sulf), sphingomyelin (SM), sphingosine (SS), gangliosides aGM1, GM1, GM2, GM3, GD1a, GD1b, GD3, GT1b, GQ1b; glycerolipids – monogalactosyldiacylglycerol (MGDG), digalactosyldiacylglycerol (DGDG) and sterols – cholesterol (chol) were obtained from Avanti Polar Lipids, Inc. (Alabama, USA), Sigma Aldrich (UK) or Enzo Life Sciences (UK). Commercial ganglioside extract (CGE) was obtained from Avanti Polar Lipids (Alabama, USA). Lipid stocks were stored at 10 mg/ml or 1 mg/ml in 2:1 chloroform:methanol at -80 ˚C. Working aliquots were stored at -20 ˚C for no more than 2 months. All lipid stocks were stored in glass vials. All lipid preparation was done in designated glassware and glass Hamilton syringes.

2.2 Recipes

Primulin (anthocyanin) 0.05% in 1:4 acetonitrile (ACN) for application.

0.25 g primulin reagent Sigma Aldrich (UK)

40 ml acetone

10 ml dH$_2$O

Theoretical Upper Phase (Folch, Lees, & Sloane Stanley, 1957)

30 ml chloroform

480 ml methanol

430 H$_2$O (HPLC grade)

Thin Layer Chromatography (TLC) Solvent (Scandroglio et al., 2009)

50 ml chloroform

42 ml methanol

11 ml 0.2% aq. calcium chloride

Weak Anion Exchange Binding Buffer A (single extract)

45 ml Chloroform

90 ml methanol

12 ml dH$_2$O

Weak Anion Exchnage Binding Buffer B (single extract)

45 ml Chloroform

90 ml methanol

12 ml 0.8M aq. sodium acetate

2.3 Preparation of Biological Samples

Brain and central and peripheral nerves were dissected for lipid extraction or tissue sectioning from wild type, GalNAc transferase knockout mice or various 'rescue' models where the GalNAc transferase gene had been placed under the control promoters that were active in specific nerve tissues. For more information on the generation and validation of these mice see (Yao et al., 2014).

2.3.1 Dissection of Brain and Nerves

Mice were killed by a rising concentration of CO_2 in accordance with UK Home Office guidelines then pinned in a supine position. For **brain dissections** the spine was severed at the neck and the skin reflected from snout to shoulder to expose the skull. The skull was removed and the brain cut away from the olfactory tissue, optical nerve and spinal nerve bundle. The brain was then removed and snap-frozen dry on dry ice and ethanol. For nerve and spinal cord dissections the rib cage was opened and the vascular system perfused with saline to drain blood. For **peripheral nerve dissections** the skin was reflected from feet to mid-back. Nerves (sciatic, saphenous) were identified and separated from the surrounding muscle then cut away from the spine, removed and placed on dry ice for extractions. For **spinal cord dissections** skin was reflected from snout to tail. Incisions were made across the base of the skull and between the shoulder blades exposing the vertebrae which were cleared of tissue. The cord was fully

exposed by breaking each vertebra then cut at the top and bottom and placed on dry ice. **Root ganglia** were dissected by Jen Barrie, an experienced technician. Spinal cord was exposed and sensory and motor ganglions defined by position, pooled from single mice into glass vials and lipid extractions performed immediately. For **imaging mass spectrometry** nerves and spinal cord were embedded in 10% gelatine solution which was then frozen in iso-pentane cooled in liquid nitrogen and stored at -80 ˚C. Gelatine was used instead of a more common embedding medium in order to avoid contamination of the tissue sections with stabilizing polymers.

2.3.2 Lipid Extraction

For full lipid extractions, tissue samples were weighed and placed in methanol-cleaned glass tubes with 1 ml 1:1 chloroform/methanol (v/v) for each 10 mg wet tissue (minimum 5 ml for tissues weighing less than 50 mg). Tissues were homogenised using an Ultra-turrax homogeniser (Janke & Kunkel, Staufen, Germany) for 1 min then incubated, sealed, at 35 ˚C overnight with agitation. Tissue debris was pelleted by centrifugation at 1430 xg for 10 minutes. The supernatant was collected and dried under a stream of nitrogen at 35 ˚C . These samples could be stored at 4 ˚C for up to two weeks.

2.3.3 Ganglioside Enrichment

Gangliosides comprise only 10-12% of the total lipid content of neuronal membranes (Posse de Chaves & Sipione, 2010). To minimise suppression or interference by highly abundant lipids steps were taken to enrich gangliosides in tissue extracts. Several processes were used throughout this work, as defined in each chapter, modified from those employed by (Koichi Furukawa et al., 1985). Where a specific process has not been defined a full enrichment (phase partitioning, solid phase extraction, weak anion exchange chromatography, solid phase desalting) was used.

2.3.3.1 Phase Partitioning

Phase partitioning uses the immiscibility of chloroform in solutions of over 5.5% water to

create a biphasic system partitioning more hydrophilic lipids such acidic polar glycolipids away from smaller, more hydrophobic lipids. This was done according to Folch *et al.* (Folch, Arsove, & Meath, 1951) Briefly, dried lipid extracts were re-suspended in 8 ml 2:1 chloroform/methanol (v/v). To this 2 ml dH_2O was added to make up a final 8:4:3 ratios of chloroform/methanol/dH_2O and vortexed to form an emulsion. Phases were separated by centrifugation. The upper (aqueous) phase was collected in a fresh glass vial. The lower phase was washed with 4 ml theoretical upper phase, vortexed and centrifuged. The upper phase was again collected and combined with the previous fraction and the lower phase discarded. This was then evaporated to dryness under a stream of nitrogen at 35 ˚C .

2.3.3.2 **Solid Phase Extraction**

Solid phase extraction using C18 cartridges was used to remove salts from lipid extracts as originally described by (Williams & McCluer, 1980). Briefly Sep-Pak C18 plus light cartridges (Waters, UK) were equilibrated in methanol, 2:1 chloroform/methanol (v/v) and theoretical upper phase. Samples were re-suspended in theoretical upper phase and applied to the cartridge. To remove salts, 10 ml dH_2O was applied to the column. Lipids were then eluted in methanol and 2:1 chloroform/methanol (v/v). Eluent was collected and dried under nitrogen.

2.3.3.3 **Weak Anion Exchange Chromatography**

Weak anion exchange chromatography was used to separate acidic lipids from neutral. DEAE sephadex A-50 (Sigma-Aldrich, UK), 1g per 30 ml binding buffer A, was equilibrated for 1 hour prior to packing gravity glass chromatography columns with 20 ml (equivalent of 0.66g) of the slurry. This was further equilibrated in-column with 20 ml binding buffer A. Dried lipids were re-suspended in 10 ml (nerve extract) or 20 ml (brain extract) of binding buffer A. This was applied to the column then washed with 30 ml binding buffer A to remove neutral lipids. Acidic lipids were eluted in 30 ml binding buffer B. The eluent was collected, dried under nitrogen at 35 ˚C and desalted using solid phase extraction as before.

2.3.4   Tissue Sectioning for Imaging Mass Spectrometry

Proper sample handling and preparation are essential to maintain the integrity of tissue and localisation of metabolites for imaging mass spectrometry (Schwartz et al., 2003). During removal the utmost care was taken not to deform the native shape the brains and nerves which were, where necessary, embedded in gelatine rather than more popular matrices. Samples were mounted on cryomicrotome platforms using water. Sections of 10 μm were cut at -22 ˚C and manually thaw-mounted (using an artist's brush to handle tissue sections) onto glass slides equilibrated at -22 ˚C. Indium-tin oxide (ITO)-coated glass slides, 75 x 25 mm (Bruker, UK) and 25 x 50 mm (Delta Technologies, CO, USA) were used for MALDI-imaging and imaging-SIMS respectively. Slides were then stored at -80 ˚C.

2.4 High Performance Thin Layer Chromatography

Aluminium backed high performance thin layer chromatography (HPTLC) silica gel 60 plates or HPTLC LiChrospher® Silica gel 60 plates (Merck, NJ, USA), 10 x 20 cm, were activated at 100 ˚C for 60 min before use. The HPTLC tank was equilibrated with TLC solvent for two hours using filter paper to saturate the environment. Samples were printed using an Automatic TLC Sampler 4 (ATS4) (CAMAG, Switzerland) in 1 cm bands (referred to as 'lanes' after chromatography) placed 2 cm above the bottom edge to avoid contact with solvent. These were placed in the HPTLC tank which was resealed and separations performed for 45 minutes (LiChrospher) or 90 minutes (regular). For primulin staining HPTLC plates were removed and dried then sprayed with an excess of 0.05 % primulin. After drying images were visualised using a handheld UV lamp (365 nm) and captured on a modified G:box (Syngene, UK) with two overhead black lamps and optimised exposure times.

Initial optimisation of HPTLC-IMS methodology employed separations of 10 μl of a 1:1 w/w mix of GM1, GM2, GM3, GD1a, GD1b and GT1b, 2.5 mg/ml each or commercial ganglioside extract at 1 mg/ml spiked with GM3 and GT1b at 0.1 mg/ml each. For biological investigations volumes were optimised but normalised between samples by initial wet tissue weight so that

relative comparisons could be made. Lanes of 10 µl commercial ganglioside extract at 1 mg/ml were included on each plate as a chromatography quality check. For imaging mass spectrometry experiments, lanes of sample were run simultaneously on the same plate for staining and for matrix preparation.

2.5 High Performance Liquid Chromatography

2.5.1 Chapter Specific Sample Preparations

2.5.1.1 Fractions for HPLC MS Using a Ternary Gradient (4.2.1)

Seven fractions (1-7) were prepared containing two or three lipids of different biochemical character (acidic phospholipid, acidic sphingolipids, neutral) at 0.05 mM each in methanol for analysis by high performance thin layer chromatography (HPLC) and MS. The components of fraction 1-7 are described in Table 6 with molecular mass of the most abundant ions according to the manufacturers, concentrations and dilution volumes.

2.5.1.2 Preparing Lipid Stocks for HPLC-MS Analyses (4.2.2, 4.2.3)

Stocks were prepared in 100% methanol (HPLC grade) to 10 µM in glass vials with 300 µl glass inserts and sealed with PTFE caps (both Chromcol, UK). Commercial ganglioside extract was prepared at 0.1 mg/ml. Individual lipid stocks were prepared at 10 µM unless specified. Brain extracts were diluted to the equivalent of 10 µg wet tissue weight per ml solvent. Motor and sensory nerve extracts were diluted to the equivalent of 0.045 mg wet tissue per ml solvent. Dilution solvents methanol, 70% methanol and 100% and 70% isopropanol were compared early on and were found to make little difference to peak intensities or retention times. Methanol was used for all subsequent preparations for ease of handling and solubility issues with other solvents. Once prepared, samples were kept on ice and vortexed immediately prior to placement on the autosampler.

Table 6. Fraction Composition and Stock Dilution Factors for Initial HPLC Method Development.

Fraction		Polarity	Predominant ion*	Stock Conc. (mg/ml)	Stock Conc. (mM)	Dilution Vol. (ul)	Final Vol. (ml)	Final Conc. (mM)	Final Conc.(mg/ml)
1	Ceramide	Neutral	565.5	1	1.77	2.83	0.1	0.05	0.028
	Phosphoserine	Acidic	747.5	1	1.34	3.74	0.1	0.05	0.037
	Ganglioside GD1a	Acidic	1836.97	1	0.54	9.18	0.1	0.05	0.092
2	Cholesterol	Neutral	386.65	1	2.59	3.87	0.1	0.1	0.039
	Phosphocholine	Neutral	746.56	1	1.34	3.73	0.1	0.05	0.037
	Ganglioside GD1b	Acidic	1836.97	1	0.54	9.18	0.1	0.05	0.092
3	Phosphoglycerol	Acidic	734.5	1	1.36	3.67	0.1	0.05	0.037
	Digalactosyldiacylglycerol	Neutral	935.27	1	1.07	4.68	0.1	0.05	0.047
	Ganglioside GD3	Acidic	1471.83	1	0.68	7.36	0.1	0.05	0.074
4	Cerebroside	Neutral	727.35	1	1.37	3.64	0.1	0.05	0.036
	Ganglioside GM1	Acidic	1545.87	1	0.65	7.73	0.1	0.05	0.077
	Ganglioside GQ1b	Acidic	2419.16	1	0.41	12.10	0.1	0.05	0.121
5	Monogalactosyl-diacylglycerol	Neutral	743.06	1	1.35	3.72	0.1	0.05	0.037
	Cardiolipin	Acidic	1403.9	1	0.71	7.02	0.1	0.05	0.070
6	Phosphoethanolamine	Neutral	703.51	1	1.42	3.52	0.1	0.05	0.035
	Ganglioside GM2	Acidic	1383.82	1	0.72	6.92	0.1	0.05	0.069
	Ganglioside GT1b	Acidic	2128.07	1	0.47	10.64	0.1	0.05	0.106
7	Sphingomyelin	Neutral	731.6	1	1.37	3.66	0.1	0.05	0.037
	Sulfatide	Acidic	807.55	1	1.24	4.04	0.1	0.05	0.040
	Ganglioside GM3	Acidic	1180.74	1	0.85	5.90	0.1	0.05	0.059

*According to manufacturer

2.5.1.3 Internal Standards for Analyses of Peripheral Nerves (6.2.3.1)

Where relative quantitation was attempted between single nerves, internal standards were added to provide values with which to normalise ganglioside signal intensities between samples. Omega-CD$_3$-monosialogangliosides GM2 and GM3 (Matreya LLC, PA, USA) and lactosylceramide d18:1/12:0 (Avanti Polar Lipids, AL, USA) were added at 0.5 µg per mg wet tissue. Taurocholic acid (TCA) (Sigma-Aldrich, UK) was added at 20 µM per mg wet tissue weight. GM2 and GM3 were added before tissue homogenisation. Lactosylceramide and TCA were added before automated injection for HPLC-MS analysis.

2.5.1.4 Autosampler Settings and Batch Set-up

An UltiMate 3000 Analytical Autosampler WPS-3000 (Dionex, Sunnyville, California) was used at 4 ˚C throughout. For each batch samples were prepared in glass vials with 300 µl glass inserts and sealed with PTFE caps (Chromacol, UK). Samples were placed on the autosampler in random order and 10 µl injected onto the column. Blanks were run at the beginning and end of each batch as well as commercial ganglioside extract injections at the beginning, end and between each five samples. Each batch was also preceded by 3 or more methanol injections to equilibrate injection volumes.

2.5.2 HPLC Solvent Gradients

All liquid chromatography was performed on an UltiMate 3000 LPG 3000 loading & micro pump (Dionex, Sunnyville, California). Solvent systems for gradient optimisation as described in Chapter 4, including normal and reverse phase, ternary and biphasic, are detailed in Table 7. All biological studies employed Gradient 4, the isopropanol gradient. HPLC grade solvents were used throughout. All solvents were degassed by sonication for 10 minutes prior to use.

2.5.3 HPLC Chromatography Columns

An UltiMate 3000 Flow Manager and Thermostatted Column Compartment (Dionex, Sunnyville, California) set at 35 ˚C was used throughout. Reverse phase chromatography was

performed on an Acclaim C30 reversed-phase LC column, 3 μm particle size, 2.1 x 150 mm (Dionex, Sunnyville, California). Normal phase chromatography was performed on a Fortis HILIC (Hydrophilic Interaction Chromatography) column, 5 μm particle size, 2.1 x 150 mm (Fortis Technology, Neston, UK).

Table 7. HPLC Solvent Gradients for Optimisation.

Chapter ref **4.2.1 Initial Separation**					
Gradient 1					
Time (min)	Flow rate (ml/min)	%A	%B	%C	
0	0.150	75	25	0	
10	0.150	20	80	0	
35	0.150	10	10	80	
50	0.150	0	5	95	
60	0.150	0	5	95	Solvent A 10 mM aq. amm. formate
61	0.150	30	70	0	Solvent B 100% acetonitrile
75	0.150	30	70	0	Solvent C 100% isopropanol

Chapter ref **4.2.2 Optimising HPLC Settings**					
Gradient 2 Ternary Gradient (system 1)					
Time (min)	Flow rate (ml/min)	%A	%B	%C	
0	0.150	70	30	0	
15	0.150	0	100	0	
35	0.150	0	5	95	
45	0.150	0	5	95	Solvent A 10 mM aq. amm. formate
46	0.150	0	30	70	Solvent B 100% methanol
50	0.150	0	30	70	Solvent C 100% isopropanol

Chapter ref **4.2.2 Optimising HPLC Settings**					
Gradient 3 Acetonitrile Gradient (system 2)					
Time (min)	Flow rate (ml/min)	%A	%B	%C	
0	0.150	50	50	0	
45	0.150	0	100	0	
50	0.150	0	100	0	Solvent A 10 mM aq. amm. formate
51	0.150	50	50	0	Solvent B 100% acetonitrile
55	0.150	50	50	0	Solvent C 100% isopropanol

Chapter ref **4.2.2 Optimising HPLC Settings**					
Gradient 4 Isopropanol Gradient (system 3)					
Time (min)	Flow rate (ml/min)	%A	%B	%C	
0	0.150	50	0	50	
45	0.150	0	0	100	
50	0.150	0	0	100	Solvent A 10 mM aq. amm. formate
51	0.150	50	0	50	Solvent B 100% acetonitrile
55	0.150	50	0	50	Solvent C 100% isopropanol

Chapter ref **4.2.2 Optimising HPLC Settings**					
Gradient 5 Normal Phase Acetonitrile Gradient					
Time (min)	Flow rate (ml/min)	%A	%B	%C	
0	0.150	100	0	0	
45	0.150	50	50	0	Solvent A 10 mM aq. amm. formate
46	0.150	50	50	0	Solvent B 100% acetonitrile
50	0.150	100	0	0	Solvent C 100% isopropanol

Chapter ref **4.2.2 Optimising HPLC Settings**					
Gradient 6 Normal Phase Isopropanol Gradient					
Time (min)	Flow rate (ml/min)	%A	%B	%C	
0	0.150	0	0	100	
45	0.150	50	0	50	Solvent A 10 mM aq. amm. formate
46	0.150	50	0	50	Solvent B 100% acetonitrile
50	0.150	0	0	100	Solvent C 100% isopropanol

Chapter ref **4.2.3 Analysis of Lipid Standards**					
Gradient 7 Isopropanol Gradient					
Time (min)	Flow rate (ml/min)	%A	%B	%C	
0	0.150	50	0	50	
35	0.150	100	0	0	
40	0.150	100	0	0	Solvent A 10 mM aq. amm. formate
41	0.150	50	0	50	Solvent B 100% acetonitrile
45	0.150	50	0	50	Solvent C 100% isopropanol

2.6 <u>Matrix Assisted Laser Desorption Ionisation Time of Flight Mass Spectrometry</u>

All MALDI-TOF mass spectrometry, including imaging, was performed on an Ultraflex III MALDI TOF/TOF equipped with smartbeam™ laser operated at 200 Hz using Bruker FlexControl™ and FlexImaging™ software (Bruker Daltonik, Bremen, Germany). After initial settings were optimised for gangliosides (4.2.1), all further data was collected in negative ion reflectron mode using minimum diameter laser at approx. 45% power for imaging or individually adjusted power for direct analysis.

2.6.1   <u>Direct MALDI-TOF Analysis of Lipid Stocks</u>

Lipids standards GM1, GM3, GD1a, GD3, GT1b, GQ1b and commercial ganglioside extract were prepared at 0.1 mg/ml in 100% methanol. These were spotted 1 µl to 1µl with matrix on an MTP 384 target plate ground steel (Bruker Daltonik, Bremen, Germany) and air dried. MALDI matrices were purchased from Sigma-Aldrich. Matrices 2,3-dihydrobenzoic acid (DHB) and 9:1 DHB:2-hydroxy-5-methoxybenzoic acid ("super-DHB") were prepared at 25 mg/ml (individually and in ratios of 1:1, 1:4 and 4:1, w/w) in 50% acetonitrile or 70% methanol; α-cyano-4-hydroxycinnamic acid and sinapinic acid at 10 mg/ml in 50% acetonitrile; and 2',6'-dihydroxyacetophenone at 10 mg/ml in 50% ethanol. Once dry the plate was loaded into the MALDI source. One thousand laser shots per spectra were collected from at least three separate spots of each matrix/lipid combination. Peak intensities were averaged.

2.6.2   <u>Preparation of HPTLC Plates for Imaging by MALDI-TOF Mass Spectrometry</u>

2.6.2.1 <u>Manual Matrix Application; Chromatography Reagent Sprayer</u>

After separation, lanes of interest were cut from HPTLC plates using a guillotine and mounted on ITO coated glass slides, 75 x 25 mm (Bruker Daltonik, Germany) using XYZ double sided electrically conductive tape (3M). A traditional chromatography sprayer (Sigma-Aldrich) with a nitrogen source was loaded with 5 ml 100 mg/ml DHB matrix in 70% acetonitrile, 0.1% TFA, 70% methanol, 0.1% TFA or chloroform containing solvents as defined in results chapters and

used to apply matrix. For **regular matrix coating** a fine mist was applied for 20 s from a height of 10-15 cm, moving the slide to ensure the coating was even. When coated, but not wet-through, a nitrogen stream was used to evaporate the solvent. This was repeated until the 5 ml reservoir was expended. For **matrix recrystallisation** matrix was applied as described, re-wet with a mist of 70% methanol and recrystallised under a low pressure nitrogen stream. **Dry matrix** was applied as described (R J A Goodwin, Scullion, Macintyre, Watson, & Pitt, 2010). Briefly DHB matrix was finely ground with a pestle and mortar then evenly applied across the surface of a slide and lane lightly dampened with 50% methanol.

2.6.2.2 <u>Manual Matrix Application; Pneumatic Airbrush</u>

Lanes of interest were mounted on ITO-slides as described. A dual action airbrush with 0.35 mm nozzle diameter (eBay, UK) with a nitrogen gas source was loaded with 5 ml 100 mg/ml DHB. Spray protocols including heavy to light application from various distances were tried on glass to obtain the most homogeneous crystal layer (judged by eye) before matrix was applied to a lane in a light spray from approximately 10 cm distance. Matrix was applied in a similar manner to the reagent sprayer; in layers, periodically dried by nitrogen, until the reservoir was exhausted.

2.6.2.3 <u>Automated Matrix Application; Automated TLC Sampler</u>

An automatic TLC sampler 4 (CAMAG, Switzerland) was used to apply DHB in 70% methanol in order to automate the process and remove the potential for human error involved in the manual application of MALDI matrices. After HPTLC separation, lanes were left *in situ* on the HPTLC plate for the application of matrix. Only once matrix had been deposited were lanes removed and mounted on ITO-glass slides as described above.

The ATS4 was programmed to deposit matrix over a 3 x 70 mm area down the centre of the lane of interest. The precise positioning of this was calculated using the known position of initial sample band on the plate and the highest position of separated bands as indicated by

staining as illustrated in Figure 13. Deposition rates of 0.5 μg DHB per mm^3 (calculated to match the amount of matrix deposited by the chromatography sprayer) and 0.2 μg DHB per mm^3 were used initially, printed at a rate of 400 nl/s, from a reservoir of 100 mg/ml DHB in 70% methanol, 0.1% TFA. Further print speeds, deposition amounts and DHB reservoir concentrations were tried as described in Results Chapter 4.2.3.3. The optimal application of DHB in 70% methanol, 0.1% TFA at 0.05 μg/mm^3 from a 25 mg/ml reservoir at 100 nl/s was observed and used for all further HPTLC-IMS investigations.
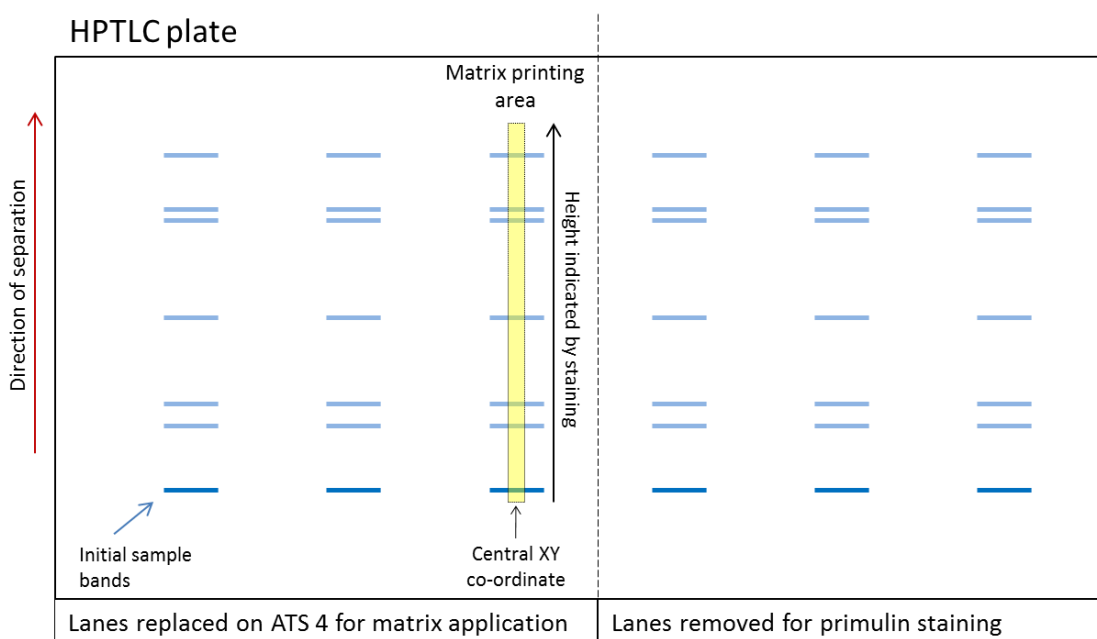
Figure 13. Matrix Printing for HPTLC-IMS using the Automatic TLC Sampler. After manual matrix sprayers proved inconsistent at best, the automatic TLC sprayer used to initially print samples onto the HPTLC plate was set up to print areas of matrix down the lanes after separation.

2.6.2.4 Printing Calibration Spots Using the ATS4

Spots of commercial ganglioside extract (CGE), the components of which had been well characterised, were printed on HPTLC lanes using the ATS4. After matrix had been applied 1 μl CGE at 0.1 mg/ml in 100% methanol was printed over a 0.5 x 0.5 μm area either to one side or in the corners of the HTPLC lanes as shown in Figure 14. This was over spotted with 1 μl DHB

from the 25 mg/ml reservoir at 100 nl/s. Spectra were collected from these spots by direct

MALDI-TOF mass spectrometry immediately before imaging runs and used to calibrate the

instrument.

2.6.2.5 **Preparation of Matrix Coated HPTLC Lanes for Imaging**

During early HPTLC-IMS method development, silica plates, hand spotted with gangliosides,

were loaded into the MALDI source on an MTP TLC Adapter Target (Bruker Daltonics,

Germany). However this target failed to consistently maintain contact, and therefore electrical

conductivity, with the back of the silica. When this was observed all silica plates were mounted

on ITO-coated glass slides as described above and loaded into the source on a Bruker Daltonics

MTP Slide Adapter II target.

Before loading the samples into the source, three pencil drawn crosses were added to silica

plates, avoiding contact with areas of interest, to act as "teach points" once inside the
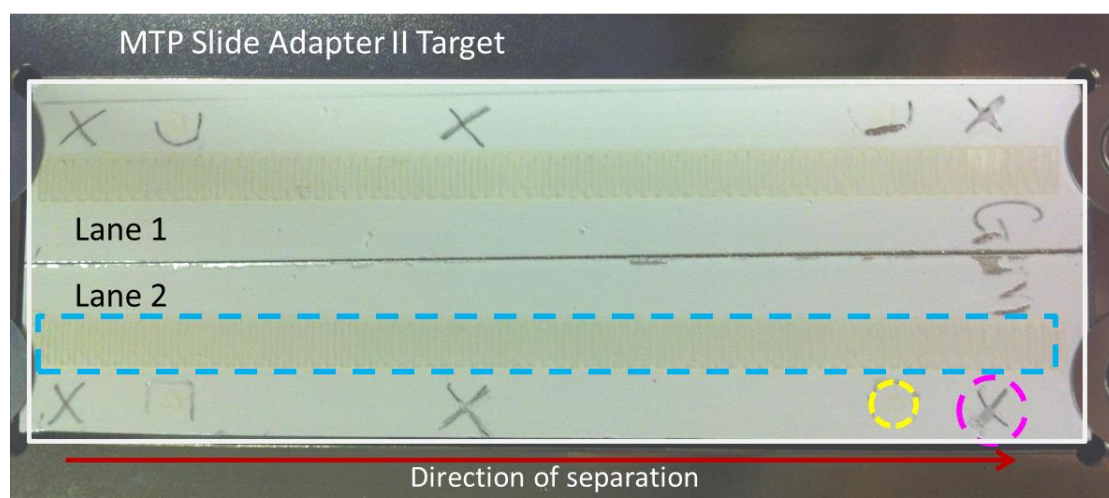
Figure 14. HPTLC–IMS Setup on Bruker MTP Slide Adapter II Target. Two bands of wild type brain extract were separated in the horizontal orientation indicated. Separated lanes were printed with DHB MALDI matrix (blue) using the ATS4. Calibration spots of commercial ganglioside extract were added (yellow) also using the ATS4. Prepared lanes were cut from the HPTLC plate and mounted onto an ITO-coated glass slide (white) using XYZ conductive tape. Pencil-drawn crosses were added (pink) to act as "teach points" once loaded into the ion source. The slide was then placed on an MTP slide adapter II target. This image was captured using a handheld smart phone camera to be uploaded into FlexImaging. The target was then loaded into the MALDI source.

instrument. An image of the HPTLC lane on the target plate was captured using a handheld smart phone camera, ensuring teach points were clearly visible, and uploaded into FlexImaging. An illustration of this is indicated in Figure 14 of two lanes of wild type extract, separated by HPTLC, printed with matrix and calibration spots, removed from the the silica plate and mounted onto an ITO-coated glass slide *in situ* on an MTP slide adapter target.

2.6.3   Preparing Tissue Sections for Imaging by MALDI-IMS

Tissue sections mounted on ITO-glass slides were brought to room temperature in a vacuum desiccator for 30 minutes to prevent condensation forming. A SunCollect MALDI Spotter (SunChrom, Germany) was used to apply MALDI matrices immediately prior to imaging. Brain sections were coated with 30 layers of 25 mg/ml DHB in 50% acetonitrile, 0.1% TFA. Several matrices were compared for imaging spinal cord sections; specific conditions for DHB, DHAP, DAN and 9-AA are detailed in Table 8. Once coated with matrix, slides were attached to a modified MTP 394 ground steel BC target (Bruker Daltonics, Germany), images scanned using an Epson flatbed scanner and uploaded into FlexImaging software and the slides loaded into the MALDI source.

Table 8. MALDI Matrix Application Specifics for Spinal Cord Tissue Imaging.			
Matrix	Concentration (mg/ml)	Solvent	Number of layers
Dihydroxybenzoic acid	20	50% acetonitrile, 0.1% TFA	30
Dihydroxybenzoic acid	20	70% methanol, 0.1% TFA	30
Dihydroxybenzoic acid	20	Chloroform/methanol/water 4:4:1	30
Dihydroxyacetophenone	15	Chloroform/methanol/water 4:4:1	30
Diaminonapthalene	10	50% acetonitrile, 0.1% TFA	15
9-Aminoacridine	10	Isopropanol/acetonitrile 6:4	20

2.6.4   MALDI-TOF-IMS; Instrument Parameters

MALDI-TOF imaging spectra were acquired on the Ultraflex III MALDI TOF in negative reflectron mode using 50 ns delayed extraction and the instrument settings mentioned above. Imaging parameters were defined in FlexImaging software as advised in the flexImaging user manual, Version 2.0. Briefly, after samples were loaded into the MALDI source a new imaging file was created using an 'arbitrary array' workflow. The AutoeXecute method, previously adapted during early HPTLC-IMS method development in FlexControl, was defined. Imaging spectra were acquired over a mass range of m/z 600-3000 from one hundred shots per pixel (unless specified) using FlexControl random walk function. The sample image was uploaded, and teach points matched between FlexImaging and FlexControl. The instrument was then calibrated using commercial ganglioside extract spotted on either the silica plate or the slide on which tissue sections were mounted. After this the area for imaging and raster step resolution were defined. Resolutions ranging from 500 – 50 μm^2 were used and are specified in each results chapter.

2.6.5   Data Analysis

2.6.5.1 Ganglioside Mass Filters in FlexImaging

Various mass filters were applied to IMS datasets in order to visualise, or perform targeted analysis for, specific gangliosides in mouse brain extracts separated by HPTLC and brain and spinal cord sections. These are described in Table 9. These filters were applied in FlexImaging using a mass range of +/- 0.5 Da, relative minimum intensity of 5-15 % and a maximum relative intensity of 60-90 % to enhance images.

2.6.5.2 Calibration of Individual Mass Spectra

A minimum of seven individual spectra from pixels in FlexImaging datasets across each spinal cord section were opened in FlexAnalysis and internally calibrated using ubiquitously detected peaks. These peaks included sulfatide d18:1/16:0 (m/z 778.51450), sulfatide d18:1/18:0 (m/z

Table 9. Glycosphingolipid Mass Filters for HPTLC-IMS datasets.				
Lipid	Molecular Mass	Ion	Nominal Mass	Filter colour
Sulfatide d18:1/18:0	807.5530	[M-H]$^-$	807	White
Sulfatide d18:1/18:0(2OH)	823.5480	[M-H]$^-$	823	White
PI C38:3	887.5655	[M-H]$^-$	887	White
Sulfatide d18:1/24:0	891.6469	[M-H]$^-$	891	White
Sulfatide d18:1/24:0(2OH)	905.6262	[M-H]$^-$	905	White
GM3 d18:1/18:0	1180.7445	[M-H]$^-$	1180	Red
GM3 d18:1/20:0	1207.7758	[M-H]$^-$	1208	Red
GM2 d18:1/18:0	1383.8238	[M-H]$^-$	1383	Pink
GM2 18:1/20:0	1411.8551	[M-H]$^-$	1411	Pink
GD3 d18:1/18:0	1471.8399	[M-H$_2$O-H]$^-$	1453	Orange
GD3 d18:1/18:0	1471.8399	[M-H]$^-$	1471	Orange
GD3 d18:0/20:0	1499.8712	[M-H$_2$O-H]$^-$	1481	Orange
GD3 d18:0/20:0	1499.8712	[M-H]$^-$	1499	Orange
9OAc-GD3 d18:1/18:0	1513.8505	[M-H$_2$O-H]$^-$	1495	Turquoise
9OAc-GD3 d18:0/20:0	1541.8818	[M-H$_2$O-H]$^-$	1523	Turquoise
GM1 d18:0/18:0	1545.8767	[M-H]$^-$	1545	Blue
GM1 d18:1/20:0	1573.9080	[M-H]$^-$	1573	Blue
GD1b d18:1/18:0	1836.9721	[M-H$_2$O-H]$^-$	1818	Cyan
GD1b d18:1/20:0	1865.0034	[M-H$_2$O-H]$^-$	1846	Cyan
GD1a d18:1/18:0	1836.9721	[M+Na-2H]$^-$	1858	Yellow
GD1a d18:1/20:0	1865.0034	[M+Na-2H]$^-$	1886	Yellow
9OAc-GD1a d18:1/18:0	1878.9827	[M+Na-2H]$^-$	1900	Violet
9OAc-GD1a d18:1/20:0	1907.0140	[M+Na-2H]$^-$	1928	Violet
GT1b d18:1/18:0	2128.0675	[M+Na-H$_2$O-2H]$^-$	2131	Green

806.54580), sulfatide d18:1/20:0 (m/z 834.57710), sulfatide d18:1/22:0 (m/z 862.60840) and sulfatide d18:1/24:0(2OH) (m/z 906.63460). Complex gangliosides GM1 d18:1/18:0 (m/z 1544.86940) and GM1 d18:1/20:0 (m/z 1572.90070) were also used to calibrate spectra from wild type datasets. Simple gangliosides GM3 d18:1/18:0 (m/z 1179.73720), GM3 d18:1/20:0

(m/z 1207.76850) and GD3 d18:1/18:0 (m/z 1470.83260) were also used to calibrate spectra from knockout datasets, which lacked complex gangliosides, and NFL rescue datasets which contain reduced levels of complex gangliosides. The masses of peaks of interest from the imaging datasets were then cross-referenced with the corresponding average mass values obtained from the calibrated spectra to obtain more accurate and consistent peak values for identification.

2.7 High Resolution Mass Spectrometry with Dissociation

All high resolution accurate mass spectrometry and dissociation was done on an Orbitrap Velos Pro™ or Obritrap Elite™ hybrid ion trap-orbitrap mass spectrometer (Thermo Fisher Scientific, Germany) equipped with heated electrospray ion source operated at a source heater temperature of 80 ˚C.

2.7.1 Direct Injection Mass Spectrometry with Dissociation

2.7.1.1 Full Scan Instrument Parameters

All direct injection analysis was done on the Orbitrap Velos Pro™. The HESI source was coupled with an automated Hamilton glass syringe using a flow rate of 3.5-5 µl/min. Sheath and auxillary gas rates of 20 and 10 were applied. The instrument was used in negative polarity with a source voltage of 3.90 kV and in positive polarity with a source voltage of 4.5 kV. Full scans were collected in a mass range of m/z 400-2000 for 20 seconds at a resolution of 60,000.

2.7.1.2 Dissociation Parameters

For each lipid, peaks were selected from the full scan for dissociation in a mass range encompassing predominant species according to the supplier/manufacturer, +/-50 Da, unless otherwise stated. Most peaks in these ranges returned a putative identification as the head-group of interest from databases, or were recognised as a lipid modification. Collision induced dissociation (CID) and high energy collision induced dissociation (HCD) were applied in the LTQ mass spectrometer. Collision energies were adjusted from 10-60 eV for CID and 20-75 eV for

HCD with 20 ms activation times to find an optimal energy. Isolation width and maximum injection time were set at 1.0 Th and 200 ms respectively. Product ion spectra were collected at a resolution of 30,000.

2.7.1.3 Analysis of Product Ion Spectra

Product ion spectra were observed in Xcalibur™ software (Thermo Fisher Scientific). Putative peak identification was done using a combination of Lipid MAPS glycosphingolipid product ion search tool, manual analysis of structural sketches and previous publications on lipid dissociation. Manual structures were investigated in ACD/ChemSketch Software (ACD/labs, Canada).

2.7.2 High Performance Liquid Chromatography with Mass Spectrometry and Dissociation

2.7.2.1 Full Scan Instrument Parameters

HPLC-MS during the initial optimisation of chromatography, as well as for motor and sensory nerve extract separations (Chapter 6) was done on the Orbitrap Velos Pro™ at 60,000 resolution. All other HPLC-MS was done on the Obritrap Elite™ at 120,000 resolution. The HESI source was coupled to the UltiMate 3000 HPLC system described above, running at 250 μl/min. Sheath and auxillary gas rates of 20 and 5 were applied on the Orbitrap Velos Pro™ and 15 and 1 on the Obritrap Elite™. Both instruments were used in negative polarity using a source voltage of 4.5 kV on the Orbitrap Velos Pro™ and 4.2 kV on the Obritrap Elite™. Full scans were collected in a mass range of m/z 500-2000.

2.7.2.2 Dissociation Parameters

For each full scan the four most intense peaks, with a minimum intensity of 5000, were selected for dissociation in the linear ion trap using CID with a collision energy of 30-35 eV, isolation width of 2, and activation time of 30 ms. On the Orbitrap Velos Pro™ dynamic exclusion for 20 seconds was applied after 2 repeat counts in 30 seconds. On the Obritrap Elite™ dynamic exclusion for 15 seconds was applied after 3 repeat counts in 20 seconds.

2.7.3 HPLC-MS Data Analysis and Applied Mass Filters

The majority of data analysis of HPLC-MS and dissociation datasets was done in Xcalibur™ software (Thermo Fisher Scientific).

2.7.3.1 Mass Filters for Commercial Ganglioside Extract

Two layout files were set up in Xcalibur containing mass filters encompassing the major glycosphingolipid components of commercial ganglioside extract in order to facilitate comparisons between different solvent systems during optimisation of the HPLC settings. The components of these are described in Table 10a & 10b. Mass filters were applied with a set mass tolerance of 10 ppm.

Table 10a. Commercial Ganglioside Extract Mass Filter 1 for Data Analysis in Xcalibur Software.

Lipid	Formula	Molecular mass	Ion	Ion mass
PS C36:1	$C_{42}H_{80}NO_{10}P$	789.5519	$[M-H]^-$	788.5447
Sulfatide d18:1/18:0	$C_{42}H_{81}NO_{11}S$	807.5530	$[M-H]^-$	806.5457
GM1 d18:1/18:0	$C_{73}H_{131}N_3O_{31}$	1545.8767	$[M-H]^-$	1544.8694
GM2 d18:1/18:0	$C_{67}H_{121}N_3O_{26}$	1383.8238	$[M-H]^-$	1382.8166
GM3 d18:1/18:0	$C_{59}H_{108}N_2O_{21}$	1180.7445	$[M-H]^-$	1179.7372
GD1 d18:1/18:0	$C_{84}H_{148}N_4O_{39}$	1836.9721	$[M-2H]^{2-}$	917.4788
GT1 d18:1/18:0	$C_{95}H_{165}N_5O_{47}$	2128.0675	$[M-2H]^{2-}$	1063.0265
GQ1 d18:1/18:0	$C_{106}H_{182}N_6O_{55}$	2419.1629	$[M-2H]^{2-}$	1208.5742

Table 10b. Commercial Ganglioside Extract Mass Filter 2 for Data Analysis in Xcalibur Software.

Lipid	Formula	Molecular mass	Ion	Ion mass
GM1 d18:1/20:0	$C_{75}H_{135}N_3O_{31}$	1573.9080	$[M-H]^-$	1572.9001
GM2 d18:1/20:0	$C_{69}H_{125}N_3O_{26}$	1411.8551	$[M-H]^-$	1410.8473
GM3 d18:1/20:0	$C_{61}H_{113}N_2O_{21}$	1209.7836	$[M-H]^-$	1208.7758
GD1 d18:1/20:0	$C_{86}H_{152}N_4O_{39}$	1865.0034	$[M-2H]^{2-}$	931.4939
GT1 d18:1/20:0	$C_{97}H_{169}N_5O_{47}$	2156.0988	$[M-2H]^{2-}$	1077.0416
GQ1 d18:1/20:0	$C_{108}H_{186}N_6O_{55}$	2447.1942	$[M-2H]^{2-}$	1222.5893

2.7.3.2 Mass Filters for Mouse Brain Extracts

Layout files were set up in Xcalibur containing mass filters for gangliosides of various chain structures in order to extract standard retention times, experimental retention times and normalised intensity values for relative quantitation between datasets from mouse brain extracts in Chapter 6. A full description of the mass filters included is given in Table 11. Mass filters were applied with a set mass tolerance of 5 ppm.

2.7.3.3 Normalisation of Nerve Rootlets Datasets

Normalised intensities were extracted from each motor and sensory nerve dataset for the [M-H]$^-$ ion of internal standards GM2 CD$_3$-d18:1/18:0 (m/z 1385.8395), GM$_3$ CD$_3$-d18:1/18:0 (m/z 1182.7601) and TCA (m/z 514.283851) and the [M+Cl]$^-$ ion of lactosylceramide (m/z 840.5240) using mass filters in Xcalibur. For each sample, extracted ganglioside intensity values were divided by internal standard intensities of GM2 CD$_3$-d18:1/18:0 and GM$_3$ CD$_3$-d18:1/18:0 in the same dataset. The two values resulting from this were averaged to obtain a normalised value for each ganglioside for each nerve extract. Student t-test and paired t-tests were performed manually in excel to test whether differences between either raw or normalised values for each ganglioside were significant between sensory (n=5) and motor (n=5) nerves. Paired t-tests could be performed as sensory and motor nerve matched pairs were removed from each mouse. Principal component analysis (PCA) was performed in microsoft excel using multibase excel add-in for PCA from NumericalDynamics.com.

2.8 Secondary Ion Mass Spectrometry

2.8.1 Preparation of Standards on Steel Targets

One microlitre of each lipid standard (gangliosides – GM1, GM2, GM3, GD1a, GD1b, GD3, GT1b, sphingolipids – SS, SM, galC, sulf, phospholipids – PC, PE, PG, PS) at 10 µg/ml (low concentration) or 100 µg/ml (high concentration) were spotted onto a steel target and air dried. Spectra were either collected directly by SIMS or spots were gold coated using a SC7640

Table 11. Mass Filters Applied to Mouse Brain Datasets for Ganglioside Data Extraction.

Ganglioside	Ceramide	Formula	m/z	Ganglioside	Ceramide	Formula	m/z
GM1	d18:1/16:0	$C_{71}H_{127}N_3O_{31}$	1516.8377	GD1	d18:1/16:0	$C_{82}H_{144}N_4O_{39}$	903.4623
	d18:1/18:1	$C_{73}H_{129}N_3O_{31}$	1542.8533		d18:1/18:0	$C_{84}H_{148}N_4O_{39}$	917.4780
	d18:1/18:0	$C_{73}H_{131}N_3O_{31}$	1544.8690		d20:1/18:0	$C_{86}H_{152}N_4O_{39}$	931.4936
	d18:0/18:0	$C_{73}H_{133}N_3O_{31}$	1546.8845		d20:1/20:0	$C_{88}H_{156}N_4O_{39}$	946.0110
				O-acetyl GD1			
	d20:1/18:1	$C_{75}H_{133}N_3O_{31}$	1570.8846		d18:1/16:0	$C_{84}H_{146}N_4O_{40}$	924.4676
	d20:1/18:0	$C_{75}H_{135}N_3O_{31}$	1572.9003		d18:1/18:0	$C_{86}H_{150}N_4O_{40}$	938.4833
	d20:0/18:0	$C_{75}H_{137}N_3O_{31}$	1574.9160		d20:1/18:0	$C_{88}H_{154}N_4O_{40}$	952.4989
	d20:1/20:0	$C_{77}H_{139}N_3O_{31}$	1600.9316		d20:1/20:0	$C_{90}H_{158}N_4O_{40}$	966.5145
GM2	d18:1/16:0	$C_{65}H_{117}N_3O_{26}$	1354.7849	GD3	d18:1/16:0	$C_{68}H_{121}N_3O_{29}$	720.8963
	d18:1/18:1	$C_{67}H_{119}N_3O_{26}$	1380.8006		d18:1/18:0	$C_{70}H_{125}N_3O_{29}$	734.9119
	d18:1/18:0	$C_{67}H_{121}N_3O_{26}$	1382.8162		d20:1/18:0	$C_{72}H_{129}N_3O_{29}$	748.9276
	d18:0/18:0	$C_{67}H_{123}N_3O_{26}$	1384.8319		d20:1/20:0	$C_{74}H_{133}N_3O_{29}$	762.9432
				O-acetyl GD3			
	d20:1/18:1	$C_{69}H_{123}N_3O_{26}$	1408.8319		d18:1/16:0	$C_{70}H_{123}N_3O_{30}$	741.9018
	d20:1/18:0	$C_{69}H_{125}N_3O_{26}$	1410.8475		d18:1/18:0	$C_{72}H_{127}N_3O_{30}$	755.9175
	d20:0/18:0	$C_{69}H_{127}N_3O_{26}$	1412.8632		d20:1/18:0	$C_{74}H_{131}N_3O_{30}$	769.9331
	d20:1/20:0	$C_{71}H_{129}N_3O_{26}$	1438.8788		d20:1/20:0	$C_{76}H_{135}N_3O_{30}$	783.9488
GM3	d18:1/16:0	$C_{57}H_{104}N_2O_{21}$	1151.7055	GT1	d18:1/16:0	$C_{93}H_{161}N_5O_{47}$	1049.0100
	d18:1/18:1	$C_{59}H_{106}N_2O_{21}$	1177.7212		d18:1/18:0	$C_{95}H_{165}N_5O_{47}$	1063.0256
	d18:1/18:0	$C_{59}H_{108}N_2O_{21}$	1179.7369		d20:1/18:0	$C_{97}H_{169}N_5O_{47}$	1077.0413
	d18:0/18:0	$C_{59}H_{110}N_2O_{21}$	1181.7526		d20:1/20:0	$C_{99}H_{173}N_5O_{47}$	1091.0569
				O-acetyl GT1			
	d20:1/18:1	$C_{61}H_{110}N_2O_{21}$	1205.7525		d18:1/16:0	$C_{95}H_{163}N_5O_{48}$	1070.0153
	d20:1/18:0	$C_{61}H_{112}N_2O_{21}$	1207.7682		d18:1/18:0	$C_{97}H_{167}N_5O_{48}$	1084.0309
	d20:0/18:0	$C_{61}H_{114}N_2O_{21}$	1209.7838		d20:1/18:0	$C_{99}H_{171}N_5O_{48}$	1098.0466
	d20:1/20:0	$C_{63}H_{116}N_2O_{21}$	1235.7995		d20:1/20:0	$C_{101}H_{175}N_5O_{48}$	1112.0622
GMx	d18:1/16:0	$C_{68}H_{119}N_3O_{28}$	1424.7904	GQ1	d18:1/16:0	$C_{104}H_{178}N_6O_{55}$	1194.5580
	d18:1/18:1	$C_{70}H_{121}N_3O_{28}$	1450.8060		d18:1/18:0	$C_{106}H_{182}N_6O_{55}$	1208.5733
	d18:1/18:0	$C_{70}H_{123}N_3O_{28}$	1452.8217		d20:1/18:0	$C_{108}H_{186}N_6O_{55}$	1222.5890
	d18:0/18:0	$C_{70}H_{125}N_3O_{28}$	1545.8374		d20:1/20:0	$C_{110}H_{190}N_6O_{55}$	1236.6046
	d20:1/18:1	$C_{72}H_{125}N_3O_{28}$	1478.8373				
	d20:1/18:0	$C_{72}H_{127}N_3O_{28}$	1480.8530				
	d20:0/18:0	$C_{72}H_{129}N_3O_{28}$	1482.8686				
	d20:1/20:0	$C_{74}H_{131}N_3O_{28}$	1508.8843				

sputter coater (Quorum Technologies, New Haven, UK) equipped with an FT7607 quartx crystal microbalance stance and FT690 thickness monitor to deposit a 1nm gold layer and then collected by SIMS.

2.8.2   SIMS and SIMS Imaging Instrument Parameters

Static SIMS mass spectrometry was performed on a BioTRIFT-II TOF SIMS mass spectrometer (Physical Electronics, Eden Prairie, MN) equipped with a 22keV gold liquid metal ion source with the Biomolecular Imaging Mass Spectrometry group at the FOM-institute AMOLF in the Netherlands. Direct analysis from steel targets was performed by manually rastering the

focused ion beam across sample spots with acquisition times of 2 or 6 minutes. SIMS imaging

spectra were obtained by automatic rastering of the focused ion beam across the sample with

an acquisition time of 20 minutes per tile. Four tiles of 50 x 50 μm and 256 x 256 pixels were

collected in a 2x2 grid from 10 μm tissues sections of sciatic nerve from wild type mouse. For

each ion detected the time of flight and primary ion beam position were recorded, allowing

post-processing of the data. All spectra and tile collection and analysis were performed in

WinCadence 4.4.0.17 software (ULVAC-PHI, Inc., Kanagawa, Japan) and DataCube Explorer

(http://www.maldi-msi.org) as described previously (Fornai et al., 2012).

Chapter 3. Coupling High Performance Thin Layer Chromatography with Imaging Mass Spectrometry Detection and Identification

3.1 Introduction

High performance thin layer chromatography (HPTLC) has been the established separation technique for gangliosides since their discovery in 1942 (Klenk, 1942). It employs a thin layer of polar stationary phase such as silica or cellulose, immobilised on a glass or aluminium back. Lipids are separated by their mobility in a non-polar mobile phase as it wicks through the layer enabling purification or profiling of lipids in complex mixtures. Much of the initial species, tissue and time specific dynamics of ganglioside composition were described using HPTLC as were many disease profiling studies correlating abnormal ganglioside profiles to cancer and neurological diseases. Despite the development of liquid, gas, ion exchange and capillary electrophoresis methods HPTLC is still employed today both preparatively and analytically.

Thin layer chromatography benefits from its simple approach, with stationary and mobile phase targeted towards subsets of lipids with specific properties. The technique therefore has a high tolerance to sample contamination and its two-dimensional nature means that results can be easier to interpret compared to more global techniques. It is however difficult to standardise the process for reproducibility. It's most significant weaknesses are the lengthy processes required for detection and identification. Traditionally HPTLC profiling of gangliosides employs lipid dyes and/or overlays for detection. Dyes, such as the universal lipid dye primulin which stains all fatty acids, or sialic-acid specific resorcinol, are simple to apply and universally detect all relevant bands. Overlays using serum or lectins are more sensitive and specific but also complex to run. However without a large bank of known comparison standards, both require further analysis such as on-plate digestion with neuraminidase enzymes to identify bands of interest. Alternatively bands or fractions can be scraped off, re-extracted and characterised by mass spectrometry but this runs the risk of contamination by adjacent species. For concurrent detection and identification, immunostaining with anti-

ganglioside antibodies can be used with high sensitivity and specificity. However immunostaining is a targeted approach and depends on the availability of high quality antibodies without cross-reactivity.

The use of mass spectrometry for the direct detection of lipids from HPTLC membrane was first published in 1995 (Gusev et al., 1995). Mass spectrometers equipped with desorption ionisation sources, most commonly matrix assisted laser desorption ionisation (MALDI), can ionise gangliosides from the HPTLC plate or a PVDF membrane after blotting. Sample preparation is relatively simple and detecting molecules by their mass to charge ratio enables confident identifications when combined with their retention factor. Despite the utility of this concept it is not in regular usage and relatively few methods have been published. These mostly employ specialist instrumentation (Dreisewerd et al., 2005), customized ion source settings (V. B. Ivleva et al., 2004), and additional blotting steps onto PVDF membrane (N Goto-Inoue, Taki, & Setou, 2010) to increase sensitivity and mass accuracy and to limit fragmentation. Lipid bands are usually located first using traditional dyes then marked and analysed individually. Consistent matrix application can be problematic and may require a specialist commercial system.

We sought to develop a quick, simple method for HPTLC-MS for ganglioside profiling directly from HPTLC plates without additional blotting using a commercially available MALDI axial-TOF without instrument modifications. Instead of locating ganglioside bands prior to mass spectrometry we used novel imaging mass spectrometry (IMS) software to collect spectra from across the entire HPTLC area.

3.2 <u>Results</u>

3.2.1 <u>Optimisation of MALDI Parameters for Ganglioside Ionisation</u>

Mass spectrometry settings for ganglioside ionisation and analysis by MALDI-TOF were optimised using mono- (GM1, GM3), di- (GD1a, GD3), tri- (GT1b) and tetra- (GQ1b) sialylated ganglioside standards co-spotted with 2,3-dihydrobenzoic acid (DHB) matrix on a steel MALDI

target plate. Settings were also investigated for non-ganglioside sphingolipids (ceramide, galactosylceramide and sulfatide). Polarity (pos/neg) and laser power (offset 55%, range 40-70%) and diameter (10 – 80 µm) were tested. In positive ion mode no signal was observed from gangliosides with two or more sialic acid components. For mono-sialylated gangliosides and sulfatide higher signal intensities were obtained in negative ion mode than positive ion mode (Figure 15) using a minimum laser diameter of 10 µm and a power of approximately 45% range, 55% offset. In negative ion mode monosialylated species GM1 and GM3 spectra were predominated by the [M-H]$^-$ ion, compared to the [M+Na]$^+$ ion in positive ion mode. Fragmentation of the sialic acid was greatly reduced in negative ion mode. The availability of additional sialic acids resulted in the formation of more complex adducts including [M-H2O-H]$^-$, [M-Na-2H]$^-$ and [M+K-2H]$^-$ ions of GD1a and an additional [M+2Na-3H]$^-$ ion of GT1b. Inclusion of excess lithium hydroxide prior to spotting did not result in homogenous formation of [M+Li-2H]$^-$ ions and other adducts were present at similar ratios from lithium treated and untreated solutions. Signal intensities of galactosylceramide and ceramide were higher in positive ion
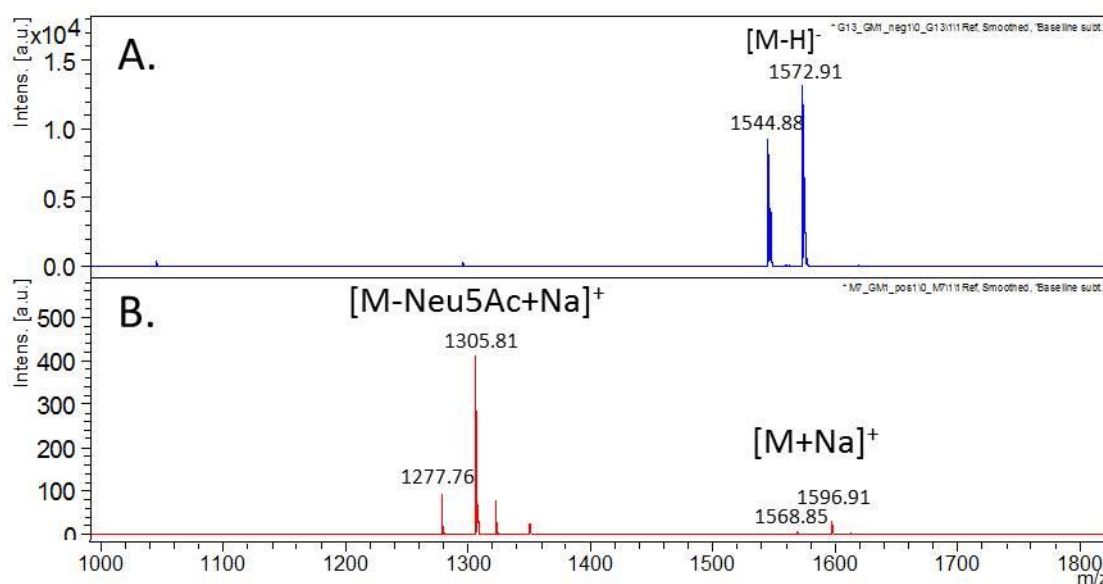
Figure 15. MALDI MS Spectra from Monosialylated Ganglioside GM1. Panel A – spectrum collected in negative ion mode. Panel B – spectrum collected in positive ion mode. During optimisation of MALDI settings negative ion mode resulted in better ionisation of gangliosides. Intensities were significantly higher compared to positive ion mode and fragmentation of the sialic acid (Neu5Ac) was greatly reduced. This was observed in all ganglioside stocks and for sulfatide.

mode. Settings for ganglioside ionisation were saved in a negative ion mode FlexControl method for ganglioside ionisation.

While the optimal MALDI matrix for gangliosides is widely reported to be DHB other matrices such as sinapinic acid (V Ivleva, Sapp, O'Connor, & Costello, 2005), 9-AA (Cerruti, Benabdellah, Laprévote, Touboul, & Brunelle, 2012) and super-DHB (sDHB, 9:1 2,5-hydroxybenzoic acid/2-hydroxy-5-methoxybenzoic acid) have also been reported to work well. GM1, GD1a and GT1b were co-spotted with CHCA, sinapinic acid, DHAP and DHB and analysed using optimised settings. Commercial ganglioside extract (CGE) was also spotted with 3 ratios of DHB:sDHB and analysed. Each ganglioside/matrix mix was spotted in 3 replicates, spectra collected from each and signal intensities averaged. Signal intensities for GM1, GD1a and GT1b were reduced using DHAP, CHCA and sinapinic acid compared to DHB to the point that quantifying intensities was unnecessary, supporting current opinion that DHB is the optimal matrix for lipids. Signal intensities from sulfatide, lactosylceramide, GM1, GM3 and GD1 from CGE using DHB, sDHB and ratios of the two were highest using DHB or a 1:4 ratio of sDHB:DHB (Figure 16). DHB was
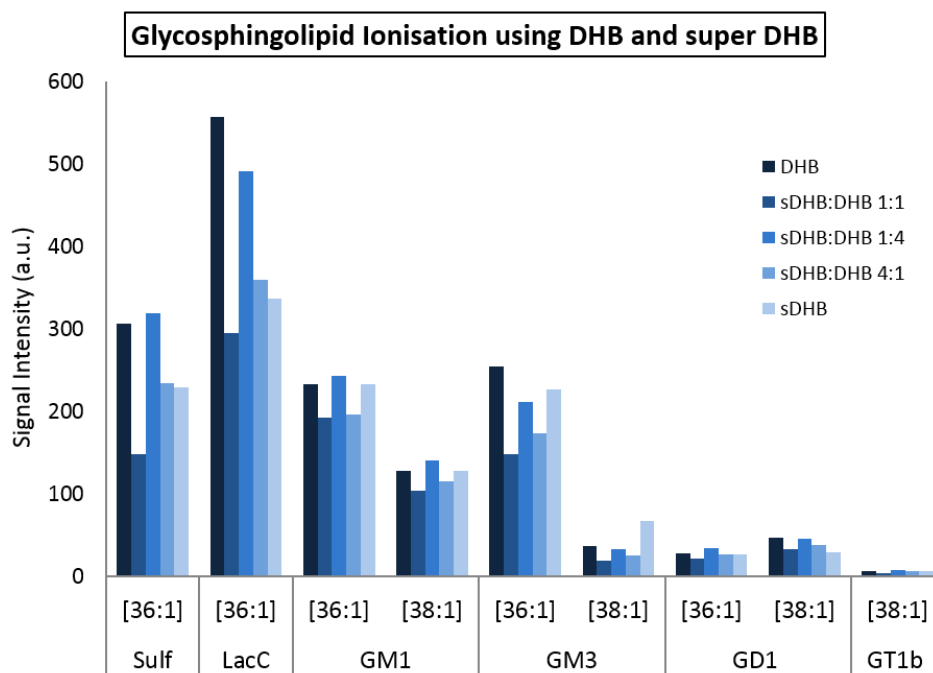
Figure 16. MALDI Matrix Optimisation. Gangliosides were spotted in triplicate with DHB, super DHB (sDHB) and various ratios of the two. Spectra collected and intensities averaged. Intensities were highest using straight DHB or a 1:4 ratio of sDHB:DHB as MALDI matrix.

chosen for ganglioside ionisation for simplicity.

3.2.2   <u>Ganglioside Ionisation Directly from HPTLC Plates</u>

For the initial ionisation of gangliosides from HPTLC plates GD1a was spotted directly onto aluminium-backed silica HPTLC plates. Spots of 50, 10, 5 and 1 µg total material were applied and coated with several light layers of concentrated DHB in 70% acetonitrile using a HPTLC reagent sprayer (TRS). Each layer was dried using nitrogen before applying the next. HPTLC plates were then loaded into the MALDI source either on a Bruker TLC target plate or stuck to an ITO coated slide on a Bruker slide adapter target plate. The laser was fired for 500 shots at the highest concentration spot and at blank silica. Signal was observed only using the latter target and the HPTLC adapter target was not used further. The silica alone produced ion peaks in the 100-600 m/z range so gated ion suppression was set at m/z 600 and scans were taken from 600-3000 m/z to prevent these ions swamping the detector.

An imaging method was created in FlexImaging software to collect 100 laser shots per pixel in a 500 x 500 µm raster from a 10 x 55 mm area covering the positions of the GD1a spots. Once spectra had been collected the overall average spectrum (OAS) was normalised (using FlexImaging inbuilt normalisation to equalise the total ion count for all spectra). Regions of interest were defined around ganglioside spots and blank membrane creating average spectra for these areas which are illustrated in Figure 17. Five peaks ranging from m/z 1825 – 1893, the distribution of the most intense of which is shown in Figure 17, were observed in spectra from 50 and 10 ug spots and not from blank membrane. Despite occurring in the right mass range, none of these peaks corresponded to the mass of the [M-H]- ions for GD1a. However no internal mass calibration was used in this experiment and it was probable that these peaks corresponded to more complex adducts of GD1a. Without internal calibration small variations in the molecular time of flight could amount to significant variations in mass value at the detector.
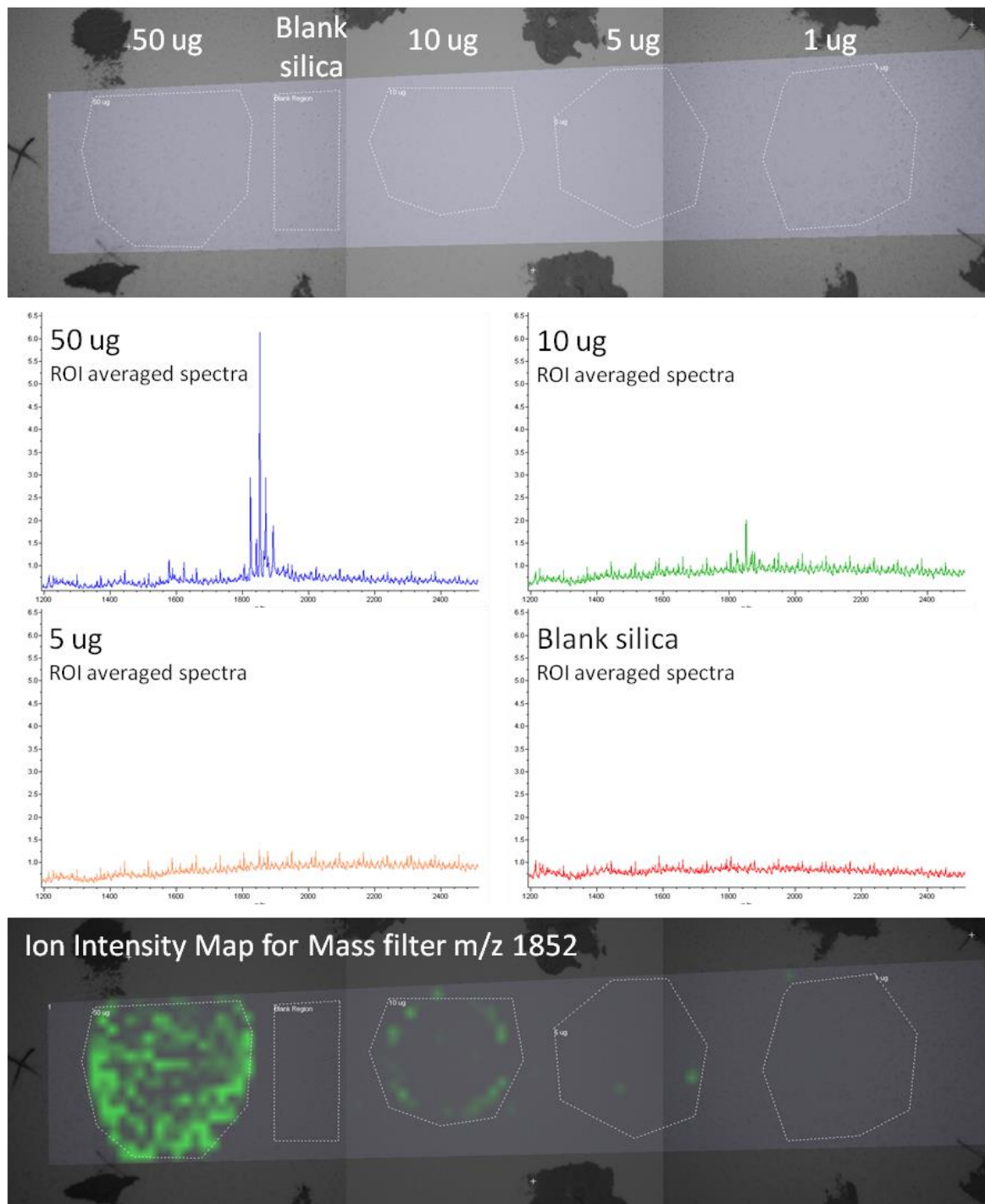
Figure 17. IMS of Ganglioside GD1a Spotted onto a HPTLC Silica Plate. After collecting an imaging dataset, regions of interest were defined around spots locations of 50, 10, 5 and 1 µg GD1a in FlexImaging software (top). Average spectra (middle panels) were extracted automatically from these regions by the software revealing peaks that are enriched in specific regions. In this case five peaks corresponding to GD1a were observed in spectra from spots of 50 µg and 10 µg GD1a, but not in spectra from 5 µg or 1 µg (not shown) GD1a, or in spectra from blank silica. A mass filter can be set up, in this case for the most intense peak observed in the first average spectra, and the software generates an ion intensity map of the detection of that mass across the imaged area (bottom).

It was noted during preparation for the imaging run that applying the matrix solution resulted in blistering of the silica. The resulting rough, flaky surface reduced peak mass accuracy and resolution preventing assignment of identifications. When acetonitrile was replaced with 70% methanol as a matrix solvent the integrity of the silica surface was maintained. Ionisation of GT1b co-spotted with DHB in 70% methanol or 70% acetonitrile was compared on a steel target. Signal intensities, fragmentation and overall spectra were found to be similar. Acetonitrile was therefore replaced with methanol in matrix solvent for HPTLC imaging. Three protocols were trialled to reduce the formation of adducts and matrix salt clusters. HPTLC plates were washed with water or methanol prior to spotting gangliosides to remove salts in the silica and 0.1% TFA was added to the matrix solvent. Washing the silica had no effect but adding 0.1% trifluoroacetic acid did reduce the formation of interfering matrix clusters and was routinely added to matrix solvent for HPTLC imaging.

The optimisations above were then applied to the detection and identification of gangliosides directly from a silica plate after HPTLC separation. A delayed extraction of 50 ns was used to combat the loss of peak resolution as a result of the uneven surface of the silica and the laser power was increased slightly to improve ionisation. A mix of GM1, GM2, GM3, GD1a, GD1b, GD3 and GT1b was separated by HPTLC and a FlexControl method set up to image an area down the centre of the excised lane at 400 μm^2 raster, 500 shots per pixel. The workflow from separation to collection of the imaging spectra is summarised in Figure 18. Areas of localised signal intensity corresponding to potential bands were identified by manual investigation of the normalised OAS. Once identified, regions of interest (ROIs) were applied to produce average spectra for each area. Seven potential species were identified. Peak m/z were extracted from each average spectra and summarised in Table 12 alongside putative assignment of the ganglioside, fatty acid chain and ion adduct based on mass, chromatographic position and known composition of the mixture. Mass error ranges from 4.5-11 Da increasing linearly with m/z partially due to the lack of on-plate calibration.

Print and separate ganglioside mixture on HPTLC silica plates. Stain and image reference repeat lanes.

Remove lane and mount on ITO glass slide using conductive tape. Mark teach points in pencil.

Coat with MALDI matrix (100 mg/ml DHB in 70% methanol, 0.1% TFA), and place on Slide Adapter II target.

GM1
Fatty acids;
(18:1/18:0)
(18:1/20:0)
(18:1/22:0)

Image sample setup and load into source. Create file in FlexImaging defining parameters (area, method, raster step).

Start imaging run to automatically collect data.

Figure 18. Workflow for HPTLC Directly Coupled to MALDI-IMS.

Table 12. Putative Assignments to Peaks of Interest in HPTLC Plate Imaging Datasets.

Observed m/z	Region of Interest	Putative Identification	Ion?	Expected m/z	Mass Error ΔDa
1184	1	GM3 d18:1/18:0	[M-H]-	1179.5	4.5
1212	1	GM3 d20:1/18:0	[M-H]-	1207.5	4.5
1388	2	GM2 d18:1/18:0	[M-H]-	1383	5
1416	2	GM2 d20:1/18:0	[M-H]-	1411	5
1551	3	GM1 d18:1/18:0	[M-H]-	1545	6
1579	3	GM1 d20:1/18:0	[M-H]-	1573	6
1459	4	GD3 d18:1/18:0	[M-H2O-H]-	1452	7
1477	4	GD3 d18:1/18:0	[M-H]-	1471	6
1499	4	GD3 d18:1/18:0	[M+Na-2H]-	1492	7
1865	5	GD1a d18:1/18:0	[M+Na-2H]-	1857	8
1893.5	5	GD1a d20:1/18:0	[M+Na-2H]-	1885	8.5
1826.5	6	GD1b d18:1/18:0	[M-H2O-H]-	1817	9.5
1844.5	6	GD1b d18:1/18:0	[M-H]-	1836	8.5
1854.5	6	GD1b d20:1/18:0	[M-H2O-H]-	1845	9.5
2141	7	GT1b d18:1/18:0	[M+Na-H2O-2H]-	2130	11
2169	7	GT1b d20:1/18:0	[M+Na-H2O-2H]-	2158	11
2180.5	7	GT1b d18:1/18:0	[M+2Na-3H]-	2170	10.5
2187.1	7	GT1b d20:1/18:0	[M+Na-2H]-	2176	11.1
2209	7	GT1b d20:1/18:0	[M+2Na-3H]-	2198	11

While accurate identifications were not feasible with such large mass errors, all gangliosides included in the mixture were potentially detected as separated bands directly from the HPTLC plate (Figure 19. GM1 (green) and GM2 (blue)). Their positions are indicated on the HPTLC plate using coloured mass filters for the observed m/z of the d18:1/18:0 and d18:1/20:0 species. Complex salt adducts were observed indicating bands of di- and tri-sialylated gangliosides. Higher intensity peaks were observed for the [M-H2O-2H]⁻ ion from GD1b and the [M+Na-2H]⁻ ion from GD1a suggesting each had a propensity to form different adducts that could be used to distinguish the two isomers.
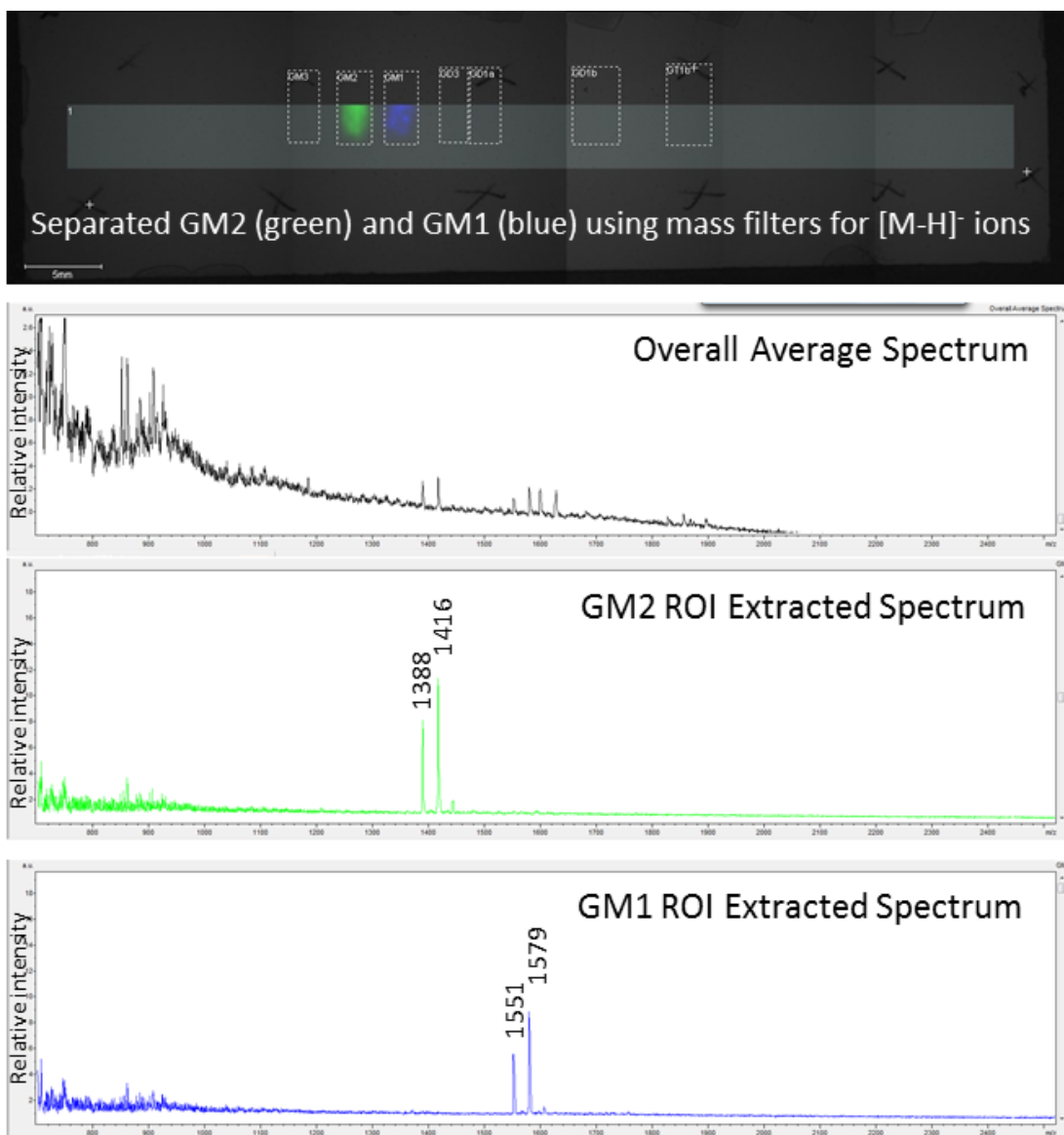
Figure 19. Identification of Separated Gangliosides Directly from the HPTLC Plate. Little was observed in the overall average spectra (OAS) of this imaging dataset collected from an HPTLC separated ganglioside mix directly from the silica. However by defining regions of interest around potential bands (top panel, white dashed lines), peaks that localised specifically to these areas were revealed in extracted average spectra. This is illustrated by the lower two spectra where peaks are now clearly visible that were barely above baseline in the OAS. Peak masses were used to allocate putative identifications and to set up for mass filters to map the ion distribution across the area. This is illustrated in the top panel where mass filters, corresponding to [M-H]- ions of GM1 and GM2 d18:1/18:0, localised to specific areas enabling the identification of bands of separated GM1 (blue) and GM2 (green).

3.2.3   Optimisation of MALDI Matrix for Imaging

In HPTLC-IMS the choice of matrix solvent and method of application are both essential for

obtaining good quality data. The solvent acts mutually as a matrix solvent and an extraction

solvent to draw analytes to the surface of the silica in order to co-crystallise with the matrix. Extraction increases with the solubility of the analyte in the solvent which must be balanced against matrix crystal size and rate of lateral diffusion (although this is not as important for imaging HPTLC as it is for imaging tissue sections). Numerous publications present novel methods for depositing MALDI matrix for IMS that maximise sensitivity, lateral resolution, dynamic range and reproducibility. Some such as ink jet printing, ImagePrep systems or sublimation MALDI (SMALDI) require specialist equipment. Others can be reproduced more easily. Matrix recrystallisation has been shown to minimise the formation of cation adducts (Monroe, Koszczuk, Losh, Jurchen, & Sweedler, 2007) and enable high spatial resolutions (Bouschen, Schulz, Eikel, & Spengler, 2010). Dry/wet matrix application has also resulted in more homogenous crystal sizes and higher signal intensities (Aerni, Cornett, & Caprioli, 2006; Ferguson, Creasey, Wolstenholme, Clench, & Francese, 2013).

3.2.3.1 <u>Matrix Solvent</u>

Chloroform is often included in lipid solutions to increase solubility and was therefore tested as an additive in matrix solvents for HPTLC-MS. A mix of gangliosides including GM1, GM2, GM3, GD1a, GD1b and GT1b was separated and coated with DHB in methanol (70%) and methanol & chloroform (50:50 v/v, 70:30 v/v). These lanes were imaged then analysed for ganglioside signal intensities as described above. Briefly bands were detected manually from the OAS, ROI's defined around them and signal intensities taken from average spectra and compared. Using a chloroform composition above 30% resulted in a solid matrix layer over the HPTLC plate and no analyte extraction. Lateral diffusion within the HPTLC membrane indicated by band width (illustrated in Figure 20) was comparable for all gangliosides in both solvent conditions. Higher signal intensities, also shown in Figure 20 alongside mass errors, were observed from all but the GD1b C38:1 species using 70% methanol, 0.1% TFA with similar mass errors in both solvent conditions (methanol = +3.5-8 Da, C/M 30/70 = +4-8 Da).
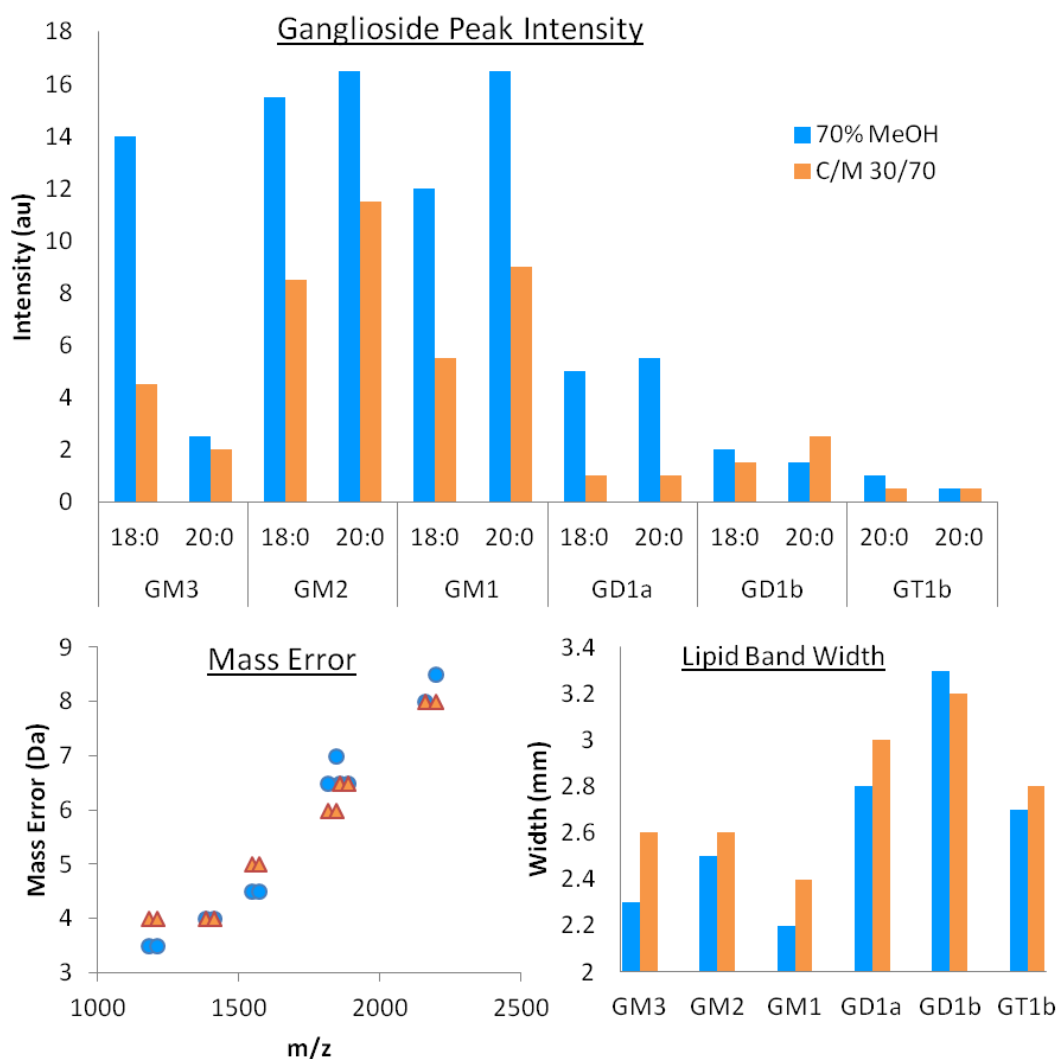
Figure 20. Parameters for Evaluating DHB Matrix Solvent Efficacy for HPTLC-IMS; Comparison of 70% Methanol in Water and Chloroform. Various factors were evaluated when assessing different matrix solvents for efficacy ionising gangliosides. In this instance peak signal intensities were higher using 70% methanol in water as matrix solvent compared to 70% methanol, 30% chloroform. Mass errors were comparable using both solvents and the width of the lipid bands was also similar, although slightly increased using chloroform, suggesting increased lateral spread with this matrix solvent. In this comparison 70% methanol was deemed the optimal matrix solvent.

3.2.3.2 <u>Matrix Application</u>

Several combinations of matrix deposition (dry and wet) and recrystallisation in 70% methanol were compared to the previously used application method. A mix of GM1, GM2, GM3, GD1a, GD1b and GT1b was separated and coated as described. Dry matrix alone resulted in no observable ganglioside signal. When matrix was applied dry and re-crystallised, hotspots of intense signal suggested heterogeneous crystal sizes or uneven analyte extraction. Ganglioside

peak intensities in the OAS of each condition were significantly reduced for all novel recrystallisation or wet matrix applications compared to the traditional spray method. This reduction in signal was replicated after further processing in average spectra from band ROIs.

3.2.3.3 Matrix Applicator

Using the TLC reagent sprayer (TRS) for matrix application had thus far produced inconsistent results. Despite attempts to standardise the manual details of the process crystals ranged from small and homogenous to large and heterogeneous with variable analyte extraction efficiencies. On occasion matrix formed a solid layer over the HPTLC plate preventing any analyte ionisation. Automated systems such as the ImagePrep (Bruker), TM-sprayer (HTXImaging) and SunCollect (SunChrom) provide control over many variables improving the consistency, efficiency and reliability of matrix application. Unfortunately they are also expensive. Using a pneumatic airbrush had also been reported to improve crystal size and homogeneity without increasing application time (Wang, Post, & Woods, 2008). In order to mimic these, an Automatic HPTLC Sampler (ATS) and an airbrush were used to apply matrix. (The ATS is a simple robotic sample application system used to apply sample spots and bands to TLC plates via contact or spray printing. It is capable of automatically spray coating programmed areas at constant speed.)

A mix of GM1, GM2, GM3, GD1a, GD1b and GT1b was separated and coated with DHB using either the TRS, ATS or an airbrush. The same volume and concentration of matrix was used with the TRS and airbrush. TRS coated slides were weighed after application and deposition calculated at 0.5 ug/mm^2. Depositions of 0.5 ug/mm^2 and 0.2 ug/mm^2 were replicated on the ATS over 3 x 55 mm areas. Matrix application was equally inconsistent using the airbrush compared to the TRS (based on three separate applications). When ganglioside peaks were obtained intensities were similar in the OAS and ROI average spectra to TRS application. Initially no ganglioside peaks were detected in the OAS or upon closer inspection using the ATS. However the matrix crystals resembled those observed when matrix applied by TRS

formed a solid layer over the plate. The same ganglioside mix was separated and matrix deposition reduced from 0.5 ug/mm^2 to 0.1 ug/mm^2. Low intensity peaks were observed in the OAS from monosialyated gangliosides GM1, GM2 and GM3 although further processing failed to find signals from di- or tri-sialylated gangliosides. Data collection was repeated using depositions of 0.05 ug/mm^2 and 0.01 ug/mm^2 at 100 nl/s and 400 nl/s. The OAS of each condition showed apparently higher peak intensities after printing at 100 nl/s and highest using 0.05 ug/mm^2 total deposition. Manual investigation detected 7 bands corresponding to all gangliosides included in the mix in all conditions except 0.01 ug/mm^2 at 400 nl/s. ROI signal intensities, summarised in Figure 21, were also highest using 0.05 ug/mm^2 matrix at 100 nl/s.

As a final optimisation of matrix deposition, different concentrations of matrix reservoir were used. A commercial ganglioside extract (CGE) from bovine brain spiked with GM3 and GT1b was separated and printed with matrix at 0.05 μg/mm^2 at 100 nl/s and 400 nl/s from stocks of 25, 50 and 100 mg/ml DHB (all in 70% methanol). Signal intensities for gangliosides GM3, GM1,
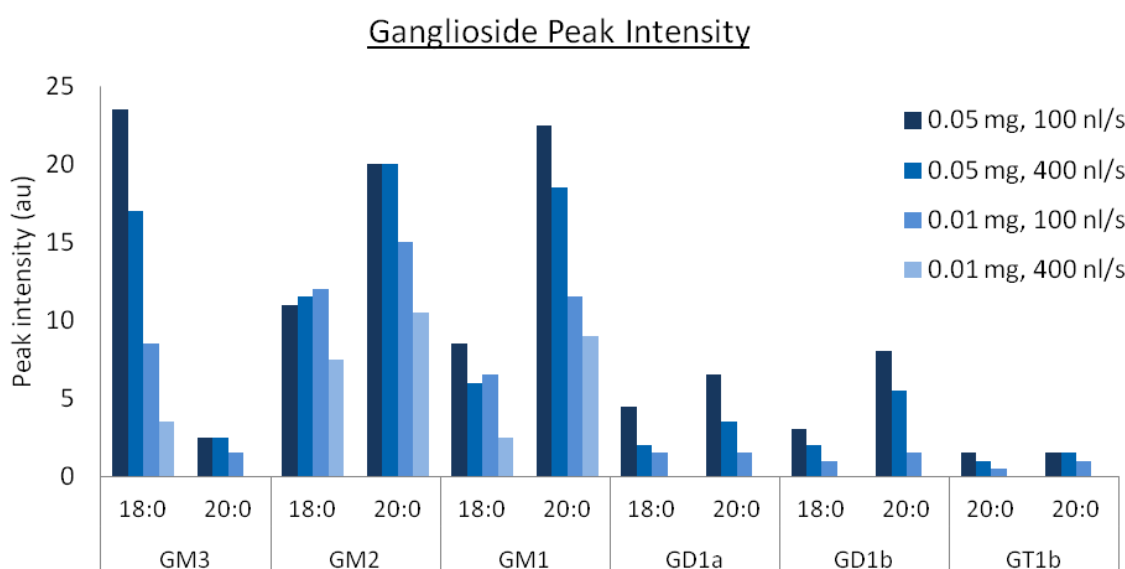
Figure 21. Assessment of Automatic TLC Sampler for Printing MALDI Matrix. The automatic TLC sprayer (ATS) was utilised for printing MALDI matrix onto HPTLC lanes to emulate automatic MALDI matrix applicators. Several factors including spray speed (100 nl/s, 400 nl/s) and matrix deposition (0.01 mg/mm^2, 0.05 mg/mm^2) were optimised and assessed by ganglioside peak intensity in imaging datasets. In this case 0.05 mg/mm^2 printed at 100 nl/s resulted in highest peak intensities.
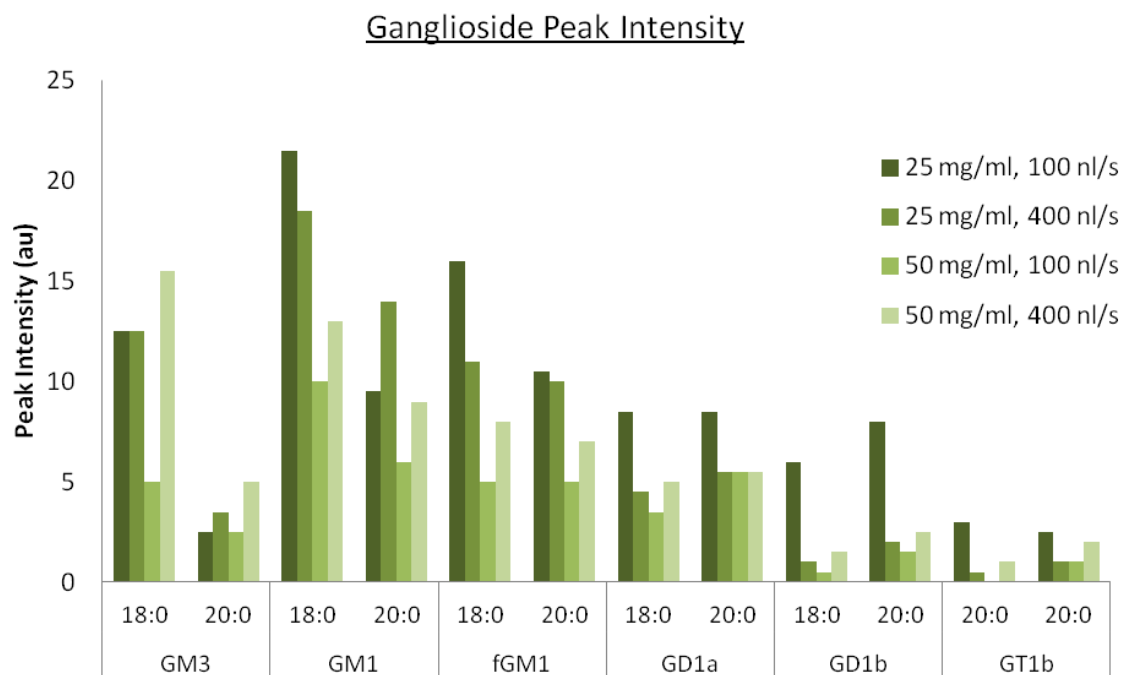
Figure 22. Effect of DHB Reservoir Concentration on Ganglioside Signal Intensity. DHB reservoirs of 25 mg/ml and 50 mg/ml were used to print 0.05 mg/mm^2 MALDI matrix onto HPTLC lanes at 100 nl/s and 400 nl/s. Effects on ionisation efficacy were again monitored by extracting ganglioside peak intensities from imaging datasets. Although the 50 mg/ml reservoir printed at 400 nl/s resulted in high signal intensities, the highest ganglioside peak intensities were observed using the 25 mg/ml reservoir printed at 100 nl/s.

fGM1 GD1a, GD1b and GT1b from ROI average spectra defined around the six identified ganglioside bands are shown in Figure 22. Peak intensities for monosialylated gangliosides were similar in all conditions and consistently higher for di- and trisialylated gangliosides using 25 mg/ml matrix stock printed at 100 nl/s. Optimal settings for matrix application appeared to be 25 mg/ml DHB applied at 100 nl/s to a total deposition of 0.05 ug/mm^2.

3.2.4   LiChrospher HPTLC Plates

The uneven surface of a silica HPTLC plate affects both the ionisation efficiency and peak resolution decreasing the quality of mass spectrometry data. A new type of LiChrospher™HPTLC plate ([LC]HPTLC) is the first to use spherical shaped silica particles of 6-8 μm with a size distribution of 3-5 μm. The manufacturers report more compact bands and lower detection limits on these plates compared to regular HPTLC ([R]HPTLC) plates. The spherical

particles could potentially provide a more even ionisation surface. [R]HPTLC and [LC]HPTLC plates were compared for ganglioside separation, optimal loading capacity and IMS analysis. Separations of 1 µl, 5 µl, 20 µl and 50 µl CGE were stained with primulin. Loading capacity and separation are shown in Figure 23a. Bands were better resolved and separated on [R]HPTLC. Separation is reported to occur faster on [LC]HPTLC plates so development time may have been suboptimal on this membrane. A lower loading capacity was observed with [LC]HPTLC plate with band distortion occurring from 50 µl although sensitivity was increased. Bands were visible from the 5 µl separation on [LC]HPTLC but not [R]HPTLC plates. Separations of 20 µl were then analysed by imaging mass spectrometry. Sensitivity was significantly increased using [LC]HPTLC plates. The intensity of ganglioside peaks in the OAS was higher, and in ROI average spectra of bands of sulfatide, GM1, fGM1, GD1a and GD1b which are shown in Figure 23b. GT1b was undetected from [R]HPTLC from the 20 µl separation. Peak and mass accuracy (ΔDa 1.5 - 4 [LC]HPTLC, 0.5-7.5 Da [R]HPTLC) were also improved using [LC]HPTLC plates compared to [R]HPTLC. Intra-band separation of different fatty acids was detected from [LC]HPTLC plates (Figure 23c) which was not seen on [R]HPTLC plates.

3.2.5   Signal Reproducibility without Source Cleaning

Sensitivity is lost between and sometimes within imaging runs as matrix and silica debris builds up in the MALDI source. The source was usually cleaned between each HPTLC-IMS run, a process that takes around 5 hours and significantly reduces throughput. To examine the potential for consecutive imaging runs three analyses (t0, t1 and t2) were performed on TLC separations of CGE without cleaning the source. Matrix was printed <2 hours before imaging in each case to prevent ionisation changes through oxidation of the matrix. Sensitivity loss, detected as reduced ganglioside peak intensity, was not obvious in the OAS' from t0, t1 and t2. However peak intensities from ROI average spectra corresponding to bands of GM1, fGM1, GD1a, GD1b and GT1b were significantly reduced through consecutive runs. Percentage loss of peak intensity was 12.2% (0% - 40%) after two consecutive runs and 39.2% (12 - 60%) after
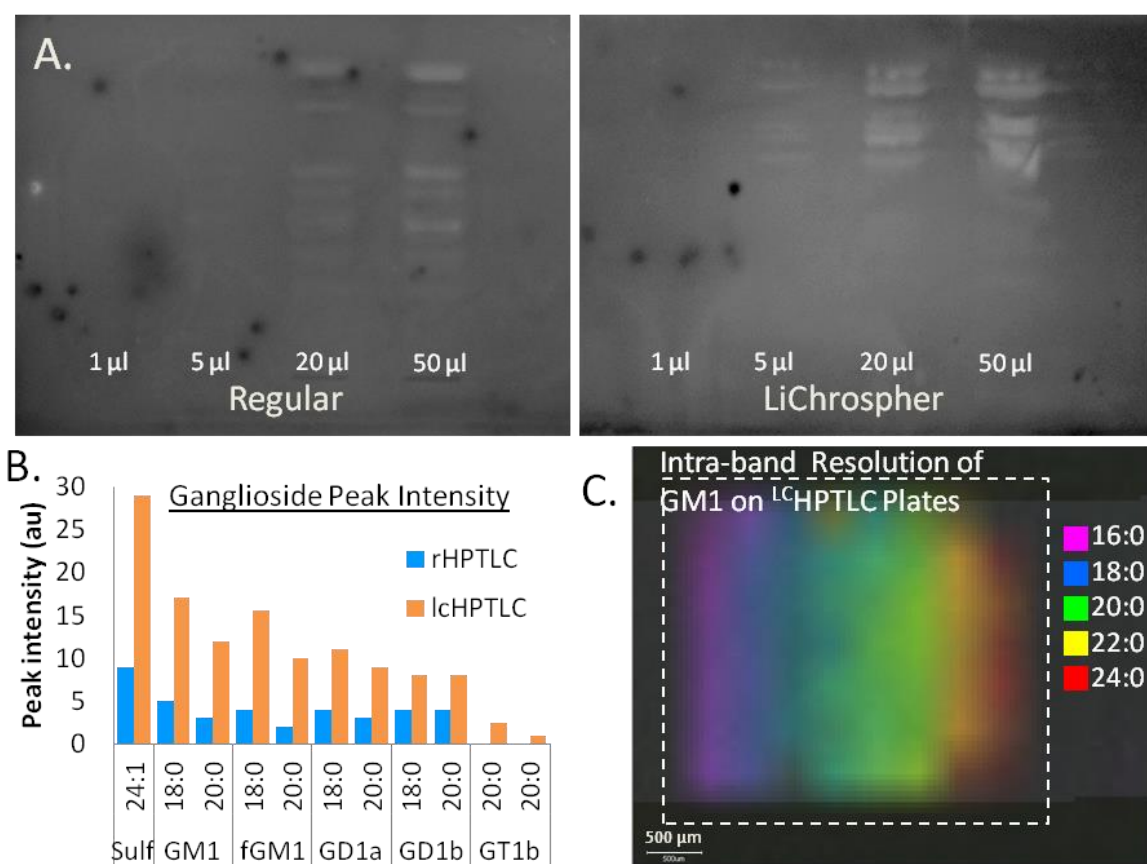
Figure 23. Ganglioside Separation and Imaging on Regular and LiChrospher® HPTLC Plates. LiChrospher HPTLC (^{LC}HPTLC) plates use spherical silica particles potentially providing a more even ionisation surface for MALDI imaging. Separation of sample loadings from 1-50 µl commercial ganglioside extract were compared (A). Loading capacity was reduced on ^{LC}HPTLC and separation poorly resolved. However higher sensitivity was observed, both by traditional staining and imaging mass spectrometry (n=1). Ganglioside peak intensities were significantly higher from ^{LC}HPTLC plates (B). Resolution of gangliosides of the same head-group with different ceramide structures was observed within bands from ^{LC}HPTLC plates only (C).

three. GT1b was hard to visualise in the third imaging dataset due to the loss of signal. It was concluded that two consecutive imaging runs without cleaning the source may be possible without significantly comprising results but that further runs may result in ganglioside bands going undetected.

3.2.6   Discussion

In this chapter a functional workflow for the analysis of separated gangliosides directly from thin layer chromatography plates was developed using imaging mass spectrometry on a

MALDI-TOF mass spectrometer for the universal detection and identification of ganglioside bands. The full work flow is illustrated in Figure 18. Thin layer chromatography is a widely used separation technique in ganglioside analysis and profiling. Traditionally, in order to identify bands of interest HPTLC preparations required either vast banks of lipid standards that could be run simultaneously or the re-extraction and further chemical analysis of bands of interest. Alternatively for more specific detection immunostaining can be used to identify individual gangliosides but anti-lipid antibodies often suffer from cross-reactivity and low affinity. Using mass spectrometry to both detect the presence of lipid bands and identify these by mass greatly assisted the recognition of lipid bands without using standards or antibodies.

The HPTLC-IMS workflow equalled traditional universal stains in sensitivity and capability for detecting separated ganglioside bands. All bands that were detected using the universal fatty acid stain primulin were detected by IMS analysis including barely visible bands. Once potential bands were identified from the OAS and defined as regions of interest they were identifiable by combining mass and retention data. The observed mass errors which were reduced from around 8 Da to less than 4 Da by the end of optimisation would still interfere with band identifications in unknown mixtures. It was thought that this loss of mass accuracy may stem in part from a lack of calibration from the surface of the thin layer chromatography plate. Commercial ganglioside extract will therefore be co-spotted with matrix adjacent to the lane for all experimental samples. Spots in each corner of the HPTLC lane will also provide information on changes in mass error across the imaging area.

The specificity of HPTLC-IMS provided an unexpected benefit over traditional staining when LiChrospher HPTLC plates were introduced. It was possible to resolve the separation of different fatty acids within bands of a single head group structure. This was especially true for more stable monosialylated gangliosides. Masses corresponding to five different fatty acid structures were detected within the band of GM1 in commercial ganglioside extract. Four fatty acid structures were detected from fucosylated-GM1 and two from GM2. For future analysis of

biological samples this would enable the detection of changes in ganglioside fatty acid composition that would not be observable using universal or immuno-staining. The fragmentation and adduct formation of larger oligo-silylated gangliosides made fatty acid modifications harder to interpret although they could still be distinguished. This fragmentation decreased the ability of HPTLC-IMS to detect these bands although sensitivity still equalled staining for the detection of GD1 and GT1 structures.

Some of these advantages of HPTLC-MS have been mentioned previously in publications using longer sample preparation or specialist equipment (Dreisewerd et al., 2005; N Goto-Inoue et al., 2010; V. B. Ivleva et al., 2004). Sufficient sensitivity and specificity were achieved here on a commercial MALDI-TOF system without bespoke equipment. Furthermore this workflow involved no blotting step in the sample preparation. After the chromatography, plates were simply dried and matrix was applied. This reduced the opportunity for introducing contamination and cut down sample preparation time and complexity significantly. Other groups have reported that blotting onto PVDF can improve sensitivity. While this was not tested here, sensitivity was sufficient to detect gangliosides that were not detected by staining. The complexity of preparation was further reduced by the utilisation of the Automatic TLC sampler for matrix application. Without a commercial system, matrix application was initially done manually which was inconsistent and wasteful of materials. Once printing on the ATS was optimised, application was reproducible and consistently resulted in successful ionisation (personal observations from repeat datasets, data not shown). Efficient delivery also reduced the amount of matrix used per run.

Another benefit of the method developed here was the use of MS imaging software to automatically collect data from the HPTLC plate. Despite its benefits only one other group can be found using similar software to investigate HPTLC preparations, which use it in combination with blotting (Valdes-Gonzalez et al., 2011). Without imaging, ganglioside bands must be located prior to mass spectrometry. This has been done using an MS compatible stain such as

primulin, which was shown to reduce sensitivity (Fuchs, Schiller, SuB, Schurenberg, & Suckau, 2007), or staining of an adjacent, more heavily loaded, lane for comparison. Spectra are then collected manually from each band to identify the ganglioside. Imaging allowed automatic collection of spectra from the length of the TLC lane without previously locating ganglioside bands. This automation reduced the set up time required for each run and, due to the high sensitivity of mass spectrometry, enabled detection of bands not visible by staining which could otherwise have been missed.

There are of course areas for further improvement. The fragmentation of larger, more complex gangliosides by MALDI ionisation and loss of mass accuracy due to the uneven surface of the silica have already been discussed. IMS peak intensities were notably inconsistent between HPTLC preparations of the same commercial ganglioside extract. Methods for quantitative HPTLC-IMS analysis such as including internal standards in the matrix application or within the lipid sample itself could be developed. However in this case, for semi-quantitative comparative profiling of biological samples a primulin stained lane can be included for traditional densitometry quantitation if necessary. The analysis of the IMS dataset is still primitive. The OAS was searched manually for m/z that localised to distinct areas which were defined as ROIs to produce average spectra. This was simplified by dividing the imaged area into ROIs and investigating the average spectra for enriched peaks to identify the bands more quickly. However were HPTLC-IMS to be applied to large numbers of samples or lipids with a wider variety of structures than natively occurring gangliosides, automated analysis would be beneficial. It would be interesting for example to apply principal component analysis to obtain correlation measures to match low intensity peaks to bands.However software was not available at the time for PCA analysis of IMS datasets.

Chapter 4. High Performance Liquid Chromatography with High Resolution Mass Spectrometry and Dissociation for Ganglioside Analysis.

4.1 Introduction

Liquid chromatography and high performance liquid chromatography (HPLC) are separation techniques that have been used extensively in the preparation and analysis of gangliosides. Traditionally these are coupled with UV detection measuring changes in absorption as lipid concentration changes in the eluate. This provides no information about the lipid species without extensive use of comparative standards or further analysis of collected fractions. More recently HPLC has proved highly compatible with online mass spectrometry using an electrospray ionisation (ESI) source interface. The eluate is ionised in real time and mass data collected in a series of full scans. This has several benefits over UV detection. Without additional complexity to the workflow the sensitivity and specificity of detection are increased. Mass data is collected so that putative identifications can be made without previous knowledge of elution times. Co-eluting species of different masses that would not be resolved by UV detection are distinguishable. Many MS configurations also now enable online dissociation between full scans providing internal structural data that can be used to support putative identifications.

Several technical papers have been published applying HPLC-MS to targeted lipid analysis. The majority of these lipid studies have used a triple quadrupole instrument configuration. Such instruments have relatively fast scan times and the three consecutive mass analysers allow for versatility in experimental design, but the mass accuracy and resolution are lower than those achievable by other MS configurations. Some groups have focused on the sphingolipids subgroup; however most have steered clear of any but the simplest glycosphingolipids (Kundu, Diego, Osovitz, & Marcus, 1985; Markham & Jaworski, 2007; Merrill et al., 2005; Sullards et al., 2007; Suzuki, Yamakawa, & Suzuki, 1991). This is surprising as the larger, polar glycosphingolipids such as gangliosides have repeatedly been shown to be biologically

important. A handful of publications were found describing HPLC-MS methods designed specifically for the targeted analysis of sulfatides and gangliosides (Fong, Norris, Lowe, & McJarrow, 2009; Ikeda, Shimizu, & Taguchi, 2008; Ikeda & Taguchi, 2010). Separation was reported using mainly hydrophilic interaction liquid chromatography (HILIC) whereby all gangliosides of a particular head-group structure elute concurrently and minor modifications may be missed. Several methods described the preparative isolation of individual gangliosides prior to characterisation by reverse phase chromatography and mass spectrometry (Ladisch, Li, & Olson, 1994; Mauri et al., 2003). Although these methods provide comprehensive, easy to interpret data on single head-groups, the extra chromatographic steps complicate the experimental setup significantly. The one publication that used reverse phase chromatography, which has the potential to separate by interactions with both the hydrophilic and hydrophobic moieties, with online MS detection reported low chromatographic resolution and poor elution peak shapes in some instances and showed significant overlap between the elution of certain ganglioside head groups such as GM1, GM2 and GM3, and sulfatides (Ikeda et al., 2008).

In this chapter we therefore aimed to develop an in-house optimised method for the mass spectrometric analysis of gangliosides separated by HPLC using a high resolution Thermo LTQ Orbitrap Velos MS for detection and dissociation. This configuration has sub ppm mass accuracy and mass resolution of up to 100,000 compared to triple quadrupole instruments' unit mass accuracy and typical <3000 resolution, while maintaining high sensitivity enabling detection and accurate identification of even low abundance gangliosides. Separation by normal and reversed phase HPLC were investigated using a hydrophilic interaction liquid chromatography (HILIC) column and an Acclaim C30 reversed phase column designed specifically for lipid separation. Several solvent gradients were tested for mass-spectrometry compatible separation. Once an optimal HPLC system was established, elution and dissociation patterns were investigated using available ganglioside, sphingolipid and phospholipid stocks and described in detail to provide orthogonal data to support identifications.

4.2 <u>Results</u>

4.2.1 <u>Initial Separation of Lipid Standards</u>

Standards including gangliosides, sphingolipids and phospholipids were analysed in fractions using a three part acetonitrile/ isopropanol/ aq. ammonium formate gradient adapted from a previous lipidomic publication (Nygren, Seppänen-Laakso, Castillo, Hyötyläinen, & Orešič, 2011). Polarity preferences were determined by normalised intensities from extracted ion chromatographs (XIC) (Table 13). The masses of protonated and deprotonated ions of the most abundant species as reported by manufacturers were used for XIC for all but cardiolipin, PC and PE where alternative predominant species were identified.

Table 13. Fractions 1 -7. Ganglioside standards analysed in fractions of three or fewer species by LCMS in positive and negative ion mode. Predominant ions are highlighted.

	Fraction	Dominant peak m/z	NI positive ion mode	NI negative ion mode	Adduct formation
Cardi	5	1461.066*	5.98E+05	1.93E+06	[M-H]$^-$ **[M-2H]$^{2-}$**
Cer	1	565.5434	4.00E+05		**[M+H]$^+$** [M-H2O+H]$^+$ [M+H2O+H]$^+$ [M+H2O+Na]$^+$
Cerebroside	4	727.596	5.57E+06	3.94E+05	**[M+H]$^+$** [M+Na]$^+$ [M-H2O+H]$^+$ [M+H2O+H]$^+$
Chol	2	386.3549			
DgDg	3	946.6593	5.23E+04		**[M+H]$^+$** [M+NH4]$^+$ [M+Na]$^+$
GD1a	1	1836.9716	8.60E+04	1.81E+06	[M-H]$^-$ **[M-2H]$^{2-}$**
GD1b	2	1836.9716	4.12E+04	4.03E+05	**[M+H]$^+$** [M+NH4]$^+$ [M+2H]$^+$
GD3	3	1471.8399	1.04E+05	3.22E+05	[M-H]$^-$ **[M-2H]$^{2-}$**
GM1	4	1545.8767	9.06E+05	1.70E+06	**[M-H]$^-$** [2M-2H]$^{2-}$
GM2	6	1383.8238	1.59E+06	2.31E+06	[M-H]$^-$
GM3	7	1180.7445	4.13E+06	5.29E+06	**[M-H]$^-$** [2M-2H]$^{2-}$ [M-H2O-H]$^-$
GQ1b	4	2418.1629			
GT1b	6	2128.0700		1.54E+05	[M-H]$^-$ **[M-2H]$^{2-}$**
MgDg	5	784.6070			
PC	2	787.6091*	2.28E+07		**[M+H]$^+$** [M+Na]$^+$ [2M+H]$^+$
PE	6	745.562*	1.70E+05	3.04E+05	[M-H]$^-$
PG	3	748.5254	5.92E+05	8.79E+06	[M-H]$^-$ **[M-2H]$^{2-}$**
PS	1	789.5520	5.85E+05	6.04E+05	**[M-H]$^-$**
Sm	7	730.5989	1.35E+07		**[M+H]$^+$** [M+Na]$^+$
Sulf	7	806.5458	4.45E+06	1.24E+07	[M-H]$^-$

* Most abundant ion not according to manufacturer.

** Higher intensity [M-2H]$^{2-}$ ion used for signal intensity measurement.

NI – normalised intensity.

Ceramide, hexosylceramide, digalactosyl diacylglycerol and glycerophosphocholine were detected at higher intensity in positive ion mode preferentially forming cations including $[M+H]^+$, $[M+Na]^+$ and $[M+NH4]^+$. Of these only hexosylceramides were also detected in negative ion mode. It was possible that the other neutral lipids formed complex negatively charged adducts that weren't identified. All gangliosides and other acidic lipids, including sulfatide and PE, PG and PS, were detected at higher intensity in negative ion mode as $[M-H]^-$ and $[2M-2H]^{2-}$ anions. Gangliosides containing more than one sialic acid ionised preferentially as $[M-2H]^{2-}$ ions. Cholesterol, which is usually analysed by GC-MS, was not detected nor was MGDG or GQ1b.

Elution peak qualities were assessed as good (1), peak tailing (2) or poor (3), illustrations of which are shown in Figure 24. Phospholipid and simple sphingolipid elution peaks scored 1; peaks were symmetrical with FWHM of <0.3 minutes. Gangliosides and phosphatidyserine had quality scores of 2 – 3. Some peaks (GM1, GD1a) were sharp but showed peak tailing. Elution peaks for more complex gangliosides and PS were poor quality with low peak resolution, high asymmetry and significant tailing. Elution times of 30.67 min for GD1a and 30.63 min for GD1b also suggested that this

- Quality 1
- Asymmetry <1.5 at 10% peak height.
- FWHM <0.3 min.
- T_f <1.5 at 5% peak height.

- Quality 2
- Asymmetry >1.5 at 10% peak height.
- FWHM >0.3 min.
- T_f >1.5 at 5% peak height.

- Quality 3
- Asymmetry >5 at 10% peak height.
- FWHM >0.5 min.
- T_f >5 at 5% peak height.
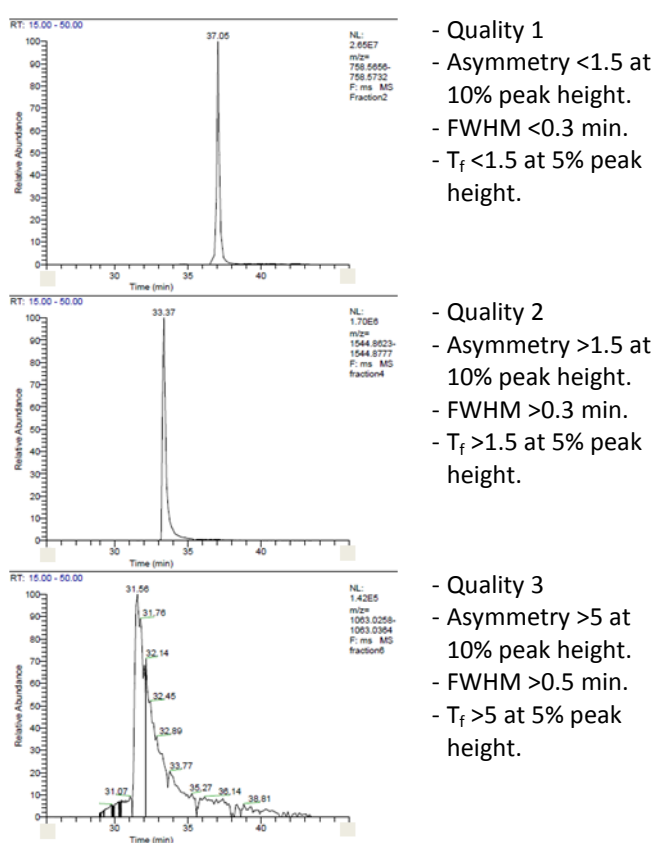
Figure 24. HPLC Peak Quality Parameters. The initial separation of standards by a three-part HPLC gradient was assessed by three parameters; peak asymmetry, full width half maximum (FWHM) resolution and USP tailing factor (T_f) (USP, 1990). Elution peaks for the predominant ions in each standard were assigned quality ratings from 1 (top) to 3 (bottom). Most simple phospho- and sphingolipids scored 1 while larger more complex glycosphingolipids scored 2-3.

gradient was not suitable for the separation of structural isomers. It was concluded that these HPLC settings, which were originally applied to the separation of more simple lipids, required optimisation for the analysis of larger more complex glycosphingolipids.

4.2.2   Optimisation of HPLC Parameters using Commercial Ganglioside Extract

4.2.2.1 Direct Injection Analysis of Commercial Ganglioside Extract

A commercial ganglioside extract (CGE) from bovine brain was used to optimise HPLC settings for ganglioside analysis. This was initially analysed by direct injection to define the major components. Peaks were picked manually and accurate mass searches performed in the Human Metabolomic Database (HMDB), Scripps Center for Metabolomics METLIN: Metabolite and Tandem MS Database and Lipid MAPS (Metabolite and Pathways Strategy) structure database.   Identifications were made for all selected m/z in the METLIN and LipidMAPS databases while only two were identified using HMDB. Many lipid species including but not exclusively gangliosides were detected as well as contaminating plasticizers, free fatty acids and other small metabolites (Figure 25). Mass filters for the major detected species, as well as mammalian gangliosides GM2, GM3, GD3 and GQ1 were prepared to simplify assessment of ganglioside separation. Details of the components of the two filters, covering either the d18:1/18:0 or d18:1/20:0 species are described in Materials and Methods 2.7.3.1 with putative identifications and expected m/z.

4.2.2.2 Optimisation of HPLC Solvent System

Three solvent systems including an adapted ternary system based on previous glycosphingolipidomic publications were compared for the separation of CGE on a reverse phase C30 column (Fong et al., 2009; Ikeda et al., 2008; Ikeda & Taguchi, 2010). Details of each system; the ternary system, an IPA gradient and an acetonitrile gradient, referred to as system 1, 2 and 3 can be found in Materials and Methods 2.5.3. The total ion chromatogram (black), and extracted ion chromatograms of sulfatide (d18:1/24:1) and phosphatidylserine,
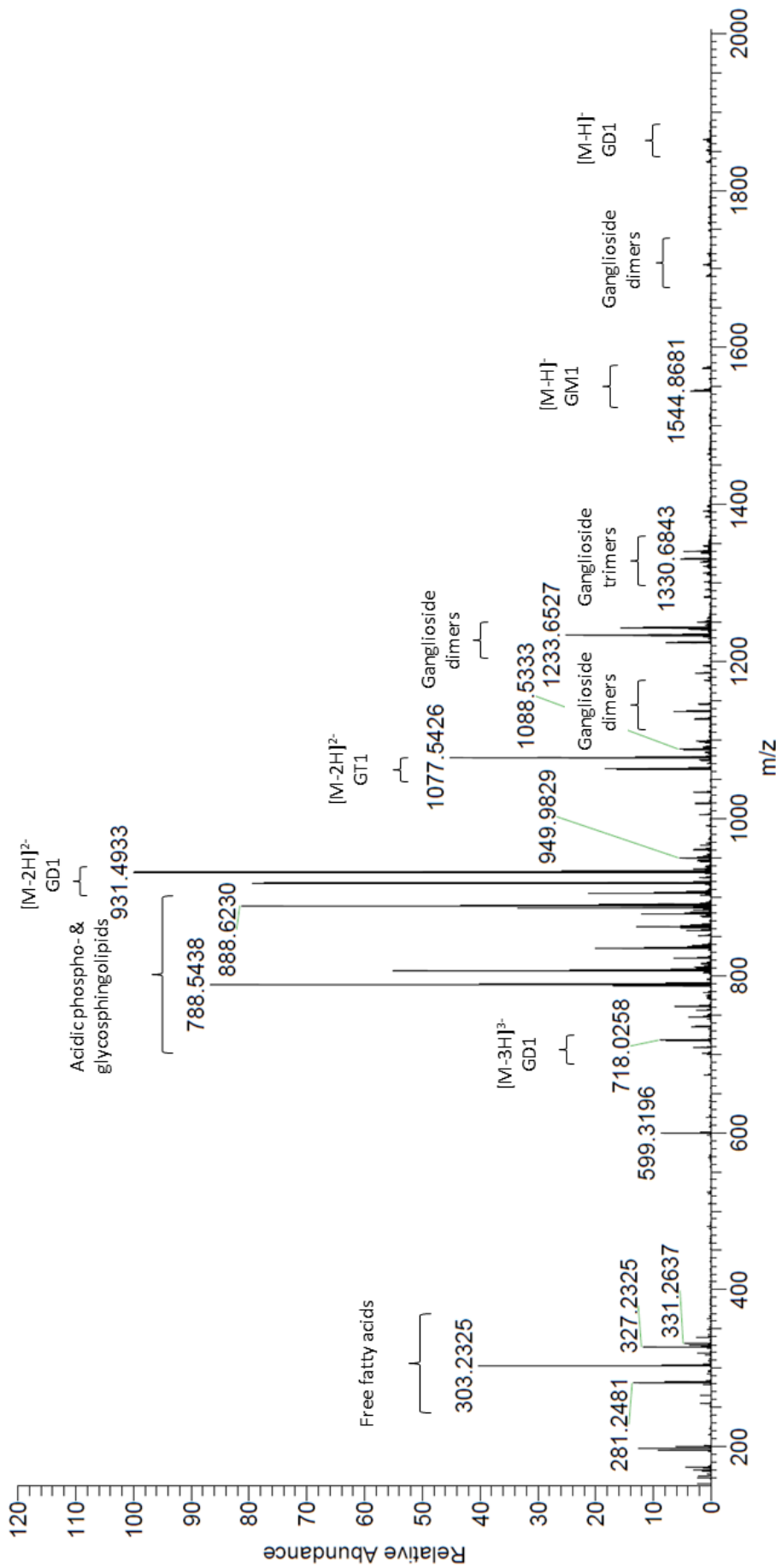
Figure 25. Direct Injection Analysis of Commercial Ganglioside Extract Composition. CGE from bovine brain was used to optimise HPLC settings. First the composition was investigated using direct injection MS-analysis. The major components corresponded to ganglioside ions in various charge states. Free fatty acids were identified in the lower mass range. Acidic phospholipids and sphingolipids were also detected as well as contaminating plasticisers and polymers. Mass filters for the major components were set up in to simplify assessment of chromatography separation during optimisation.

GM1, GM3, GD1, GT1 and GQ1 (all d18:1/18:0) (green) and GM1, GM3, GD1, GT1 and GQ1 (all d18:1/20:0) (blue) are shown for each system in Figure 26.

Brackets indicate elution of gangliosides (red), simple sphingolipids and phospholipids (purple) and polymers (orange). It was apparent that system 3, the IPA gradient provided the optimum separation of the three conditions tested. Lipids of interest eluted over 14.08 min compared to 1.82 min using system 1 and over 15.98 min with significant variability using system 2 (raw retention data can be found in Appendix 1). Individual elution peaks were well resolved with symmetrical if slightly broad peak shapes and gangliosides separated by lipid head and tail group. System 3 was also the only system capable of near base line separation of structural isomers such as GD1a and GD1b. These isomeric species co-eluted in systems 1 and 2.

4.2.2.3 Hydrophilic Interaction and Reverse Phase Columns

Systems 2 and 3 were then used to compare separation of a ganglioside extract from murine brain by normal and reverse phase (RP) chromatography. In both cases the isopropanol gradient resulted in superior separation and elution peak quality over the acetonitrile gradient. Figure 27 shows base peak chromatograms and ganglioside (d18:1/18:0 mass filter) separation using normal (base peak chromatogram – black, XIC – green) and reverse phase (base peak – blue, XIC – red) columns for this gradient. Inserts show full scan mass spectra at the retention time of ganglioside GT1 d18:1/18:0 on the normal (Figure 27b) and reverse phase (Figure 27c) columns. Red stars indicate the GT1 d18:1/18:0 species, blue the d18:1/18:1 and green the d20:1/18:1. Elution peak shapes were comparable on both columns. Gangliosides with the same head groups co-eluted on the HILIC column regardless of fatty acid structure. While this made identification of the head group (without dissociation) easier, distinguishing adducts from structural modifications and overlapping isotopic peaks was simpler on the reverse phase column. The base peak chromatograms shown in Figure 27 also indicated that non-ganglioside lipids such as sulfatide and phosphatidylserine did not elute cleanly from the HILIC column.
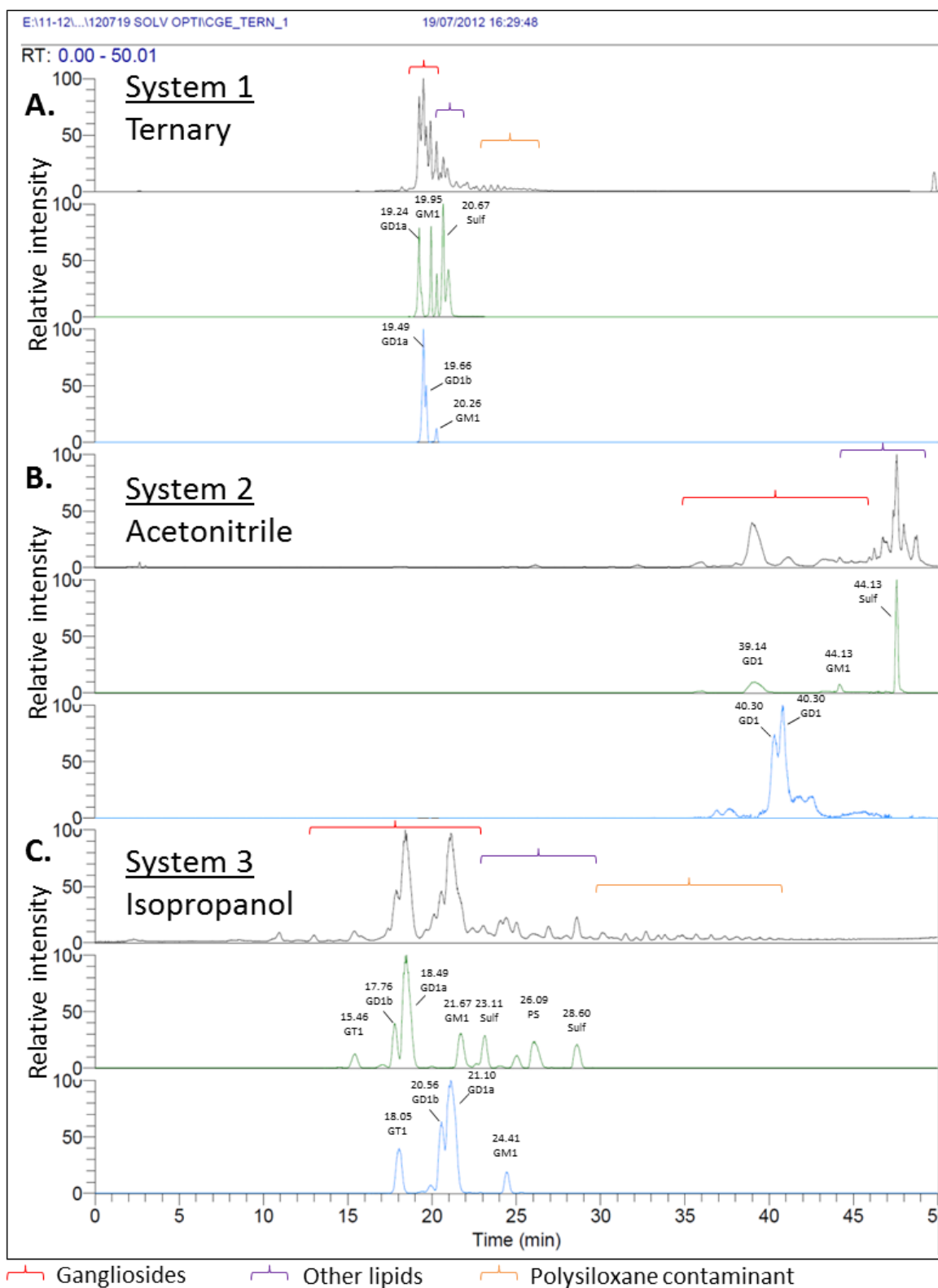
Figure 26. Separation of CGE by Three Reverse Phase Solvent Systems. System 1 – ACN/IPA/amm. form. System 2 – binary ACN/amm. form. System 3 – binary IPA/amm. form. Full chromatograms (black) indicated optimal separation of gangliosides (red bracket), other lipids (purple bracket) and polymers and plasticisers (yellow bracket) using system 3. This was clarified when mass filters for d18:1/18:0 gangliosides (green) and d18:1/20:0 gangliosides (blue) were applied. System 3 clearly provided the best separation of different ganglioside species.
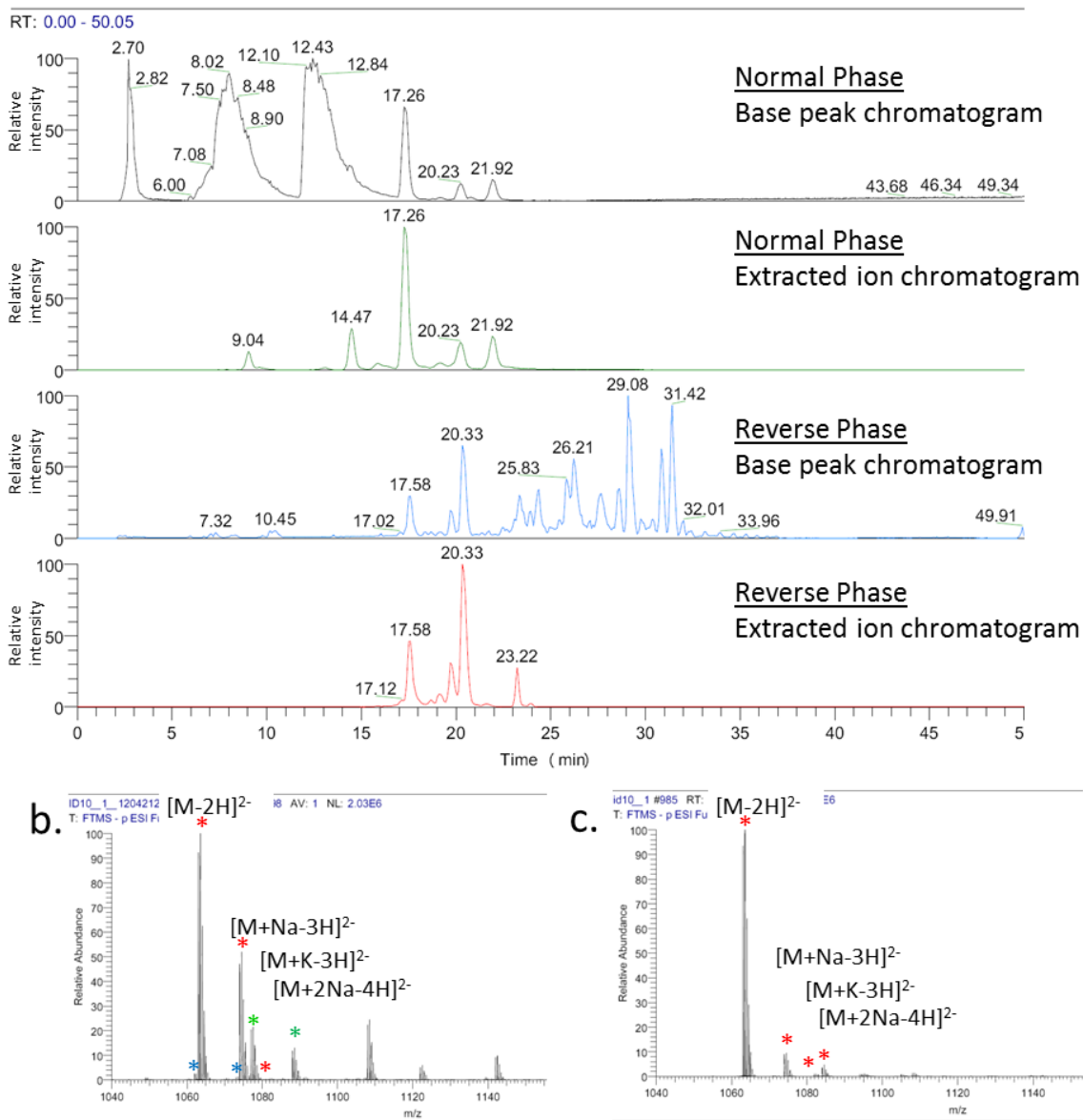
Figure 27. Separation of CGE by Normal and Reverse Phase Chromatography using an Isopropanol Gradient. Lipid separation (base peak chromatograms) of a ganglioside extract from murine brain was cleaner using reverse phase chromatography. Using a normal phase column, non-ganglioside lipids showed significant peak tailing. Extracted ion chromatograms using mass filters for ganglioside d18:1/18:0 species indicated similar quality separation of ganglioside by both methods. However closer inspection of individual spectra (panels b and c, full spectra from the time point of the elution of ganglioside GT1b) showed that spectra were easier to interpret using reverse phase chromatography. Using normal phase chromatography (b) the GT1b head-groups eluted at a single time point regardless of ceramide structure. The full spectrum contained multiple adducts of the d18:1/18:0 (red star), d18:1/18:1 (blue star) and d20:1/18:0 (green star) species. Minor modifications to the ceramide structure could be missed in the complexity of this spectrum. Reverse phase chromatography resulted in separation by head group and by ceramide structure. The full spectrum contained only adducts of the d18:1/18:0 species. The other ceramide structures eluted at distinct time points. Minor modifications were therefore easier to detect and distinguish by reverse phase chromatography.

4.2.3 Analysis of Lipid Standards by MS Dissociation and HPLC-MS to Build a Databank of Standard Retention Times and Product Ion Spectra

The configuration used here is capable of monoisotopic mass detection with better than 5 ppm accuracy. This significantly narrows the search breadth for putative identifications. For example the monoistopic m/z of sulfatide (d18:1/24:1) is 888.623461. A LIPID MAPS database search using 0.05 Da mass tolerance (56.2 ppm) returns 13 different lipid entries. Reducing tolerance to 0.005 Da returns one entry; sulfatide (d18:1/24:1). That said, according to the Metabolomics Standards Initiative evidence should come from two independent and orthogonal data sources in order to confirm identifications. Orthogonal sources include known retention times and tandem mass spectrometry data. In order to amass these available standards including gangliosides, sphingolipids and phospholipids were analysed by direct injection to optimise dissociation and describe fragmentation pathways in depth. Standards were then analysed using the HPLC method described above to establish retention times.

4.2.3.1 Selection of Peaks for Dissociation

Lipid standards were ionised in their preferred polarities as described in Table 13. Full scans were collected from m/z 400-2000 for 20 seconds. For each standard the top 20 peaks were extracted from a defined mass range encompassing the m/z of the most abundant ion (as reported previously) +/- 50 Da. This range was used in order to capture possible variations in the fatty acid chain structure. Database searches were then used for putative identification of the extracted masses. Peaks of interest that did not return an identification were included if they were recognised as common modifications of an identified species. All standards investigated contained multiple fatty acid structures. For gangliosides this was almost exclusively ceramide substructures of d18:1/18:0 and d20:1/18:0 ionised as simple cations ($[M-H]^-$, $[M-2H]^{2-}$) and more complex adducts including multiply charged dimers and trimers. Other sphingolipids such as sphingomyelin and hexosylceramides showed more diverse fatty acid structures. The most common fatty acid modifications observed were the addition or loss

of a double bond (+/- 2.0157 Da) or a change in fatty acid chain length by C2H4 (+/- 28.0313 Da).

4.2.3.2 HCD and CID Dissociation – Establishing Collision Energies

Putatively identified peaks from each standard were selected for dissociation using collision induced dissociation and high energy collision induced dissociation. Collision energies from 10-60 eV were applied for CID and 20-75 eV for HCD. Product ion spectra for non-ganglioside lipids were similar using CID or HCD although in positive ion mode HCD resulted in higher product peak intensities for all but sphingomyelin. For gangliosides and acidic lipids other than phosphatidylserine product ion intensities were higher and more unique fragments observed using CID.

4.2.3.3 Analyisis of Product Ion Spectra

Product ion spectra for each lipid standard were analysed for characteristic ions and neutral losses that were conserved and could be used to support putative identifications by accurate mass in unknown mixtures. Analysis was done using a combination of Lipid MAPS glycosphingolipid product ion search tool, manual analysis of structural sketches and previous publications on lipid fragmentation.

4.2.3.3.1 Glycerophospholipids

Phospholipid fragmentation has been documented previously using various instrumental set ups (X. Han & Gross, 1994; Ivanova, Milne, Byrne, Xiang, & Brown, 2007; Pulfer & Murphy, 2003). Ion transfer schemes have been proposed for the formation of the most ubiquitously reported product ions such as the loss of the phospholipid head-group. This neutral loss has been used diagnostically in triple quad reaction monitoring studies for the detection of different subclasses including glycerophosphocholine and glycerophosphoethanolamine. These and other commonly published phospholipid product ions or neutral losses are described in Table 14. A rudimentary glycerophospholipid MSMS database and MSMS

Table 14. Commonly Reported Product Ions for Phospholipid Classes.

Lipid	Loss of strucure	Mass
Glycerophosphocholine	Choline	[M+H-59]-
	phosphocholine	[M+H-184]-
	Fatty acyl as free fatty acid	[M+H-$R_{1/2}$'COOH]+
	Fatty acyl as ketene	[M+H-$R_{1/2}$'CH=C=O]+
Glycerohosphoethanolamine	Ethanolamine	[M+H-141]+
	Fatty acyl as ketene	[M-H-$R_{1/2}$'CH=C=O]-
Glycerophosphoinositol	Fatty acyl as free fatty acid	[M-H-$R_{1/2}$'COOH]-
	Fatty acyl as ketene	[M-H-$R_{1/2}$'CH=C=O]-
Glycerophosphoglycerol	Fatty acyl as free fatty acid	[M-H-$R_{1/2}$'COOH]-
	Fatty acyl as ketene	[M-H-$R_{1/2}$'CH=C=O]-
	Both acyls as ketene and acid	m/z 227
	Both acyls as acids	m/z 209
Glycerophosphoserine	phosphoserine	[M+H-185]+
	phosphoserine + fatty acyl as ketene	[M+H$R_{1/2}$'CH=C=O-185]+
Sphingomyelin	phosphocholine	[M+H-184]-

spectrum prediction tool are also available on the LIPID MAPS website, although these are exclusively for negative ion mode analysis. Both literature and LIPID MAPS search tools simplified product ion analysis, providing guidance and inspiration for product ion structural elucidation, and support for dissociation pathways using CID and HCD in the LTQ Orbitrap. Because product ion masses are usually reported by their nominal mass the high mass accuracy obtained here sometimes confused product ion identification, so putative product ion structures were checked in ChemSketch for their accurate masses.

Two major conserved dissociations were observed here in glycerophospholipid fragmentation. The first was the neutral loss (NL) of the head group; the breakage of which is illustrated for positive (red) and negative (green) ions in Figure 28. In positive ion mode this occurred at the glycerol 3-sn-phosphoester bond leaving a positively charged carbon in place of the 3-sn-hydroxyl. This was observed in product ion spectra from PC and PE species after a NL of 141.0191 Da (observed 141.0182 Da) and 183.0660 Da (observed 183.0651 Da) respectively. In negative ion mode this occurred at the second bond of the phosphodiester, leaving a characteristic product ion with a phosphatidic acid in place of the original head group. This was
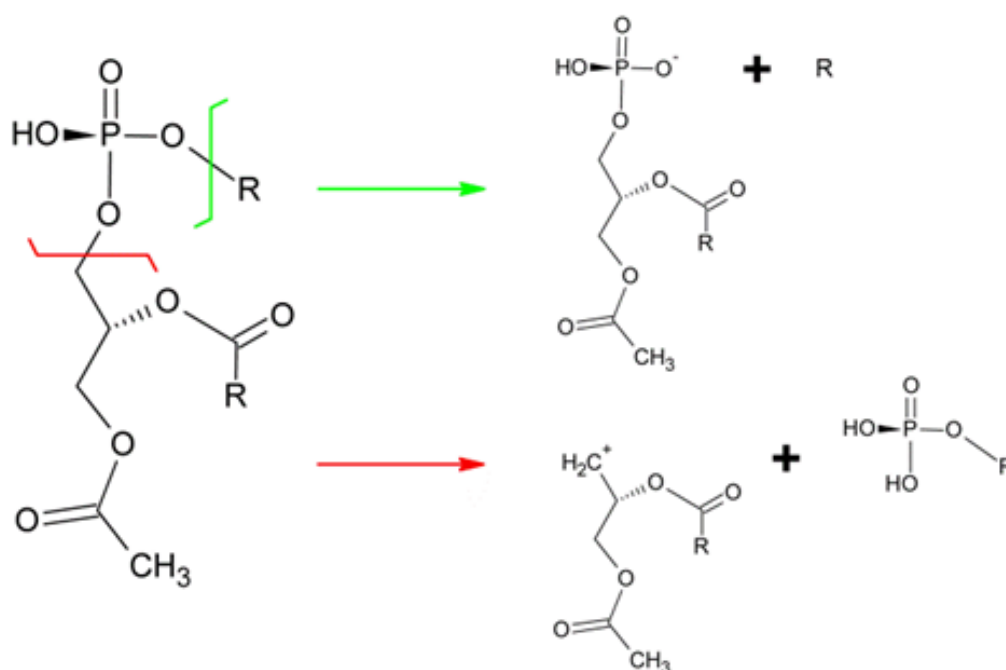
Figure 28. Phospholipid Headgroup Breakage Positions in Negative (green) and Positive (red) Ion Mode.

observed from glycerohosphoserines after a NL of 87.0320 Da (87.0319 Da observed) and from glycerophosphoglycerols in combination with the neutral loss of one of the fatty acids.

Other dissociations were consistently observed in the product ion spectra of PC, PG and PS as well as cardiolipin. These included the dissociation of a fatty acid at the *sn*-1 and *sn*-2 position (positions could not be distinguished without further investigation) as reported in Table 2. Product ions corresponding to the resulting lyso-glycerophospholipid were identified both with and without the third glycerol *sn*-3-hydroxyl within single spectra confirming the NL of free fatty acids and fatty acid ketenes. In product ion spectra from glycerophospholipids containing distinguishable fatty acids (different carbon number and/or saturation), product ions were detected corresponding to the NL of both fatty acids suggesting that dissociation can occur from glycerol *sn*-1 and *sn*-2 positions. Figure 29 illustrates product ions corresponding to the dissociation of both fatty acids and also the breakage positions either side of the ester oxygen for PC C18:1/16:0 in positive ion mode and PG C18:1/16:0 in negative ion mode. This has been
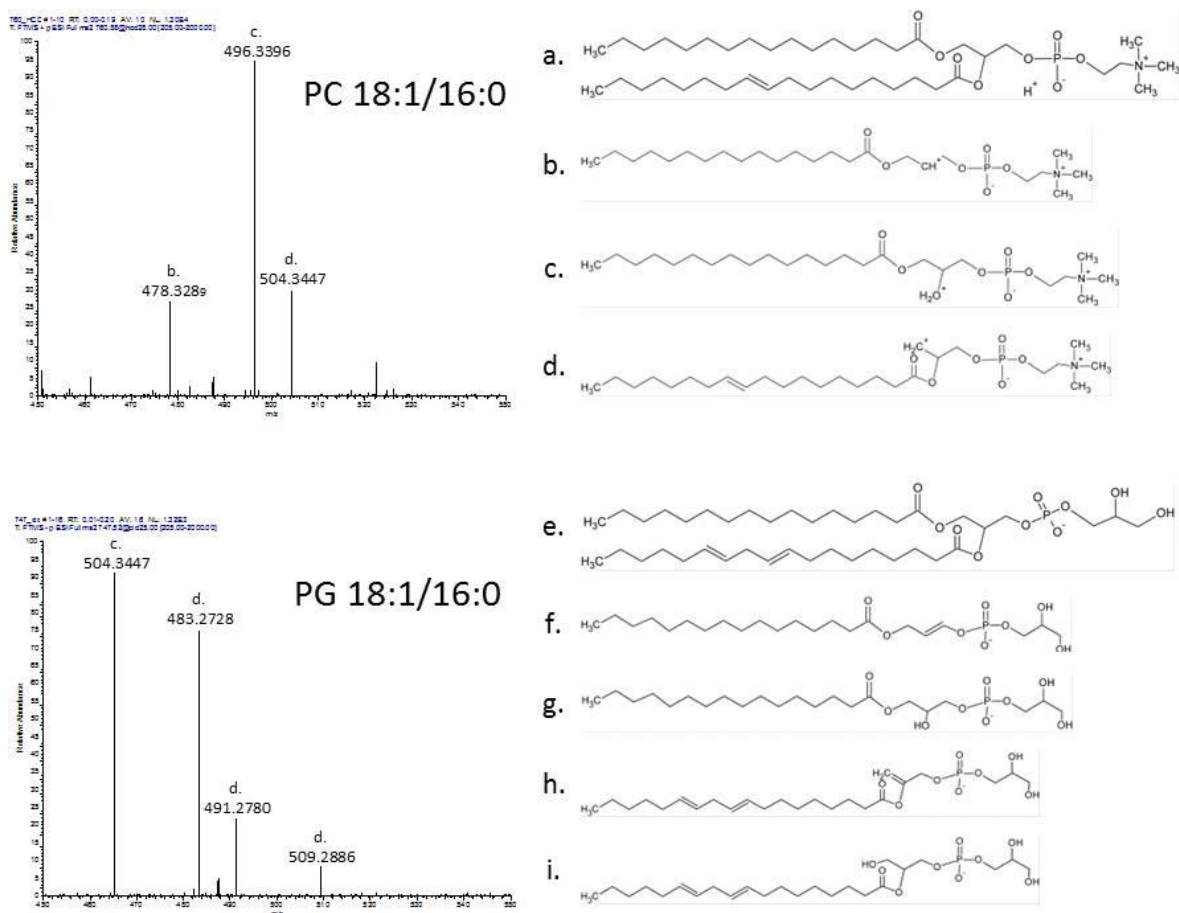
Figure 29. Phospholipid Product Ion Spectra; Glycerophosphocholine and Glycerophospho-glycerol. Several dissociations were consistently observed between product ion spectra from different glycerophospholipid species including PC, PG, PS and cardiolipin. Product ion spectra are shown from PC 18:1/16:0 in positive ion mode after HCD and PG 18:1/16:0 in negative ion mode after CID to illustrate this. (Few unique peaks were observed for HCD or CID). These included dissociations of the fatty acid in either the *sn*-1 or *sn*-2 position (it was not possible to distinguish these positions without further dissociation) (product ions a-i) before (c, g, i) and after (b, d, f, h) the glycerol hydroxyl group from the loss of fatty acids and fatty acids ketenes. For glycerophospholipids with distinguishable fatty acids, like those shown here, neutral losses pertaining to the loss of both fatty acid masses were detected, suggesting that dissociations occur from both *sn-* positions, or that one *sn-* position is more volatile and could be occupied by different fatty acids.

observed before and can apparently change in ratio of *sn*-1 and *sn*-2 carboxylate ions with

collision energy (Hvattum, Hagelin, & Larsen, 1998) and sn-2 acyl structure (Huang, Gage, &

Sweeley, 1992).

Cardiolipin had a more complex product ion spectrum. Cardiolipins are often excluded from

phospholipid publications and the LIPID MAPS phospholipid database which made

identification of product ions more difficult. Still several targeted studies were found to assist

product ion analysis and the majority of detected peaks were putatively identified (F.-F. Hsu et

al., 2005; Lesnefsky, Stoll, Minkler, & Hoppel, 2000; Minkler & Hoppel, 2010). Some ions were

common to product ion spectra from both the [M-H]$^-$ and [M-H]$^{2-}$ precursor ions (Fig 30, a,b)

while others were unique to each precursor charge state (Fig. 30, product ion spectra from
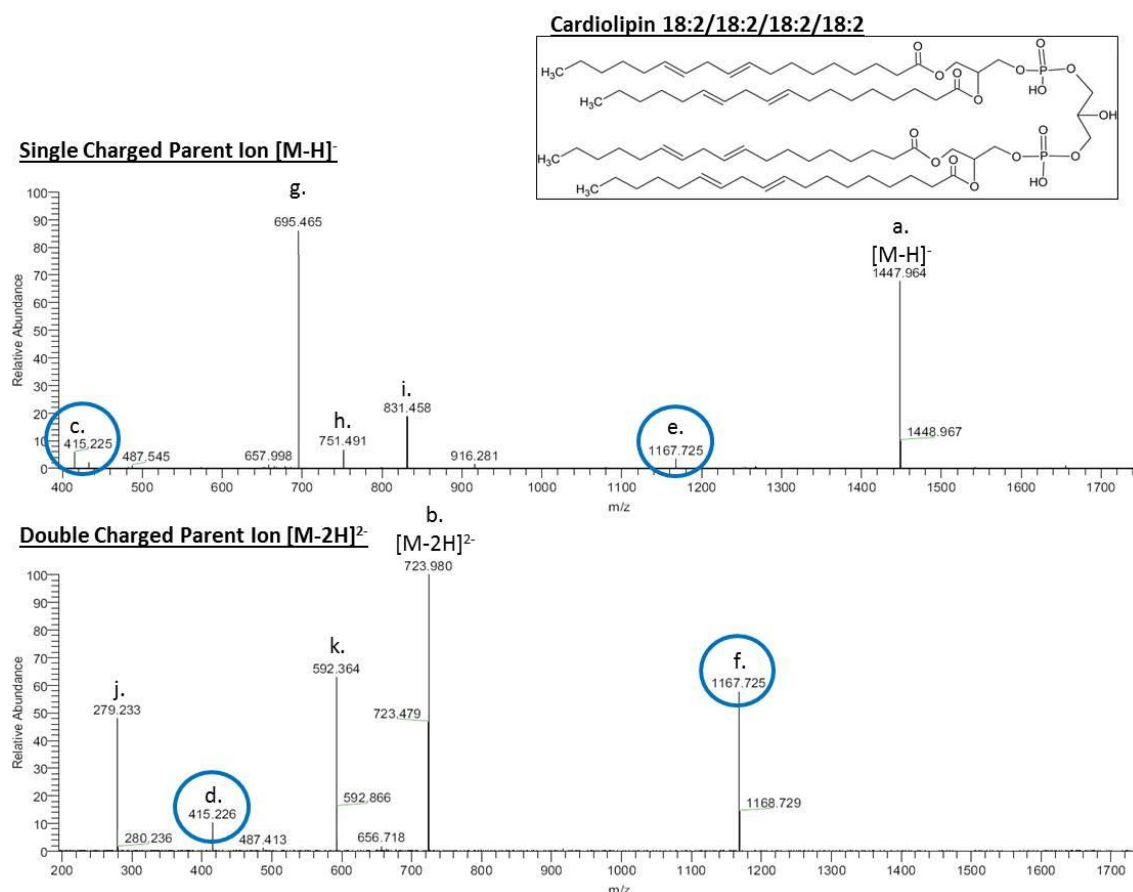
Figure 30. Cardiolipin Product Ion Spectra. CID dissociation of cardiolipin precursor ions in different charge states resulted in some unique and some conserved product ions. This is illustrated in negative ion mode for cardiolipin 18:2/18:2/18:2/18:2 [M-H]$^-$ (a) and [M-2H]$^{2-}$ (b) ions. Several ions, circled in blue, were common to both product ion spectra, including a fatty acid fragment ester linked to a cyclic 2-carbon phosphate structure (c, d, m/z 415.225) and the product ion of a neutral loss of a complete PC structure (e, f, m/z 1167.725). Other product ions were however unique to the different charge states. From the [M-H]- precursor these included phosphatidic acid (g, m/z 695.465), glycerol-linked phosphatidic acid (h, m/z 751.491) and glycerophopho-linked phosphatidic acid (i, m/z 831.458). From the [M-2H]$^{2-}$ precursor unique product ions included a dissociated fatty acid (j, m/z 279.233) and the corresponding lyso-cardiolipin (k, m/z 592.364).

cardiolipin C18:2/18:2/18:2/18:2 [M-H]$^-$ and [M-H]$^{2-}$). Common product ions included the neutral loss of a complete PC structure through dissociation of the glycerol sn-3 ester on the biphosphate-linked (central) glycerol (Fig. 30 e, f) and a fatty acid fragment ester linked to a cyclic 2-carbon phosphate structure (Fig. 30 c,d). Products ions exclusively arising from fragmentation of the [M-H]$^-$ precursor ion included a phosphatidic acid, glycerol-linked phosphatidic acid and a glycerophospho-linked phosphatidic acid (Fig. 30 g, h, i) from consecutive dissociations of the ester bonds that link the phospho-glycerol-phosphate head group. A similar pathway has been described before for diacyl cardiolipin product ions involving the exchangeable hydrogens on the phosphate (F.-F. Hsu et al., 2005). Products ions exclusively arising from fragmentation of the [M-2H]$^{2-}$ precursor included a lyso-cardionlipin from the loss of one of the four fatty acids by dissociation of the glycerol ester bond and the corresponding fatty acid (Fig. 30 j, k). Identifications largely agreed with those already published. It must be mentioned that the complication of multiply charged ions and a lack of conserved cardiolipin dissociation nomenclature made the results of previous studies difficult to apply during analysis and were more useful for retroactive confirmation of putative identifications.

4.2.3.3.2   Simple Sphingolipids

Compared to phospholipids fewer resources exist for the analysis of simple sphingolipids. Review publications are not as abundant and LIPID MAPS has only an MS precursor ion search tool. That said fragmentation of simple sphingolipids has been reported previously on triple quad instruments by CID (F.-F. Hsu, Bohrer, & Turk, 1998; Merrill et al., 2005; Yang, Cheng, Gross, & Han, 2009). It was therefore surprising then when good quality data was not obtained from sulfatide nor sphingomyelin precursors in either polarity using CID or HCD. Sulfatide MS scans in negative ion mode revealed many intense peaks that were putatively identifiable as sulfatides and easily isolated for dissociation. However product ion spectra were very low intensity despite adjusting several of CID and HCD settings. Previously reported product ions at

m/z 259, 257 and 241 from the 3-sulfogalactosyl structure and neutral loss of 242, the sulfatide head group, were not detected (F.-F. Hsu & Turk, 2004). The [HSO4]$^-$ ion sometimes reported was below the lower mass cut-off of the instrument used here (R. Sandhoff et al., 2002; Whitfield, Sharp, Johnson, Nelson, & Meikle, 2001). Two low intensity product ions (m/z 656.7 and m/z 487.5) that were consistently observed in sulfatide product ion spectra could not be assigned structures or identified from the literature. No other peaks were observed that could be used to confirm sulfatide identifications. However this characteristic lack of dissociation, even at high collision energies, could be used to indicate sulfatide precursors in complex mixtures.

Sphingomyelin ionised poorly in negative ion mode but putatively identifiable peaks were observed in full scans in position ion mode. Unlike sulfatide when these were selected for dissociation, product ion spectra contained good quality peaks several of which were consistently observed from multiple precursor ions. However reported dissociations on triple quad instruments, such as the loss of the fatty ester and glycerophosphocholine head-group, were not observed (Bielawski, Szulc, Hannun, & Bielawska, 2006; Byrdwell, 1998; Isaac, Bylund, Månsson, Markides, & Bergquist, 2003). Instead loss of water from the [M+H]$^+$ ion was the most consistent alteration. Peaks at m/z 321.32, 338.35 and 378.82 were observed in product ion spectra from three or more different sphingomyelin precursors but could not be identified. These could have been the result of complex rearrangements dependent upon very specific conditions such as the presence of a contaminant. As sphingomyelin ionises poorly if at all in negative ion mode it was concluded that this lack of confirmatory dissociation data should not interfere with ganglioside analysis by HPLC-MSMS in negative ion mode.

Fragmentation of ceramide, illustrated in Figure 31 for the d18:1/18:0 species, was more successful in positive ion mode (ionisation was poor in negative ion mode). Peaks were observed at [M+H-18.0102]$^+$ and [M+H-30.0103]$^+$ from neutral loss of water and a consequent carbon, most likely from the C_1 position. Other peaks were identified from various breakages

of the sphingosine-fatty acid amide bond (Fig. 31 m/z 300.290, 282.279, 252.269), with the neutral loss of the C_1 and C_3 hydroxyls (Fig. 31 m/z 264.269). Variations in the fatty ester and sphingosine base meant that products ions were specific to each ceramide without being characteristic of the group which was consistent with previous studies (Bielawski et al., 2006; Colsch et al., 2004). Similar ceramide-like product ions were observed in spectra from hexosylceramides which also ionised more efficiently in positive ion mode. Other hexosylceramide fragments corresponded to the distinctive neutral loss of the hexose before and after the oxygen of the glycosidic bond and after the C_1 carbon of the sphingosine. Schemes for this head-group loss, which is also used diagnostically in reaction monitoring studies, have been described previously (F. F. Hsu & Turk, 2001).
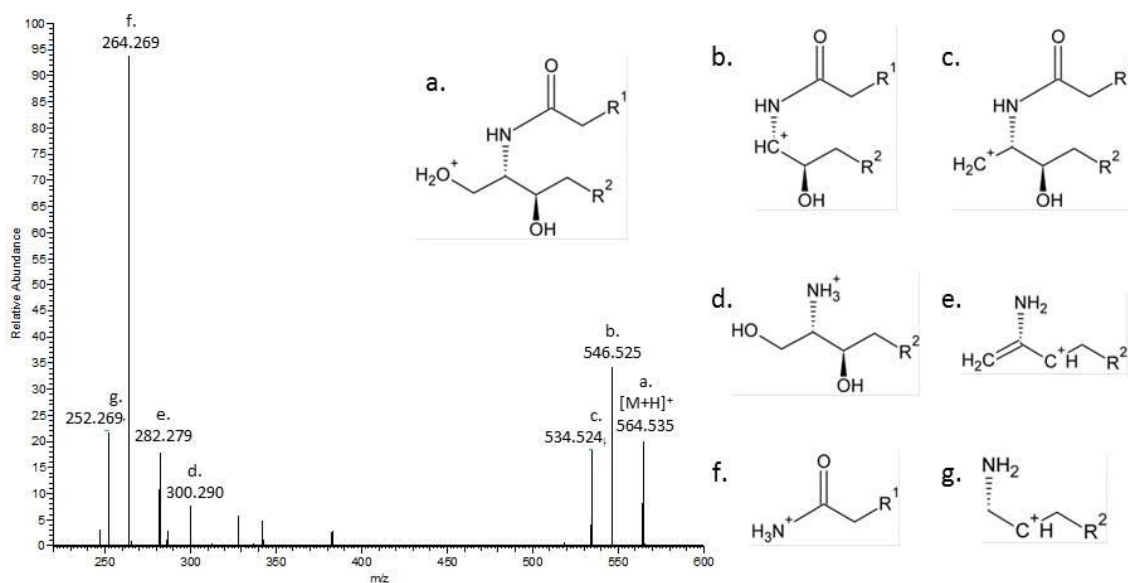
Figure 31. Ceramide Product Ion Spectra. A series of dissociations were consistently observed in the product ion spectra of ceramide species. These are illustrated for the precursor ion ceramide d18:1/18:1 (a, m/z 564.535) [M+H]$^+$ ion in positive ion mode after HCD where R^1 refers to C14:1 and R^2 to C16:1. Product ions included the neutral loss of water from the molecular ion and further loss of a carbon (b, m/z 546.525 and c, m/z 534.524). Other peaks were identified from breakages of the sphingosine-fatty acid amide bond (d, m/z 300.290, e, m/z 282.279 and f, m/z 264.269) and loss of the C_1 and C_3 hydroxyls (g, m/z 252.369). Because most of these dissociations encompassed the fatty acid/spingosine moieties, which were not unique to ceramides, no diagnostic fragments were identified.

124

4.2.3.3.3 Complex Glycosphingolipids

Ganglioside fragmentation was originally addressed in 1988 by Domon and Costello who dissociated several glycolipids including gangliosides so comprehensively by FAB-MS/MS that a new naming system was required (B Domon & Costello, 1988). It is this system (Figure 32) that is used throughout this section (Domon & Costello 1988[b]). Since this early effort not many publications have systematically addressed ganglioside fragmentation and few if any appear to use an LTQ orbitrap to do so. Many studies simply monitor for the loss of a sialic acid fragment (m/z 291) in order to identify gangliosides (Tsui et al., 2005). Still the limited background of literature alongside a LIPID MAPS glycosylceramide MS/MS search tool assisted product ion assignment in this section and confirmed similar dissociation patterns in the LTQ orbitrap to those previously observed. Manual rearrangement of structural sketches was also employed to identify some fragments and confirm accurate masses for others as again most publications report nominal masses. The d18:1 and d20:1 sphingosine structures were assumed, although no dissociation of the fatty acid and sphingosine were observed in negative ion mode, in order to simplify analysis. This is consistent with previous negative ion mode fragmentation. Product
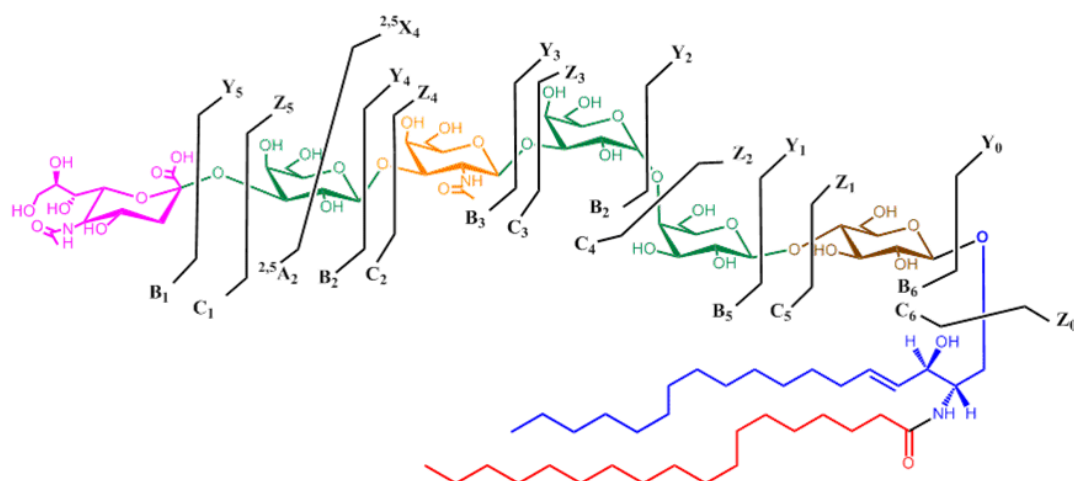
Figure 32. Ganglioside Fragmentation Nomenclature (Domon & Costello 1988)**.** Image adapted from LipidMAPS. In 1988 Domon and Costello dissociated gangliosides and gylcosphingolipids to such a high degree that a new nomenclature was required to define the position of breakages in the individual sugars and within the carbohydrate chain. This nomenclature, similar to the ion labels given to peptide fragmentations, is shown here and used throughout the chapter to describe glycosphingolipid dissociation.

ion spectra were initially collected from the d18:1/18:0 precursor unless stated. Identified

fragments were then confirmed from the d20:1/18:0 precursor.

Monosialylated gangliosides produced the simplest product ion spectra to interpret due to the

formation of only singly charged ions. Despite the available resources several minor peaks

including m/z 1346.7960 from GM1, mz 1184.7428 from GM2 (both from a neutral loss of

198.074) and m/z 884.6101 and 708.5776 from GM3, as well as m/z 487.5 detected in spectra

from all three, were not identified manually or from the literature and LIPID MAPS resources.

Identified product ions are described in Table 15 and in product ion spectra in Figure 33. [M-

H2O-H]$^{-}$ and [M-COOH]$^{-}$ ions (Δmz -18.0106 and Δmz -43.9898 respectively) were detected in

Table 15. Identified Monosialylated Ganglioside Product Ions.

Precursor	Ion	m/z	Product Ion	m/z	NL
GM1	[M-H]$^{-}$	1544.8694		**487.515	
d18:1/18:0			Y_1	726.5889	GalGalNAc(Neu5Ac)GalGlu
			$Y_{2\alpha}/Y_{2\beta}$	888.6418	GalGalNAc & NeuAc
			$(Z_{2\alpha}/^{3,5}X_{2\beta})$ or		
			$(^{2,4}X_{2\alpha}/Z_{2\beta})$	983.6789	
			$Z_{3\alpha}/Y_{2\beta}$	1073.7106	
			$Y_{3\alpha}Y_{2\beta}$	1091.7211	Gal & NeuAc
			$Y_{2\alpha}$ [M-COOH]-	1136.7469	GalGalNAc
			$Y_{2\alpha}$	1179.7372	GalGalNAc
			$Y_{2\beta}$	1253.774	Neu5Ac
			[M-CH3COOH]-	1484.8477	
			[M-COOH]-	1500.879	
			[M-H2O-H]-	1526.8583	
GM2	[M-H]$^{-}$	1382.8166		**487.4957	
d18:1/18:0			$Y_{2\beta}$	888.6418	GalNAc & NeuAc
			$Y_{3\alpha}/Y_{2\beta}$	1091.7211	
			[M-COOH]-	1338.8262	
			[M-H2O-H]-	1364.8055	
GM3	[M-H]$^{-}$	1179.7372		**487.4919	
d18:1/18:0			Y_0	564.5361	Neu5Ac
			Y_1	726.5889	Neu5AcGal
			Y_2	888.6418	Neu5AcGalGlu
			$^{0,2}X_2$	958.6473	^{0,2}A Neu5Ac
			[M-COO]-	1135.7468	
			[M-H2O-H]-	1161.7261	
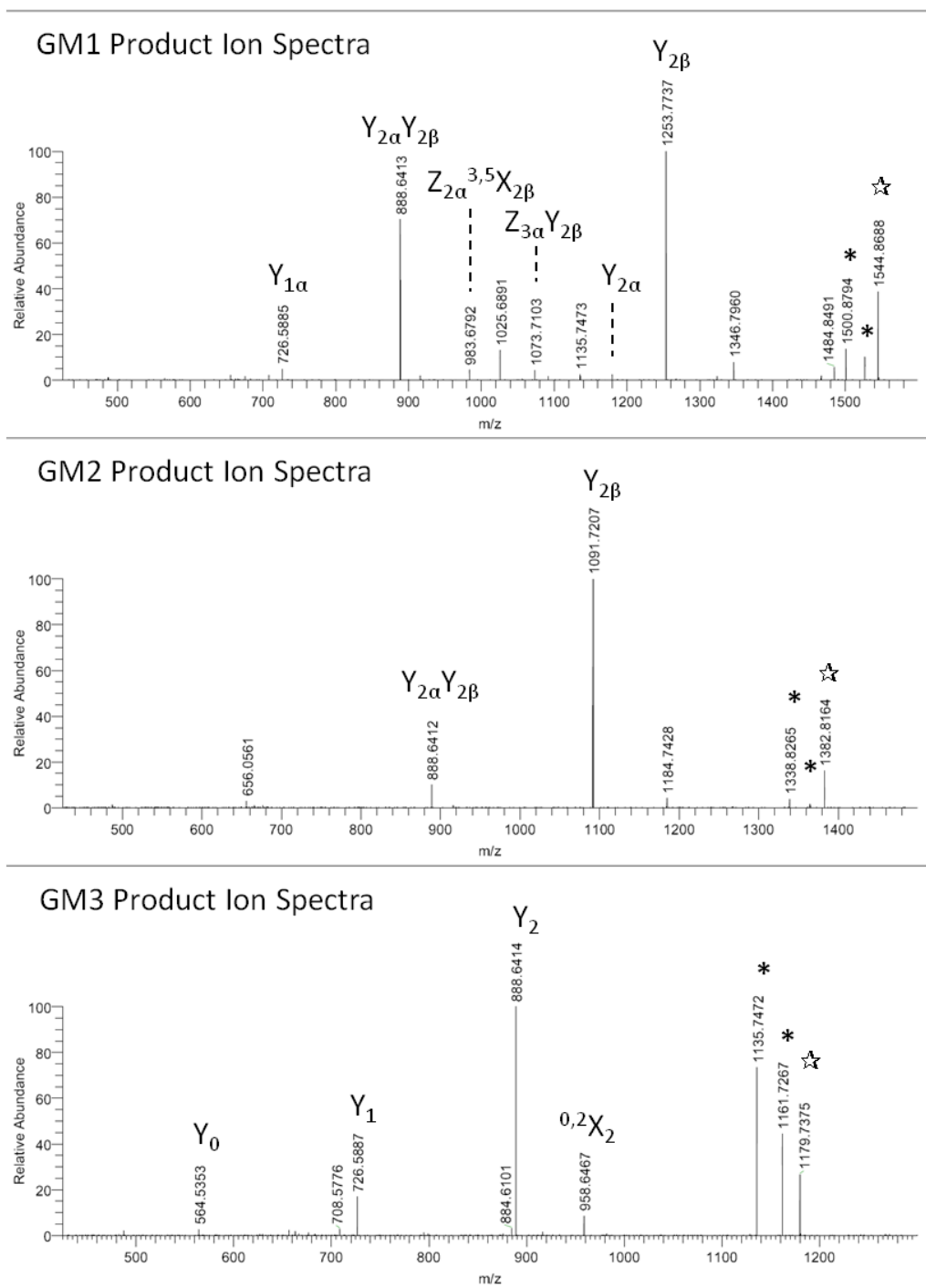
Figure 33. Assignment of Structures to Monosialylated Ganglioside Product Ions. Spectra were collected from the [M-H]$^-$ ions of the d18:1/18:0 species of GM1, GM2 and GM3 in negative ion mode. Many of the peaks identified in the product ion spectra of monosialylated gangliosides were identified as Y-type ions resulting dissociation of the glycan subunits after the reducing termini. These included, for example, Y1, Y2α, Y2β and Y2α/Y2β product ions at m/z 726.5889, 1179.7372, 1253.774 and 888.6418 from GM1, resulting from loss of GalGalNAc(Neu5Ac)GalGlu, GalGalNAc, Neu5Ac, and GalGalNAc & Neu5Ac respectively. Similar step-wise loss of sugars was observed in product ion spectra from GM2 where Y2β and Y2αY2β ionswere identified at m/z 1091.7207 and 888.6412, and GM3 where Y0, Y1 and Y2 ions were identified at m/z 564.5353, 726.5887 and 888.6414. For all monosialylated gangliosides the most abundant product ions came from the loss of the sialic acid (Y2β from GM1 and GM2, Y2 from GM3). Cross-ring fragmentations were also identified from GM1 (Z$_{2\alpha}$/^{3,5}X$_{2\beta}$ or ^{2,4}X$_{2\alpha}$/Z$_{2\beta,}$ m/z 983.6789) and GM3 (^{0,2}X$_2$, m/z 958.6473).

spectra from all three (Fig. 33, marked with a *****).

Remaining peaks were identified mostly as Y-ions from loss of sugars after the glycosidic link. Such Y-ions were the most commonly reported dissociations in early FAB-MS/MS and later CID-MS/MS reports in negative ion mode (B Domon & Costello, 1988; Egge & Peter-Katalinic, 1987; Zaia, 2004). Z-ions arising from neutral loss of sugars after the glycosidic link have been observed less frequently and were not detected here. The most abundant product ions arose from the neutral loss of the sialic acid (Δmz – 291.0954, GM1 m/z 1253.7737, GM2 1091.7207, GM3 m/z 888.6414), a bond that is reported to be particularly labile. Few intra-sugar dissociations were identified. Those that were, included product ions corresponding to $Z_{2\alpha}/^{3,5}X_{2\beta}$ or $^{2,4}X_{2\alpha}/Z_{2\beta}$ at m/z 983.6789 from GM1 and an $^{0,2}X_2$ product ion at m/z 958.6473 from GM3.

Product ion spectra were collected from disialylated gangliosides GD1a, GD1b and GD3 from [M-2H]$^{2-}$ d18:1/18:0 precursor ions as the most abundant in full scan spectra (Fig. 34, ☆). Identified product ions are described in Table 16 and in Figure 34. Peaks corresponding to the neutral loss of water were observed in all spectra (Fig. 34, *). Again few internal sugar dissociations or Z-ions were observed. The most abundant product ions corresponded to recognisable glycosphingolipid sub-structures after the loss of one of more sialic acids. These included GM1 at m/z 1544.8694 (GD1a, GD1b), GA1 at m/z 1253.774 (GD1a, GD1b), GM3 at m/z 1179.7372 (GD3, GD1a) and lactosylceramide at m/z 888.841 (GD1a, GD1b, GD3). Characteristic sialic and disialic acid fragments were also observed at m/z 290.089 (GD1a, GD1b, GD3) and m/z 581.185 (GD1b, GD3). These dissociation patterns provided some insight into the sequence of the glycan head-group and could be used to distinguish structural isomers such as GD1a and GD1b. The literature provides little direct support for this disialylated ganglioside product ion analysis – often they have been excluded from studies for their complexity or, in the case of early FAB-MS papers, analysed as singly charged sodium adducts. That said the patterns of sugar loss observed from singly charged adducts and from

Table 16. Identified Disialylated Ganglioside Product Ions.

Precursor	Ion	m/z	Product Ion	m/z	NL
GD3 d18:1/18:0	$[M-2H]^{2-}$	734.9127	B_1	290.0881	
				493.1675	
			B_2	581.1836	
			Y_2	888.6418	Neu5AcNeu5Ac
			Y_3	1179.7372	Neu5Ac
			$[M-H2O-2H]^{2-}$	*725.9073	
GD1a d18:1/18:0	$[M-2H]^{2-}$	917.478	$B_{1\beta}$ OR $B_{1\alpha}$	290.0881	
			$B_{3\alpha}$	655.2203	
			$C_{3\alpha}$	673.23036	
			$Y_{2\alpha}Y_{2\beta}$	888.6418	Neu5AcGalGalNAc & Neu5Ac
			$Y_{3\alpha}Y_{2\beta}$	1091.7211	Neu5AcGal & Neu5Ac
			$Y_{2\alpha}$	1179.7372	NeuAcGalGalNAc
			$Y_{3\alpha/2\beta}$	1253.774	Neu5Ac & NeuAc
			$Y_{3\alpha}$	1382.8166	NeuAcGal
			$Y_{4\alpha}$ OR $_{2\beta}$ $[M-H]^-$	1544.8694	Neu5Ac
			$Y_{4\alpha}$ OR $_{2\beta}$ $[M-2H]^{2-}$	*771.9329	Neu5Ac
			$^{0,2}X_{4\alpha}$ - COOH	1569.8767	
			$^{0,2}X_{4\alpha}$ $[M-H]^-$	1614.8749	
			$^{0,2}X_{4\alpha}$ $[M-2H]^{2-}$	*806.9360	
			$[M-COO-2H]^{2-}$	1790.9666	
			$[M-H2O-2H]^{2-}$	*908.4756	
GD1b d18:1/18:0	$[M-2H]^{2-}$	917.478	$B_{1\beta}$	290.0881	
				493.1675	
			$B_{2\beta}$	581.1836	
			$Y_{2\alpha}Y_{2\beta}$	888.6418	GalGalNAc & Neu5AcNeu5Ac
			$^{0,5}X_{2\alpha}$	916.6367	
			$Z_{3\alpha}Y_{2\beta}$	1073.7106	
			$Y_{2\beta}$	1253.774	Neu5Ac & NeuAc
			$Y_{3\beta}$	1544.8694	Neu5Ac
			$^{0,2}X_{4\alpha}$	*806.9363	
				*887.4705	
			$[M-COO-2H]^{2-}$	*895.4864	
			$[M-H2O-2H]^{2-}$	*908.4758	

* doubly charged ions
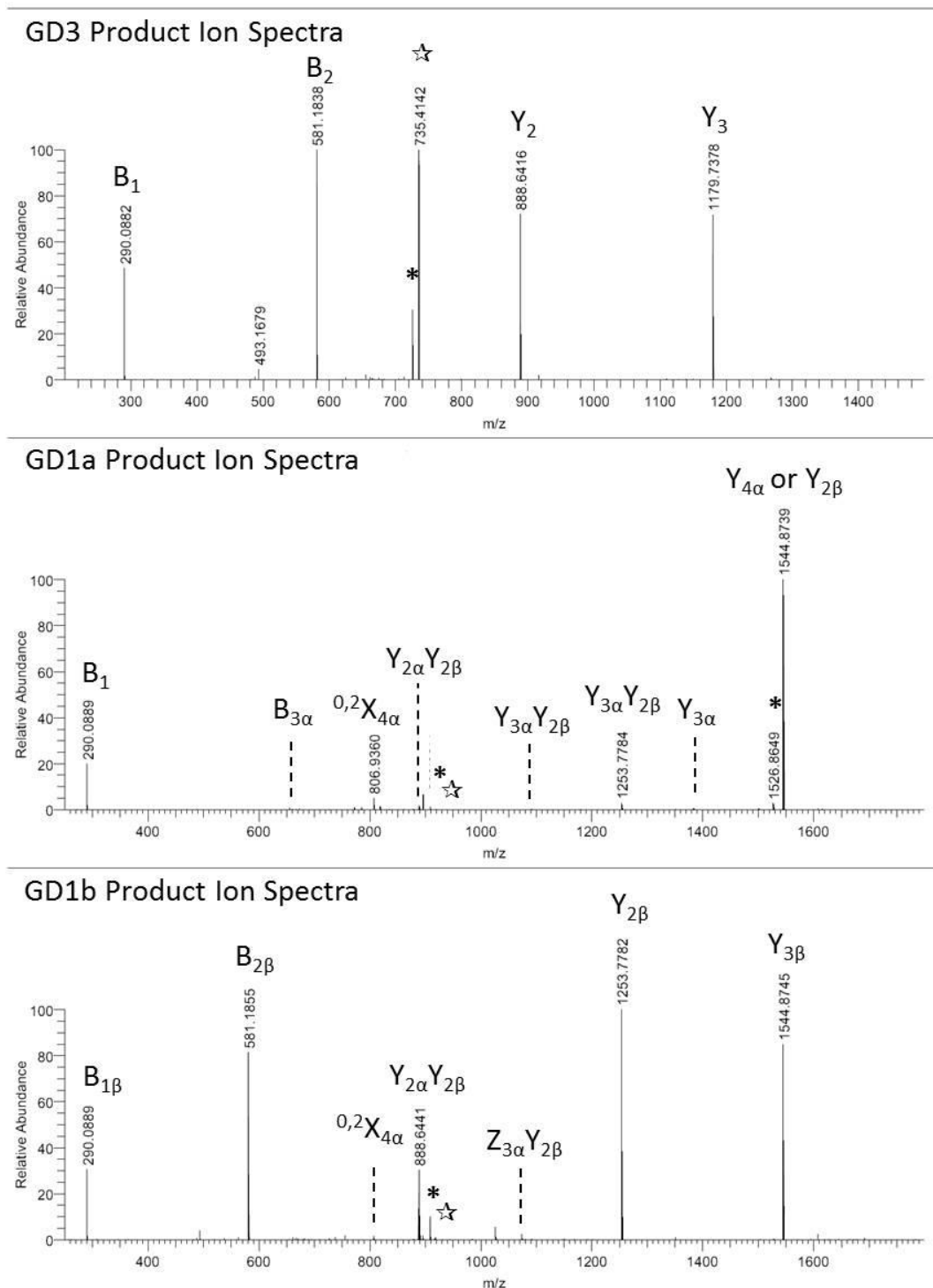
Figure 34. Assignment of Structures to Disialylated Ganglioside Product Ions. Spectra were collected from the [M-2H]$^{2-}$ ions of the d18:1/18:0 species of GD3, GD1a and GD1b in negative ion mode. Many of the peaks were identified as Y-type ions from dissociation of the glycan subunits after the reducing termini. These included Y_2 and Y_3 ions at m/z 888.6416 and 1179.7378 from GD3, from loss of Neu5Ac Neu5Ac & Neu5Ac respectively. The sugar fragment ions, B_1 and B_2, were detected at m/z 290.0882 and 581.1838. Similar dissociations were observed in product ion spectra from GD1a and GD1b resulting in various Y ion formations. The disialic acid product ion was detected at m/z 581.1855 only from GD3 and GD1b and not from GD1a, where the linked sialic acid structure does not occur. The most abundant product ions came from the loss of one sialic acid ($Y_{4\alpha}$ or $Y_{2\beta}$ from GD1a), two sialic acids ($Y_{2\beta}$ from GD1b) or from the sialic acid B ion (B_2 from GD3). Cross-ring fragmentations were identified only occasionally from GD1a ($^{0,2}X_{4\alpha}$, m/z 806.9380) and GD1b ($^{0,2}X_{4\alpha}$, m/z 806.9363).

monosialylated gangliosides were very similar to the dissociation patterns of doubly charged disialylated gangliosides. Understanding, provided by previous ganglioside fragmentation both in this and other publications, greatly simplified the elucidation of product ions in these spectra.

Product ions from the [M-2H]$^{2-}$ and [M-3H]$^{3-}$ d18:1/18:0 precursor of trisialylated ganglioside GT1b are described in **Table 5.** Peaks corresponding to the neutral loss of water were observed at m/z 711.688 and 1068.036. The most abundant ions again corresponded to glycosphingolipid sub-structures from the loss of one, two or three sialic acids to form GD1, GM1 and GA1 (m/z 931.4937 and 1863.9947, m/z 1572.9000 and m/z 1267.4859). This was very similar to fragmentation patterns described in (Serb, Schiopu, Flangea, Sisu, & Zamfir, 2009) and (Vukelić et al., 2005) for the [M-2H]$^{2-}$ precursor, although relative product ion peak intensities were slightly different. In these papers, which both applied CID, the GM1-fragment was the most abundant; in this instance the GD1 [M-H]$^{-}$ peak was the most abundant. Interestingly the GM1-like fragment was present as both [M-H]$^{-}$ and [M-2H]$^{2-}$ ions in spectra from the [M-3H]$^{3-}$ precursor, suggesting the presence or transfer of the charge onto something other than the sialic acid. Only the [M-H]$^{-}$ ion was observed from the [M-2H]$^{2-}$ precursor. Neither publication investigated the triply charged precursor ion so this was unconfirmed by previous research.

Product ion spectra from the [M-2H]$^{2-}$, [M-3H]$^{3-}$ and [M-4H]$^{4-}$ d20:1/18:0 precursor ions of tetrasialylated ganglioside GQ1b are described in Table 17. Previous description of this ganglioside appeared to be unavailable. However the dissociation patterns of less complex gangliosides was again applicable here. Product ions were similar from each precursor but present in different charge states and stemmed mostly from the loss of sialic acids. For example GT1 and GD1-like fragments were identified as the [M-2H]$^{2-}$ and [M-H]$^{-}$ ions from the [M-2H]$^{2-}$ precursor; as the [M-2H]$^{2-}$ and [M-2H]$^{2-}$ ions from the [M-3H]$^{3-}$ precursor and as the [M-3H]$^{3-}$ and [M-2H]$^{2-}$ions from the [M-4H]$^{4-}$ precursor. Disialic acid ions were observed as [M-

Table 17. Identified Tri- and Tetrosialylated Ganglioside Product Ions.

Precursor	Ion	m/z	Product Ion	m/z
GT1b	[M-2H]$^{2-}$	1063.0259		487.48
d18:1/18:0			B$_{2\beta}$	581.184
			B$_{3\alpha}$	655.1667
			Y$_{2\alpha}$Y$_{2\beta}$	888.64
			Y$_{4\alpha}$Y$_{2\beta}$	1253.772
			Y$_{2\beta}$ OR Y$_{4\alpha/1\beta}$	1544.8692
			Y$_{4\alpha}$ OR Y$_{3\beta}$ [M-H]$^{-}$	1835.9642
			Y$_{4\alpha}$ OR Y$_{3\beta}$ [M-2H]$^{2-}$	*917.4781
			[M-COO-2H]$^{2-}$	*1041.0311
			[M-H2O-2H]$^{2-}$	*1054.0203
	[M-3H]$^{3-}$	708.348	B$_{1\alpha}$	290.0881
				487.4253
			B$_{2\beta}$	581.183
				*771.9304
			Y$_{2\beta}$ OR Y$_{5\alpha}$Y$_{1\beta}$	1544.8688
			Y$_{5\alpha}$	*917.4776
			^{0,4}X$_{5}$	*952.4804
			[M-COO-3H]$^{3-}$	**693.6843
			[M-H2O-3H]$^{3-}$	**702.3445
GQ1b	[M-2H]$^{2-}$	1222.5898	B$_{2\alpha}$ or B$_{2\beta}$	581.1836
d18:1/20:0			Y$_{5\alpha}$Y$_{2\beta}$ OR Y$_{4\alpha}$Y$_{3\beta}$	1572.9001
			Y$_{4\alpha}$ OR Y$_{2\beta}$ OR Y$_{5\alpha}$Y$_{3\beta}$	1863.9956
			Y$_{5\alpha}$ OR Y$_{3\beta}$	*1077.0415
	[M-3H]$^{3-}$	814.7241	B$_{2\alpha}$ or B$_{2\beta}$	581.1836
			Y$_{4\alpha}$ OR Y$_{2\beta}$ or Y$_{5\alpha}$Y$_{3\beta}$	*931.4941
			Y$_{5\alpha}$ OR Y$_{3\beta}$	*1077.5438
	[M-4H]$^{4-}$	610.7913	B$_{1\alpha}$ OR B$_{1\beta}$	290.0881
			Y$_{4\alpha}$ OR Y$_{2\beta}$ or Y$_{5\alpha}$Y$_{3\beta}$	*931.4939
			Y$_{5\alpha}$ OR Y3β	**717.6918

* doubly charged ion
**triply charged ion

H]$^-$ ions from the [M-2H]$^{2-}$ and [M-3H]$^{3-}$ precursors. This product ion was not observed in spectra from the [M-4H]$^{4-}$ precursor unless the ion at m/z 290.0881 was the doubly charged ion.

4.2.3.4 <u>Lipid Standard Separations by HPLC-MS</u>

Each lipid standard was analysed by HPLC-MS in negative ion mode using the chromatography settings optimised above in order to collect data on standard retention times that may assist identifications in unknown samples. Typical chromatograms from phospholipids and sphingolipids can be found in Appendix 2. Collision induced dissociation was applied to the 5 predominant peaks in the range m/z 600-2000 from each full scan. While analysis focused on obtaining data from gangliosides and larger sphingolipids, all available standards were analysed in order that the method could later be applied, if required, to more heterogeneous samples containing a wider range of lipids. At any rate the data collected could be used to recognise and eliminate non-gangliosides from focused analysis. Commercial ganglioside extract was also separated by the same method on separate occasions to investigate the reproducibility of the method. Ganglioside retention times were compared to those obtained from commercial standards.

4.2.3.4.1 <u>Data Analysis</u>

MZmine 2 software (Pluskal et al., 2010), an open-source pipeline for processing HPLC-MS data, was used to generate mass lists, detect and de-convolute chromatograms and remove isotopes. Despite chromatographic peak resolutions (FWHM) of ≤ 0.5 minutes for nearly all peaks, maximum peak duration had to be set to 1.8 minutes in order to detect predominant peaks from several standards. Time range limits were applied to each dataset to simplify the analysis. The top 15-25 extracted m/z with normalised intensities over 100,000 were then analysed for all but the ceramide standard where a cut-off point of 75,000 was used. Extracted peak values were manually checked in raw files since MZmine occasionally identified an incorrect isotopic peak as the monoisotopic mass, especially for multiply charged ions.

Mass lists were then entered into the Scripps METLIN database for putative identifications. Multiple identifications were often returned with isomeric fatty acid or sugar structures. For example twenty one masses from the extracted mass list from the ganglioside GD3 returned 57 identifications with ≤ 2 ppm mass accuracy. Therefore where identifications were made ganglioside and sphingolipids were assumed to have the expected ganglio-series carbohydrate structure and to contain the d18:1 sphingosine (the d20:1 sphingosine is nearly as abundant, however for simplicity sake in reporting the results in this paragraph only the d18:1 sphingosine is mentioned). This issue was even more prominent in phospholipid standard data where biological variation in fatty acid structure is higher. In results phospholipids are therefore reported only as a total acyl carbon number and degree of saturation. Finally manual analysis was applied to classifying unidentified masses using mass differences known to correspond to fatty acid modifications and by comparing product ion spectra. Product ion spectra were also used here to confirm putative identifications and the intramolecular position of some novel modifications that were identified. Full mass lists from each standard with putative identifications and retention times (RT) can be found in Appendix 2.

4.2.3.4.2 Glycerophospholipids

Ten glycerophosphocholine species with 32 to 40 fatty acid carbons and 0 to 6 double bonds were identified with RT from 20.5 to 25.7 minutes. All product ion spectra showed a neutral loss of 50 Da corresponding to the loss of CH_3Cl (from chlorine adduct ions) from the terminal choline. Addition of C_2H_4 to the fatty acid moiety resulted in retention shifts of over 2 minutes (32:1 → 34:1 = +2.14 min, 34:1 → 36:1 = +2.26 min) and loss of a double bond in shifts of over 1.4 min (34:3 → 34:2 = +1.41 min, 34:2 → 34:1 = +1.59 min, 32:1 → 32:0 = +1.7 min). Fourteen glycerophosphoethanolamines were identified with RTs from 19.0 to 26.0 minutes. Similar retention shifts were observed for loss of a double bond (34:2 → 34:1 = +1.72 min, 34:1 → 34:0 = +1.83 min) and addition of C_2H_4 (32:1 → 34:1 = +2.15 min, 34:1 → 36:1 = +2.28 min). Fourteen glycerophosphoglycerols were identified with RT from 18.4 to 22.7 minutes. Each

showed a neutral loss of 74 Da in product ion spectra from neutral loss of the glycerol head group. Similar changes in fatty acid length and saturation resulted in retention shifts of over 2 minutes (32:1 → 34:1 = +2.13 min, 34:1 → 36:1 = +2.14 min), and over 1.25 minutes (34:2 → 34:1 = +1.29 min, 34:1 → 34:0 = +1.65 min). Eleven PS species were identified with RTs from 20.7 to 28.6 minutes. Loss of a double bond resulted in a shift of less than 1.5 min (36:2 → 36:1 = 1.45 min, 40:6 → 40:5 → 40:4 = 0.84 min and 0.61 min) while additions of C_2H_4 resulted in shifts of over 2 minutes (36:2 → 38:2 = 2.67, 36:1 → 38:1 = 2.12). Initially PS appeared to elute later than other phospholipids, however this was due to increases in the predominant fatty acid lengths in the standard. Retentions times of 25.7, 26.0, 22.6 and 22.2 min were observed for the 36:1 species of PC, PE, PG and PS respectively showing that PS actually eluted earlier than other phospholipids.

Cardiolipins eluted later due to the hydrophobic influence of four fatty acids. Two lyso cardiolipins, 54:6 and 54:5, were identified with RTs of 23.9 and 24.5 minutes respectively. Six other cardiolipins were identified with RTs of 29.9 to 32.0 minutes.

4.2.3.4.3 Simple Sphingolipids

Seven ceramides were identified, five of which contained a 2-hydroxyl modification, with retention times from 21.6 to 27.1 minutes. Similar to phospholipids additions of C_2H_4 to the fatty acid resulted in retention shifts of over 2 minutes (d18:1/16:0(2OH) → d18:1/18:0(2OH) = +2.2 min, d18:1/18:0(2OH) → d18:1/20:0(2OH) = +2.2 min). Only one example of double bond loss was observed between ceramides containing sphingosine and dihydrosphingosine resulting in a RT shift of 0.8 minutes. Eleven hexosylceramides were identified with retention times from 23.0 to 30.8 minutes. The fatty acid moieties detected in these hexosylceramides, as well as in sphingomyelins and sulfatides, were predominantly longer chain ranging from the d18:1/18:0 species upwards. Hexosylceramide identifications were supported by a neutral loss of 198 Da observed in all product ion spectra equating to the loss of a hexose chlorine adduct ($C_6H_{11}O_5Cl$ = 198 Da). Addition of C_2H_4 or loss of a double bond resulted in retention shifts of

over 1.6 minutes and 1.7 minutes respectively. Thirteen sphingomyelins were identified with RT between 22.4 and 29.8 minutes. Like PC these were identifiable by the neutral loss of 50 Da in product ion spectra from the loss of CH_3Cl from the choline head group. Additions of C_2H_4 and loss of a double bond resulted in retention shifts of around 2 minutes. The modification from sphingosine (d18:1) to dihydrosphingosine (d18:0) also resulting from loss of a double bond however only produced shifts of around 0.7 minutes. Finally 20 sulfatide species were identified, 9 of which contained a 2-hydroxyl modification, with relatively early RT from 18.9 to 27.4 minutes. Addition of C_2H_4 resulted in RT shifts of around 1.7 minutes. Unexpectedly, considering previous MSMS experiments, lyso-sulfatide fragments containing the sphingosine moiety were detected in product ion spectra from all identified sulfatides.

4.2.3.4.4 **Complex Glycosphingolipids**

Retention times were collected for gangliosides GM1, GM2, GM3, GD1a, GD1b, GD3, GT1b and GQ1b, as well as GA1 (asialo-GM1), including ceramide structures ranging from d18:1/16:0 (GA1, GM2, GM3, GD3) to d18:1/24:0 (GM1, GM3, GD1b, GD3, GT1b). Gangliosides eluted earlier than the majority of lipid standards thus far investigated, between 13.3 (GQ1b) and 25.5 (GM3) minutes which should simplify their analysis in unknown mixtures even in the presence of other lipids. The structural variation in the ceramide moiety was lower than observed in other lipid standards and limited exclusively to one or no double bonds in the fatty acid and sphingosine, compared to 0-5 desaturations in most phospholipids. Addition of C_2H_4 resulted in retention shifts of 2 to 2.5 minutes, similar to other lipids. The only variation in saturation observed in gangliosides apart from GA1 was the presence of species containing dihydrosphingosine instead of sphingosine. This modification caused an RT shift of 0.5 to 1 minute, again significantly lower than retention shifts for the loss of a double bond in the fatty acid moiety. In GA1 the loss of a double bond not involving the sphingosine was observed in two cases and resulted in shifts of 1.5 and 1.7 minutes.

4.2.3.4.5 **Retention Time Reproducibility in Separations of Commercial Ganglioside Extract**

Commercial ganglioside extract was analysed by the same HPLC method on separate occasions to test the reproducibility of ganglioside retention times. Elution times were extracted for major gangliosides that had been detected in single standards that were also present in CGE so that they could be compared to standard RT. This included a minimum of 2 species of GM1, GM2, GM3, GD1a, GD1b, GD3 and GT1b. Raw data is reported in Appendix 3. It must be noted that tubing was changed on the HPLC equipment between standards analysis and CGE analysis which resulted in a consistent 10.3 +/- 2.6 second shift ahead of the retention times observed previously. Retention times across 26 different ganglioside species showed a pooled mean standard deviation (PMSD) of 0.1 min (8 repeats, 19 gangliosides). Further investigation showed that reproducibility was highest for mono-sialylated gangliosides (PMSD SD = 0.07 min) and decreased slightly for disialylated (PMSD SD = 0.11 min) and trisialylated gangliosides (SD = 0.15 min). Intensities were also extracted for the major ganglioside species and showed a relative standard deviation of 9.93% which was consistent between mono-, di- and trisialylated gangliosides.

4.3 Discussion

In this chapter we set out to develop an in-house optimised HPLC-MS method with dissociation for the analysis of gangliosides. Comprehensive lipidomic methods, even those concentrating on acidic sphingolipid analysis, have tended to neglect gangliosides detecting only the simplest glycosphingolipids (Kundu et al., 1985; Markham & Jaworski, 2007; Merrill et al., 2005; Sullards et al., 2007; Suzuki et al., 1991). The few methods previously published that focus on ganglioside separation report a variety of HPLC settings, resulting in sub-optimal separation, failure to separate isomeric species, or overlapping head-group modifications in the case of normal phase chromatography (Fong et al., 2009; Ikeda et al., 2008; Ikeda & Taguchi, 2010). We therefore tested different solvent systems adapted from the literature and

observed better ganglioside separation using a simple isopropanol gradient including near baseline separation of isomers GD1a and GD1b. Unusually for lipidomic HPLC, methanol did not appear to improve or contribute to the separation. When normal and reverse phase columns were compared, optimal separation of gangliosides and other sphingolipids and acidic lipids was observed on the latter. Many lipidomic publications have favoured normal phase HPLC as head groups elute concurrently, simplifying identifications. Here however we found that, especially for the larger gangliosides that formed a series of adduct ions, this concurrent elution confused the differentiation of adducts from structural modifications and minor structural changes such as loss of a double bond from dominant isotopic peak distributions.

We also report using a high resolution Thermo LTQ Orbitrap mass spectrometer for detection and dissociation. While this high resolution mass spectrometer has previously been applied to direct injection analysis of gangliosides the majority of HPLC-MS based lipidomic studies use a triple quadrupole configuration. This enables precursor ion scanning so that the characteristic loss of particular structures; often the head-group from lipids or a sialic acid from glycosphingolipids, can be easily detected throughout the data. This allows species of a particular group to be identified quickly although this risks missing unknown native modifications in biological samples. Single and multiple reaction monitoring are also possible for targeted studies. Compared to the triple quadrupole configuration however, the LTQ orbitrap has higher mass accuracy and resolution enabling detection and accurate mass identifications of even low abundance gangliosides such as the unusual d18:0/18:0 species and long chain fatty acid configurations detected here. Online dissociation and accompanying software also enabled examination of MS^2 scans for neutral losses or characteristic ions similar to precursor ion scanning. The accurate mass detection allowed false identifications to be rejected on several occasions throughout the analysis of standards. Considering many lipidomic publications work in either nominal mass or single decimals this could become a stand-out benefit in the analysis of unknown mixtures.

Once an optimal HPLC system was established, mass spectrometry settings and MS^2 dissociation were optimised for online detection and identification of gangliosides. This was investigated using available purified and commercial ganglioside standards. Software to assist with this was hard to find and the most useful but non-comprehensive database was the LipidMAPS Glycosphingolipid MS/MS product ion search tool. Therefore much of the analysis was done using literature searches and manually in ChemSketch. The fragmentation of gangliosides occurred in a conserved manner for all standards via the loss of consecutive sugars from the carbohydrate moiety, some of which also ionised, to produce extremely characteristic product ion spectra. To the best of our knowledge dissociations by ESI-CID-MSMS in this instrument occurred in a similar manner to those observed in 1988 by FAB-MS/MS which remains to be the most comprehensive study of ganglioside fragmentation to date (B Domon & Costello, 1988). Because the fatty acid and sphingosine components did not dissociate from one another they could not be described individually. That said, fragment ions were observed that could be used to map modifications to either sugar or ceramide moiety and characteristic ions were identified that could distinguish regioisomers. This detailed description has provided insight into how various gangliosides not available as standards, such as GM1b, GD1c, GT1a and LM1, may fragment to produce unique product ions.

In order that putative ganglioside identifications made by accurate mass detection and dissociation pattern could be confirmed during the analysis of complex biological samples an orthogonal data source was also investigated in the form of standard retention times for a range of lipid species using the method developed here. Ganglioside standards were analysed using the HPLC-MS method in order to build a database of standard retention times. This use of chemical reference standards is commonly applied in metabolomics and is a suggested criterion for reporting chemical analysis by the Metabolomics Standards Initiative, although reports are less common in lipidomics. This may be because, unlike chemical standards which are synthesised rather than purified and commonly contain a single chemical, lipid standards are often defined by head-group structure. They contain, as was consistently found here,

multiple species of said structure with different fatty acid/sphingosine components. With accurate mass detection and dissociation, identifications were possible without details of the ceramide composition, but this complicated data processing somewhat and perhaps decreases the reliability of the figures. Still standard retention times were collected for a variety of gangliosides. The reproducibility of the method appeared to be good. However as a security measure it was a decided that the commercial ganglioside extract used to assess this, which was now well characterised in terms of retention times, should be included as a QC at the beginning and end of future batches. An unexpected benefit of the impurity of the standards was that data could be collected on average retention time shifts arising from common modifications. These could be used to support putative identifications assigned to novel gangliosides if confirmed identifications of well-defined gangliosides can be made in the same sample.

Similar investigations into MSMS patterns and standard retention times were made into lipids other than gangliosides where standards were available in order that the HPLC-MS method could be applied to wider lipidomic studies in the future. This encompassed sphingolipids, glycosphingolipids and phospholipids including neutral and acidic. It had also already been observed that commercial ganglioside extract contained non-ganglioside lipids implying that even enriched samples contained contamination. Collecting data on other lipids would allow this contamination to be recognised and excluded from targeted analysis. Neutral lipids including the majority of phospholipids and sphingomyelin ionised preferentially in positive ion mode which should eliminate them from ganglioside investigations which will be performed in negative ion mode. Due to the comparatively large polar structures of gangliosides, other lipids investigated tended to elute after gangliosides which should simplify analysis further. It was noted that elution peak shapes and species separation for non-gangliosides were acceptable using this method, should it be possible to apply it to larger scale lipidomic investigations.

Chapter 5 – Molecular Phenotyping in Mouse Models of Guillain-Barré Syndrome.

5.1 Introduction

Modelling disease in animals enables researchers to investigate and clarify aspects that cannot be studied in humans. This is especially true for heterogeneous autoimmune syndromes such as Guillain-Barré Syndrome where many of the subtleties of the disease remain a mystery. Questions relating to onset, autoimmune antibody affinity and clinical subtypes, symptoms and severity are still unanswered. Several models have been used to understand specific aspects of GBS. Experimental autoimmune encephalomyelitis/neuritis in mice, resulting from inoculation with central nervous system tissue or lipids, has been used to investigate autoimmune-mediated demyelination as occurs in Autoimmune demyelinating polyradiculoneuropathy, the prevalent subtype of GBS. However the heterogeneity of the biological material used for inoculation often results in physiological damage outside of the nervous system creating a syndrome that is not specific to GBS (Gold, Hartung, & Toyka, 2000).

Animal infection or immunisation with microbes, campylobacter lipo-oligosaccharides (LOS) and gangliosides has been used to study molecular mimicry and the induction of cross-reactive antibodies as is thought to occur in GBS. In rabbits this has been reported to cause a GBS-like neuropathy and different neuropathies have been associated with specific gangliosides. For example spastic or flaccid paralysis has been associated with anti-GM1 or GD1a antibodies respectively (Nobuhiro Yuki et al., 2001). This echoes the association of anti-GQ1b with the human GBS subtype Miller Fisher Syndrome although a strong link has not been established for other syndromes/affinities (A Chiba et al., 1992). In mice the success of these studies has been limited by murine self-tolerance to gangliosides and/or auto-antibody binding to self-antigens (Karlsen & Dyrberg, 1998; Kawashima et al., 1992). Goodyear *et al*. found that mice immunized with purified *C.jejuni* LOS were non-specifically unwell but showed no overt clinical neuropathy despite a positive serological response producing ganglioside reactive antibodies. Cloned antibodies were shown to bind peripheral nerves in *ex vivo* preparations causing

electrophysiological malfunction and in passive *in vivo* immunisations (Goodyear et al., 1999).

Various synthetic enzyme knockouts (α-2,8-sialyltransferase II (STII) knockout, β-1,4-N-acetylgalactosaminyltransferase (GalNAcT) knockout) (Handa et al., 2005; Takamiya et al., 1996), developed originally to understand the role of complex gangliosides, have been applied to circumventing this tolerance. These mice are incapable of synthesising certain branches of the ganglioside anabolic pathway (Figure 35) and are therefore immunologically naïve to these lipids. Changes to the ganglioside profile in these mice have been described previously by HPTLC and are shown in Figure 36 (Takamiya 1996; Okada et al. 2002). Upon inoculation, serological responses are increased and many IgG and IgM antibodies with various specificities have been cloned from these mice (Lunn et al., 2000). However they cannot be used themselves to model neurodegenerative disease for two reasons; the mice often have a mild to severe phenotype associated with the gene knockout, and they contain no native target epitopes for the auto-antibodies raised to bind (Koichi Furukawa, Tokuda, Okuda, Tajima, & Furukawa, 2004). Wild type animals must therefore be immunised with the extracted monoclonal antibodies often with an external source of complement to produce a neurodegenerative model.

A novel concept in this area is the genetic rescue of the GalNAcT gene in the knockout mouse under promoters regulating genes that are predominantly expressed in distinct neurological tissues. Theoretically these so-called 'rescue mice' are unable to synthesis complex gangliosides in most tissues so are systemically immunologically naïve to complex gangliosides enabling a strong serological response upon inoculation. However target epitopes are synthesised in designated tissues enabling a targeted autoimmune response. The Neuroimmunology Research Group at the Glasgow Biomedical Research Centre has developed several such mice with GalNAcT rescue in the neurological tissue. These mice are undergoing genotypic and phenotypic description but thus far no molecular profiling has been performed and the presence of complex gangliosides, which is essential to their function, has not been

Synthetis Enzymes   1. α-2,3-sialyltransferase I   2. α-2,8-sialyltransferase II

3. α-2,8-sialyltransferase III   4. β-1,4-N-acetylgalactosaminyltransferase

5. β -1,3-galactosyltransferase   6. β-2,3-sialyltransferase IV   7. α-2,8-sialyltransferase V/X
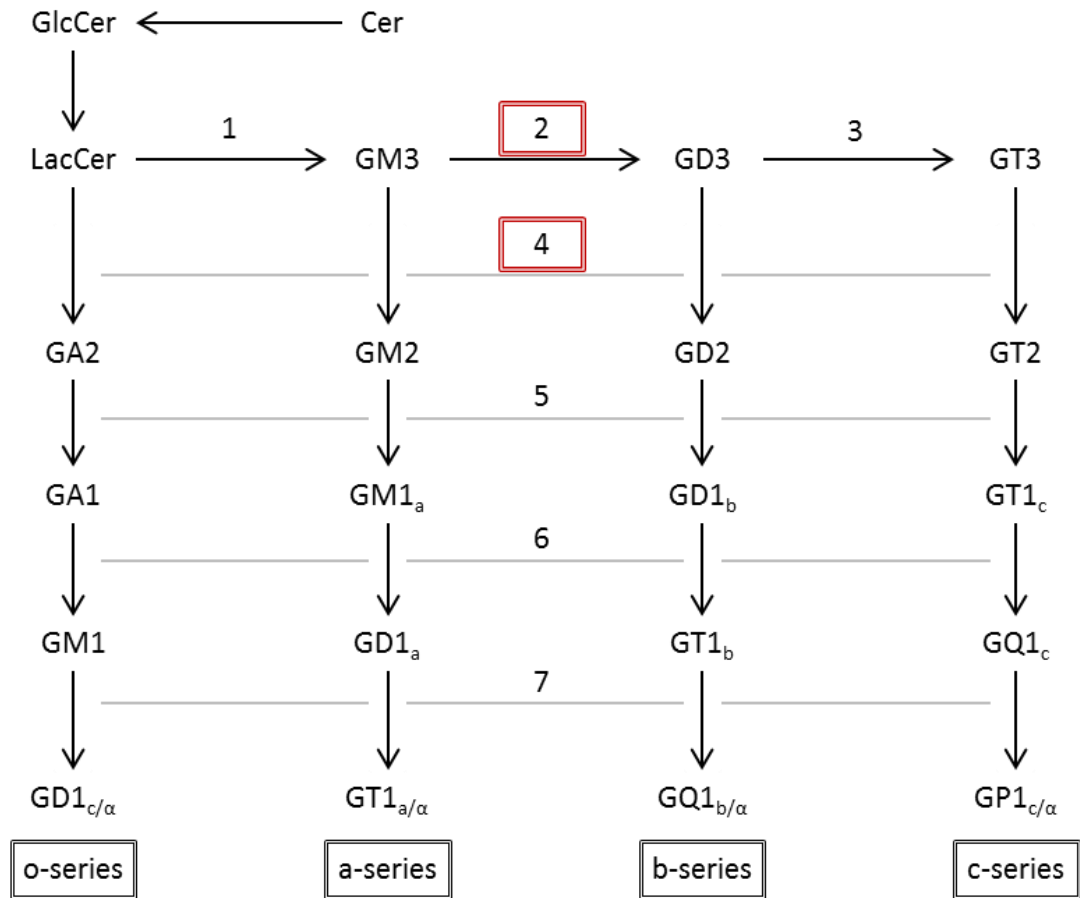
Figure 35. Ganglioside Synthesis and Pathway Knockouts in STII and GalNAcT Knockout Mice. Enzyme knockouts indicated by red boxes. These mice are genetically engineered to be unable to synthesise certain pathways in ganglioside metabolism. The ST II (2) knockout cannot produce neolipids in the b- and c-series pathways while the GalNAcT (4) knockout can only produce simple gangliosides GM3, GD3 and GT3.
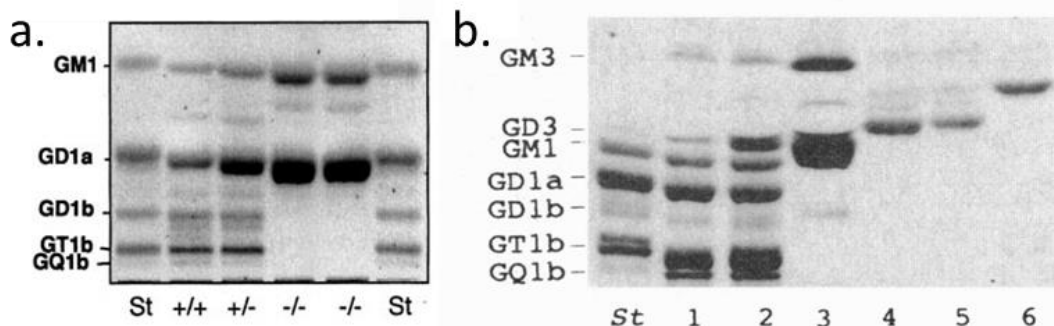
Figure 36. Ganglioside Profiles in STII Knockout and GalNAcT knockout Mice. Both mouse models have been profiled previously by HPTLC with staining. Reproduced from (Okada et al. 2002; Takamiya et al. 1996). A. STII knockout brain gangliosides. St standards, +/+ wild type, +/- heterozygous KO, -/- homozygous KO. The profile was dominated by a-series gangliosides. B. GalNAcT knockout, 1-3 brain and 4-6 liver gangliosides. 1,4 wild type, 2,5 heterozygous KO, 3,6 homozygous KO. The knockout lacked complex gangliosides in liver or brain.

confirmed.   In this chapter we extracted lipids from the brains of wild type (WT), STII knockout, GalNAcT knockout , NFL rescue, PLP rescue, THY1 112 rescue and THY1 115 rescue mice and enriched for gangliosides using weak anion exchange chromatography and phase partition. These extracts were separated by HPTLC and parallel lanes visualised using primulin stain and analysed by imaging mass spectrometry to identify ganglioside profiles. Data was collected by HPLC-MSMS for more sensitive, in-depth analysis, to confirm putative identifications and describe several unknown species putatively identified by HPTLC-IMS. Comparative profiling was performed using intensity measurements from both methods.

5.2 Results

5.2.1   HPTLC-IMS Analysis of Brain Extracts

5.2.1.1 HPTLC Separations

To ascertain an optimum volume for separation, four volumes of WT extract, corresponding to 2.5 to 50 mg wet tissue weight, were separated by HPTLC alongside a commercial ganglioside extract (CGE) and stained with the fatty acid stain primulin. Band distortion was observed with the equivalent of 20 or 50 mg wet tissue weight due to overloading with lipid material. A volume of 25 ul equivalent of 12.5 mg wet tissue weight was selected for further separations unless specified. Extracts (n=2) were then separated by HPTLC alongside CGE to compare profiles by conventional staining. These are shown in Figure 37. Gangliosides bands GM3, GM1, GD1a and GD1b were putatively identified in WT (lane 1) mice. Contradictory to previous publications no GT1b or GQ1b were observed. These publications used resorcinol, a sialic-acid specific stain, that may amplify the visual intensity of these highly sialylated gangliosides. The absence of detection here may have been due to the use of a non-sialic acid specific stain. Only simple gangliosides GM3, GD3 and 9-O-AcGD3 were identified in GalNAcT knockout mice (lane 2), and only a-series gangliosides GM3, GM1 and GD1a in STII knockout mice (lane 3). Interpretation of the rescue mice profiles was more complex due to overlapping bands and weak staining. The NFL (lane 4) and PLP rescues (lane 5) appeared to contain similar
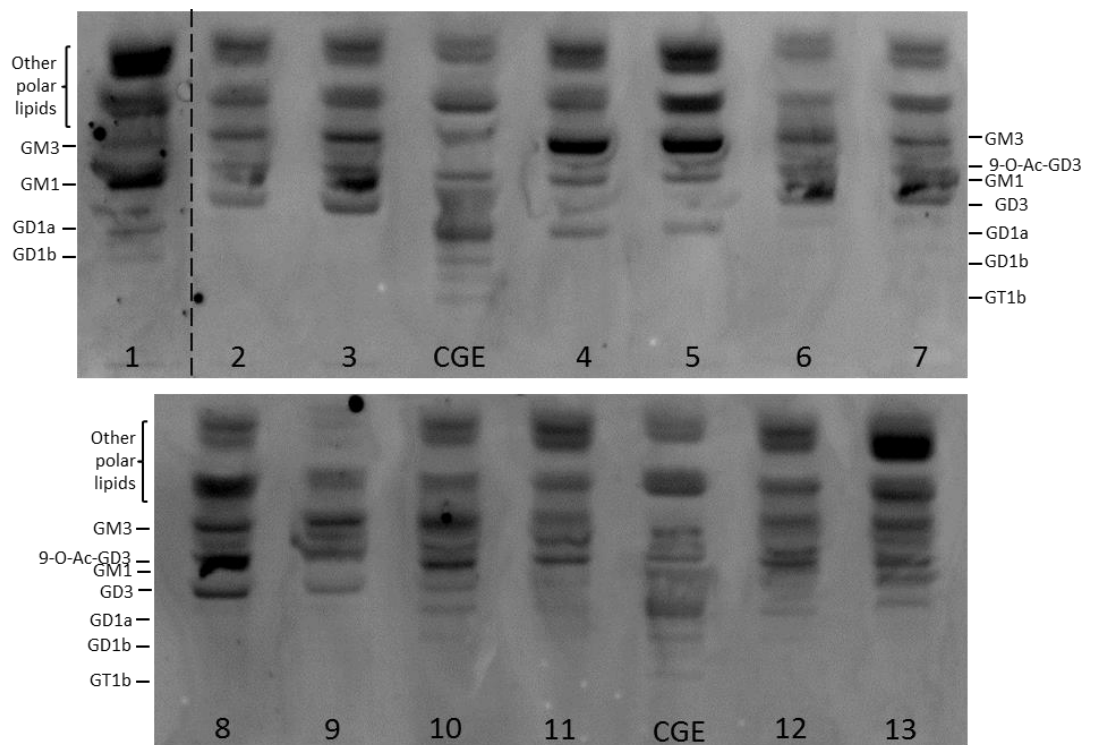
Figure 37. HPTLC Separations of Brain Extracts Stained with Primulin. 1 – wild type, 2,3 – GalNAcT knockout, 4,5 – ST II knockout, 6,7 – NFL rescue, 8,9 – PLP rescue, 10,11 – THY1 112 rescue, 12,13 – THY1 115 rescue, CGE – commerciarl ganglioside extract. Colours inverted for visualisation. Bands were identified as GM3, GM1, GD1a and GD1b (simple and complex gangliosides) in wild type. No GT1b or GQ1b were observed, despite previous reports, possibly due to the choice of stain. Profiles from knockouts largely agreed with previous publications containing only simple, or a-series, gangliosides, as expected. Interpretation of rescue mice profiles was complicated by overlapping bands. However bands corresponding to both simple and complex species were putatively detected.

accumulation of simple gangliosides GM3, GD3 and 9-O-Ac-GD3 to the GalNAcT knockout.Faint bands possibly corresponding to complex gangliosides GM1 and GD1a were observed. The THY1 112 (lane 6) and THY1 115 (lane 7) rescue profiles appeared similar to the NFL and PLP rescue mice with stronger staining of the putative GM1 and GD1a bands.

5.2.1.2 Plate Calibration for IMS

In order to improve mass accuracy from the uneven surface of the HPTLC silica CGE was co-spotted with matrix in the four corners of the HPTLC lane to be imaged. Spectra were collected from each spot and calibration performed using the spot providing median mass values. Mass accuracy was improved to < 1 Da by calibrating the mass spectrometer in this way. Calibration spots were therefore applied to each of the experimental HPTLC lanes to be analysed by IMS.

However a mass shift was still observed across the plate from right to left (Δtop = 0.71 Da, Δbottom = 0.66 Da) and from top to bottom (Δright = 0.53 Da, Δleft = 0.48 Da) that could not be compensated for by calibrating in this manner. Attempts to flatten the surface by increasing the pressure applied when attaching the HPTLC plate to the glass slide failed to improve this. It was therefore necessary to work with nominal mass for experimental analyses. Identifications were still possible using nominal mass since the presence of unknown, non-ganglioside lipids was limited by the extraction procedure, and the relative chromatographic positions of the major gangliosides are well documented.

5.2.1.3 HPTLC-IMS Data Processing

5.2.1.3.1   Wild Type Dataset

As the best described ganglioside profile, analysis and description of the HPTLC-IMS data began with the wild type extract. Ten distinct bands were identified from the overall average spectra (OAS). These are shown, alongside primulin staining, visualised using 1-3 mass filters per band, in Figure 38a. Raw data relating to mass filters, putative identifications, and intensities are provided in Appendix 4. Based on chromatographic position and the observed m/z in the ROI averaged spectra these bands were identified, from the top of the HPTLC lane to bottom, as sulfatide, PI, GM3, GM2, GM1, GD3, GD1a, GD1b and GT1b. For all gangliosides the predominant peak in the ROI average spectra came from the d18:1/18:0 ceramide structure. A region at the bottom of the imaging area may have corresponded to GQ1b, showing strong localisation of very weak signal in the m/z 2350-2500 range and intensity from the GT1 mass filter possibly after loss of sialic acid from the GQ1 molecule. However signal intensities were so weak that this could not be concluded with confidence. Although signal was thought not to be quantitative in HPTLC-IMS analysis, higher intensities were acquired from bands GM1, GD1a and GD1b, which showed the strongest primulin staining and are reported to be the predominant gangliosides in WT mice. This suggested that peak intensities were partially proportional to ganglioside quantity. Two intensity
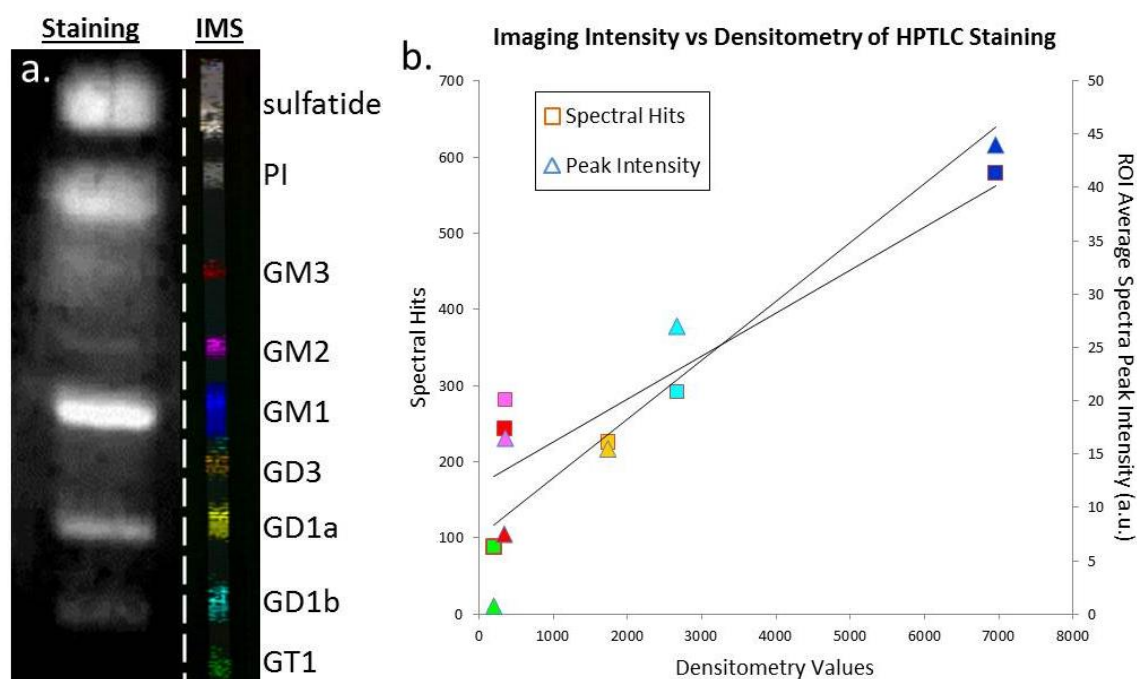
Figure 38. HPTLC and HPTLC-IMS Detected Lipids in Wild Type Mice. Lipids in wild type brain extract are shown in (a), detected by staining on the left and imaging mass spectrometry (IMS) on the right. Six bands were observed by staining, not all of which were identifiable by position alone. Compared to this ten bands were observed in imaging dataall of which were assigned putative identifications based on mass and position. Using this dataset intensity was measured traditionally (densitometry on stained lanes) and using two factors from MSI datasets; spectral hits from the mass filter and normalised peak intensity from ROI average spectra for GM3, GM2, GM1, GD1a, GD1b and GT1b (colour coded according to mass filters in IMS data). A plot of densitometry and IMS values is shown in panel b. Both IMS measures showed strong positive correlation with traditional densitometry, however this was slightly stronger for peak intensity than spectra hits, suggesting that IMS peak intensities could be used for relative quantitation.

measurements; ROI average spectra peak intensity ('intensity'), and mass filter spectra hits ('hits'), were extracted from the IMS data for GM1, GM2, GM3, GD1a, GD1b and GT1b and plotted against traditional densitometry values for primulin staining (Figure 38b). Positive correlations were observed for both and were marginally stronger for ROI intensities (R^2 of 0.94 vs 0.91).

5.2.1.3.2 Knockout Datasets

The ganglioside profiles of the GalNAcT knockout and STII knockout mice have also been investigated previously by HPTLC and resorcinol staining, identifying predominantly GM3, GD3 and 9OAcGD3 in the former and GM1 and GD1a in the latter (Figure 36) (Okada et al. 2002b;

Takamiya et al. 1996). Here, five bands were visualised from the former by primulin staining and by imaging mass spectrometry (Figure 39a). These potentially corresponded to sulfatide, PI, GM3, 9-O-acetyl GD3 (9OAcGD3) and GD3 by position. Identifications were supported by m/z in IMS datasets (incorporated in mass filters described in 2.6.5.2 and applied in Figure 39 IMS datasets). Six bands were visualised by staining in the STII knockout extract which were putatively identified as sulfatide, PI, GM3, GM2, GM1 and GD1a by chromatographic position. This was supported by m/z in IMS data (Figure 39b, mass filters from 2.6.5.2). Examination of the OAS also revealed a weak seventh band with the putative mass of an acetylated GD1.

Specific application of mass filters for other gangliosides revealed no intensity in either dataset above background, indicating the absence of these gangliosides. Raw data relating to the application of mass filters described in 2.6.5.2, putative identifications and intensity measures are given in Appendix 4. Predominant ganglioside peaks belonged to the d18:1/18:0 species.

5.2.1.3.3 Rescue Model Datasets

Raw data pertaining mass filters, identifications and intensities is provided in Appendix 4. Analysis of ganglioside profiles by staining alone was more complex. Certain bands, such as GM1 and 9OAcGD3, overlapped and could not be distinguished by staining, while others did not match the position of known gangliosides. From the NFL rescue seven bands were detected by staining, which corresponded to sulf, PI, GM3, GM2, 9OAcGD3, GM1 and GD3 identified in the WT and knockout. However in IMS data, ten bands (Figure 40a) were clearly located after investigation of the OAS. Sulfatide and PI were identified at the top of the plate. Simple gangliosides GM3, 9OAcGD3 and GD3 were detected with high intensities, which corresponded to staining intensity. Complex gangliosides GM1, GM2, GD1a and GD1b were clearly identified from the imaging data despite being barely visible by staining. A mass filter at m/z 2132, shown in separate lanes in green in Figure 40a, also indicated a weak band of GT1b that was detected exclusively by IMS. A final band was detected between GM3 and GM2 at m/z 1453, the mass of GD3 – H_2O, which was designated GMx. Chromatographic position and

adduct formation in the ROI extracted spectrum suggested that this was a monosialylated ganglioside rather than an artefact of GD3 ionisation.

In the remaining rescue extracts sulfatide and PI were identified by staining and IMS (Figure 40b, c, and d). In PLP rescue three additional bands were visible by staining, corresponding to the positions of simple gangliosides GM3, GD3 and 9OAcGD3. Identifications were confirmed in IMS data and two further bands located that were identified by mass, position and adduct formation as complex gangliosides GM1 and GD1a. In THY1 112 and THY1
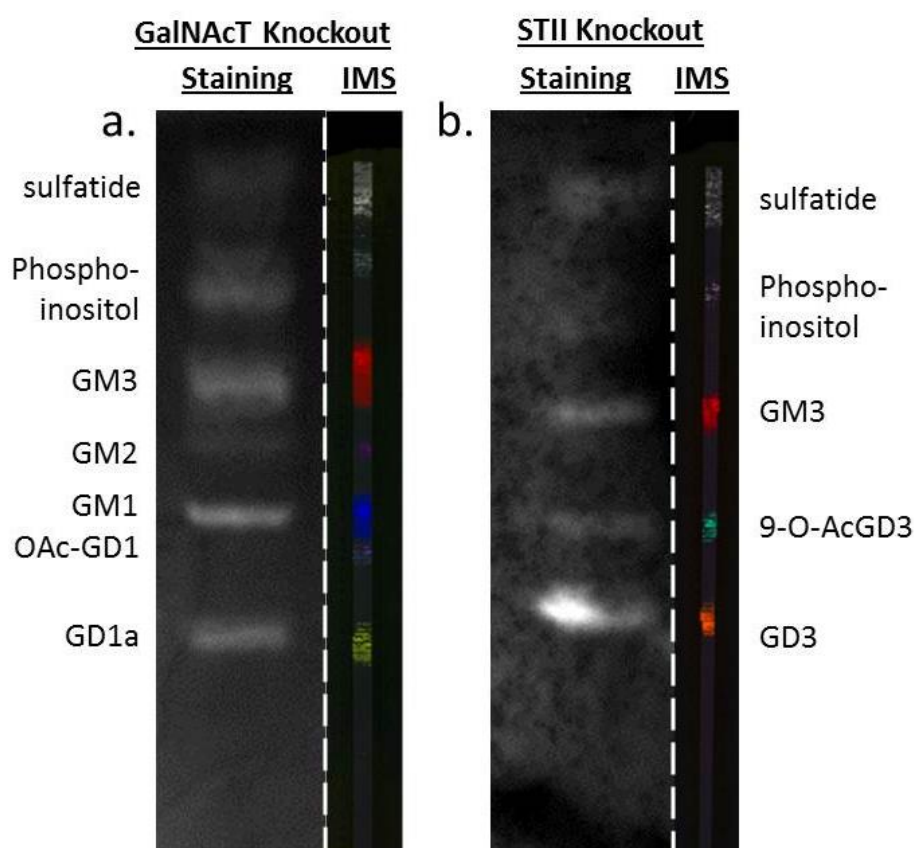
Figure 39. HPTLC and HPTLC-IMS Detected Lipids in Knockout Mice. Lipids in GalNAcT (a) and STII knockout (b) brain extracts are shown, detected by staining (left lanes) and IMS (right lanes). Six bands were visualised from the STII by staining and assigned putative identifications of sulfatide, PI, GM3, GM2, GM1 and GD1a. Five bands were detected from the GalNAcT by staining that were assigned putative identifications of sulfatide, PI, GM3, 9-O-acetyl GD3 (9OAcGD3) and GD3. While these agreed with previous profiling studies of these models (Figure 36), identifications were based on chromatographic position alone. However, via the application of mass filters for gangliosides and other polar lipids, which are defined in 2.6.5.2, to IMS datasets, bands were simultaneously detected, and putatively identified based upon mass and chromatographic position. In this manner, seven bands were identified from GalNAcT knockout, including an additional possible acetylated GD1 structure, and five from the STII knockout. Identifications agreed with those suggested by staining.
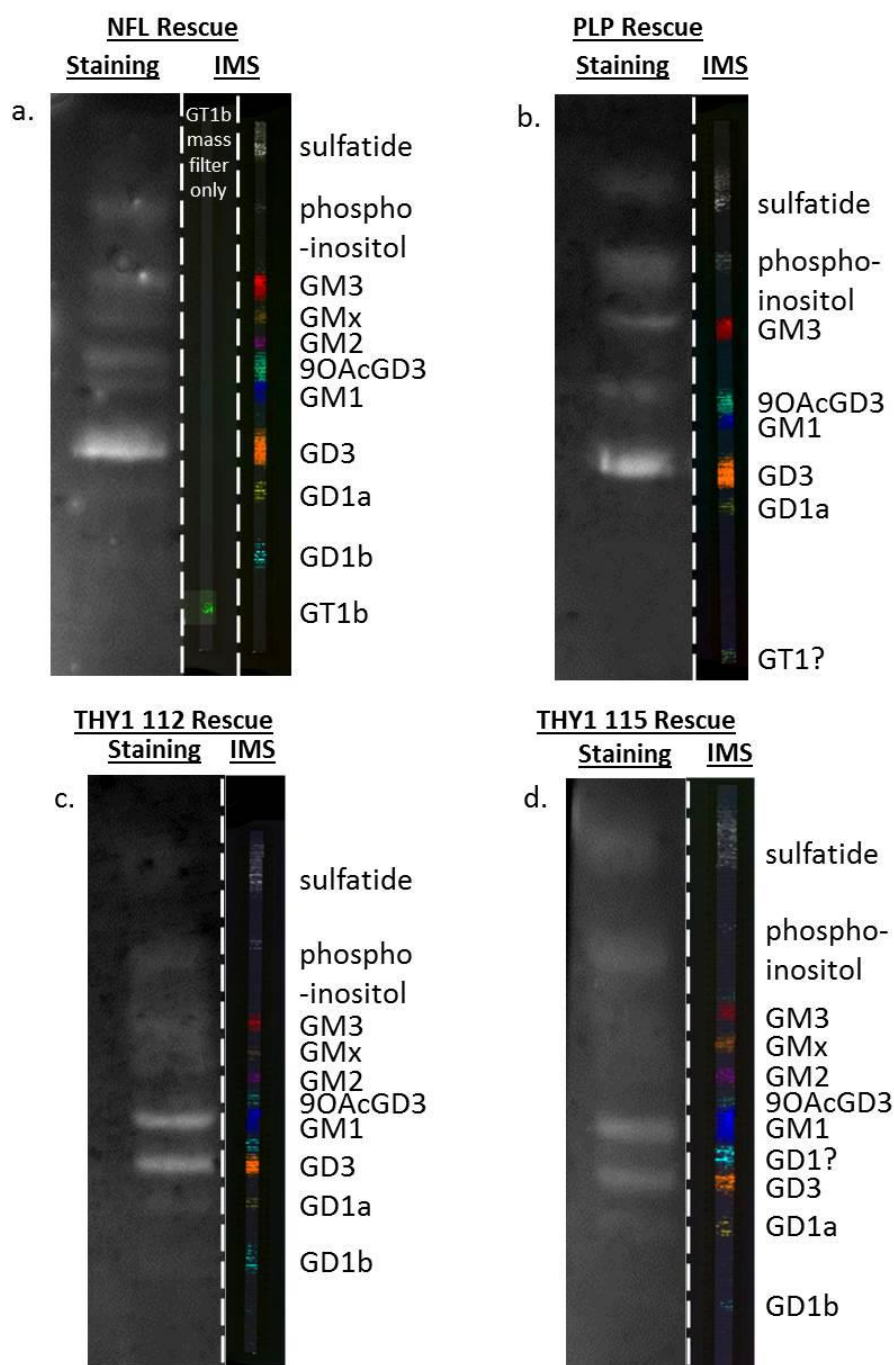
Figure 40. HPTLC and HPTLC-MS Detected Lipids in Rescue Mice. Lipids in brain extracts are shown from NFL, PLP, THY1 112 and THY1 115 rescue mice, detected by staining (left lanes) and IMS (right lanes). Identifications were difficult from the staining. Reference profiles were not available for these mice, and some bands were faint, overlapping or did not correspond to known chromatographic positions. Putative identifications were assigned for gangliosides GM3, GD3 and 9OAcGD3 in all four mice and for complex gangliosides GD1a and GD1b in THY1 rescues and GD1a in NFL and PLP rescues. Via the application of mass filters for gangliosides and other polar lipids, which are defined in 2.6.5.2, to IMS datasets, complex gangliosides GM1, GM2, GD1a, GD1b and, in the NFL rescue, GT1b, as well as GM3, GD3 and 9OAcGD3, were simultaneously detected, and putatively identified based on mass and position. GM1 and 9OAcGD3, which have similar positions, were easily distinguished in IMS data using their distinct masses and a novel structure, GMx, with the mass of a monodehydrated GD3 structure was identifiable only from IMS data.

115 rescue profiles staining revealed six bands, which were putatively identified as GM3, may have corresponded to GM2 but did not match the position accurately. In IMS datasets discrete region of intensity was observed between bands of GD3 and GM1 using the GD1b this, and all other, identifications were confirmed by mass in both models. Investigation of the OAS also revealed bands of GD1b and GMx in THY1 112 and THY1 115 rescues. Another mass filter in both THY1 rescues indicating a possible third GD1 structure.

5.2.2   HPLC-MSMS Analysis of Brain Extracts with Dissociation

HPTLC-IMS provided a simple method to build basic brain ganglioside profiles in model mice with sensitivity and specificity above and beyond that of staining alone. Structures were inferred by chromatographic position and additionally by mass and adduct formation. However identifications were made using nominal mass due to the loss of mass resolution/accuracy from the HPTLC plate surface, reducing confidence. Several species were present at such low intensity that identifications were speculative at best. Novel bands that were detected, including a potential OAcGD1 structure in the STII knockout extract, and a monosialylated structure deemed 'GMx' in NFL, THY 112 and THY 115 rescue extracts, could not be characterised in detail using this workflow.

Conventionally lengthy immunostaining and chemical processes would be necessary to confirm identifications and elucidate the structure of these unknowns. In this instance however we applied the sensitive and specific HPLC-MSMS method. Mass accuracy and resolution were improved compared to HPTLC-IMS so identifications by mass could be made with higher confidence while CID dissociation throughout the separation provided strucutral information that could be used to corroborate these identifications and describe unknowns. Higher specificity also enabled some degree of ceramide structural analysis. Data was collected from each of the brain extracts. Commercial ganglioside extract was injected before and after the batch as a QC and to obtain retention times to assist and confirm identifications.

5.2.2.1 <u>Confirmation of an Acetylated GD1 structure in STII knockouts</u>

A mass filter was applied to the data from the STII knockout brain extract at m/z 938.4841; the accurate mass of an [M-2H]$^{2-}$ ion of OAcGD1 d18:1/18:0, at 5 ppm mass accuracy. An elution peak, shown in Figure 41a below the full base peak chromatogram, was observed at 16.0 min. The full scan mass spectrum from time point 15.97 min (Figure 41b) showed a doubly charged ion at m/z 938.4829. The putatively identified OAcGD1 eluted at a similar time to GD1a itself. The single elution peak indicated only one acetylated d18:1/18:0 GD1 structure was present in this extract. By applying further mass filters elution peaks were revealed from OAcGD1a d20:1/18:0 at RT 18.2 min and from OAcGD1a d20:1/20:0 at RT 20.4.

Product ion spectra were then used to elucidate some of the internal structure of this species. Product ion spectra from GD1a at this time point contained fragment ions including sialic acid (Fig. 41c, m/z 290.1) and GM1 (Fig. 41d, m/z 1544.9). Similar product ions (marked with *) were observed in the dissociation spectra from m/z 938.4841 at this time point, as well as peaks indicating the same plus an acetyl group (+42 Da) (Fig. 41c & d). This established the acetylation position on one of the sialic acids, although not specifically on the galactose-linked inner group. The presence of GM1 and AcGM1 product ions indicated that this modification occurred on both sialic acids; intensity suggested it was more common on the outer sugar. The absence of a disialic acid fragment ion confirmed the GD1a backbone. 9-O-acetylation could not be confirmed without further fragmentation but is the most commonly reported linkage in the literature.

In order to investigate whether this modification was exclusive to the STII knockout mouse, the mass filter for OAcGD1 d18:1/18:0 was applied to data sets from WT, GalNAcT and rescue mice. Elution peaks corresponding to m/z 938.3841 were observed in all chromatograms showing that this modification was not specific to the STII knockout. Normalised intensities were, however, at least one order of magnitude lower, suggesting that substrate abundance is a contributing factor. In the wild type and all four rescue mice, three separate elution peaks
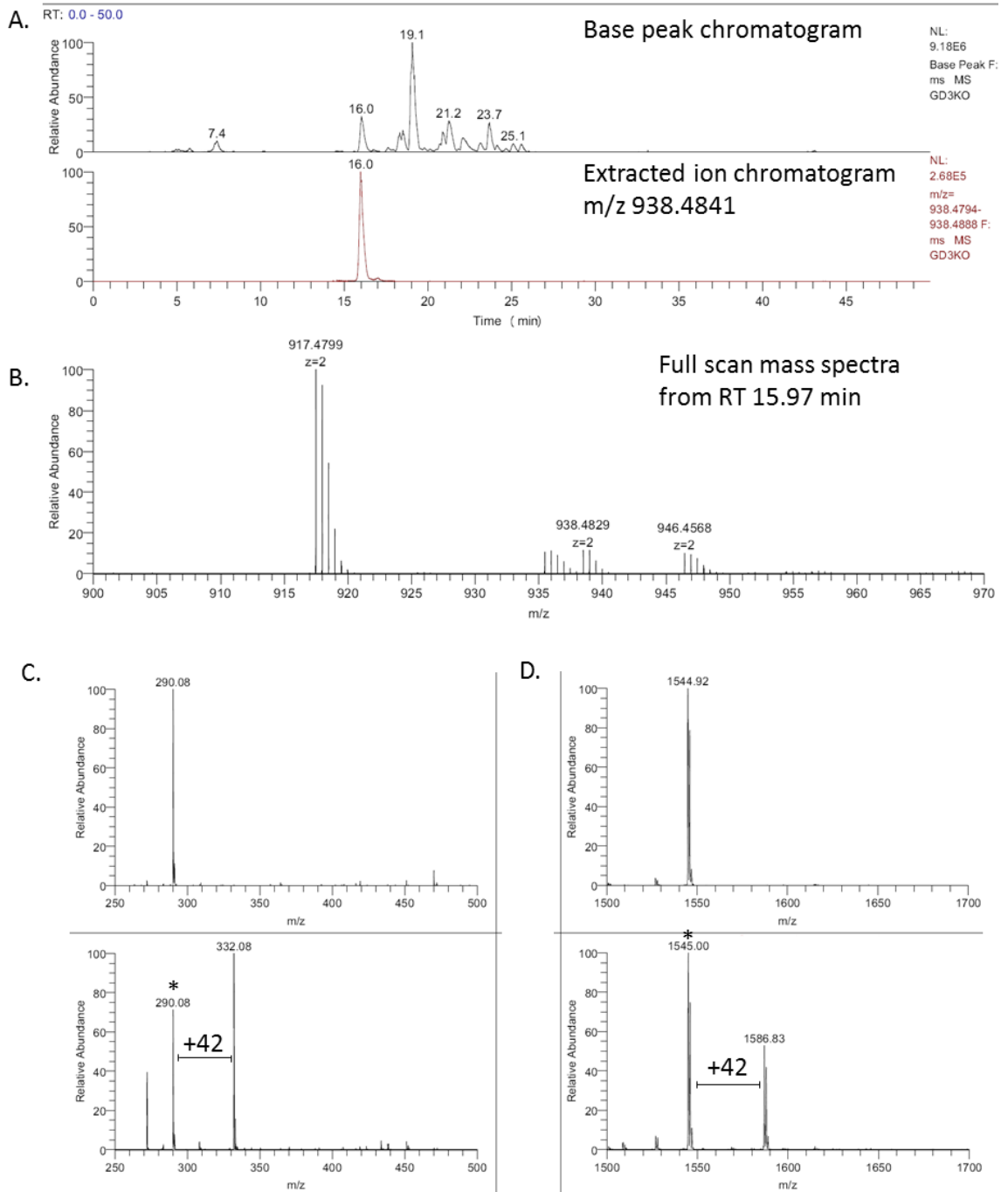
Figure 41. Confirmation of an Acetylated GD1a in STII Knockout Extract. A novel band in HPTLC-IMS data from STII knockout extract was conjectured to be an acetylated GD1a structure. This was investigated in HPLC-MSMS data by applying a mass filter for a putative $[M-2H]^{2-}$ ion of d18:1/18:0 structure (A). This showed a single elution peak with a similar retention time to GD1a itself. A doubly charged ion of this mass was identified in the full scan from this time point (B) which, when dissociated, showed a similar dissociation pattern to GD1a except that characteristic fragments at m/z 1544.9 (GM1) and 290.1 (sialic acid) were also detected with a +42 modification (C,D) corresponding to the addition of an acetyl group on a sialic acid. Similar modifications were then confirmed in data from all other extracts suggesting this is a native low abundance modification.
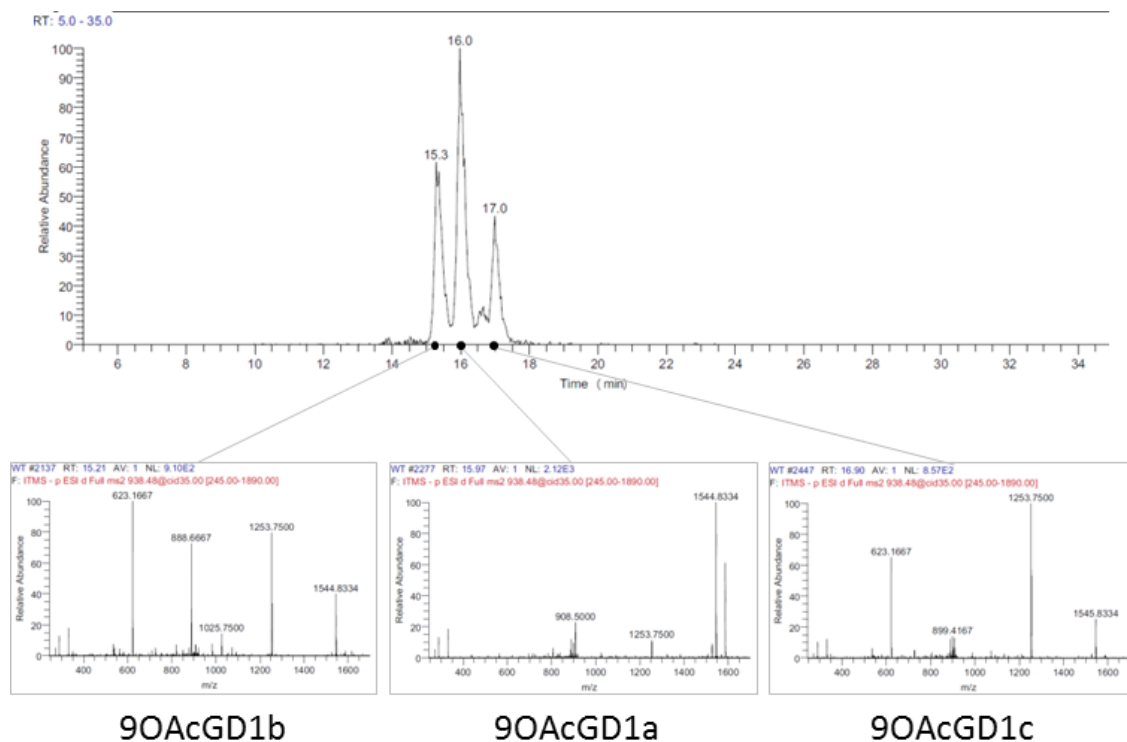
Figure 42. Identification of Three Acetylated GD1 Structures in Wild Type Brain Extract. When the mass filter for the $[M-2H]^{2-}$ ion of d18:1/18:0 structure of acetylated GD1 was applied to the wild type dataset three separate elution peaks were observed. Product ion spectra from the mass of interest at these time points suggest acetylated GD1a, GD1b and GD1c, which has a similar structure to GD1b so also contains a characteristic disialic acid product ion but with different peak intensity ratios.

were observed, possibly reflecting acetylated forms of GD1a, GD1b and GD1c. Retention times were similar to those of GD1a and GD1b and a third GD1 peak conjectured to be GD1c, which has a structure similar to GD1b in that the two sialic acids are linked. Product ion spectra from m/z 938.3841, taken from the three retention time points, supported this (Figure 42). A characteristic acetylated disialic acid product ion (m/z 623.1667) was observed in the m/z 938.3841 dissociation spectra from the retention time point of OAcGD1b and the putative OAcGD1c structure but not from OAcGD1a. Relative intensities of OAcGD1a, OAcGD1b and OAcGD1c differed between extracts and did not correlate with GD1a, GD1b and GD1c intensities in any but wild type extracts. This suggested that the addition of the O-acetyl group was not an artefact of extraction nor solely regulated by the abundance of the substrate.

The mass filter was finally applied to the GalNAcT knockout datasets. One elution peak was

154

observed at the retention time of the putatively identified OAcGD1c in wild type and rescue extracts (data not shown). Blank runs ruled out carry over between samples. It may be that while these mice cannot synthesise complex gangliosides via the a- and b-series there is an alternative enzymatic pathway along the o-series branch (Figure 35) that enables the production of GD1c and its consequent O-acetylation.

5.2.2.2 Description of GMx in Rescue Mice

HPTLC-IMS data from NFL, THY1 112 and THY1 115 rescue mice indicated a novel ganglioside band corresponding to the m/z 1453; the mass of GD3 minus water. Adduct formation in ROI spectra and chromatographic position suggested this was a monosialylated species. This was then investigated in HPLC-MSMS data. A mass filter was applied to the NFL rescue dataset for m/z 1452-1454. A single chromatographic peak was located at RT 18.7 from m/z 1452.8234. The mass filter was adjusted (m/z 1452.8234, 5 ppm) and applied to the THY112 and THY115 rescue HPLC-MSMS datasets revealing similar peaks at RT 18.7 min in both. This species eluted over two minutes after GD3 itself (RT 16.0) suggesting that GMx was less hydrophilic than GD3. Ionisation occurred exclusively as the [M-H]$^-$ ion also suggesting a monosialylated species.

The GMx product ion spectrum, which were consistent between datasets, contained a peak at m/z 563.2 equating to the mass of a disialic acid minus water, placing the dehydration on the sialic acids. The exclusive presence of a dehydrated GM3 product ion, rather than GM3 itself, suggested this occurred on the primary galactose-linked sialic acid. Deoxydidehydro-sialic acids (dehydrated sialic acids) have been reported before. Soluble 2-deoxy-2,3-didehydro-sialic acid has been detected in fluids including serum, saliva and urine (Nohle et al., 1985; Varki & Schauer, 2009). In this instance the dehydration may involve the carboxylic acid or N-acetyl group due to the loss of the second charge. The precise position was not established.

The monosialylated GMx strucutre was confirmed in NFL, THY112 and THY115 rescue and in the GalNAcT knockout datasets. Inconclusive traces were identified in the WT and STII

knockout extracts at < $5.5E^3$ normalised intensity. If GMx was present in these mice, it was synthesised at low levels. It was unknown if GMx was an artefact of extraction or a modification made before or after the incorporation of the sialic acid into the ganglioside. The detection of GMx in extracts that contained a build-up of GD3, rather than GM3, suggested that the modification occured after the addition of the second sialic acid, and was driven by an abundance of the GD3 structure. Intensity values from the GalNAcT knockout and rescue mice indicated a negative correlation (0.84) between GD3 and GMx intensity suggesting that levels of GD3 decrease as levels of GMx increase. This could indicate that the dehydration of GD3 occurred post-extraction in samples containing an absolute level of GD3 or that the modification accumulates with age in these mice while synthesis of GD3 plateaus.

5.2.2.3 Profiling in HPLC-MS Datasets Using Standards Analysis to Confirm Identifications

5.2.2.3.1 Extracting Retention Times from CGE Separations

Standard retention times (SRT) have been used previously to confirm identifications made by accurate mass. Here these were generated from CGE samples, the components of which were well characterised, run at the beginning and end of each experimental batch. Mass filters were applied for gangliosides including GM1, GM2, GM3, GD1, GD3, GT1, GQ1 and OAc-GD3 and GD1 with various ceramide strucures. A number of hypothetical head groups, such as acetylated or dehydrated GM1 and GT1, were also included. Retention times were extracted for at least one ceramide structure, primarily the d18:1/18:0 structure, for most gangliosides. GMx was not identified. Retention time shifts of 0.08-0.23 min were revealed across the batch so an average SRT was calculated for each. Ganglioside profiles for each mouse were then constructed by applying ganglioside mass filters to experimental datasets and extracting detection, intensity and retention time for each. To confirm identifications extracted retention times had to agree with mean SRT +/- 0.1 min and/or a minimum of three other extracts (# matches WT=29, GD3 KO = 18, GM/D2 KO = 8, NFL = 20, PLP = 20, THY112 = 25, THY115 = 19). Where applicable, ganglioside RT deviation was ≤ 0.07 min between extracts.

5.2.2.3.2 Ganglioside Detection in Experimental Datasets

Only gangliosides with normalised intensity > 10,000 were included in profiles; intensities below this were obtained on occasion from background noise alone. Normalised intensity under the extracted ion chromatogram was recorded as a correlative measure of abundance. If more than one elution peak was present (eg. GD1 filters) the maximum peak intensity was taken from under each elution peak. All identifications were supported by product ion spectra containing characteristic ganglioside fragment ions as identified in Chapter 5. Acetylated sialic acid fragments were identified in product ion spectra from all mentioned acetylated species although the 9-O-position was not confirmed. Normalised intensities for the major complex ganglioside species (GM1, GM2, GD1a, GD1b, GT1b, d18:1/18:0) are indicated for WT and rescue mice in Figure 43.

In wild type extract complex gangliosides GM1, GM2, GD1a, GD1b, GT1b and GT1a and simple gangliosides GM3 and GD3 were detected. Acetylated forms of GD1a and GD1b, GT1b and GT1a were also identified. If OAcGD3 was present it was below the intensity cut-off. The predominant peaks corresponded to the d18:1/18:0 species of GM1, GD1a and GD1b. GQ1b, which is sometimes reported as a component of wild type gangliosides by HTPLC, was not detected here. In the STII knockout gangliosides GM1, GM2, GM3, GD1a and OAcGD1a were identified (data not shown). The predominant gangliosides were GM1 and GD1a, detected at similar intensities to the wild type,and GM3 which was detected at intensities an order of magnitude higher. In GalNAcT knockout mice only simple gangliosides were identified; predominantly GM3 and GD3 both at high intensity, as well as 9OAcGD3 and GMx at lower intensities.

In the NFL rescue simple gangliosides GM3, GD3, 9OAcGD3 and GMx were detected with mid- to high-intensity levels. Complex gangliosides including GM1, GM2, GD1a, GD1b, GT1b and acetylated forms of GD1a, GD1b and GT1b were also detected albeit at intensities an order of
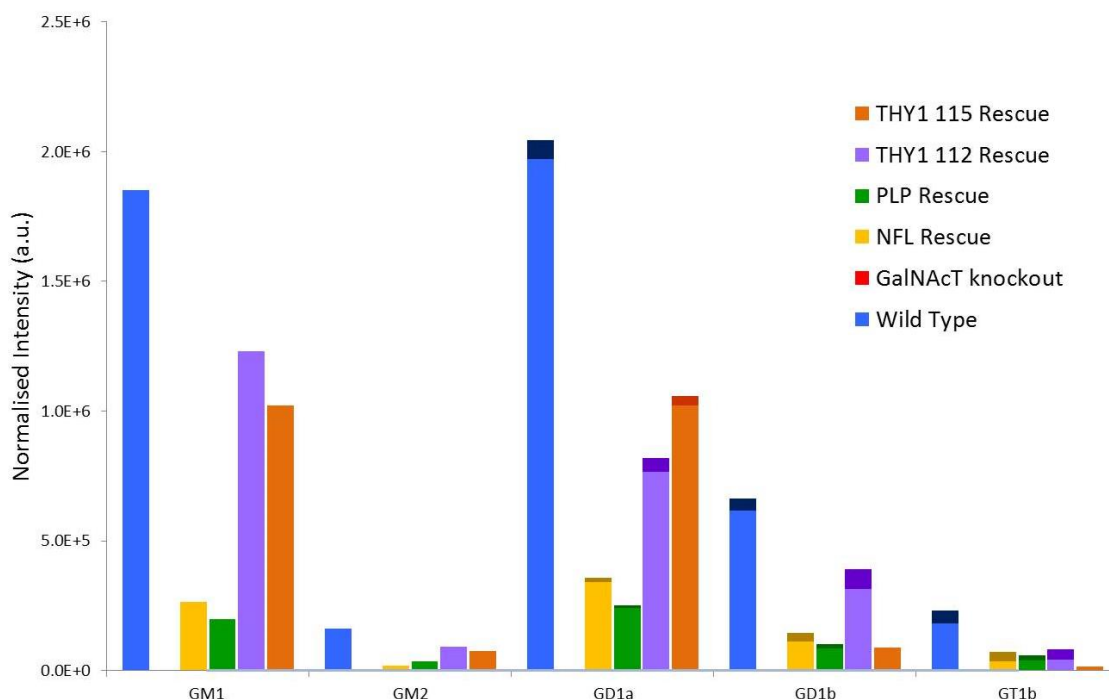
Figure 43. Relative Abundance of Complex Gangliosides in Brain Tissue Extracts from Rescue Models. Total elution peak intensities are shown for the d18:1/18:0 species of the major complex gangliosides GM1 , GM2, GD1a, GD1b and GT1b found in wild type brain for wild type, GalNAcT knockout, and NFL, PLP, THY1 112 and THY1 115 rescue model brain extracts (n=2). Acetylated species are shown as darker bands at the top of each bar and were not detected for monosialylated gangliosides. Complex gangliosides were not detected in GalNAcT knockout extracts (red) but were detected, including acetylated species, at various relative abundances from all rescue model extracts, although always at lower abundance compared to the wild type.

magnitude lower than observed in the wild type. Similar identifications were made in PLP rescue extract (green) and THY112 (purple) and THY115 (red) rescue extracts.

5.2.2.3.3 Relative Quantitation of Ganglioside profiles

For each ganglioside the MS signal intensities from the two major ceramide structures; d18:1/18:0 and d20:1/18:0 (where detected), were processed from HPTLC-IMS and HPLC-MSMS datasets into percentages of the total detected ganglioside intensity to create comparative profiles for each extract. The d18:1/18:0 ceramide structure was predominant in all identifications followed by the d20:1/18:0 structure. In HPLC-MSMS data other minor ceramide structures were identified for the most abundant gangliosides, such as GM1 in wild type, and GM3 in STII and GalNAcT knockout extracts. These included diverse chain lengths (d18:1/16:0 and d20:1/20:0), further desaturations (d18:1/18:1 and d20:1/18:1) and

Wild Type GM1 Ceramides   **THY1 112 Rescue GM1 Ceramides**   **STII Knockout GM3 Ceramides**

Legend: d18:1/16:0, d18:1/18:0, d20:1/18:0, d20:1/20:0, d18:0/18:0, d18:1/18:1, d20:0/18:0, d20:1/18:1
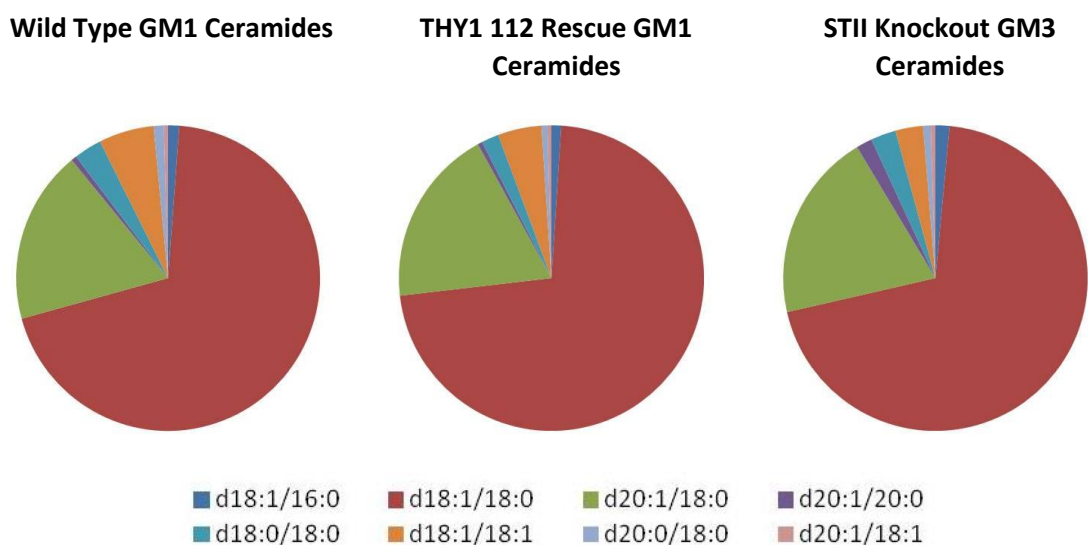
Figure 44. Relative Abundance of Ceramide Moieties in Monosialylated Gangliosides in Wild Type, Knockout and Rescue Mice. Although peak intensity is by no means quantitative, under certain conditions comparisons can be made between normalised intensities to infer relative abundance. Here intensities were processed into percentages of total ganglioside intensity in order to compare the inclusion of different ceramide moieties in the major monosialylated ganglioside species (wild type – GM1, THY1 112 – GM1, STII KO – GM3). Ceramide inclusion patterns were similar between the three, with nearly 75% of the major monosialylated gangliosides containing the d18:1/18:0 species in each mouse model. Similar ceramide patterns were observed in monosialylated gangliosides in other mouse models.

dihydrosphingosine-based ceramides (d18:0/18:0 and d20:0/20:0). Where detected the relative abundance of these different ceramide structures was consistent in WT, knockout, and rescue model extracts. Figure 44 illustrates this similarity in ceramide variation in monosialylated ganglsiodes in WT, STII knockout and THY1 112 rescue; the d18:1/18:0 and d20:1/18:0 structures accounted for 88-90% of the signal intensity from each. This relative abundance was consistent in other models, and across other gangliosides, including disialylated species. However, since the minor ceramide structures contributed negligible intensity values to the ganglioside intensity totals they were excluded from further relative quantitation.

Ganglioside profiles from HPTLC-IMS and HPLC-MS for wild type and GalNAcT knockout brain extracts and for NFL, PLP, THY1 112 and THY1 115 rescue brains are shown in Figure 45. The

relative profiles of complex gangliosides only are shown in the right column of Figure 45. All gangliosides identified from HPTLC datasets were included and >96% of the total intensity observed from ganglioside mass filters in HPLC-MSMS data was accounted for. Profiles from HPLC-MSMS data were noticeably more complex than those from HPTLC-IMS data due to the additional sensitivity and specificity of the technique. Several minor components such as GT1a and acetylated forms of GD1a and GD1b were only detected by HPLC-MSMS. It was also apparent that monosialylated gangliosides were perhaps over-represented in HPTLC-IMS datasets while larger polysialylated species were under-represented. The discete composition of the rescue profiles, excluding the minor components, was largely similar.

The WT ganglioside profile was dominated by complex gangliosides GM1, GD1a and GD1b and (in HPLC-MSMS data) GT1b. Less abundant complex gangliosides included GM2, GT1a and acetylated forms of GD1a, GD1b, GT1a and GT1b (indicated by the darker colours in Figure 45). Simple gangliosides GM3 and GD3 contributed a minor component of the overall ganglioside profile. Acetylated GD3 was not detected.

Figure 45. Comparative Relative Profiling of Gangliosides in Brain Extracts from HPTLC-IMS and HPLC-MSMS Datasets. (Figure follows on page 161). Normalised intensity was extracted for the d18:1/18:0 and d20:1/18:0 species of GM1 (blue), GM2 (pink), GM3 (red), GD1a (yellow), GD1b (cyan), GD3 (red), GT1a (pale purple) and GT1b (green) and acetylated forms of GD1a, GD1b, GD3, GT1a and GT1b (same colours, darker palette) from extracted chromatograms in HPTLC-IMS datasets and HPLC-MSMS datasets. Normalised intensities were further processed into percentage of total ganglioside signal for wild type, STII (data not shown), GalNAcT knockout, and NFL, PLP, THY1 112 and THY1 115 rescue brain extracts and incorporated into relative profiles. The wild type profile was dominated by GM1, GM2, GD1a and GD1b in HPTLC-IMS data and GM1, GD1a and GD1b in HPLC-MSMS data. Simple gangliosides GM3 and GD3 and complex gangliosides GM2 and GT1a were detected with low relative abundance. Only simple gangliosides and 9OAcGD3 were detected in the GalNAcT knockout by HPTLC-IMS. An additional species, GMx (purple), with the mass of dehydrated GD3, was detected by HPLC-MSMS. In rescue models, both HPTLC-IMS and HPLC-MSMS data revealed that profiles were dominated by simple precursor gangliosides GM3, GD3 and 9OAcGD3. However all wild type complex gangliosides were also detected by HPLC-MSMS except GT1a and the acetylated form. Proportionally, a higher extent of the profile in the THY1 rescues came from these complex gangliosides compared to the NFL and PLP rescues (>50% vs. 18% and 8% respectively). However closer inspection of the relative profile of the complex gangliosides only showed that the PLP and NFL profiles more closely resembled the relative abundance of complex gangliosides in the wild type.
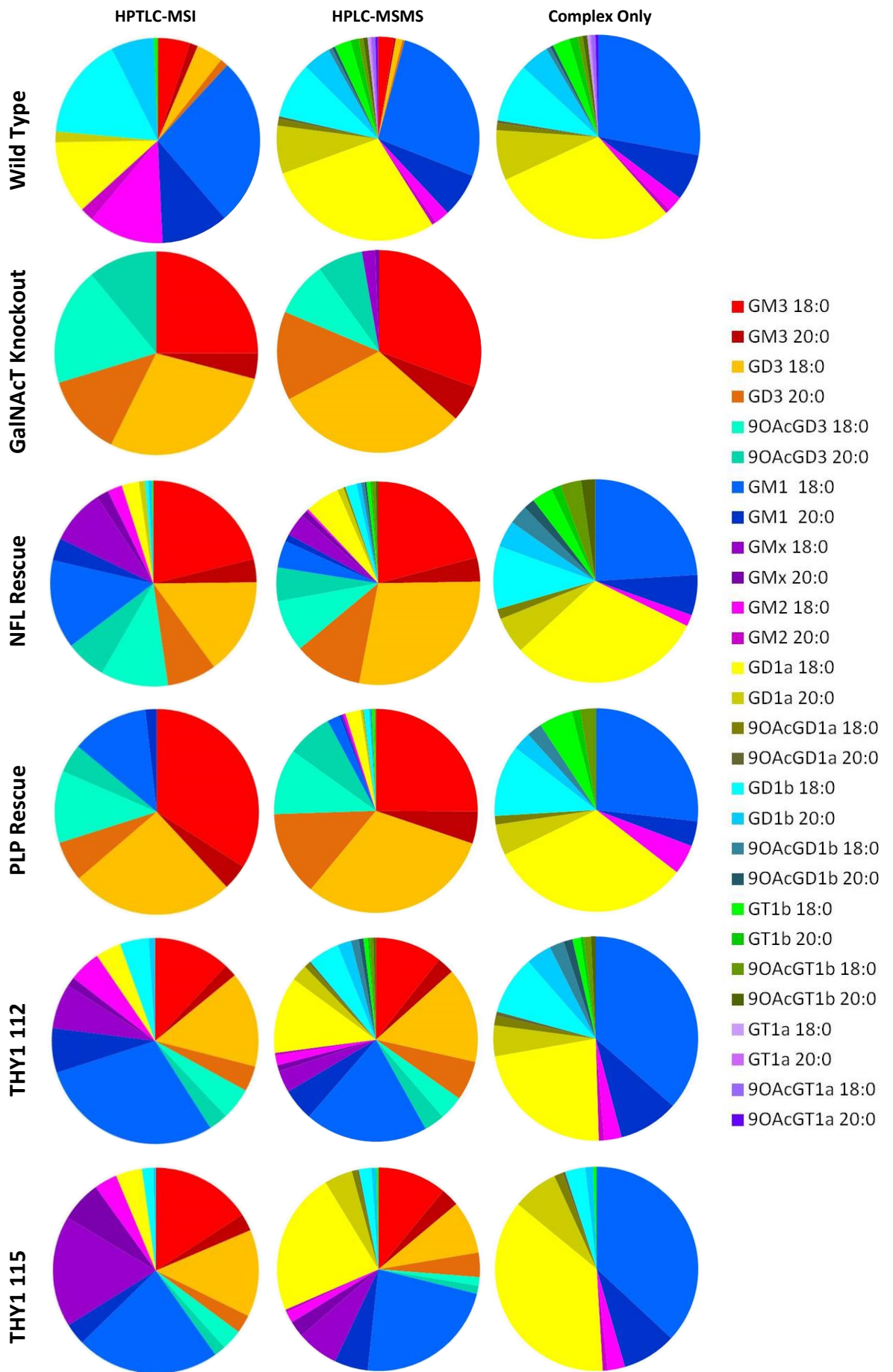
The STII knockout profile was dominated by a-series gangliosides; GM3 and, less so, by GD1a

and GM1. GM2 was detected as a minor component as well as an acetylated-GD1; OAcGD1a

which was first observed by HPTLC-IMS, then confirmed and described in HPLC-MSMS data.

GD3 was identified at low intensity in the STII model by HPLC-MSMS. This was unexpected as

this mouse lacks the GD3 synthase enzyme necessary to synthesise this ganglioside suggesting

that alternative synthetic pathways may be available. As can be seen in Figure 45 (orange) this

formed an extremely small component of the total ganglioside composition. Only simple

gangliosides GM3, GD3, 9OAcGD3 and GMx (GD3 minus water, only detected by HPLC-MS)

were identified from the GalNAcT knockout.

Figure 45 shows the ganglioside profiles of the rescue mice being described here for the first

time, compared to the wild type. The rescue profiles still showed the build-up of simple

gangliosides GM3, GD3 and 9OAcGD3 above wild type levels that was characteristic of the

GalNAcT knockout on which they were based. This was less pronounced in the THY1 112 and

THY1 115 rescues, where simple gangliosides comprise <50 % of the total profile, compared to

approximately 50 – 60 % in the NFL rescue and 70-75 % in the PLP rescue. However complex

gangliosides were also identified in all rescue mice. By HPLC-MSMS a near full range of WT

complex gangliosides (GM1, GM2, GD1a, GD1b and GT1b as well as acetylated GD1a, GD1b

and GT1b), excluding GT1a and its acetylated form, were identified from all rescue mice. The

complex ganglioside profiles, indicated in the right hand column of Figure 45, while at lower

absolute abundance, were similar between WT and rescue mice, indicating comparable

amounts of each complex species relative to each other. The main exception to this was that

GM1 appeared over-represented in THY1 112 and THY1 115 profiles, and GD1a over-

represented in the THY1 115 profile.

5.3 Discussion

In this chapter we applied novel profiling methods developed in earlier chapters to the

molecular profiling of biological samples and the identification of unknowns. Both HPTLC-IMS

and HPLC-MSMS were employed to analyse brain gangliosides from wild type and engineered mouse models of relevance to autoimmune neuropathies such as Guillain-Barré Syndrome. The gangliosides of wild type and the two knockout mice, STII and GalNAcT have been described previously thus providing a basis for assessing the accuracy of the MS techniques (Takamiya et al. 1996; Okada et al. 2002; Handa et al. 2005). This earlier profiling appears to have exclusively employed conventional HPTLC using a sialic acid specific resorcinol stain.

The gangliosides of wild type mouse brain are reported to consist primarily of complex gangliosides GM1, GD1a, GD1b and GT1b. Gangliosides GM3 and GD3 are occasionally described as minor components (Figure 36). These species were all detected in WT extracts by HPTLC-IMS, despite GT1b being undetectable by staining alone. Based on peak intensities, which appreared to be semi-quantitative, the predominant species appeared to be GM1, GM2, GD1a and GD1b, which agrees with previous publication. The intensity of GT1b, which is normally reported to be a major WT ganglioside component, was low in IMS data. Possible explainations are 3-fold; the IMS sample preparation may not extract GT1b from the HPTLC plate as well or as fast as smaller less polar gangliosides during sample preparation for IMS. The structural size and complexity of GT1b may also hinder efficient ionisation compared to smaller gangliosides. And finally resorcinol is a sialic acid specific stain that amplifies the intensity of gangliosides with a higher degree of sialylation such as GT1b and may have over-represented its abundance in the literature. This issue could be investigated further using ganglioside standards to compare relative signal from GT1b and smaller species by HPTLC-resorcinol and HPTLC-IMS. If the HPTLC-IMS workflow is under-performing for GT1b, further optimisation of the preparative steps could improve the extraction and ionisation of larger, more polar gangliosides.

By HPLC-MSMS, GM1, GD1a, GD1b and GT1b were identified as the major components of wild type extract, mirroring previous reports. The abundance of GT1b, while still under-represented compared to resorcinol stained HPTLC plates, comprised a more significant proportion of the

profile suggesting that electrospray ionisation is more efficient than MALDI for the ionisation of larger gangliosides. Minor components GM2, GM3 and GD3 were also detected, as well as GT1a and acetylated forms of GD1a, GD1b, GT1a and GT1b, all confirmed by CID, which are rarely reported in conventional HPTLC studies. Identification of these acetylated gangliosides is supported by previous results from Furukawa *et al*. who observed several unknown bands in wild type extract after HPTLC-overlay with an anti-9-OAcGD3 antibody. This indicated several 9-O-acetyl sialic acid containing gangliosides that were not accurately identified at the time (Keiko Furukawa et al., 2008).

STII and GalNAcT knockout ganglioside profiles also widely agreed with previous reports (Figure 36) by both HPTLC-IMS and HPLC-MSMS. These results demonstrated the accuracy of the MS methods for ganglioside profiling in biological samples. Specific benefits were observed for each technique. HPTLC-IMS had increased simplicity and compatibility with traditional techniques while HPLC-MS had higher sensitivity, specificity and was more appropriate for relative quantitation. Profiles differed slightly in their representation of monosialylated and disialylated species. This was possibly due to the more efficient ionisation of smaller species by MALDI, suggesting that the HPLC-MSMS profiles were a more accurate depiction. Again quantitative studies using commercial ganglioside standards could be undertaken to investigate this.

Both methods were then applied to profiling genetically engineered rescue mice in which ganglioside profiles were thus far unknown. These novel rescue mice are based upon the GalNAcT knockout model but have the gene rescued under promoters exclusively active in distinct tissues; in this instance either in nerve (NFL, THY112, THY115) or glial cells (PLP). Phenotypically the NFL, THY112 and THY115 rescue mice are normal while the PLP suffers age-related neurodegeneration similar to the knockout. It is essential to their functional relevancy modelling heterogeneous human diseases that the synthesis of complex gangliosides is rescued to some degree in these mice. Thus far it was only known that synthesis of the

enzyme itself is rescued at low levels in the nervous tissue. Whether the synthesis of complex gangliosides is rescued in each model and to what degree was not known. These questions have now been answered using these novel MS techniques.

Results by both HPTLC-IMS and HPLC-MSMS confirmed that synthesis of complex gangliosides was rescued in the brain tissue of all rescue models investigated. Relative profiling was done using absolute intensities (Figure 43) and relative intensities (Figure 45, 46). The latter was more tolerant of inconsistencies in sample preparation that may affect ganglioside extraction efficiencies. The build-up of downstream precursor gangliosides GM3, GD3 and 9OAcGD3 which characterise the GalNAcT knockout profile was still observed in the rescues, comprising up to 75% of the ganglioside profile. This was to be expected since the examined organ, the brain, is made up of a complex mix of both nerve and glial cells. Regardless of the cell specificity of the promoter under which the GalNAcT gene was rescued, many brain cells would remain GalNAcT -/-. Additionally glycosyltransferase activity assays showed low GalNAcT activity in rescue mice compared to the wild type (5.3% NFL rescue and 11.7% in the PLP rescue).

That said complex gangliosides were also detected from all rescue mice by HPTLC-IMS and HPLC-MSMS. By HPLC-MSMS, the more sensitive method, all wild type complex gangliosides aside from GT1a were identified in the rescues including minor acetylated species. It appeared that, out of the rescue models, in absolute terms (Fig. 43) and regarding the ratio of simple to complex gangliosides (Fig. 46), the synthesis of complex gangliosides was rescued to a higher degree in the THY1 112 and THY1 115 rescue mice. This may be a consequence of the protomer activity, which could be investigated using mRNA hybridisation or protein assays. In profiles however this increase appeared to relate primarily to GM1, or to the a-series pathway in the THY1 115. In terms of complex gangliosides only, the NFL rescue profile most closely resembled the wild type, which may have significance when it comes to modelling Guillain-Barré Syndrome. Differences in rescue phenotype appeared not to relate to the presence of a

particular complex ganglioside or to relative composition, as these were similar in all rescue mice. Rather these results suggested differences in phenotype were most likely due to the cellular location of complex gangliosides. It would be interesting however to do an longitudinal study to investigate whether age-related changes in profile may also contribute to neurodegeneration.

Finally it is worth noting in this discussion that the capabilities of the HPLC-MSMS method were further demonstrated by the description of two unknown species, GMx and OAcGD1a, that were initially detected in HPTLC-IMS datasets. Modifications were identified in other datasets with relative ease and mapped onto the sialic acid moieties by MSMS. More specific localisation could be achieved by applying further MS^n. These observations led to the detection of other acetylated species including GD1a, GD1b, putative GD1c, GT1b and GT1a. These species are not usually detected in ganglioside profiling studies but may occur as low abundance native modifications at higher frequency than previously thought. This may be of biological significance considering autoantibodies specifically against the 9-O-acetylated form of GD3 have been correlated previously with cranial nerve involvement (Koga, Yuki, Ariga, & Hirata, 1999).

Chapter 6. Single Nerve Glycosphingolipidomics; Profiling in Peripheral Motor and Sensory Nerves

6.1 Introduction

Guillain-Barre Syndrome and similar conditions such as Miller-Fisher Syndrome (MFS) and Multifocal Motor Neuropathy (MMN) cover a number of related but distinct diseases. One of the defining characteristics is the focal nerve or tissue; MFS affects the optical nerves, MMN the motor nerves, and GBS covers a range of pathological subtypes that affect specifically motor nerves (acute motor axonal neuropathy, AMAN), motor and sensory nerves (acute motor and sensory axonal neuropathy, AMSAN), or the associated Schwann cells (acute inflammatory demyelinating polyneuropathy (AIDP)). Clear causes for this specificity have not yet been identified amongst the complex onset of these conditions. It is partially linked to the presentation or enrichment of particular ganglioside epitopes on different cell types, combined with the presence of corresponding autoantibodies, as appears to be the case in MFS. MFS is clinically characterised by ophthalmoplegia, ataxia and areflexia, and has been strongly associated with anti-GQ1b IgG antibodies (A Chiba et al., 1992). Studies have since shown GQ1b to be abundantly expressed in oculomotor nerves linking the predominant site of epitope presentation with one of the primary clinical symptoms. Anti-GQ1b antibodies have also since been associated with GBS presenting with ophthalmoplegia, Bickerstaff's brainstem encephalitis, a syndrome thought to be on the same spectrum as MFS, and acute ophthalmoparesis (A. Chiba, Kusunoki, Obata, Machinami, & Kanazawa, 1993; N. Yuki, Sato, Tsuji, Hozumi, & Miyatake, 1993; N Yuki, 1996).

Unfortunately such clear cut associations are rare in peripheral autoimmune neuropathies. Ganglioside GQ1b has in fact been identified at low levels in peripheral nerves around the body; thus far, despite many hypotheses, there is no absolute explanation why anti-GQ1b antibodies direct damage to the oculomotor nerves when the epitope occurs ubiquitously (Atsuro Chiba, Kusunoki, Obata, Machinami, & Kanazawa, 1997; Lars Svennerholm et al.,

1994). Similarly, a robust correlation has been observed between anti-GM1 and GM1:GalC complex antibodies and MMN, a pure motor neuropathy (Galban-Horcajo et al., 2013; Pestronk et al., 1988). Yet the target epitope GM1 is found on both motor and sensory nerves with similar distribution and only mild motor enrichment with no explanation why anti-GM1 antibodies characteristic of MMN should direct damage to motor nerves only (O'Hanlon, Paterson, Veitch, Wilson, & Willison, 1998; Sheikh, 1999). Other less robust correlations have been found in many of these neuropathies; for example between the presence of anti-GM1 IgG and anti-GD1a antibodies and presentation of motor nerve-specific AMAN over AMSAN or demyelinating AIDP despite the detection of both GM1 and GD1a in sensory and motor nerve axons and myelin (Ho et al., 1999; Ogawa-Goto, Funamoto, Ohta, Abe, & Nagashima, 1992; Willison & Yuki, 2002). The instances mentioned here are the better examples drawn from a vast bank of literature identifying weak, inconsistent and often contradictory correlations between antibody affinities and syndrome, symptom and severity. Clearly the relationship between pathogenesis, antibody specificity and ganglioside presentation is not straightforward and involves factors beyond the simple co-existence of epitope and autoantibody.

A comprehensive profile of tissue-specific gangliosides is therefore an essential foundation on which to base these investigations in order to know the abundance and distribution of potential target epitopes. From the literature it is clear that the major gangliosides profiling experiments still referenced today were performed over a decade ago by TLC/HPTLC profiling and resorcinol stain despite recent improvements in technology and sensitivity (Atsuro Chiba et al., 1997; Ogawa-Goto et al., 1993; Lars Svennerholm et al., 1994). The low availability of biological tissue, which is unavoidably taken post-mortem, has also limited the description of unknown species or modifications beyond basic profiling. Low abundance components may have gone undetected by these methods. This is despite reports that antibodies against minor gangliosides such as GM1b and GalNAcGD1a correlate with clinical factors such as previous gastro-intestinal illness, faster progression, increased severity, distal weakness and lack of

cranial or sensory involvement (Kaida, Kusunoki, Kamakura, Motoyoshi, & Kanazawa, 2008; Kusunoki et al., 1996; Nobuhiro Yuki et al., 2000). In previous chapters we demonstrated the sensitivity and specificity of the HPLC-MSMS method developed in this thesis, particularly for describing unanticipated ganglioside modifications. In this chapter we therefore applied this technique to profiling gangliosides from extremely low sample masses to test the limits of sensitivity for ganglioside profiling using this method. As a pilot study total lipid was extracted from sciatic and sural peripheral nerves from wild type mice amounting to 3 - 12 mg tissue and profiled by HPLC-MSMS. Once it had been confirmed that the sensitivity limits allowed the detection of gangliosides from single nerve samples, several extraction and enrichment methods were compared to examine their effects on detection sensitivity by HPLC-MS. Finally sensory and motor roots were dissected from the spinal nerve of wild type mice, thereby avoiding much of the connective tissue, prepared with internal standards and profiled using HPLC-MS.

6.2 Results

6.2.1 Pilot Extraction from Wild Type Sciatic Nerve

In the profiling studies discussed above, with the exception of Chiba et al., extractions were performed on a minimum of 0.5 g of tissue and samples were pooled from up to 10 individuals from a mixture of backgrounds, ages and causes and times of death. Here we attempted to extract material from single nerves from mice, starting with less than 50 mg of tissue. To test whether this would yield detectable ganglioside levels total lipids were extracted from single sensory sural (30 mg) and mixed sciatic (11.5 mg) nerves from wild type mouse. Data was collected by HPLC-MSMS, analysed using M/Z Mine software and identifications made using the Scripps METLIN database. Over 500 lipids were putatively identified from peaks with normalised levels over $4e^4$ from both datasets; predominantly phospholipids PE, PG, PS and PI and including hexosylceramides, sulfatides, and larger glycosphingolipids. No ganglioside peaks were extracted using automated software. However the application of specific mass filters

revealed peaks corresponding to GM1, GM3, GD1a, GD1b, GT1a, GT1b and GQ1b from sciatic nerve and GM3, GD1a, GD1b, GD3 and GT1b from sural nerve. It was concluded that gangliosides could be detected in total extract from single nerve tissue samples, but signal intensity was over two orders of magnitude lower than other lipids.

6.2.2   Comparison of Extraction Methods

The next process was to discern whether further sample preparation improved ganglioside sensitivity by enrichment and reduction of ion suppression, or resulted in a reduction of signal through unavoidable material losses during additional preparative steps. No literature could be found on starting material limits for the preparations used. However it must be considered that no preparative re-extraction is 100% efficient and each process introduces an amount of absolute material loss. It must also be considered that as the initial amount of material decreases this loss will account for a larger proportion of the total. When applied to such small amounts of initial material it may occur that the loss introduced by extensive sample preparation accounts for such a high proportion that the end sensitivity is reduced rather than improved by processing.

To investigate this, lipids were extracted from an available saphenous nerve (25 mg) from an NFL rescue mouse. Extract was divided into four volumes, three of which were processed further using phase partitioning, solid phase extraction and weak anion exchange as described in Chapter 3. Data was collected from the four fractions by HPLC-MSMS, normalised by wet tissue weight. Figure 46 shows the base peak chromatograms (top per pair) and extracted ion chromatograms for gangliosides (d18:1/18:0, bottom per pair) from total lipid extract (black) compared to Folch upper phase (blue), upper phase followed by solid phase extraction (green) and upper phase after weak anion exchange enrichment (red). Signal from gangliosides increased in intensity with successive sample preparations from $3.51E^{4}$ in total lipid extract to $4.89E^{5}$ after weak anion exchange; an increase of an order of magnitude. This suggested that even using such small tissue samples the extra preparative steps were recompensed by

additional ganglioside sensitivity. Ganglioside analysis was also simplified after solid phase

extraction or weak anion exchange after which gangliosides comprised many of the observable

peaks in the base peak chromatogram (see Figure 46 comparison of peaks in extracted ion

chromatograms for gangliosides and base peak chromatograms).
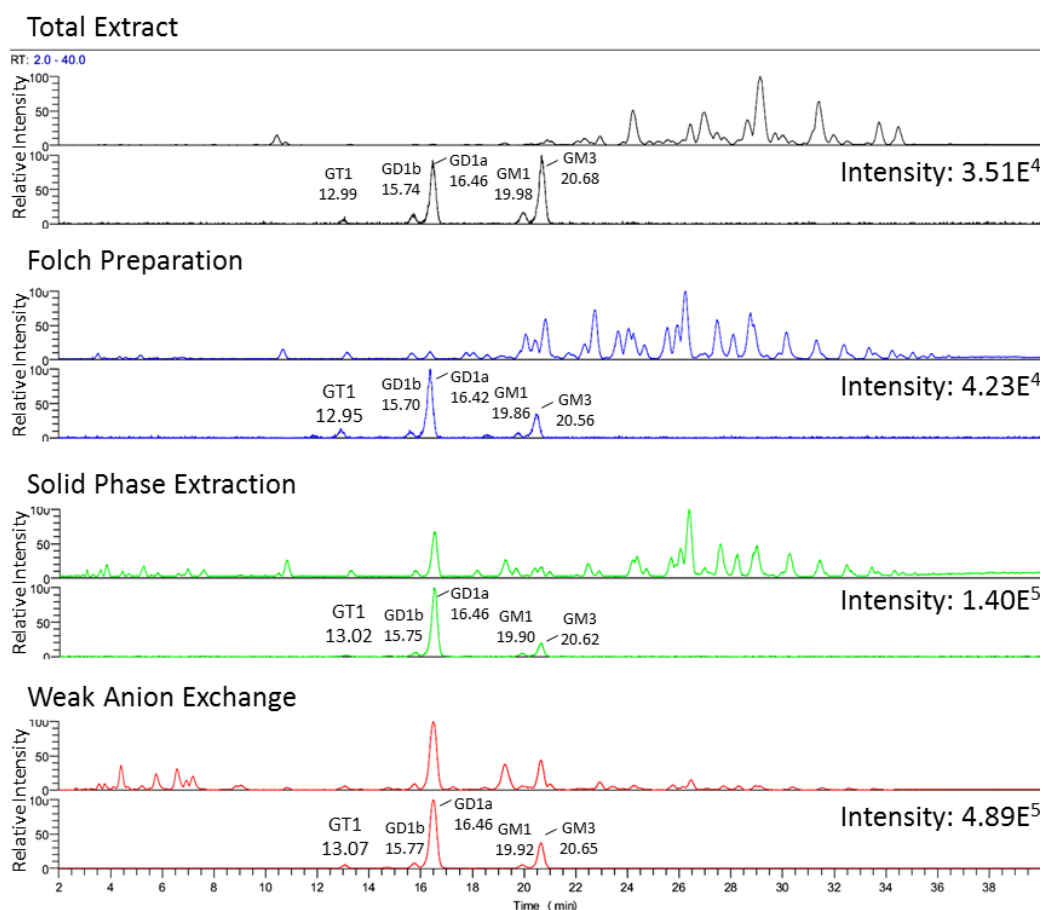
Figure 46. Optimising Ganglioside Extraction using Different Sample Enrichment Strategies. Four sample preparation procedures; total extraction (black), Folch partition (blue), solid phase extraction (green) and weak anion exchange (red), were used to extract lipids and enrich gangliosides in samples from sciatic nerve tissue in order to select an optimal sample preparation for extracts from small samples. The base peak chromatogram is shown above the extracted ion chromatogram from the d18:1/18:0 species of GM1, GM2, GM3, GD1a, GD1b, GD3 and GT1b for each preparation method. The suitability of each method was assessed on the normalised intensity under the extracted ion chromatogram and the presence of ganglioside peaks in the base peak chromatogram (matched on retention time). Significant contamination by other lipids was observed in all preparations but weak anion exchange, indicated by the presence of many elution peaks besides gangliosides in the base peak chromatograms. The relative intensity under the extracted ion chromatogram was also nearly four times after weak anion exchange compared to solid phase extraction; the next most intense. Both measures suggested weak anion exchange as the optimal sample preparation method to minimise ganglioside ion suppression and maximise ganglioside detection for small sample extractions.

6.2.3   Analysis of Sensory and Motor Nerve Roots

6.2.3.1 Extraction of Internal Standard Data

It had been observed in earlier experiments that variation in signal intensity by HPLC-MSMS increased when analyte abundance was very low. This was likely to be the case here where spinal roots from individual wild type mice were the targeted tissues. Therefore internal standards (IS) were introduced so that data could be normalised by more than wet tissue mass during processing. Deuterated gangliosides GM2 and GM3 were introduced to each sample before the initial lipid extraction at 0.5 µg/mg and 0.2 µg/mg tissue weight respectively. These standards were first analysed by direct injection and HPLC-MS with dissociation. The $[M-H]^-$ ion of the CD_3-d18:1/18:0 species was identified as the predominant peak in both, as well as GM2 CD_3-d18:0/18:0 and CD_3-d20:1/18:0 and GM_3 CD_3-d18:1/16:0, CD_3-d18:0/16:0 and CD_3-18:1/17:0. Undeuterated GM2 and GM3 were not detected. However product ion spectra and HPLC retention times were near-identical to the undeuterated counterparts.

After data collection the relative standard deviation in IS intensity between the 10 extracts was 68.9% for GM2 CD_3-d18:1/18:0 and 60.6% for GM3 CD_3-d18:1/18:0 despite normalising injection volumes by wet tissue weight. The predominant peaks at the respective elution times were identified as the expected deuterated ions, suggesting this variation was not a result of ion suppression. The correlation between the intensity of GM2 CD_3-d18:1/18:0 and GM3 CD_3-d18:1/18:0 within extracts was high (0.99) and both IS were applied to normalising ganglioside intensities.

6.2.3.2 Relative Quantitation in Sensory and Motor Nerve Datasets

6.2.3.2.1   Data Processing

Initial investigation found that the predominant peaks in base peak chromatograms came not from gangliosides but other acidic polar lipids including sulfatides and PI. Ganglioside peaks were detected but at low peak intensities. Automated analysis and comparison were attempted using MZmine 2 software, Scripps Centre's XCMS Online and in-house Excel-based

Ideom (Creek, Jankevics, Burgess, Breitling, & Barrett, 2012; Pluskal et al., 2010). However reliable and consistent detection and processing of gangliosides at such low levels was not possible using these softwares despite lowering threshold and quality levels. Ganglioside intensities were therefore manually extracted using mass filters applied in Xcalibur software and normalised using IS intensities.

6.2.3.2.2 <u>Extraction of Ganglioside Data</u>

Gangliosides GM1, GM3, GD1a, GD1b, GD3 and 9OAcGD3 of the d18:1/18:0 species were detected in all extracts regardless of whether they came from sensory or motor roots. The d20:1/18:1 species were also detected where these lipids were abundant. GT1b was detected in all samples bar one motor extract. Other less ubiquitous gangliosides that were identified included GM2 detected in two motor root extracts, GMx detected in one motor root extract, O-acetylated GD1a identified in all but one sensory and one motor root extract (incidentally from the same mouse) and GQ1b which was detected in one motor extract. Other gangliosides epitopes where antibodies have been shown to be linked to certain syndromes such as GM1b and GalNAcGD1a were not detected, nor were ceramide moieties other than the d18:1/18:0 and d20:1/18:0 structures. The mean intensities of each ganglioside in motor and sensory root extracts before and after normalisation are shown in Figure 47. Data from one mouse was removed from the mean intensity of GD3 after being found to be abnormally high in both motor and sensory extracts. Several gangliosides including GM1, GD1a and O-acetylated GD1 and GD3 were detected at similar levels in sensory and motor roots. Complex b-series gangliosides GD1b and GT1b were detected at higher levels in sensory than motor roots while the simple b-series precursor GD3 was detected at lower levels. Where detected the d20:1/18:0 ceramide structures followed suit in all but GD1a where the d18:1/18:0 was higher in motor extracts while the d20:1/18:0 was higher in sensory extracts.

Figure 47. Abundance of Motor and Sensory Gangliosides Before and After Normalisation. Because the nerve tissue samples from which lipids were extracted were so small, deuterated gangliosides GM2 and GM3 were included as internal standards prior to extraction in order that ganglioside intensities could be normalised, sample to sample, at the end of analysis. The two graphs above show the relative intensities (mean, n=5) of gangliosides from motor (blue) and sensory (green) datasets before (above) and after (below) normalisation. Error bars were not included as the variation in signal intensities was too high in both motor and sesnroy datasets.

Statistical analysis revealed that variability within motor and sensory groups was however very high with coefficient of variance over 1 for several of the gangliosides detected. No statistical significance was found between mean intensities, either raw or normalised (p<1 in all cases) and principal component analysis revealed no clustering of the groups along components 1, which only accounted for 64% of the variance, 2 or 3. Transformation of the data into percentage total ganglioside intensities or matched pair ratios failed to improve the variability sufficiently to discover consistent patterns in ganglioside abundance between motor and sensory root extracts.

6.3 Discussion

There are few examples in the literature of peripheral nerve ganglioside profiling studies in mice with which to compare the results obtained here. This lack of study may be partially due to the challenge of the unavailability of material. Here, a range of simple and complex gangliosides have been detected by HPLC-MSMS from both sensory and motor roots and identified using a combination of accurate mass, retention time and dissociation. These included gangliosides GM1, GM3, GD1a, GD1b, GD3 and GT1b, as well as O-acetylated forms of GD1 and GD3. This widely agreed with the detection if not quantitation of two previous studies that were found. The first of these describes the ganglioside profiles of sensory root ganglion and sciatic nerve from an unspecified number of mice as having 'a normal repertoire of gangliosides' (Gong, 2002). It can be assumed that this also describes those identified here. The latter publication by Harpin *et al.* details the ganglioside composition of 100 pooled sciatic nerves which are a mix of motor and sensory roots (Harpin, Portoukalian, & Baumann, 1982). The major components of peripheral nerve were identified as GM1, GM3, GD1a, GD1b and GT1b as was found here. Several minor unidentified densitometric peaks were observed by Harpin *et al*. which may correspond to the O-acetylated varieties. They also detected sialosylparagloboside (SPG), an isomer of GM1, which was not identified in this study. This is difficult to explain as the paper contains no account of how identifications were made. The SPG identification may have been a misdiagnosis of O-acetylated GD3 which was identified in this study and occupies a similar thin layer chromatographic position to GM1; this is pure conjecture however without knowledge of their identification methods. GD3 was not identified in this paper despite being found to be a major contributor in this chapter. Initially GD3 appeared to be the predominant ganglioside in both sensory and motor roots. Closer inspection however showed much of the signal intensity to come from the extracts from a single mouse. The participation of GD3 was significantly lower in other samples. Once this anomaly was removed from mean analysis GD3 intensities fell below those of GD1a which Harpin *et al*. also identified as the predominant ganglioside of peripheral nerve.

Regarding the relative quantitation of gangliosides using signal intensities normalised by internal standards the variation within groups was too high in this study for analysis to reveal any significant and consistent differences in composition between motor and sensory roots. Assuming that the variation in peripheral nerve ganglioside composition is not naturally this high, which is probable, inconsistency must have been introduced during sample preparation and/or analysis. It was unlikely to come from HPLC-MS analysis; much of the process is automated by a high performance liquid chromatography system with high reliability in which performance affecting factors such as pressure, flow rate and column temperature are monitored. Auto-injection volumes were stabilised by initial methanol injections prior to running samples and MS instrument performance was checked using QC CGE injections at the beginning, middle and end of the sample batch. It is equally unlikely to have been introduced during sample collection; sensory and motor rootlets were dissected and separated by Jennifer Barrie, an experienced animal technician, in a consistent manner mouse to mouse. It was most likely therefore to have been introduced during tissue weighing, homogenization and/or ganglioside enrichment which may not be suitable methods for preparing sample masses this small. The loose correlation between intensity from internal standards and total gangliosides suggested a combination of these three procedural points.

Accurately weighing and homogenizing such small amount of tissue was challenging but could be improved by adapting the method carefully. Enrichment reproducibility could also be potentially improved by simplifying the process for example by using a single Sep-Pak C18 solid phase extraction rather than traditional DEAE sephadex weak anion exchange chromatography in large gravity driven columns. The reduced surface area of the C18 cartridge compared to a packed WAX column may result in more efficient re-elution of gangliosides when there is very little material available. SPE can also be automated, increasing the reproducibility, not to mention the throughput, of the extraction. Ultimately when applied to a larger organism such as a human peripheral nerve, where more material is available, this variability may become less influential. This would need investigating beforehand.

It is worth noting here that the analytical method itself, despite the poor reliability and reproducibility of the preparation, was capable of detecting and identifying a range of gangliosides from spinal roots from single mouse subjects including minor lipids such as acetylated GD1 and GD3 that have not, to the best of our knowledge, been detected from peripheral nerve before. With further optimisation of sample preparation HPLC-MS could enable the characterisation of human peripheral nerve gangliosides with unprecedented sensitivity. Several studies on peripheral nerves have reported significant differences in the ceramide composition between motor and sensory gangliosides (Ogawa-Goto et al., 1990; Lars Svennerholm et al., 1994). While this was not observed here this method of HPLC separation and detection by accurate mass allowed clear separation of ceramide modifications and could be used to clarify and expand upon these reports with relative ease.

Chapter 7. Imaging Mass Spectrometry in Central and Peripheral Nerve Tissue

7.1 Introduction

Mass spectrometry has demonstrable benefits for detecting and identifying gangliosides in complex or enriched mixtures with high sensitivity and specificity compared to traditional methods. However one of the major pitfalls of any profiling investigation is the loss of spatial information. This applies to both traditional and novel profiling techniques, where lipids must be extracted from whole tissues and sometimes pooled from multiple individuals. Achievable spatial resolution has therefore been restricted to the separation of, for example, sensory and motor nerves, or nerve myelin and axons through special preparative methods. The difficulties that arise attempting these small-scale separations, especially for low abundance lipids like gangliosides, have been discussed in previous chapters. Any localisation to morphological features or tissue strata is lost and yet may be vital to understanding the role of gangliosides and other lipids in development and disease.

Immunohistochemistry (IHC) and fluorescence microscopy can be used to investigate sub-cellular and tissue-wide distribution and has revealed the localisation of various gangliosides to nodes of Ranvier, paranodal Schwann cells, and nodal and intermodal axolemma (Sheikh, 1999). However for many glycosphingolipids IHC is plagued by difficulties beyond those typical of the technique. Antibody cross-reactivity between gangliosides and other glycosylated cell membrane components can occur. For rarer, modified or uncharacterised glycosphingolipids the necessary antibodies are unavailable and, without access to good quality standards, are impossible to generate. It is also worth noting that IHC reveals no information on the fatty acid arrangement of the ceramide moiety of which several native variations are known.

Imaging mass spectrometry (IMS), described in detail in Chapter 1.6.4, combines the specificity of mass spectrometry with the spatial detail of imaging. While the technique is compatible with several ion sources, the majority of biological imaging has been done in conjunction with matrix assisted laser desorption ionisation (MALDI). While MALDI-IMS lacks the sub-cellular

resolution of microscopy MALDI is a relatively soft ionisation technique that minimises fragmentation of large molecules enabling simultaneous detection across a relatively wide mass range. MALDI-IMS has been used to map the distribution of many metabolites in tissue sections but has been most widely applied to drug metabolite studies and more recently for lipid imaging. The few IMS papers that have been published on glycosphingolipids use MALDI-IMS exclusively and focus on mouse brain tissue; most likely because brain tissue is ganglioside-rich and mouse tissue easy to obtain (Chan et al., 2009; Colsch & Woods, 2010; Naoko Goto-Inoue et al., 2010). Simple detection of gangliosides in these tissues has been achieved but studies with biological context are rare. One interesting observation has been the differential distribution of sphingosine and eicososphingosine containing gangliosides in the hippocampal region and age-related enrichment of eicosasphinganine containing species in the dentate gyrus; an observation which, as mentioned, would not be possible by IHC (Chan et al., 2009; Colsch & Woods, 2010; Sugiura, Shimma, Konishi, Yamada, & Setou, 2008).

Secondary ion imaging mass spectrometry (SIMS) is a high-resolution alternative to MALDI-IMS. SIMS is the oldest mass spectrometry based imaging technique, originally developed in 1962 for chemical surface analysis and applied to elemental imaging in biological samples throughout the 1980's (M. S. Burns, 1982; Chandra & Morrison, 1992). During the 1990's SIMS was applied to the analysis of glycosphingolipid TLC preparations, including the detection of gangliosides, but has been overshadowed by online HPTLC-MALDI-IMS (Kasama, Hisano, Nakajima, Handa, & Taki, 1996; Kushi, Rokukawa, & Handa, 1988). More recently SIMS has branched into the detection of lipids in cell cultures and tissue sections (Johansson, 2006; Mas et al., 2007; D. Touboul et al., 2007). Unlike a MALDI source, SIMS resolution is not limited by the diameter of a laser beam, using instead a beam of primary ions to sputter secondary ions from a surface. The technique is therefore capable of sub-micrometer resolution and has already been used to achieve sub-cellular images of biological samples (McDonnell et al., 2005; Passarelli & Winograd, 2011). It must be noted though that SIMS experiments have thus far focused on the detection of only the most abundant membrane lipids such as cholesterol and

phosphocholine/sphingomyelin head group fragments. The only application of SIMS to the imaging of gangliosides in a membrane context has been the detection of labelled fragments from artificially mono-fluorinated GM1 in a supported lipid bilayer (Lozano et al., 2013).

Both MALDI-IMS and SIMS necessitate a significant trade-off between sensitivity and resolution and it is not yet known whether either will be applicable to glycosphingolipid or ganglioside imaging outside of the brain, where these lipids are less abundant. In this chapter we have applied both methods to imaging nerve tissue cross sections. MALDI-IMS was initially applied to imaging brain tissue sections from wild type and GalNAc T knockout mice to confirm a functional method. Different matrices were tested and an optimal matrix was then used to image spinal column sections from wild type, GalNAcT knockout and NFL rescue mice. This was done in order to answer both the question of MALDI-IMS applicability to ganglioside imaging and to investigate the occurrence and the detection and distribution of lipids in a novel genetic mouse model in relation to the wild type. The knockout mouse acted as a negative control for the detection of complex gangliosides in the wild type. We also report on attempted SIMS imaging of peripheral nerve cross sections to observe differences in myelin and axon composition. In order that ganglioside-specific fragments could be recognised, standards including phospholipids, sphingolipids and gangliosides were first analysed individually by SIMS. The resulting spectra were processed for peaks that were complex ganglioside-specific. Tiles of 50 x 50 μm were then collected from sciatic nerve sections and data sets processed for the presence and distribution of various ions.

7.2 Results

7.2.1 Imaging in the Central Nervous System

7.2.1.1 Developing a MALDI-IMS Method in Brain Tissue Sections

Sections of brain tissue were imaged to confirm a MALDI-IMS method capable of ionising and detecting gangliosides from tissue sections. The mass spectrometer was operated exclusively in negative ion mode as this was optimal for ganglioside ionisation. Tissue sections of 10 μm

thickness on ITO-glass slides were coated with DHB matrix using an automated system and imaged at 150 x 150 µm as described in materials and methods. Ion source and mass analyser settings were similar to those used in Chapters 4 & 5 for HPTLC imaging. Ganglioside peaks were visible in the overall average spectrum (OAS) of both wild type and knockout datasets which are shown in Figure 48b & c. In the OAS of wild type brain complex gangliosides GM1, GD1 and GT1, containing sphingsosine and eicososphingosine moieties were identified. Only simple gangliosides GM3, GD3 and OAc-GD3 were detected in the OAS of the GalNAcT knockout. Other acidic lipids were putatively identified in the lower mass range including PI, PS and PE species as well as several sulfatides. These other non-ganglioside lipids were detected at significantly higher peak intensity than gangliosides which were clearly minor components of the detected lipid repertoire.

As this was method optimisation, brain sections were taken at random without standardising the angle or depth of cryosectioning for initial experiments so it was not possible to map lipids to tissue features. However gangliosides and other lipids were observed to localise to specific strata in the mouse brain, examples of which are exemplified in Figure 48. Figure 48d & e show coloured mass filters for a putative cholesterol ester (cyan) and PI 18:0/20:4 (orange) that localised to distinct strata. Figure 48f & g shows the distributions of sulfatides and gangliosides using mass filters for sulfatide d18:1/20:4 (green) and monosialyated sphingosine-containing gangliosides (red) in the wild type (Fig. 48f) and knockout (Fig. 48g). The tissue distributions of sulfatide d18:1/20:4 and GM1 and GM3 were typical of others detected in these groups. In reference to previous MALDI-IMS publications Figure 48h show mass filters for sphingosine and eicososphingosine containing GM1 in blue and red respectively. Areas of mauve indicate overlap between the two species. It was clear that although both species localised to the same stratum of tissue there was some distinct localisation (visualised as areas of pure blue and pure red). This was observed for GD1
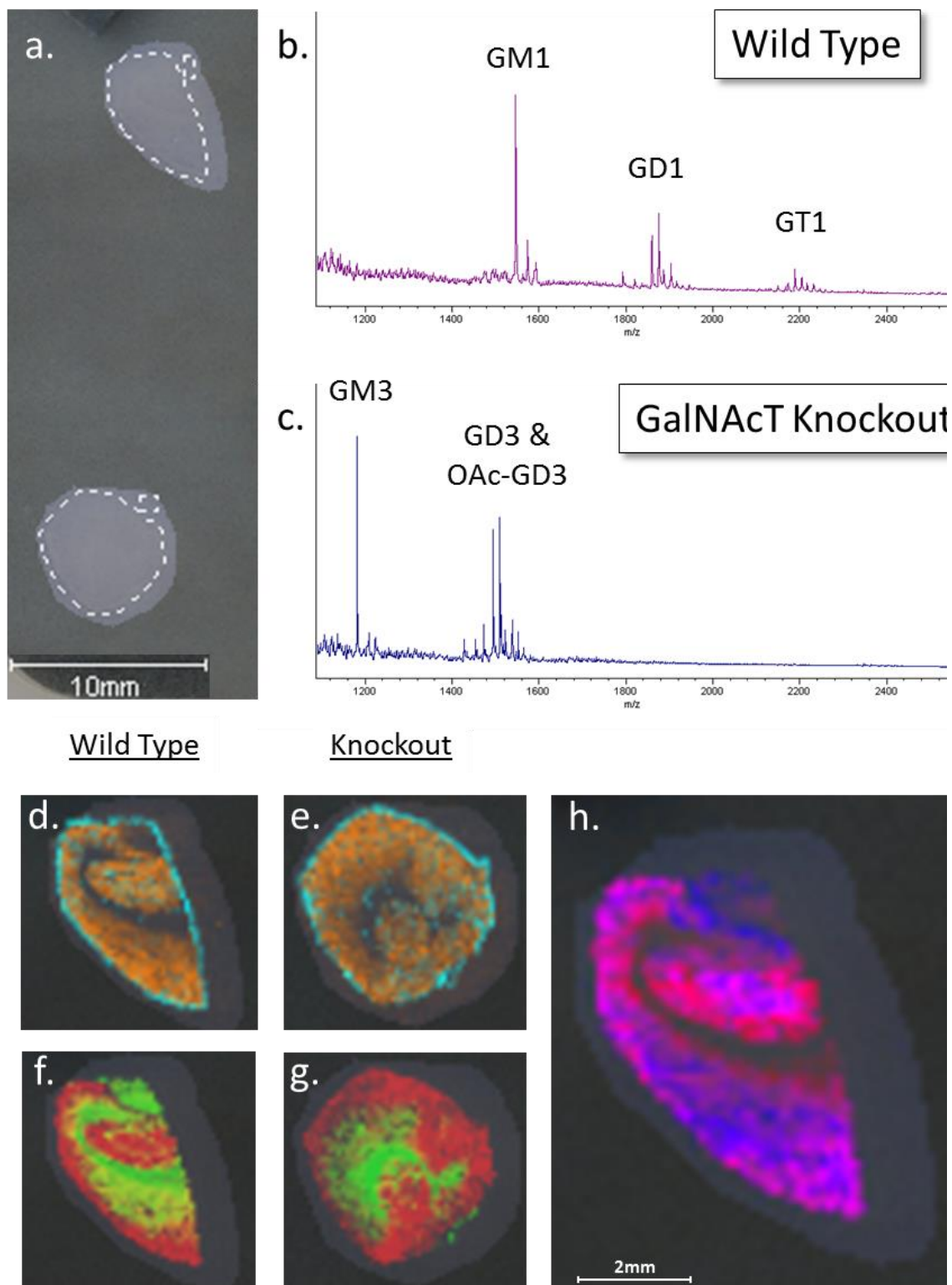
Figure 48. Imaging Mass Spectrometry in Wild Type and GalNAcT Knockout Brain Tissue. Wild type and knockout sections were imaged on a single slide by MALDI-IMS (a). Expected ganglioside peaks were detected in the total ion spectra from both datasets (b & c). Other lipids were detected that showed localisations to different tissue strata including a cholesterol ester (cyan) and PI (orange) (d & e), and sulfatide (green) and monosialyated gangliosides (red) (f & g). In accordance with previous publications GM1 (h) containing sphingosine (red) and eicososphingosine (blue) showed overlapping (mauve) but also discrete localisations in wild type brain tissue.

as well but not GD3, 9OAcGD3, GM3 or GT1; for these gangliosides near-identical distributions were observed for the sphingosine and eicososphingosine containing species.

7.2.1.2 <u>Optimising a MALDI Matrix in Spinal Cord Tissue Sections</u>

While DHB is classically used as a matrix for lipid imaging other MALDI matrices have been reported to work equally well, depending on the method of deposition, tissue of interest and targeted lipids (Dong et al., 2013; Shrivas et al., 2010; Thomas, Charbonneau, Fournaise, & Chaurand, 2012). As most of these investigations have focused on lipids under 1000 Da, several matrices were assessed for their suitability with our method in a mass range extending above 1000 Da. Gelatin embedded wild type spinal cord sections were coated with 2,3-dihydrozybenzoic acid (DHB) in 50% acetonitrile, 50% methanol or 4:4:1 chloroform/methanol/water (data not shown), or 9-aminoacridine (9-AA), 2,6-dihydroxyacetophenone (DHA) and 1,5-diaminonaphthalene (DAN) prepared using pre-optimised in-house solvents and application protocols. Sections were then imaged at 100 x 100 µm resolution. A region of interest (ROI) was defined around tissue and matrix only regions. Extracted spectra from these regions were compared for lipid-specific peaks across mass ranges from m/z 600-1000 and 1000-2000. Extracted spectra for each matrix are shown in Figure 49. Spectra are shown and were assessed without the normalisation (by the sum of each spectrum) that can be performed in FlexImaging. This was because low background signal intensity from matrix only regions resulted in ganglioside signal, which was low intensity and occurred exclusively in spectra alongside other high intensity lipid signals, mapping only to the matrix after normalisation. The results suggested 9-AA as an optimal matrix for imaging gangliosides and other smaller lipids. Little lipid-specific signal was observed using DHA which was discarded. When chloroform was included in the matrix solvent for DHB, lipid peaks were observed in both tissue and matrix-only regions suggesting that chloroform increased lateral diffusion during matrix application. This was also discarded. Of the remaining matrices extracted spectra from matrix-only regions were relatively clean with few interfering noise
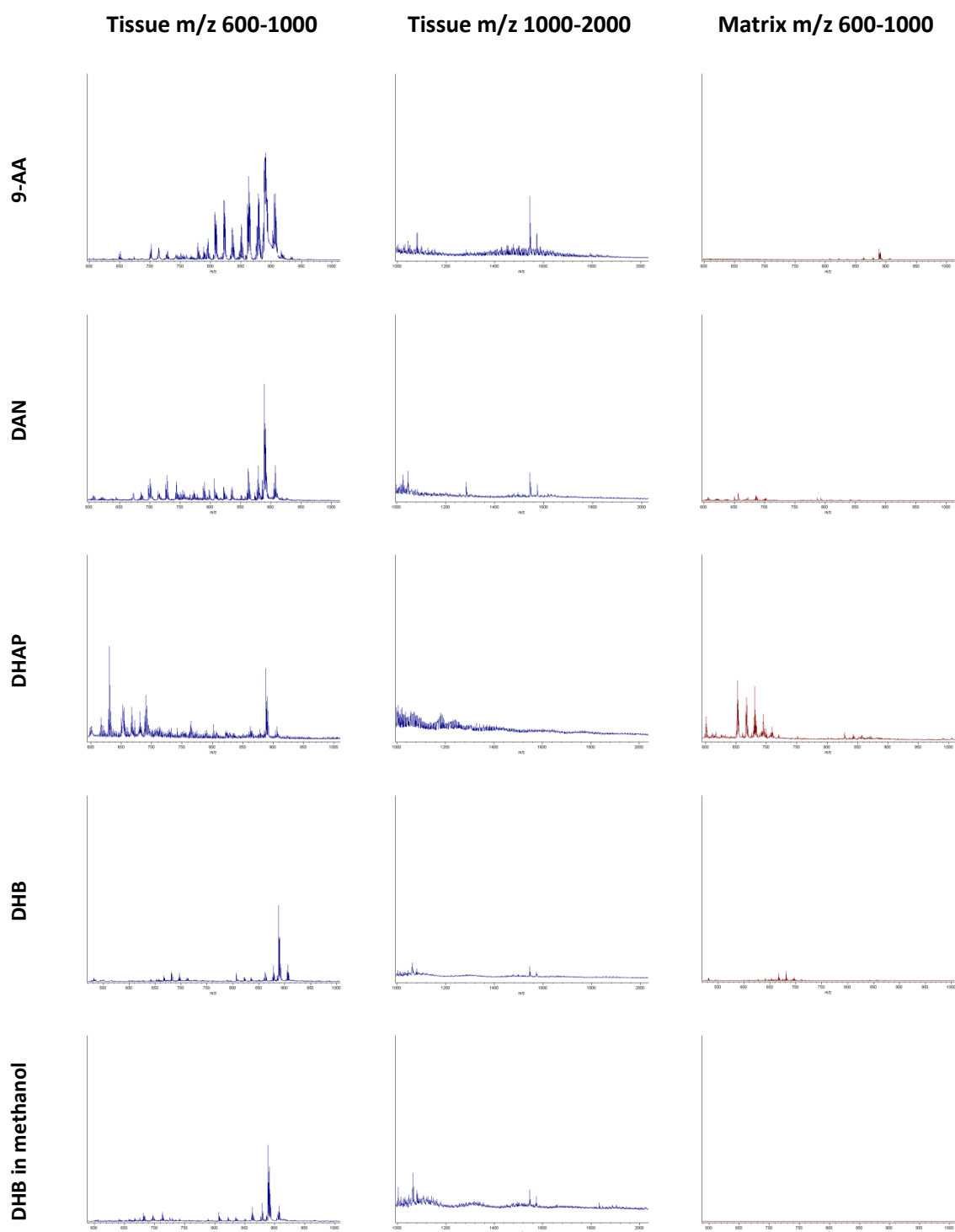
Figure 49. Comparison of MALDI Matrices for Lipid Detection in Spinal Cord. Four matrices; DHB (2,3-dihydrobenzoic acid), DHAP (2,6-dihydroxyacetophenone), DAN (1,5diaminonaphthalene) and 9AA (9-aminoacridine) in pre-optimised solvents described in 2.6.3, and DHB in 50% methanol or chloroform/methanol (data not shown), were investigated for lipid ionisation from spinal cord tissue sections in low (left column,m/z 600-1000) and high (central column, m/z 1000-2000) mass ranges and for matrix peaks in the low mass range (right column) in negative ion mode. DHAP and DHB in all matrix solvents resulted in fewest lipid peaks in both mass ranges as well as abundant matrix peaks. 9-AA and DAN resulted in fewer matrix peaks and good ionisation of lipids in both mass ranges. However 9-AA resulted in the highest intensities and widest range of ionised lipid species so was used for all further spinal cord analysis.

peaks over m/z 600. Peak distributions in the lower mass range using 9-AA, DAN, and DHB in methanol or acetonitrile were similar using observed using DHA which was immediately discarded. When chloroform was included in the each matrix. However the range of identifiable lipid peaks in the lower mass range was highest using 9-AA and to some extent DAN compared to DHB. On average lipid peak intensities were also highest using 9-AA in both the low and high mass range. MALDI-IMS studies reported here therefore used 9-aminoacridine as a MALDI matrix.

7.2.1.3 Lipid Imaging in Spinal Cord Datasets

Transverse spinal cord sections of 10 μm embedded in 10% gelatin were coated with 9-AA and imaged at 50 x 50 μm resolution. Due to the trade off between sensitivity and resolution, 50 μm was thought to be capable of distinguishing the major features of spinal cord without sacrificing the sensitivity required to detect low abundance gangliosides. Tissue from wild type (n=3), GalNAc transferase knockout (n=3) and NFL rescue mice (n=4) were imaged.

7.2.1.3.1 Data Processing

It had been noted previously that peak masses 'slipped' during imaging runs resulting in mass changes of up to 1 Da within a single dataset. This reduced peak mass accuracy and resolution in the overall average spectra and made accurate identifications from FlexImaging data less confident. In order to improve this, a minimum of seven randomly selected individual spectra were opened from each imaging dataset in FlexAnalysis. These spectra were internally calibrated using lipid peaks that were ubiquitously present as detailed in the materials and methods. Masses of peaks of interest from the imaging datasets were then cross-referenced with these calibrated spectra to obtain more accurate and consistent peak values. These were then used in metabolomic and lipidomic database searches. While the lack of accurate mass detection and fragmentation means that all identifications are putative, this method increased
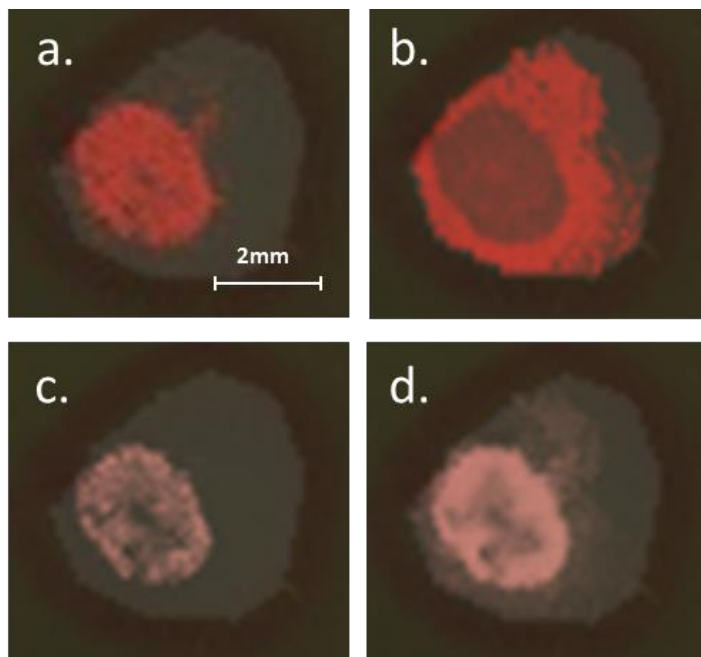
Figure 50. Effects of FlexImaging Normalisation on Ion Maps. The software used provides an option for data normalisation by total spectrum intensity. This can smooth inconsistencies in ionisation across the section to produce a cleaner ion map, as illustrated for sulf d18:1/22:1, before (c) and after (d) normalisation. However, It was observed that leaching of highly abundant lipids, such as sulf d18:1/24:1 (a,b), into the gelatin, where total spectrum intensities were low, meant that these lipids appeared falsley enriched in these areas after normalisation (b) . Normalisation therefore was not applied.

the confidence assigned to identifications, especially when combined with previous knowledge of the ionisation preference and abundance of lipids of the nervous system.

Normalisation in FlexImaging software was not used. A small amount of leaching had occurred into the embedding gelatine during initial tissue embedding. Normalisation resulted in the most abundant lipids appearing greatly enriched in the gelatine layer where total signal intensity was lower. This is illustrated in Figure 50 for Sulfatide d18:1/24:1 before (a) and after (b) normalisation. This did affect the image integrity of other lipids as illustrated in Figure 50 for Sulfatide d18:1/22:1 before (c) and after (d) normalisation. This time the ion map after normalisation shows a smoother image of this sulfatide species enriched in the white matter.

7.2.1.3.2   Wild Type Dataset

More than 50 peaks were identified in the lower mass range from wild type sections, a full list of which can be found in Appendix 5. These included phospholipids including -inositols, -glycerols, -ethanolamines and -serines, as well as hexosylceramides and sulfatides. Five distinct patterns of tissue distribution were observed, identified using the Allen Spinal Cord Atlas (Allen

186

Institute for Brain Science 2012), and are illustrated in Figure 51. These were; evenly distributed throughout the tissue (Fig. 51b); localised in the white matter (Fig. 51c); localised in the grey matter (Fig. 51d); enriched in what may have been the base of a spinal ganglion (data not shown) and in the posterior horns (Fig. 51e). Lipids that were detected evenly throughout the tissue included short and medium chain glycerophospho-serines (C26:1, C26:0 and C36:1), medium and long chain glycerophospho-ethanolamines (C46:6 and C46:5) and sulfatides and hydroxyl sulfatides ranging from d18:1/14:0 to d18:1/24:0. Lipids that were enriched in the white matter included short chain

a. Allen Spinal Cord Atlas
P56 Altlas Ref AChE L4 Section

b. Sulfatide d18:1/24:0
m/z 862.6

c. Phosphoglycerol C40:6
m/z 849.56

d. Phosphoglycerol C34:1
m/z 747.5

e. Lacto-glycosphingolipid
d18:1/24:0
m/z 1792.2

f. GM1 d18:1/18:0 – red
GM1 d20:1/18:0 – green
Overlap - yellow
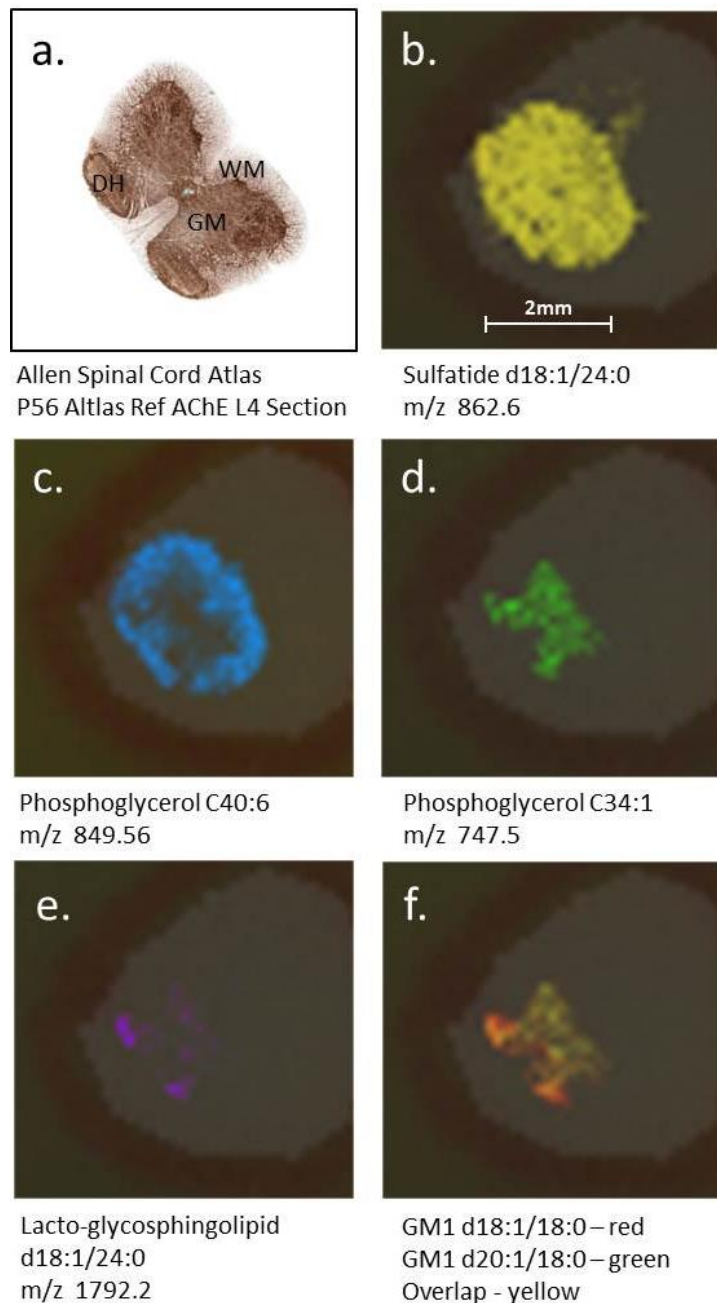
Figure 51. Lipid Distributions in Wild Type Spinal Cord. WM – white matter. GM – grey matter. DH – dorsal horn. Data collected in negative ion mode. Application of mass filters revealed distinct molecular distributions in wild type spinal cord sections, illustrated for sulfatide d18:1/24:0 (b), PG C40:6 (c), PG C34:1 (d) and and lacto-GSL d18:1/24:0 (e). Distributions were mapped to white (c) and grey (d) matter, and dorsal horn (e), using the Allen Spinal Cord Atlas resource (Allen Institute for Brain Science 2012). An acetylcholinesterase (AChE) stained lumbar section (Image index 5, tissue index 1179, structure L4) is shown for reference (a). Differences in distribution were noted for gangliosides GM1 (f) containing sphingosine (red) and eicososphingosine (green), as observed in the brain.

PI (C30:0, C34:1) and PIP C38:4, long chain polyunsaturated PGs, lactosyl-ceramide (d18:1/16:0 and d18:1/20:0(2OH)) and the majority of identified cerebro-sides. One specific species of sulfatide, d18:1/20:0(2OH) was also enriched in the white matter. Few lipids in the lower mass range were enriched in the grey matter. These included PG C34:1, several species of medium to long chain saturated and polyunsaturated PE species and glycerophosphoinositol bisphosphate C34:1. Several lipids were detected at higher levels from a distinct region of approximately 0.5 mm^2 on the posterior edge of the tissue section. This may have been the base of a posterior nerve or a spinal ganglion. Lipids localised in this area included several long chain glycerophosphoserines (C42:1, C44:4 and C44:3), lactosylceramides (d18:1/14:0, d18:1/18:1, d18:1/20:2 and d18:1/20:0) and sulfatides (d18:1/16:0 and d18:1/20:1).

In the mass range above m/z 1000 fewer peaks were observed, and at significantly lower intensity. Two peaks at m/z 1080.7 and 1082.7 were detected equally distributed across the tissue which could not be identified from databases or the literature. These peaks could correspond either to large, long chain phospholipids or oligoglycosylated glycosphingolipids containing unusual sugars such as fucose or a deaminated neuraminic acid (KDN, ketodeoxyglycerogalactononnic acid). A series of peaks were detected between m/z 1425 and 1550 that corresponded to long chain, polyunsaturated cardiolipins. These were detected at low intensity exclusively from the grey matter of the tissue section. Another peak at m/z 1792.0 was detected which localised to the posterior region of the grey matter. The intensity map of this lipid is shown in Figure 51e. Only one database identification was found for this mass, that of a neutral fucosylated glycosphingolipid of the lacto or neolacto sequence Gal(Fuc)Gal(Fuc)GlcNAcGalGlc-Cer d18:1/24:0 ([M-H]- m/z 1792.04). Of the gangliosides, only mono-sialylated species GM1 d18:1/18:0 and d18:1/20:0 and GM2 d18:1/18:0 were identified. These were detected almost exclusively from the grey matter indicating enrichment in this tissue. Different distributions within the grey matter were observed for the sphingosine and eicososphingosine containing species of ganglioside GM1. The overlaid intensity maps of mass filters for both of these are shown in Figure 51f. While eicosasphingosine-GM1 (green) was

evenly distributed through the grey matter, sphingosine-GM1 (red) appeared to be enriched in the posterior region from which the anterior roots emerge. No other gangliosides were identified.

7.2.1.3.3 GalNAc Transferase Knockout Dataset

A similar series of phospholipids, hexosylceramides and sulfatides, described in Appendix 5, were identified in the GalNAc T knockout mouse to the wild type. Typical spectra taken from the anterior white matter are shown in Figure 52a & b to illustrate this. The tissue distributions of the peaks was also similar between the two as demonstrated in Figure 53. Intensity maps are shown for mass filters of sulfatide d18:1/20:0 (Fig. 53a,b), hexosyl-ceramide d18:0/20:0 (Fig. 53e,f), PI C34:1 (Fig. 53h,i), PG C34:1 (Fig. 53k,l) and monosialylated ganglioside GM1 (Fig. 53m,n). These images demonstrate the similar distributions of these lipids in the wild type tissue and the knockout tissue. Four patterns of distribution were observed in the knockout; distributed throughout the tissue; enriched in the white matter; enriched in the grey matter;
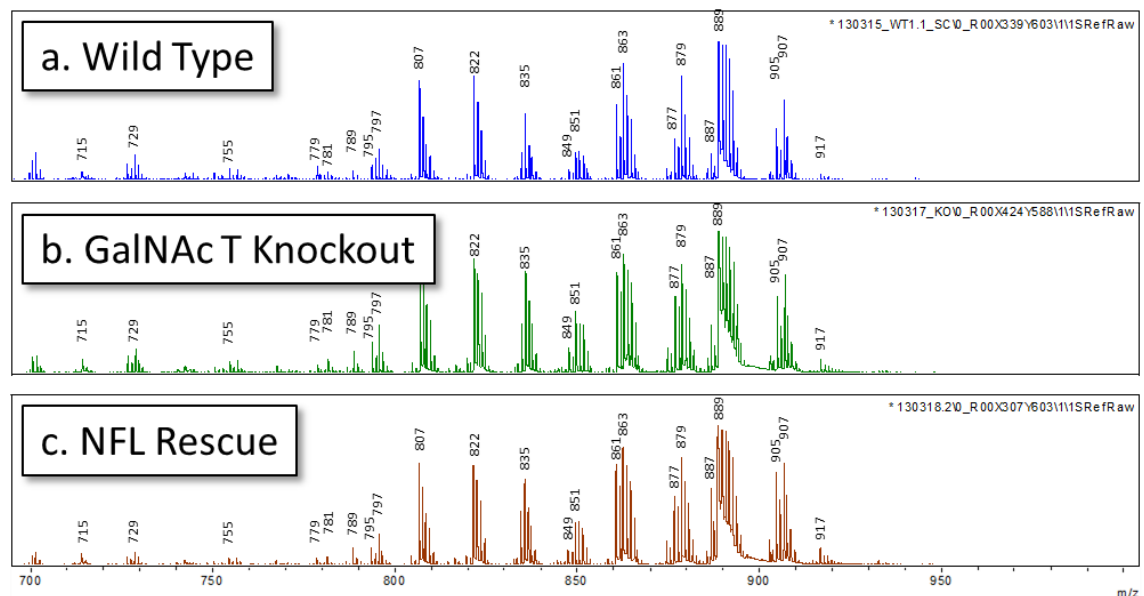
Figure 52. Single Pixel Mass Spectra from IMS Datasets. Taken from anterior white matter of each tissue section. Collected in negative ion mode. Single pixel spectra taken from anterior white matter from wild type, GalNAcT knockout and NFL rescue sections
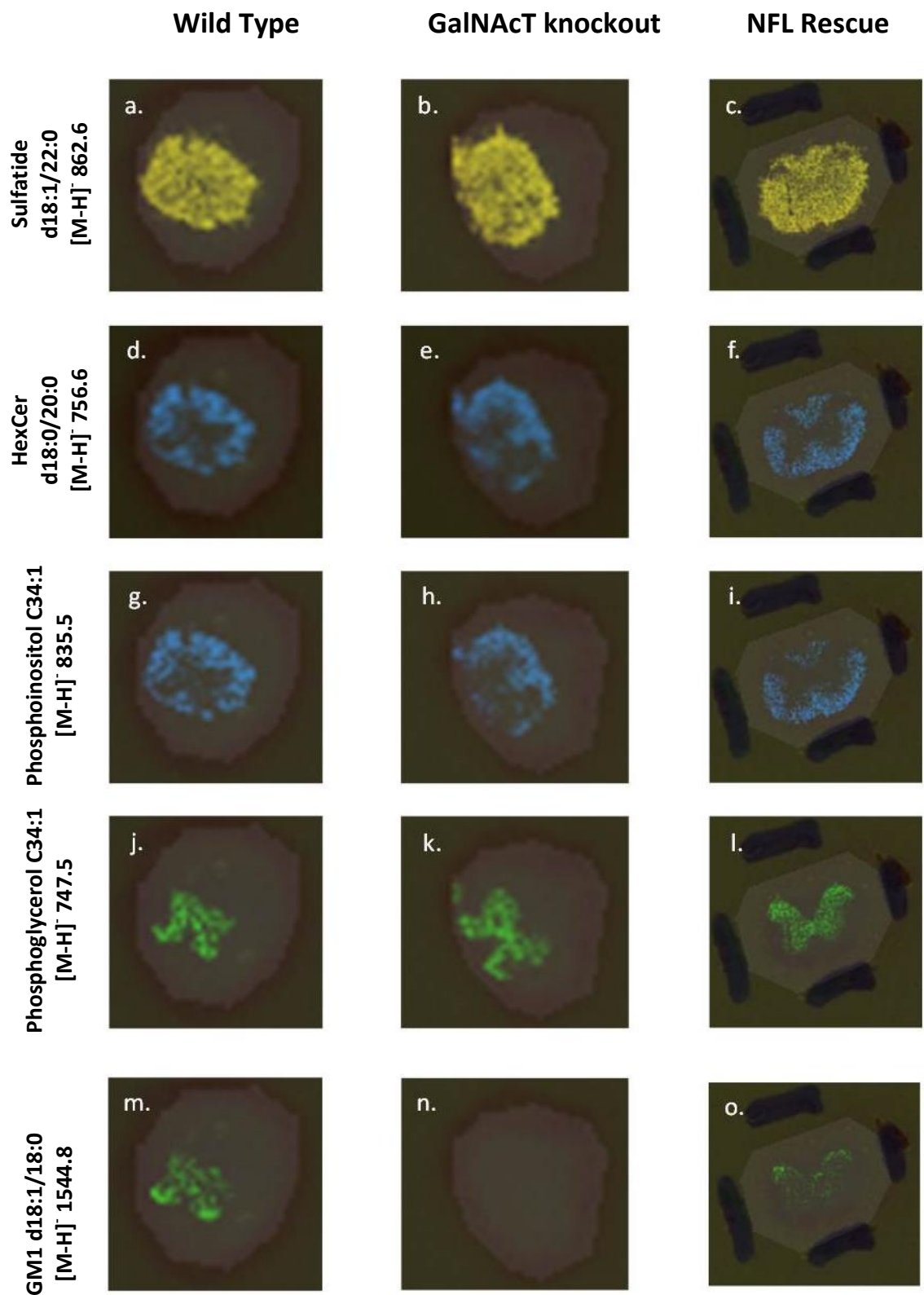
Figure 53. Lipid Distributions Compared between Spinal Cord Datasets. The tissue distributions of over 50 different lipids in MALDI-IMS datasets were similar in wild type (a,d,g,j,m), GalNAcT knockout (b,e,h,k,n) and NFL rescue (c,f,l,l,o) tissue sections. This is illustrated above for different phospho- and glycosphingolipids. The distributions of the complex ganglioside GM1 was also similar in wild type and NFL rescue sections but absent from the GalNAcT knockout.

and enriched in the posterior horn. Morphological features such as the root ganglion were not observed in KO tissue sections probably as an artefact of the tissue sectioning. However many of the lipids that had localised to this feature were identified in knockout tissue sections at lower relative signal intensities suggesting enrichment in the feature, rather than absolute absence from the rest of the tissue.

Again fewer peaks were detected in the upper mass range and at lower signal intensity than smaller lipids. These included unidentified peaks at m/z 1080.7 and 1082.7, also observed in the wild type dataset, and a series of cardiolipins between m/z 1425 and 1550, all of which showed consistent distributions in wild type and knockout. Simple gangliosides GM3 d18:1/18:0 and d18:1/20:0 (m/z 1179.74 and 1207.8) and GD3 d18:1/18:0 (m/z 1470.8) were identified from the grey matter exclusively. The sphingosine containing species of each localised to the posterior horn and laminae I, II and III regions while the eicososphingosine species of GM3 was detected evenly across the grey matter. Acetylated GD3 and complex gangliosides were not detected despite targeted analysis. The 9-OAcGD3 peak, expected m/z 1512.8 and 1540.8, may have been masked by the cardiolipin peaks if the latter were more abundant in the tissue. The peak at m/z 1792.0 was also undetected suggesting the GalNAc transferase enzyme may also be responsible for the synthesis of this glycosphingolipid.

7.2.1.3.4 NFL Rescue Dataset

Similar peaks, intensities and distributions were observed in the NFL rescue tissue sections to those observed in the wild type and knockout, in both the lower and upper mass ranges. A full description of the identified peaks can be found in Appendix 5. This similarity is illustrated in Figure 52 where typical spectra taken from the anterior white matter of the NFL rescue (Fig. 53c) are shown below examples from the wild type and knockout tissue. The major peaks and relative intensities were similar between the three. Similarities in the distributions of the lipids was also observed and is demonstrated in Figure 53. Intensity maps in the NFL rescue are shown for mass filters of sulfatide d18:1/20:0 (Fig. 53c), hexosyl-ceramide d18:0/20:0 (Fig.

53g), PI C34:1 (Fig. 53j), PG C34:1 (Fig. 53l) and monosialylated ganglioside GM1 (Fig. 53o) on the right next to images from the wild type and knockout. The localisation patterns of these and other lipids were similar between the three mouse types. Four distinct distributions were observed in the NFL rescue tissue; throughout the tissue; enriched in the white matter; enriched in the grey matter and localised to the posterior horn of the grey matter from which the motor roots emerge. Tissue features such as the root ganglion were not observed.

In the upper mass range unidentified peaks were detected in the NFL rescue tissue at m/z 1080.7 and 1082.7 from across the section and a series of cardiolipins were identified from the grey matter exclusively. As in the wild type, a peak was detected at m/z 1792.0 that specifically localised to the portion of the grey matter from which the posterior roots emerge. Sphingosine and eicososphingosine containing monosialylated gangliosides GM3 and GM1 were identified. The detection of the complex ganglioside GM1 indicated the partial rescue of complex ganglioside synthesis in this mouse model in the central nervous system. The d18:1/18:0 species of the simple ganglioside GD3 was also identified. Again sphingosine containing gangliosides were enriched in the posterior horn and laminae I, II and III while the eicososphingosine containing species were detected evenly across the grey matter.

7.2.2   Secondary Ion Mass Spectrometry in Peripheral Nerve

Secondary ion mass spectrometry (SIMS) is currently the only imaging mass spectrometry technique capable of sub-micron spatial resolution in biological tissues. Here we report its application to the analysis of gangliosides, and the complex ganglioside GM1 in particular, in peripheral nerves in wild type; GalNAc transferase knockout and NFL rescue sections. Wild type mice are capable of synthesising both simple and complex gangliosides including the monosialylated ganglioside GM1. Cholera toxin β-subunit (CTB) staining, which is thought to be highly specific for GM1, has shown GM1 predominantly in the myelin that sheathes peripheral nerve axons (Figure 54a, Rhona McGonical, personal communication).
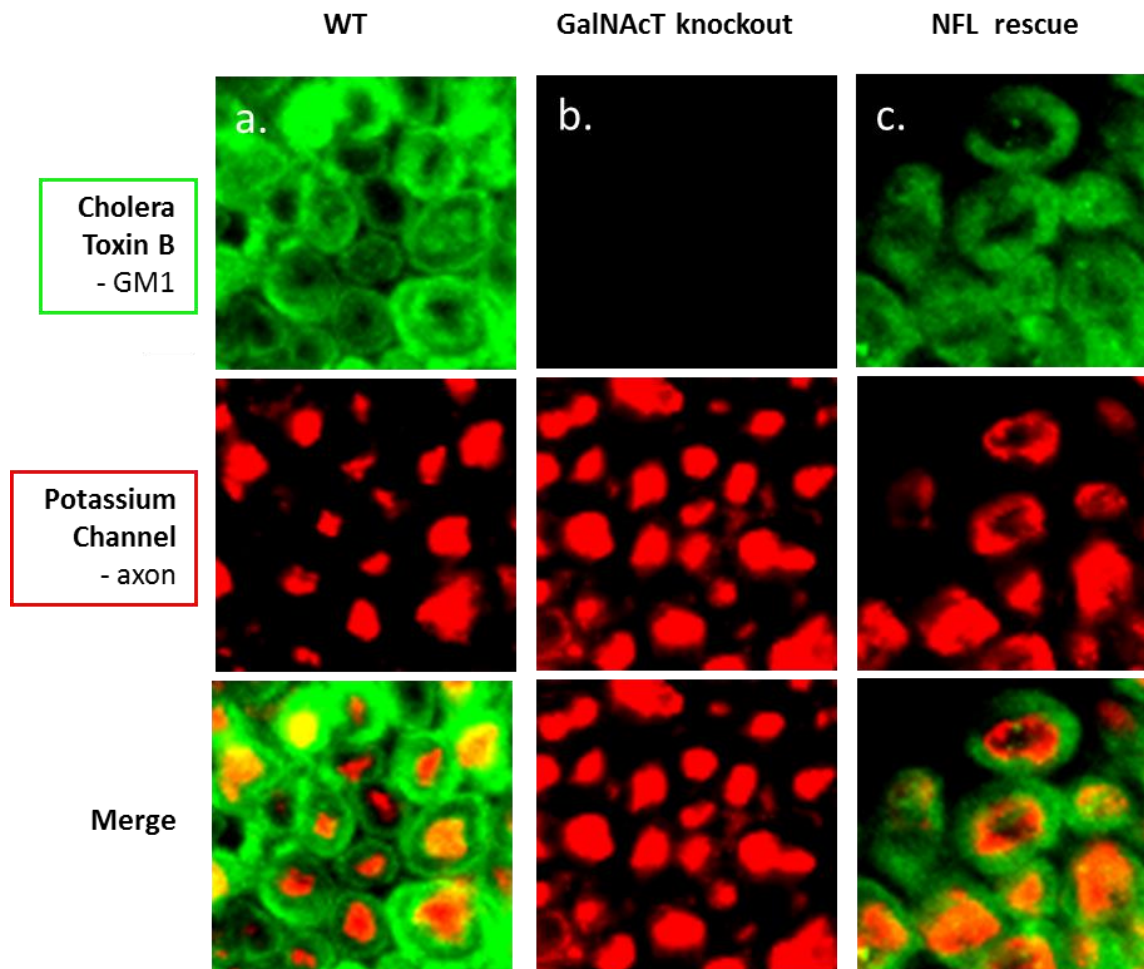
Figure 54. Cholera Toxin Staining of GM1 in the Myelin Sheathes of Peripheral Nerves.
Cholera toxin B subunit (green), which is highly specific for GM1, detects this ganglioside almost exclusively in the myelin sheath of wild type peripheral nerves. In GalNAtT knockout GM1, a complex ganglioside, is not detected. In the NFL rescue GM1 is unexpectedly again detected in the myelin sheaths, rather than the axon, where complex ganglioside synthesis is rescued, presenting something of a mystery (Rhona McGonigal, personal communication).

In knockout mice, which are unable to synthesise GM1, CTB staining was negative in both the nerve myelin and axons (Figure 54b). NFL rescue mice have the GalNAc transferase gene, which is required for the synthesis of GM1, knocked out systemically and placed under control of a promoter that is active in nerve axons. While it would follow that GM1 should be detected in the axons of peripheral nerves, CTB staining has indicated that, like the wild type, GM1 is enriched in the myelin in these mice. We applied SIMS in an attempt to understand whether this observation was a realistic representation of the distribution of GM1 in NFL tissue or an artefact of unreported cross-reactivity of the CTB subunit. SIMS spectra were collected from

lipid standards on a steel target and analysed for complex-ganglioside specific peaks or fragment patterns. The analysis of standards was repeated on ITO-coated slides with and without gold coating to confirm peaks of interest and investigate whether metal coating improved signal intensity (Altelaar et al., 2005). Peripheral nerve sections were then imaged by SIMS and analysed for the presence of peaks of interest.

7.2.2.1 Extraction of Lipid Specific Peaks in SIMS Spectra

SIMS spectra were collected for 2 minutes in negative ion mode from lipid standards including gangliosides (GA1, GM1, GM2, GM3, GD1a, GD1b, GD3, GT1b), sphingolipids (sphingosine, sphingomyelin, galactoceramide, sulfatide) and phospholipids (PC, PE, PG and PS) on a steel target. Spectra were also collected from the steel target itself. Datasets were analysed manually for peaks across m/z ranges 50-500, 500-1000 and 1000-2000 and cross-referenced with spectra from blank steel in order to eliminate non-specific peaks. A full description of extracted peaks can be found in Appendix 6. As previously reported in negative ion mode SIMS analysis of lipids, peaks were observed from pamioleic acid, palmitic acid and oleic acid at m/z 253, 255 and 281 respectively (Malmberg et al., 2007; D. Touboul, Brunelle, Halgand, De La Porte, & Laprévote, 2005). Other unique and group specific fragments were detected from phospho- and sphingolipids that have not been structurally analysed here. Instead these were used to eliminate non-ganglioside specific peaks. The stepwise fragmentation of sugars that might be expected from gangliosides was not observed, and conserved peaks were sparse. That said eight peaks were detected from complex gangliosides exclusively. Three of these, m/z 641, 833 and 861, were only observed in spectra from GA1 which was not of great interest. Four peaks were identified that might be used to detect complex gangliosides including one at m/z 371 which appeared specific to GM1 and one at m/z 592 which appeared to be specific for complex gangliosides GM1, GM2, GD1a, GD1b and GT1b.

In order to confirm that these peaks were ganglioside specific and could be used diagnostically in tissue imaging experiments, SIMS spectra were collected from ganglioside and sphingolipids
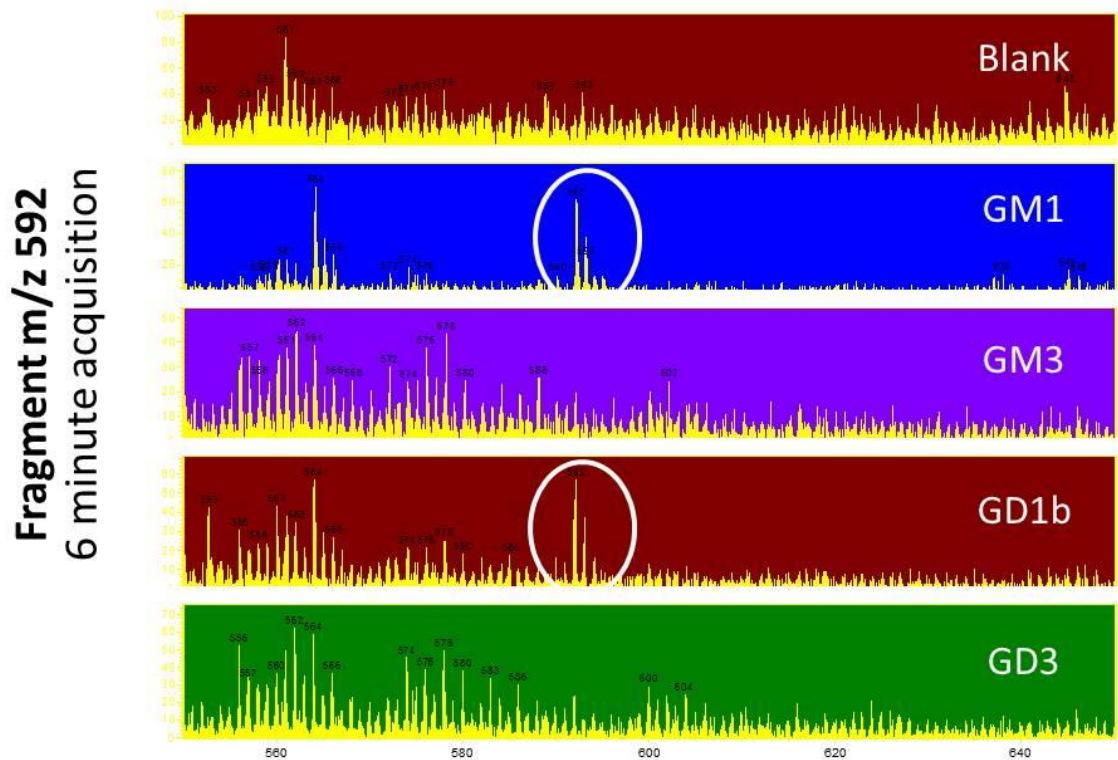
Figure 55. Confirmation of Ion m/z 592 from Complex Gangliosides. A fragment at m/z 592 had been detected exclusively from complex ganglioside stocks. This was confirmed using higher stock concentrations and longer acquisition times where the peak appeared to still be exclusively detected from complex (GM1, GD1b) and not simple (GM3, GD3) ganglioside stocks nor blanks.

standards at three concentrations; the original concentration of 0.5 ng; 5 ng and 50 ng. Spectra were acquired by negative ion mode SIMS for 2 minutes and 6 minutes. After 6 minute acquisitions all but one peak had been detected from non-ganglioside or simple ganglioside stocks, ruling them out as diagnostic fragments. Only one fragment was confirmed from complex gangliosides. The 592 fragment was detected, albeit at low intensity, from complex gangliosides and not from blank spectra or simple gangliosides as illustrated in Figure 55 for GM1, GD1b, GM3 and GD3. Unexpectedly for a primary ion beam without any ionisation enhancement, peaks corresponding to intact lipids were observed in GM1, GM2, hexosylceramides and sulfatide stocks.

7.2.2.2 <u>Investigation of Gold Coating for MeSIMS</u>

Gold coating has previously been reported to improve the quality of imaging by both SIMS and MALDI (Altelaar et al., 2005; Stoeckli et al., 2005). In SIMS imaging of brain tissue sections and single neuroblastoma cells with metal-enhancement (MetA-SIMS) showed an altered series of peaks compared to SIMS without enhancement, including more peaks in the mass range m/z 500-900. Although poorly annotated, these peaks were thought to include whole membrane lipids ionised as various complex adducts. To test whether a similar effect might be observed for gangliosides, spectra were collected by SIMS and MetA-SIMS from ganglioside standards with and without a 1.5 nm gold coating. Spectra from non-treated standards contained identical peaks to previous analyses. These were absent however in spectra from gold-treated standards which contained only peaks that were also observed in blank spectra from gold coating alone.

7.2.2.3 <u>SIMS Imaging of Sciatic Nerve Transections</u>

SIMS imaging was used to collect data from a wild type sciatic nerve section and was then analysed for lipid-related fragments. Tiles of 50 x 50 µm in a 2x2 grid were collected for 20 minutes per tile in negative ion mode. Ion counts for all ions including total ion count, phosphoric acid ($H_2PO_3^-$, m/z 81) and hydrogen sulphate (HSO_4^-, m/z 97) which are indicative of phospholipids and sulfatides were low compared to previous datasets, especially for peaks above m/z 300 and showed little morphological information. Diagnostic ions for complex or simple gangliosides were virtually undetected across all tiles (not shown). Due to the negative results from the wild type tissue, possible sources of which are discussed below, data was not collected from knockout or rescue tissue sections.

7.3 <u>Discussion</u>

This chapter reports the application of two imaging mass spectrometry (IMS) techniques; matrix assisted laser desorption ionisation-IMS (MALDI-IMS) and secondary ion IMS (SIMS), to

the analysis of gangliosides and other lipids in the central and peripheral nervous system of mice. Imaging mass spectrometry (IMS) combines the specificity MS analysis with the spatial detail of imaging thus enabling the occurrence of specific molecules, identified by mass and relatively quantitated by signal intensity, to be mapped across morphological features in biological tissue samples. While IMS techniques show distinct promise, they incur a strict trade-off between sensitivity and spatial resolution. The imaging of low abundance lipids such as gangliosides outside of enriched tissues such as the brain had not previously been reported. This investigation was undertaken in order to address both the question of IMS applicability to ganglioside imaging and to investigate the occurrence and distribution of lipids in a novel genetic mouse model in relation to the wild type.

MALDI-IMS, which uses 'soft' ionisation to ionise intact lipids and is limited to super-cellular resolution, was applied to map gangliosides and other lipids in spinal cord from wild type and NFL rescue mice. GalNAc transferase mice were used as a negative control for the detection of complex gangliosides. An optimised method was established in mouse brain tissue sections. The results from brain illustrated both the major benefits and limitations of IMS. The most abundant gangliosides GM1, GD1 and GT1 were identified from wild type tissue alongside many other lipids including hexosylceramides and phospholipids. Simultaneous to detection the distribution of these lipids was revealed, with gangliosides, phospholipids and sulfatides distinctly enriched in specific tissue strata. In accordance with previous publications the distribution of sphingosine and eicososphingosine containing species of GM1 and GD1 was subtly different; an observation enabled by the IMS technique. These complex gangliosides were not detected from GalNAc transferase knockout tissue where simple gangliosides GM3, GD3 and 9OAc-GD3 were identified. These simple gangliosides also comprise minor components of the repertoire of wild type mice; however they were not detected from the wild type tissue. Other minor complex gangliosides such as GM2 and GQ1 were also not detected, demonstrating the limited sensitivity of MALDI imaging. It is also worth mentioning that structural isomers such as GD1a and GD1b could not be differentiated in this experiment;

the incorporation of dissociation or ion mobility into the imaging workflow should be investigated to distinguish these.

After establishing 9-aminoacridine as an optimal matrix for nerve imaging, spinal cord trans-sections from wild type, GalNAc transferase knockout and NFL rescue mice were imaged by MALDI-IMS. The variety, relative abundance and distribution of phospholipids and sphingolipids were practically identical between the three mouse models. Interestingly a group of polyunsaturated cardiolipins, which have been indicated in several inflammatory and autoimmune disorders, were identified from grey matter and especially the posterior horn from all three tissue types (Lai & Lan, 2000; Marie, Jouen, Hellot, & Levesque, 2008; Petri, 2000). This consistency between modes was surprising as it suggests that the knockout and cell-type specific rescue of the GalNAc transferase enzyme do not have significant knock on effects on lipid metabolism outside of the ganglioside pathway. This means that the build up of precursors from the loss of complex ganglioside synthesis is entirely absorbed by the increased synthesis of simple gangliosides. That said it must be noted that data was collected only in negative ion mode in a relatively narrow (m/z 600-3000) mass range. Datasets therefore excluded nonpolar or free fatty acid lipids that function upstream of ganglioside metabolism, several of which form important interconnections with other pathways. Additionally gangliosides are reported to have important roles in membrane organisation (S Sonnino & Prinetti, 2010). While the data shows that other lipids have similar intensities and distributions, MALDI-IMS cannot achieve anywhere near the sub-cellular resolution necessary to conclude that these lipids were correspondingly organised in the membranes or cell types in all three mice.

One of the main interests of this chapter was of course to discern the usefulness of MALDI-IMS for imaging gangliosides in tissues other than the brain. In spinal cord only the mono-sialylated ganglioside GM1 was identified in wild type tissue. This species is known to be a major component of the gangliosides of the nervous system and this is the first report to our

knowledge of its detection by MALDI-IMS outside of the brain tissue. Sphingosine and eicosasphingosine containing GM1 were detected from the grey matter exclusively. While this disagreed with conventional immunostaining in rat spinal cord (Kotani, Kawashima, Ozawa, Terashima, & Tai, 1993), which detected GM1 from grey and white matter, a more recent immunohistochemical study by Gong *et al.* found similar localisation of GM1 in the grey matter of mouse spinal cord (Gong, 2002). It may be that ganglioside distribution is more markedly different between some species than previously realised, or this may illustrate the major issue of cross-reactivity in anti-ganglioside antibodies. The major species, GM1 d18:1/18:0, while detected throughout the grey matter, suggested enrichment in what was thought to be the posterior horn. The minor GM1 20:1/18:0 species was detected more evenly across the grey matter. As this relates to the hydrophobic moiety of GM1, which has a strong influence over interactions with intra-membrane components such as cholesterol and the hydrophobic domain of membrane proteins, this enrichment may have structural, associative or interactive consequences for the sensory neurons that are abundant in the posterior horn.

In the GalNAc transferase knockout mouse; a model unable to synthesise complex gangliosides resulting in the build of simple ganglioside precursors, GM1 was not detected. Instead only simple gangliosides GM3 and GD3 were detected. As before gangliosides were detected exclusively in grey matter and an enrichment of the sphingosine species was observed in the posterior horn. The similar localisation of gangliosides in the wild type and knockout mouse, with its neurodegenerative phenotype, demonstrated the importance of the head group structure in function and the maintenance of the nervous system. In spinal cord from the NFL rescue mouse, both simple gangliosides GM3 and GD3, and complex ganglioside GM1 were detected in the grey matter. This concurs with the profiling studies in Chapter 6 which identified the partial rescue of complex ganglioside in these mice. Again sphingosine and eicosasphingosine containing GM3 and GM1 were identified and showed an enrichment of the sphingosine species in the posterior horn of the grey matter. Using signal intensity as a measure of relative quantitation, the level of GM1 was reduced in the NFL rescue compared to

the wild type but is sufficient to rescue the phenotype.

It has been shown here that while MALDI-IMS is applicable to imaging lipids outside of brain tissue, the technique is not yet suitable to investigate gangliosides in detail. Only the major ganglioside species; GM1, GM3 and GD3 were identified while minor components were not detected. The low abundance of many gangliosides means that sensitivity needs to improve, either through instrumentation or preparative enhancement of signal, before IMS is truly applicable to ganglioside analysis. Complex sample preparations including ionic matrices and gold nanoparticles have reportedly been used to increase the sensitivity of MALDI-IMS in brain tissue enabling the detection of minor gangliosides including GM2, GM3 and GQ1b (Chan et al., 2009; Colsch & Woods, 2010; Naoko Goto-Inoue et al., 2010). These could be investigated to increase the sensitivity of MALDI-IMS for ganglioside detection in nerves also.

It must also be noted that other major ganglioside components such as GD1 and GT1 were not detected. The absence of these species was more difficult to explain. It has been suggested that labile sialic acids on the di- and trisialylated species may fragment during MALDI. However by returning to previous MALDI-IMS datasets from HPTLC separations, collected under near-identical ionisation conditions, we concluded that this could not explain the complete absence of GD1 and GT1 species. No less than two thirds of the peak intensity from bands of GD1 and GT1 came from adducts of the whole molecular ions. Therefore a combination of low native tissue abundance, poor ionisation and a degree of ion suppression by lower mass lipids was probably the cause. Other sample preparations or instrument settings that may increase the extraction, ionisation or detection of minor lipids need to be investigated before MALDI-IMS becomes applicable to imaging gangliosides outside of the brain.

Secondary ion imaging mass spectrometry (SIMS) is an alternative imaging mass spectrometry technique that we report the application of to lipid and ganglioside imaging in peripheral nerves. SIMS uses a primary ion beam to ionise secondary fragments so SIMS is capable of sub-micron resolution that could hypothetically distinguish features such as myelin sheath from

nerve axon. However SIMS suffers from lower sensitivity and the loss of whole molecular ions. Few recognisable fragment peaks were observed from ganglioside stocks. This was surprising considering the observations of previous glycosphingolipid investigations using secondary ion and fast atom bombardment mass spectrometry that have revealed the loss of consecutive sugars (Arita, Iwamori, Higuchi, & Nagai, 1984; Ilyas et al., 1998; Kushi et al., 1988). That said, an apparently complex-ganglioside specific fragment was identified at m/z 592. However this fragment was not detected from tissue sections. The intensity of elemental and head-group ions was also surprisingly low compared to previous (unpublished) data. The SIMS instrument was not routinely operated in negative ion mode so it was thought that further optimisation of the instrument settings may have been needed. There were also issues with the hardware and electronics that required addressing after the experiment and may have prevented data collection. SIMS obviously has great potential for high resolution imaging but is still in very early days for detecting even the most abundant of lipids. The technique may not be applicable to the investigation of lipids such as gangliosides without significant further adaptation to enhance either the ionisation or detection of these low abundance lipids.

Chapter 8. And Go on Till You Come to the End…

8.1 Conclusions and Future Directions

This work aimed to bring together the benefits of existing mass spectrometry (MS) techniques with the separation and analysis of large glycosylated membrane sphingolipids, specifically sialic acid containing gangliosides. Biologically this group of membrane lipids are low abundance but essential in human disease and development, especially in the central and peripheral nervous system. They are known to interact with extracellular components including antibodies. It is here where gangliosides are of particular interest. Anti-ganglioside autoantibodies have been identified in a number of different human diseases. In several instances the roles of these antibodies are as yet unknown. In autoimmune neuropathies such as Guillain-Barre Syndrome and Multifocal Motor Neuropathy, evidence suggests a clearer role. The binding of these antibodies is part of the primary disease pathology, signalling the immune-mediated degradation of peripheral nerves resulting in acute bouts of localised paralysis. While the basic pathogenesis is understood, there are many unknowns relating to these diseases. In particular, the connection between antibody specificities and nerve susceptibility, clinical syndrome, and disease severity are not well established. Genetically engineered mouse models, based on previously existing knockouts in ganglioside synthesis that are described in Chapter 1, are currently undergoing development at the University of Glasgow to better replicate the generation and onset of human GBS to increase our understanding of this group of syndromes.

The work performed here was motivated by the need for novel profiling technologies capable of native ganglioside analysis with minimal chemical derivitisation and higher sensitivity, specificity and greater independence from available lipid standards than conventional techniques. This was in part in order to describe the molecular ganglioside biology of the aforementioned mouse models, which have interrupted and rescued ganglioside synthesis in specific tissues, in unprecedented detail. For these mice to be used in relevant animal studies,

it was essential to know whether ganglioside synthesis had been rescued in the nervous tissue, and to what degree it resembled wild type ganglioside profiles. Conventional high performance thin layer chromatography can be used for this but lacks reproducibility, sensitivity and specificity. For example, in publications relating to the original knockout mouse, over 10 years elapsed between the initial recognition of a novel band in ganglioside profiles and the identification of said band using, amongst other methods, direct injection mass spectrometry as a novel GD3 structure containing an O-acetylation on the sialic acid. This modification is not usually described in wild type profiles by HPTLC but was observed in this project in wild type extracts, suggesting that it is in fact a native modification that occurs at low levels on multiple species of gangliosides in mice.

In a larger sense motivation also came from the relative exclusion of gangliosides from the larger MS field of lipidomics.   Lipidomics; the separation and MS description of the lipid component of a given system, has received growing attention over the previous decades. However due to the unconventional nature of gangliosides, many otherwise comprehensive lipidomic publications have ignored this group. A handful of publications have focused on the separation and MS detection and identification specifically of gangliosides; namely by HPTLC-MALDI-MS or HPLC-MSMS. Reports on the former however often use complex preparation steps such as membrane blotting, or adaptation of instrumentation such as an orthogonal ion source or collisional cooling gas. These requirements reduce the applicability of HPTLC-MS to wider ganglioside studies. Several different HPLC methods have been reported for the latter using different solvent systems and phases. All of these have employed triple quadrupole instruments, which were not used here. Instead a high resolution Thermo LTQ Orbitrap was used, enabling higher sensitivity and exact mass detection. Due to the lack of consistent methodology for ganglioside analysis, method development tailoring protocols for ganglioside analysis formed a large part of this project.

Two optimised methods were developed for the separation, detection and identification of

underivatised intact gangliosides. Each method had distinct advantages and limitations over those already available, which have been discussed in detail in individual chapters, and compared to each other. High performance liquid chromatography coupled to accurate mass spectrometry with dissociation was the more automated, more reproducible and more information rich of the two. Standard deviations in retention times were below 6.5 seconds across more than 30 different ganglioside species. This could potentially be reduced with more stringent controls to parameters such as environmental temperature or system pressure monitoring. Peak intensities were also relatively reproducible (s.d. <10% for 15 species) enabling relative quantitation of ganglioside species within sample batches. Compared to available methodologies this workflow provided a more complete chromatographic separation enabling distinction of adduct ions from structural modifications, sensitive MS detection with high mass accuracy and dissociation above and beyond the loss of the sialic acid which is consistently used in SRM experiments on triple quad instruments. Additional online rounds of dissociation could be used to increase the structural information provided by this method even further.

From the analysis of other non-ganglioside lipid standards it appeared that the HPLC-MSMS set up used here not exclusively applicable to gangliosides. Chromatographic peak shapes were good for phospholipids and sphingolipids, which eluted after gangliosides and ionised effectively into the mass analyser using similar source settings (although optimal dissociation parameters differed). With minimal further development this method could provide a comprehensive lipidomic analysis for at least the larger membrane lipids, which has been lacking in the literature. Failing that, the method, by separating low abundance gangliosides from more abundant lipids that cause ion suppression, could eliminate the long and inefficient sample preparations used to enrich gangliosides. Shorter, simplified sample preparation without additional ion suppression of gangliosides would be beneficial. For example solid-phase extraction has been shown by HPTLC to extract similar ganglioside profiles to weak anion exchange (Williams & McCluer, 1980). Simple SPE can be automated to increase

reproducibility and throughput, opening up sample preparation to larger sample numbers or smaller tissue samples, which could then be analysed comprehensively for membrane lipids including gangliosides. Were this possible the unsuccessful single nerve profiling study performed in Chapter 6 could be repeated without the significant limitations of the current sample preparation.

While the HPTLC-IMS workflow designed here also has certain advantages over previously published methods; namely its simplicity and low requirement for extra sample preparation steps or modified instrumentation, it is out-performed for profiling by HPLC-MS in many parameters. That said, HPTLC-IMS is not obsolete. The chromatography requires less specialist equipment and running costs and data interpretation is simplified if a head-group ganglioside glycan profile is all that is required. Perhaps more importantly, and what has not been taken advantage of here, is the complementarity of the method with a variety of immunological techniques such as HPTLC-overlay. Consecutive lanes can be stained with serum and imaged by mass spectrometry. Considering the capabilities of IMS in establishing the composition of bands with great detail, and distinguishing overlapping bands, this combination has the opportunity to reveal novel details in the binding patterns of human serum antibodies. With more complex instrumentation something similar could be achieved with HPLC-MSMS. Using a flow splitter fractions of the elution could be analysed by mass spectrometry and applied as discrete spots to an array for interrogation using serum samples.

A comparison of these two methods can be found in more detail in Chapter 5 where both were applied to the profiling of gangliosides in novel mouse models of Guillain-Barré Syndrome. Molecular phenotyping of these animals had not been performed before and was essential to assessing their usefulness for modelling complex human neuropathies. It was confirmed for the first time, using both methods, that complex gangliosides were present in the brain tissue of four different rescue models; NFL rescue, PLP rescue, THY1 112 rescue and THY1 115 rescue. While the absolute abundance of complex gangliosides was significantly lower in

rescues, the relative profiles of complex gangliosides were similar to those observed in the wild type, agreeing with current models of ganglioside anabolism. Ceramide inclusion profiles were also similar in monosialyated gangliosides in wild type, knockout and rescue mice. The sensitivity of HPLC-MSMS also revealed that native acetylations to the sialic acids in disialylated species was more abundant that previously indicated. This modification has been suggested on multiple gangliosides aside from GD3 via Influenza virus C haemagluttinin esterase assays (Fahr & Schauer, 2001) and 2D-HPTLC (Sturgill et al., 2012) but is not observed by routine ganglioside profiling. The modification was detected on GD3 in the knockout, as previously observed, and on GD1a, GD1b and GT1b in the wild type and rescue models. In this instance the linkage position was not investigated and may have corresponded to a 9-O-acetlyation or the less abundant 7-O-acetlyation (Erdmann et al., 2006). However this could be established using multiple rounds of dissociation.

The presence of complex gangliosides in the brains of these rescue mice confirmed to some degree their usefulness in modelling human autoimmune neuropathies. Antibody targets were present in the brain that have not been detected by immunostaining elsewhere in the body. Hypothetically this should lower or negate systemic self-tolerance to these antigens enabling the raising of serum antibodies to complex gangliosides. Antibody targets are then present in the brains of these animals encouraging immune-induced degradation in neurological tissue. It may be beneficial to confirm the absence of complex ganglioside targets around the body by profiling other tissues using highly sensitive HPLC-MSMS. It is worth noting as well that many human autoimmune neuropathies target nerves outside of the brain. If sample preparation could be simplified and automated as mentioned, nerve profiling by HPLC-MS could also confirm complex ganglioside targets in peripheral nerves and compare profiles to those observed in wild types. This would indicate closer relevancy of these models for human disease modelling. The presence of these targets in central nerves has been suggested here using imaging mass spectrometry of spinal cord tissue sections. GM1 was detected in both wild type and NFL rescue mice with similar tissue distributions in the grey matter of the spinal

cord. However detection was limited to the most abundant and stable mono-sialylated species. With improved sample preparation HPLC-MS could be applied to investigating full ganglioside profiles in peripheral nerves.

It was concluded during this study that the sensitivity of imaging mass spectrometry is not currently sufficient for the analysis of rare or more complex gangliosides outside of brain material where they are highly enriched. Development of novel preparations, such as an on-tissue permethylation (Juhasz & Costello, 1992) or methyl-ester conversion (A. K. Powell & Harvey, 1996), or instrumental modifications, such as the cooling gas sometimes applied in HPTLC-IMS analysis (V. B. Ivleva et al., 2004), may increase the sensitivity of MALDI methods for gangliosides. This conclusion was more true for high resolution SIMS; the only IMS technology which has the capability to image individual cells. This was concluded after applying SIMS to peripheral nerve cross sections in an attempt to investigate the distribution of GM1 in peripheral nerve myelin and axons. In the NFL rescue mice the knocked out GalNAc transferase enzyme is rescued under the neurofilament light promoter which is reportedly active only in neurons (Julien, 1999) and not supporting glial cells. However immunohistochemistry in the NFL rescue mouse has detected GM1 in the nerve myelin. While traditional SIMS imaging using a gold primary ion beam failed to detect ganglioside molecular or fragment ions here, a C60 cluster source may yield larger secondary ions with less fragmentation (Fletcher et al., 2006). Alternatively purified myelin preparations could be prepared, although this would involve significant amounts of tissue, and analysed by HPLC-MSMS to investigate the presence of complex gangliosides in the helper glial cells of these mice .

This project has clearly demonstrated the benefits of mass spectrometry to ganglioside profiling as well as highlighting the limitations and areas for future work, both in the field of glycosphingolipid research and within lipidomics. MS detection had many benefits including increased sensitivity, specificity and automation compared to conventional methods. There

was also a high degree of independence from ganglioside standards which is a limiting factor for many conventional techniques. Profiling using mass spectrometry in model mice not only detected the presence of extremely low abundance complex gangliosides in brain and nerve tissue, confirming their future usefulness for modelling autoimmune neurological diseases, but performed this to a greater degree of specificity than previously achieved, and with relative quantitation between and within datasets. Because gangliosides are analysed intact and without chemical modification this included details on native modifications and ceramide moieties. As our understanding of the functional nature of lipids increases, including roles for both hydrophobic and hydrophilic moieties, this capability for intact, unmodified molecular analysis will become more and more important. Future directions for the technology need to include the development of methods that incorporate the capabilities of those developed here for comprehensive lipidomics including the unusual and low abundance lipids such as gangliosides. Simplifying pre-analysis preparation to avoid sample loss as well as increasing the reproducibility for relative quantitation or potentially developing methods for absolute quantitation would also be useful. More generally we need to increase these collaborations between mass spectrometrists and lipid research groups in order to inform and take full advantage of the benefits of MS as a unique and complimentary data source. Only then can the utility of lipidomics be fully realised.

Bibliography

Adibhatla, R.M., Hatcher, J.F. & Dempsey, R.J., 2006. Lipids and lipidomics in brain injury and diseases. The AAPS journal, 8(2), pp.E314–21.

Aerni, H.-R., Cornett, D.S. & Caprioli, R.M., 2006. Automated acoustic matrix deposition for MALDI sample preparation. Analytical chemistry, 78(3), pp.827–34.

Allen Insitute for Brain Science. 2012. Allen Spinal Cord Atlas (internet). Available from: http://mousespinal.brain-map.org/

Altelaar, A.F.M. et al., 2005. Gold-Enhanced Biomolecular Surface Imaging of Cells and Tissue by SIMS and MALDI Mass Spectrometry. Analytical Chemistry, 78(3), pp.734–742.

Ando, S., Chang, N.C. & Yu, R.K., 1978. High-performance thin-layer chromatography and densitometric determination of brain ganglioside compositions of several species. Analytical biochemistry, 89(2), pp.437–50.

Angström, J., Teneberg, S. & Karlsson, K. a, 1994. Delineation and comparison of ganglioside-binding epitopes for the toxins of Vibrio cholerae, Escherichia coli, and Clostridium tetani: evidence for overlapping epitopes. Proceedings of the National Academy of Sciences of the United States of America, 91(25), pp.11859–63.

Ariga, T., McDonald, M. & Yu, R.., 2008. Thematic Review Series: Sphingolipids. Role of ganglioside metabolism in the pathogenesis of Alzheimer's disease—a review,. Journal of Lipid Research, 49(6), pp.1157–1175.

Arita, M. et al., 1984. Positive and negative ion fast atom bombardment mass spectrometry of glycosphingolipids. Discrimination of the positional isomers of gangliosides with sialic acids. Journal of biochemistry, 95(4), pp.971–81.

Arnon, R. et al., 1980. Anti-ganglioside antibodies in multiple sclerosis. Journal of the Neurological Sciences, 46(2), pp.179–186.

Asbury, A.K., 1981. Diagnostic considerations in Guillain-Barré syndrome. Annals of Neurology, 9(S1), pp.1–5.

Asbury, A.K. & Cornblath, D.R., 1990. Assessment of current diagnostic criteria for Guillain-Barré syndrome. Annals of Neurology, 27(S1), pp.S21–S24.

Ashcroft, A.E., 1997. Ionization Methods in Organic Mass Spectrometry N. W. Barnett, ed., Cambridge: Royal Society of Chemistry.

Basu, M. et al., 2000. Properties of animal ceramide glycanases. Methods in enzymology, 311, pp.287–97.

Benabdellah, F. et al., 2010. Mass spectrometry imaging of rat brain sections: nanomolar sensitivity with MALDI versus nanometer resolution by TOF-SIMS. Analytical and bioanalytical chemistry, 396(1), pp.151–62.

Bennaceur, K. et al., 2009. Different mechanisms are involved in apoptosis induced by melanoma gangliosides on human monocyte-derived dendritic cells. Glycobiology, 19(6), pp.576–82.

Bielawski, J. et al., 2006. Simultaneous quantitative analysis of bioactive sphingolipids by high-performance liquid chromatography-tandem mass spectrometry. Methods (San Diego, Calif.), 39(2), pp.82–91.

Birklé, S. et al., 2003. Role of tumor-associated gangliosides in cancer progression. Biochimie, 85(3-4), pp.455–463.

Bogoch, S., 1957a. Cerebrospinal fluid neuraminic acid deficiency in schizophrenia; a preliminary report. American Journal of Psychiatry, 114(2), p.172.

Bogoch, S., 1957b. Inhibition of viral hemagglutination by brain ganglioside. Virology, 4(3), pp.458–466.

Bogoch, S., 1958. Studies on the structure of brain ganglioside. The Biochemical journal, 68(2), pp.319–26.

Bouschen, W. et al., 2010. Matrix vapor deposition/recrystallization and dedicated spray preparation for high-resolution scanning microprobe matrix-assisted laser desorption/ionization imaging mass spectrometry (SMALDI-MS) of tissue and single cells. Rapid communications in mass spectrometry : RCM, 24(3), pp.355–64.

Bowes, T., Wagner, E. & Boffey, J., 2002. Tolerance to self gangliosides is the major factor restricting the antibody response to lipopolysaccharide core oligosaccharides in Campylobacter jejuni strains associated with Guillain-Barre Syndrome. Infection andImmunity, 70(9), pp.5008–5018.

Burns, M.S., 1982. Applications of secondary ion mass spectrometry (SIMS) in biological research: a review. Journal of Microscopy, 127(3), pp.237–258.

Burns, T., 2008. Guillain-Barré Syndrome. Seminars in Neurology, 28(02), pp.152–167.

Buzby, J., Allos, B.M. & Roberts, T., 1997. The Economic Burden of Campylobacter-Associated Guillain-Barre Syndrome. Journal of Infectious Diseases, 176(Supplement 2), pp.S192–S197.

Byrdwell, W.C., 1998. Dual parallel mass spectrometers for analysis of sphingolipid, glycerophospholipid and plasmalogen molecular species. Rapid communications in mass spectrometry : RCM, 12(5), pp.256–72.

Cavanna, B. et al., 1999. Anti-GM2 IgM antibodies: clinical correlates and reactivity with a human neuroblastoma cell line. Journal of neuroimmunology, 94(1-2), pp.157–64.

Cerruti, C.D. et al., 2012. MALDI imaging and structural analysis of rat brain lipid negative ions with 9-aminoacridine matrix. Analytical chemistry, 84(5), pp.2164–71.

Chan, K. et al., 2009. MALDI mass spectrometry imaging of gangliosides in mouse brain using ionic liquid matrix. Analytica Chimica Acta, 639(1), pp.57–61.

Chandra, S. & Morrison, G.H., 1992. Sample preparation of animal tissues and cell cultures for secondary ion mass spectrometry (SIMS) microscopy. Biology of the cell / under the auspices of the European Cell Biology Organization, 74(1), pp.31–42.

Chiavegatto, S. et al., 2000. A functional role for complex gangliosides: motor deficits in GM2/GD2 synthase knockout mice. Experimental neurology, 166(2), pp.227–34.

Chiba, A. et al., 1997. Ganglioside composition of the human cranial nerves, with special reference to pathophysiology of Miller Fisher syndrome. Brain Research, 745(1), pp.32–36.

Chiba, A. et al., 1993. Serum anti-GQ1b IgG antibody is associated with ophthalmoplegia in Miller Fisher syndrome and Guillain-Barre syndrome: Clinical and immune-histochemical studies. Neurology, 43(10), pp.1911–1911.

Chiba, A. et al., 1992. Serum IgG antibody to ganglioside GQ1b is a possible marker of Miller Fisher syndrome. Annals of Neurology, 31(6), pp.677–679.

Choo-Smith, L.-P. et al., 1997. Acceleration of Amyloid Fibril Formation by Specific Binding of Aβ-(1-40) Peptide to Ganglioside-containing Membrane Vesicles. J. Biol. Chem., 272(37), pp.22987–22990.

Christie, W., 1989. Gas chromatography and lipids: a practical guide., Ayr, Scotland: Oily.

Chughtai, K. et al., 2012. Mass Spectrometry Images Acylcarnitines, Phosphatidylcholines and Sphingomyelin in MDA-MB-231 Breast Tumor Models . Journal of Lipid Research .

Coetzee, T. et al., 1996. Myelination in the absence of galactocerebroside and sulfatide: normal structure with abnormal function and regional instability. Cell, 86(2), pp.209.

Colsch, B. et al., 2004. Characterization of the ceramide moieties of sphingoglycolipids from mouse brain by ESI-MS/MS: identification of ceramides containing sphingadienine. Journal of lipid research, 45(2), pp.281–6.

Colsch, B. & Woods, A.S., 2010. Localization and imaging of sialylated glycosphingolipids in brain tissue sections by MALDI mass spectrometry. Glycobiology, 20(6), pp.661–667.

Creek, D.J. et al., 2012. IDEOM: an Excel interface for analysis of LC-MS-based metabolomics data. Bioinformatics (Oxford, England), 28(7), pp.1048–9.

Crespo, P.M., Demichelis, V.T. & Daniotti, J.L., 2010. Neobiosynthesis of glycosphingolipids by plasma membrane-associated glycosyltransferases. The Journal of biological chemistry, 285(38), pp.29179–90.

Crocker, P., Paulson, J. & Varki, A., 2007. Siglecs and their roles in the immune system. Nat Rev Immunol, 7(4), pp.255–266.

Daniotti, J.L. & Iglesias-Bartolomé, R., 2011. Metabolic pathways and intracellular trafficking of gangliosides. IUBMB life, 63(7), pp.513–20.

Desplats, P.A. et al., 2007. Glycolipid and ganglioside metabolism imbalances in Huntington's disease. Neurobiology of disease, 27(3), pp.265–77.

Dewald, H.D., 1999. Electrospray Ionization Mass Spectrometry: Fundamentals, Instrumentation and Applications (ed. Cole, Richard B.). Journal of Chemical Education, 76(1), p.33.

Domon, B. & Costello, C., 1988. Structure elucidation of glycosphingolipids and gangliosides using high-performance tandem mass spectrometry. Biochemistry, 27(5), pp.1534.

Domon, B. & Costello, C.E., 1988. A systematic nomenclature for carbohydrate fragmentations in FAB-MS/MS spectra of glycoconjugates. Glycoconjugate Journal, 5(4), pp.397–409.

Dong, W. et al., 2013. Phospholipid analyses by MALDI-TOF/TOF mass spectrometry using 1,5-diaminonaphthalene as matrix. International Journal of Mass Spectrometry, 343, pp.15–22.

Downes, C.P., Gray, A. & Lucocq, J.M., 2005. Probing phosphoinositide functions in signaling and membrane trafficking. Trends in cell biology, 15(5), pp.259–68.

Draganesco, H. & Claudian, J., 1927. Sur un cas de radiculo-névrite curable (syndrome de Guillain-Barré) apparue au cours d'une osteomyelite du bras. Revue Neurologique, 2, pp.517–521.

Dreisewerd, K. et al., 2005. Analysis of Gangliosides Directly from Thin-Layer Chromatography Plates by Infrared Matrix-Assisted Laser Desorption/Ionization Orthogonal Time-of-Flight Mass Spectrometry with a Glycerol Matrix. Analytical Chemistry, 77(13), pp.4098–4107.

Duh, J. & Her, G., 1992. Analysis of permethylated glycosphingolipids by desorption chemical ionization/triple-quadrupole tandem mass spectrometry. Biological Mass Spectrometry, 21(8), pp.391–396.

Egge, H. & Peter-Katalinic, J., 1987. Fast atom bombardment mass spectrometry for structural elucidation of glycoconjugates. Mass Spectrometry Reviews, 6(3), pp.331.

Elola, M. et al., 2007. Galectins: matricellular glycan-binding proteins linking cell adhesion, migration, and survival. Cellular and Molecular Life Sciences, 64(13), pp.1679–1700.

El-Rassi, Z., 2002. Carbohydrate Analysis by Modern Chromatography and Electrophoresis (Google eBook), Elsevier.

Erdmann, M. et al., 2006. Differential surface expression and possible function of 9-O- and 7-O-acetylated GD3 (CD60 b and c) during activation and apoptosis of human tonsillar B and T lymphocytes. Glycoconjugate journal, 23(9), pp.627–38.

Ewers, H. & Helenius, A., 2011. Lipid-mediated endocytosis. Cold Spring Harbor perspectives in biology, 3(8), p.a004721.

Fahr, C. & Schauer, R., 2001. Detection of sialic acids and gangliosides with special reference to 9-O-acetylated species in basaliomas and normal human skin. The Journal of investigative dermatology, 116(2), pp.254–60.

Fahy, E. et al., 2005. A comprehensive classification system for lipids. Journal of Lipid Research, 46(5), pp.839–862.

Fahy, E. et al., 2005. A comprehensive classification system for lipids. Journal of lipid research, 46(5), pp.839–61.

Fahy, E. et al., 2009. Update of the LIPID MAPS comprehensive classification system for lipids. Journal of lipid research, 50 Suppl, pp.S9–14.

Fenn, J. et al., 1989. Electrospray ionisation for mass spectrometry of large biomolecules. Science, 246(4926), pp.64-71

Ferguson, L.S. et al., 2013. Efficiency of the dry-wet method for the MALDI-MSI analysis of latent fingermarks. Journal of mass spectrometry : JMS, 48(6), pp.677–84.

Fletcher, J.S. et al., 2006. TOF-SIMS analysis using C60. Effect of impact energy on yield and damage. Analytical chemistry, 78(6), pp.1827–31.

Folch, J., Arsove, S. & Meath, J., 1951. ISOLATION OF BRAIN STRANDIN, A NEW TYPE OF LARGE MOLECULE TISSUE COMPONENT. Journal of Biological Chemistry, 191(2), pp.819–831.

Folch, J., Lees, M. & Sloane Stanley, G.H., 1957. A simple method for the isolation and purification of total lipides from animal tissues. The Journal of biological chemistry, 226(1), pp.497–509.

Fong, B. et al., 2009. Liquid Chromatography–High-Resolution Mass Spectrometry for Quantitative Analysis of Gangliosides. Lipids, 44(9), pp.867–874.

Fornai, L. et al., 2012. Three-dimensional molecular reconstruction of rat heart with mass spectrometry imaging. Analytical and bioanalytical chemistry, 404(10), pp.2927–38.

Freddo, L. et al., 1986. Gangliosides GM1 and GD1b are antigens for IgM M-protein in a patient with motor neuron disease. Neurology, 36(4), pp.454–8.

Fuchs, B. et al., 2007. A direct and simple method of coupling matrix-assisted laser desorption and ionization time-of-flight mass spectrometry (MALDI-TOF MS) to thin-layer chromatography (TLC) for the analysis of phospholipids from egg yolk. Analytical and Bioanalytical Chemistry, 389(3), pp.827–834.

Fuchs, B., SuB, R. & Schiller, J., 2010. An update of MALDI-TOF mass spectrometry in lipid research. Progress in Lipid Research, 49(4), pp.450–475.

Fujiwaki, T., Tasaka, M. & Yamaguchi, S., 2008. Quantitative evaluation of sphingomyelin and glucosylceramide using matrix-assisted laser desorption ionization time-of-flight mass spectrometry with sphingosylphosphorylcholine as an internal standard. Practical application to tissues from patients with . Journal of chromatography. B, Analytical technologies in the biomedical and life sciences, 870(2), pp.170–6.

Furukawa, K. et al., 1985. Analysis of the specificity of five murine anti-blood group A monoclonal antibodies, including one that identifies type 3 and type 4 A determinants. Biochemistry, 24(26), pp.7820–7826.

Furukawa, K. et al., 2008. Disruption of GM2/GD2 synthase gene resulted in overt expression of 9-O-acetyl GD3 irrespective of Tis21. Journal of neurochemistry, 105(3), pp.1057.

Furukawa, K. et al., 2004. Glycosphingolipids in engineered mice: insights into function. Seminars in Cell & Developmental Biology, 15(4), pp.389–396.

Furukawa, K., Hamamura, K. & Nakashima, H., 2008. Molecules in the signaling pathway activated by gangliosides can be targets of therapeutics for malignant melanomas. PROTEOMICS, 8(16), pp.3312–3316.

Furusato, M. et al., 2002. Molecular cloning and characterization of sphingolipid ceramide N-deacylase from a marine bacterium, Shewanella alga G8. The Journal of biological chemistry, 277(19), pp.17300–7.

Furuya, S. et al., 1994. Ganglioside GD1 alpha in cerebellar Purkinje cells. Its specific absence in mouse mutants with Purkinje cell abnormality and altered immunoreactivity in response to conjunctive stimuli causing long-term desensitization. The Journal of biological chemistry, 269(51), pp.32418–25.

Galban-Horcajo, F. et al., 2013. Antibodies to heteromeric glycolipid complexes in multifocal motor neuropathy. European journal of neurology : the official journal of the European Federation of Neurological Societies, 20(1), pp.62–70.

Gobley, N., 1846. Recherches chimiques sur le jaune d'oeuf Rapport sur un mémoire ayant pour titre "Recherches chimiques sur le jaune d'oeuf, Paris: impr. de Fain et Thunot.

Gold, R., Hartung, H.-P. & Toyka, K. V, 2000. Animal models for autoimmune demyelinating disorders of the nervous system. Molecular Medicine Today, 6(2), pp.88–91.

Gong, Y., 2002. Localization of major gangliosides in the PNS: implications for immune neuropathies. Brain, 125(11), pp.2491–2506.

Goodwin, R.J.A., 2012. Sample preparation for mass spectrometry imaging: small mistakes can lead to big consequences. Journal of proteomics, 75(16), pp.4893–911.

Goodwin, R.J.A. et al., 2008. Time-dependent evolution of tissue markers by MALDI-MS imaging. Proteomics, 8(18), pp.3801–8.

Goodwin, R.J.A. et al., 2010. Use of a solvent-free dry matrix coating for quantitative matrix-assisted laser desorption ionization imaging of 4-bromophenyl-1,4-diazabicyclo (3.2.2)nonane-4-carboxylate in rat brain and quantitative analysis of the drug from laser microdissected tissue . Analytical chemistry, 82(9), pp.3868–73.

Goodyear, C.S. et al., 1999. Monoclonal antibodies raised against Guillain-Barré syndrome-associated Campylobacter jejuni lipopolysaccharides react with neuronal gangliosides and paralyze muscle-nerve preparations. The Journal of clinical investigation, 104(6), pp.697–708.

Goto-Inoue, N. et al., 2012. Imaging mass spectrometry visualizes ceramides and the pathogenesis of dorfman-chanarin syndrome due to ceramide metabolic abnormality in the skin. PloS one, 7(11), p.e49519.

Goto-Inoue, N. et al., 2010. The Detection of Glycosphingolipids in Brain Tissue Sections by Imaging Mass Spectrometry Using Gold Nanoparticles. Journal of the American Society for Mass Spectrometry, 21(11), pp.1940–1943.

Goto-Inoue, N., Taki, T. & Setou, M., 2010. TLC-Blot-MALDI-IMS. In M. Setou, ed. Imaging Mass Spectrometry. Springer Japan, pp. 169–177.

Greenshields, K. et al., 2009. The neuropathic potential of anti-GM1 autoantibodies is regulated by the local glycolipid environment in mice. The Journal of Clinical Investigation, 119(3), pp.595–610.

Griffiths, W.J. et al., 2001. Electrospray and tandem mass spectrometry in biochemistry. The Biochemical journal, 355(Pt 3), pp.545–61.

Grimm, M.O.W. et al., 2012. Amyloid precursor protein (APP) mediated regulation of ganglioside homeostasis linking Alzheimer's disease pathology with ganglioside metabolism. PloS one, 7(3), p.e34095.

Grizard, G. et al., 2000. Separation and quantification of cholesterol and major phospholipid classes in human semen by high-performance liquid chromatography and light-scattering detection. Journal of Chromatography B: Biomedical Sciences and Applications, 740(1), pp.101–107.

Gu, M. et al., 1997. Ceramide profiling of complex lipid mixtures by electrospray ionization mass spectrometry. Analytical biochemistry, 244(2), pp.347–56.

Gu, Y. et al., 2008. Silencing of GM3 synthase suppresses lung metastasis of murine breast cancer cells. Breast Cancer Research, 10(1), p.R1.

Guillain, G., Barré, J. & Strohl, A., 1916. Sur un syndrome de radiculonévrite hyperalbuminose du liquide céphalorachidien sans réaction cellulaire. Bulletins et mémoires de la Société médicale des hôpitaux de Paris, 40, pp.1462–70.

Guittard, J., Hronowski, X. & Costello, C., 1999. Direct matrix-assisted laser desorption/ionization mass spectrometric analysis of glycosphingolipids on thin layer chromatographic plates and transfer membranes. Rapid Communications in Mass Spectrometry, 13(18), pp.1838–1849.

Gusev, A.I. et al., 1995. Imaging of thin-layer chromatograms using matrix-assisted laser desorption/ionization mass spectrometry. Analytical Chemistry, 67(24), pp.4565.

Hammarstrom, S., 1970. Mass Spectrometric Characterization of Ceramides. Derived from Brain Cerebrosides. European Journal of Biochemistry, 15(3), pp.581–591.

Han, X. & Gross, R.W., 1994. Electrospray ionization mass spectroscopic analysis of human erythrocyte plasma membrane phospholipids. Proceedings of the National Academy of Sciences, 91(22), pp.10635–10639.

Han, X. & Gross, R.W., 2005. Shotgun lipidomics: electrospray ionization mass spectrometric analysis and quantitation of cellular lipidomes directly from crude extracts of biological samples. Mass spectrometry reviews, 24(3), pp.367–412.

Handa, Y. et al., 2005. GD3 synthase gene knockout mice exhibit thermal hyperalgesia and mechanical allodynia but decreased response to formalin-induced prolonged noxious stimulation. Pain, 117(3), pp.271–9.

Harizi, H., Corcuff, J.-B. & Gualde, N., 2008. Arachidonic-acid-derived eicosanoids: roles in biology and immunopathology. Trends in molecular medicine, 14(10), pp.461–9.

Harpin, M.-L., Portoukalian, J. & Baumann, N., 1982. Modifications of ganglioside composition in peripheral nerve of myelin deficient trembler mutant mouse. Neurochemical Research, 7(11), pp.1367–1373.

Harvey, D.J., 1995. Matrix-assisted laser desorption/ionization mass spectrometry of

phospholipids. Journal of Mass Spectrometry, 30(9), pp.1333–1346.

Haymaker, W.E. & Kernohan, J.W., 1949. The Landry-Guillain-Barré syndrome; a clinicopathologic report of 50 fatal cases and a critique of the literature. Medicine, 28(1), pp.59–141.

Heimburg, T., 2009. Physical Properties of Biological Membranes. In H. G. Bohr, ed. Handbook of Moelcular Biophysics. Wiley-VCH, pp. 593–616.

Henion, T.R. et al., 2001. Cloning of a mouse beta 1,3 N-acetylglucosaminyltransferase GlcNAc(beta 1,3)Gal(beta 1,4)Glc-ceramide synthase gene encoding the key regulator of lacto-series glycolipid biosynthesis. The Journal of biological chemistry, 276(32), pp.30261–9.

Herrler, G., Hausmann, J. & Klenk, E., 1995. Sialic acid as receptor determinant of Ortho- and Paramyxoviruses. In A. Rosenberg, ed. Biology of the Sialic Acids. Boston, MA: Springer US, pp. 314–336.

Herzog, R. et al., 2012. LipidXplorer: a software for consensual cross-platform lipidomics. PloS one, 7(1), p.e29851.

Hillenkamp, F. et al., 1991. Matrix-assisted laser desorption/ionisation mass spectrometry of biopolymers. Analytical Chemistry, 63(24), 1193A-1203A.

Hillenkamp, F. & Karas, M., 2007. Chapter 1. The MALDI Process and Method. In F. Hillenkamp & Peter-K, eds. MALDI MS: A Practical Guide to Instrumentation, Methods and Applications. Wiley-Blackwell, pp. 1–28.

Hirabayashi, Y. et al., 1990. Isolation and characterization of extremely minor gangliosides, GM1b and GD1 alpha, in adult bovine brains as developmentally regulated antigens. The Journal of biological chemistry, 265(14), pp.8144–51.

Hirabayashi, Y. et al., 1992. Structural characterization of a novel cholinergic neuron-specific ganglioside in bovine brain. The Journal of biological chemistry, 267(18), pp.12973–8.

Ho, T.W. et al., 1999. Anti-GD1a antibody is associated with axonal but not demyelinating forms of Guillain-Barr� syndrome. Annals of Neurology, 45(2), pp.168–173.

Honke, K. et al., 2002. Paranodal junction formation and spermatogenesis require sulfoglycolipids. Proceedings of the National Academy of Sciences, 99(7), pp.4227.

Hsu, F. & Turk, J., 2000. Characterization of phosphatidylinositol, phosphatidylinositol-4-phosphate, and phosphatidylinositol-4,5-bisphosphate by electrospray ionization tandem mass spectrometry: a mechanistic study. Journal of the American Society for Mass Spectrometry, 11(11), pp.986–999.

Hsu, F.-F. et al., 2005. Structural characterization of cardiolipin by tandem quadrupole and multiple-stage quadrupole ion-trap mass spectrometry with electrospray ionization. Journal of the American Society for Mass Spectrometry, 16(4), pp.491–504.

Hsu, F.-F., Bohrer, A. & Turk, J., 1998. Electrospray ionization tandem mass spectrometric analysis of sulfatide. Biochimica et Biophysica Acta (BBA) - Lipids and Lipid Metabolism, 1392(2-3), pp.202–216.

Hsu, F.F. & Turk, J., 1999. Structural characterization of triacylglycerols as lithiated adducts by electrospray ionization mass spectrometry using low-energy collisionally activated dissociation on a triple stage quadrupole instrument. Journal of the American Society for Mass Spectrometry, 10(7), pp.587–99.

Hsu, F.F. & Turk, J., 2001. Structural determination of glycosphingolipids as lithiated adducts by electrospray ionization mass spectrometry using low-energy collisional-activated dissociation on a triple stage quadrupole instrument. Journal of the American Society for Mass Spectrometry, 12(1), pp.61–79.

Hsu, F.F. & Turk, J., 2000. Structural determination of sphingomyelin by tandem mass spectrometry with electrospray ionization. Journal of the American Society for Mass Spectrometry, 11(5), pp.437–49.

Hsu, F.-F. & Turk, J., 2009. Electrospray ionization with low-energy collisionally activated dissociation tandem mass spectrometry of glycerophospholipids: mechanisms of fragmentation and structural characterization. Journal of chromatography. B,

Analytical technologies in the biomedical and life sciences, 877(26), pp.2673–95.

Hsu, F.-F. & Turk, J., 2003. Electrospray ionization/tandem quadrupole mass spectrometric studies on phosphatidylcholines: the fragmentation processes. Journal of the American Society for Mass Spectrometry, 14(4), pp.352–63.

Hsu, F.-F. & Turk, J., 2004. Studies on sulfatides by quadrupole ion-trap mass spectrometry with electrospray ionization: structural characterization and the fragmentation processes that include an unusual internal galactose residue loss and the classical charge-remote fragmentation. Journal of the American Society for Mass Spectrometry, 15(4), pp.536–46.

Hu, C. et al., 2009. Analytical strategies in lipidomics and applications in disease biomarker discovery. Journal of chromatography. B, Analytical technologies in the biomedical and life sciences, 877(26), pp.2836–46.

Huang, Z.H., Gage, D.A. & Sweeley, C.C., 1992. Characterization of Diacylglyceryl-phosphocholine Molecular Species by FAB-CAD-MS/MS: A General Method Not Sensitive to the Nature of the Fatty Acyl Groups. Journal of the American Society for Mass Spectrometry, 3(1), pp.71–8.

Huwiler, A. et al., 2000. Physiology and pathophysiology of sphingolipid metabolism and signaling. Biochimica et biophysica acta, 1485(2-3), pp.63–99.

Hvattum, E., Hagelin, G. & Larsen, A., 1998. Study of mechanisms involved in the collision-induced dissociation of carboxylate anions from glycerophospholipids using negative ion electrospray tandem quadrupole mass spectrometry. Rapid communications in mass spectrometry : RCM, 12(19), pp.1405–9.

Hwang, J. et al., 2010. Gangliosides induce autophagic cell death in astrocytes. British journal of pharmacology, 159(3), pp.586–603.

Iber, H. et al., 1990. pH-dependent changes of ganglioside biosynthesis in neuronal cell culture. European journal of cell biology, 52(2), pp.236–40.

Ii, T., Ohashi, Y. & Nagai, Y., 1995. Structural elucidation of underivatized gangliosides by electrospray-ionization tandem mass spectrometry (ESIMS/MS). Carbohydrate Research, 273(1), pp.27–40.

Ikeda, K., Shimizu, T. & Taguchi, R., 2008. Targeted analysis of ganglioside and sulfatide molecular species by LC/ESI-MS/MS with theoretically expanded multiple reaction monitoring. Journal of lipid research, 49(12), pp.2678–89.

Ikeda, K. & Taguchi, R., 2010. Highly sensitive localization analysis of gangliosides and sulfatides including structural isomers in mouse cerebellum sections by combination of laser microdissection and hydrophilic interaction liquid chromatography/ electrospray ionization mass spectrom. Rapid communications in mass spectrometry : RCM, 24(20), pp.2957–65.

Ilyas, A.A. et al., 1998. Antibodies to GT1a ganglioside in patients with Guillain-Barré syndrome. Journal of neuroimmunology, 82(2), pp.160–7.

Imokawa, G., 2009. A possible mechanism underlying the ceramide deficiency in atopic dermatitis: expression of a deacylase enzyme that cleaves the N-acyl linkage of sphingomyelin and glucosylceramide. Journal of dermatological science, 55(1), pp.1.

Inoue, M. et al., 2002. Refractory skin injury in complex knock-out mice expressing only the GM3 ganglioside. The Journal of biological chemistry, 277(33), pp.29881–8.

Isaac, G. et al., 2003. Analysis of phosphatidylcholine and sphingomyelin molecular species from brain extracts using capillary liquid chromatography electrospray ionization mass spectrometry. Journal of Neuroscience Methods, 128(1-2), pp.111–119.

Israelachvili, J.N., Mitchell, D.J. & Ninham, B.W., 1976. Theory of self-assembly of hydrocarbon amphiphiles into micelles and bilayers. Journal of the Chemical Society, Faraday Transactions 2, 72, p.1525.

IUPAC-IUB, 1978. The nomenclature of lipids (Recommendations 1976) IUPAC-IUB Commission on Biochemical Nomenclature. The Biochemical journal, 171(1), pp.21.

Ivanova, P.T. et al., 2007. Glycerophospholipid identification and quantitation by electrospray ionization mass spectrometry. Methods in enzymology, 432, pp.21–57.

Ivleva, V. et al., 2005. Ganglioside Analysis by Thin-Layer Chromatography Matrix-Assisted Laser Desorption/Ionization Orthogonal Time-of-Flight Mass Spectrometry. Journal of the American Society for Mass Spectrometry, 16(9), pp.1552–1560.

Ivleva, V., Elkin, Y. & Budnik, B., 2004. Coupling thin-layer chromatography with vibrational cooling matrix-assisted laser desorption/ionization Fourier transform mass spectrometry for the analysis of ganglioside mixtures. Analytical Chemistry, 76(21), pp.6484–6491.

Ivleva, V.B. et al., 2004. Coupling Thin-Layer Chromatography with Vibrational Cooling Matrix-Assisted Laser Desorption/Ionization Fourier Transform Mass Spectrometry for the Analysis of Ganglioside Mixtures. Analytical Chemistry, 76(21), pp.6484–6491.

Jacobs, B.C. et al., 1998. The spectrum of antecedent infections in Guillain-Barré syndrome: a case-control study. Neurology, 51(4), pp.1110–5.

Jennemann, R. et al., 2005. Cell-specific deletion of glucosylceramide synthase in brain leads to severe neural defects after birth. Proceedings of the National Academy of Sciences of the United States of America, 102(35), pp.12459–12464.

Johansson, B., 2006. ToF-SIMS imaging of lipids in cell membranes. Surface and Interface Analysis, 38(11), pp.1401–1412.

Juhasz, P. & Costello, C.E., 1992. Matrix-assisted laser desorption ionization time-of-flight mass spectrometry of underivatized and permethylated gangliosides. Journal of the American Society for Mass Spectrometry, 3(8), pp.785–96.

Julien, J.P., 1999. Neurofilament functions in health and disease. Current opinion in neurobiology, 9(5), pp.554–60.

Kabayama, K. et al., 2007. Dissociation of the insulin receptor and caveolin-1 complex by ganglioside GM3 in the state of insulin resistance. Proceedings of the National Academy of Sciences of the United States of America, 104(34), pp.13678–83.

Kaida, K. et al., 2007. Anti-ganglioside complex antibodies associated with severe disability in GBS. Journal of Neuroimmunology, 182(1-2), pp.212–218.

Kaida, K. et al., 2004. Ganglioside complexes as new target antigens in Guillain–Barre syndrome. Annals of Neurology, 56(4), pp.567–571.

Kaida, K. et al., 2008. Guillain-Barré syndrome with antibody to a ganglioside, N-acetylgalactosaminyl GD1a. Journal of the Peripheral Nervous System, 5(4), pp.237.

Karlsen, A.E. & Dyrberg, T., 1998. Molecular mimicry between non-self, modified self and self in autoimmunity. Seminars in immunology, 10(1), pp.25–34.

Karlsson, K.A., Samuelsson, B.O. & Steen, G.O., 1969. Mass spectrometry of polar complex lipids. Analysis of a sulfatide derivative. Biochemical and biophysical research communications, 37(1), pp.22–7.

Kasama, T. et al., 1996. Microscale analysis of glycosphingolipids by TLC blotting/secondary ion mass spectrometry: a novel blood group A-active glycosphingolipid and changes in glycosphingolipid expression in rat mammary tumour cells with different metastatic potentials. Glycoconjugate journal, 13(3), pp.461–9.

Kawai, H. et al., 2001. Mice expressing only monosialoganglioside GM3 exhibit lethal audiogenic seizures. The Journal of biological chemistry, 276(10), pp.6885–8.

Kawai, T. et al., 1991. Quantitative determination of N-glycolylneuraminic acid expression in human cancerous tissues and avian lymphoma cell lines as a tumor-associated sialic acid by gas chromatography-mass spectrometry. Cancer research, 51(4), pp.1242–6.

Kawashima, I., Nakamura, O. & Tai, T., 1992. Antibody responses to ganglio-series gangliosides in different strains of inbred mice. Molecular immunology, 29(5), pp.625–32.

Kind, T. et al., 2013. LipidBlast in silico tandem mass spectrometry database for lipid identification. Nature methods, 10(8), pp.755–8.

Klenk, E., 1942. Über die ganglioside, eine neue gruppoe von zuckerhaltigen gehirnlipoiden. Hoppe-Seyler's Zeitschrift für physiologische, 273(1-2), pp.76–86.

Koga, M. et al., 1999. Antibodies to GD3, GT3, and O-acetylated species in Guillain-Barré and Fisher's syndromes; their association with cranial nerve dysfunction. Journal of the

Neurological Sciences, 164(1), pp.50-55.

Koivusalo, M. et al., 2001. Quantitative determination of phospholipid compositions by ESI-MS: effects of acyl chain length, unsaturation, and lipid concentration on instrument response. Journal of lipid research, 42(4), pp.663–72.

Kolter, T., Proia, R.L. & Sandhoff, K., 2002. Combinatorial ganglioside biosynthesis. The Journal of biological chemistry, 277(29), pp.25859–62.

Kotani, M. et al., 1993. Differential distribution of major gangliosides in rat central nervous system detected by specific monoclonal antibodies. Glycobiology, 3(2), pp.137–146.

Kracun, I. et al., 1991. Human brain gangliosides in development, aging and disease. The International journal of developmental biology, 35(3), pp.289–95.

Krarup, C. et al., 1990. A syndrome of asymmetric limb weakness with motor conduction block. Neurology, 40(1), pp.118–27.

Krivit, W. & Hammarström, S., 1972. Identification and quantitation of free ceramides in human platelets. Journal of lipid research, 13(4), pp.525–30.

Kundu, S.K. et al., 1985. Glycosphingolipids of human plasma. Archives of Biochemistry and Biophysics, 238(2), pp.388–400.

Kushi, Y., Rokukawa, C. & Handa, S., 1988. Direct analysis of glycolipids on thin-layer plates by matrix-assisted secondary ion mass spectrometry: application for glycolipid storage disorders. Analytical biochemistry, 175(1), pp.167–76.

Kusunoki, S. et al., 1996. GM1b is a new member of antigen for serum antibody in Guillain-Barre syndrome. Neurology, 47(1), pp.237–242.

Labrada, M. et al., 2009. Direct validation of NGcGM3 ganglioside as a new target for cancer immunotherapy. Expert Opinion on Biological Therapy, 10(2), pp.153–162.

Ladisch, S., Li, R. & Olson, E., 1994. Ceramide structure predicts tumor ganglioside immune-suppressive activity. Proceedings of the National Academy of Sciences of the United States of America, 91(5), pp.1974–8.

Lai, N.-S. & Lan, J.-L., 2000. Evaluation of cerebrospinal anticardiolipin antibodies in lupus patients with neuropsychiatric manifestations. Lupus, 9(5), pp.353–357.

Landry, O., 1859. Note sur la paralysie ascendante aiguë. Gazette hebdomadaire de médecine et de chirurgie, 6, pp.472–4, 486–8.

Lehmann, H. & Sheikh, K., 2008. Guillain-Barré Syndrome. In H. E. Gendelman & T. Ikezu, eds. Neuroimmune Pharmacology. Boston, MA: Springer US, pp. 263–281.

Lesnefsky, E.J. et al., 2000. Separation and quantitation of phospholipids and lyso-phospholipids by high-performance liquid chromatography. Analytical biochemistry, 285(2), pp.246–54.

Liebisch, G. et al., 2006. High throughput quantification of cholesterol and cholesteryl ester by electrospray ionization tandem mass spectrometry (ESI-MS/MS). Biochimica et biophysica acta, 1761(1), pp.121–8.

Lozano, M.M. et al., 2013. Colocalization of the ganglioside G(M1) and cholesterol detected by secondary ion mass spectrometry. Journal of the American Chemical Society, 135(15), pp.5620–30.

Lucchinetti, C. et al., 2000. Heterogeneity of multiple sclerosis lesions: implications for the pathogenesis of demyelination. Annals of neurology, 47(6), pp.707–17.

Lunn, M. et al., 2000. High-Affinity Anti-Ganglioside IgG Antibodies Raised in Complex Ganglioside Knockout Mice. Journal of Neurochemistry, 75(1), pp.404–412.

Ma, X. et al., 2007. Evaluation of sphingolipids changes in brain tissues of rats with pentylenetetrazol-induced kindled seizures using MALDI-TOF-MS. Journal of chromatography. B, Analytical technologies in the biomedical and life sciences, 859(2), pp.170–7.

Malmberg, P. et al., 2007. Imaging of lipids in human adipose tissue by cluster ion TOF-SIMS. Microscopy research and technique, 70(9), pp.828–35.

Marconi, S. et al., 2006. Anti-GD2-like IgM autoreactivity in multiple sclerosis patients. Multiple sclerosis (Houndmills, Basingstoke, England), 12(3), pp.302–8.

Marie, I. et al., 2008. Anticardiolipin and anti-beta2 glycoprotein I antibodies and lupus-like

anticoagulant: prevalence and significance in systemic sclerosis. The British journal of dermatology, 158(1), pp.141–4.

Markham, J.E. & Jaworski, J.G., 2007. Rapid measurement of sphingolipids from Arabidopsis thaliana by reversed-phase high-performance liquid chromatography coupled to electrospray ionization tandem mass spectrometry. Rapid communications in mass spectrometry : RCM, 21(7), pp.1304–14.

Martin, S. & Parton, R.G., 2006. Lipid droplets: a unified view of a dynamic organelle. Nature reviews. Molecular cell biology, 7(5), pp.373–8.

Mas, S. et al., 2007. Lipid cartography of atherosclerotic plaque by cluster-TOF-SIMS imaging. The Analyst, 132(1), pp.24–6.

Mauri, L. et al., 2003. Procedure for separation of GM2 ganglioside species with different ceramide structures by a flash reversed-phase silica gel liquid chromatography. Journal of Chromatography B, 796(1), pp.1–10.

McDonnell, L.A. et al., 2005. Subcellular imaging mass spectrometry of brain tissue. Journal of mass spectrometry : JMS, 40(2), pp.160–8.

McLafferty, F.W., 1981. Tandem mass spectrometry. Science (New York, N.Y.), 214(4518), pp.280–7.

McMahon, H.T. & Gallop, J.L., 2005. Membrane curvature and mechanisms of dynamic cell membrane remodelling. Nature, 438(7068), pp.590–6.

Van Meer, G., Voelker, D.R. & Feigenson, G.W., 2008. Membrane lipids: where they are and how they behave. Nat Rev Mol Cell Biol, 9(2), pp.112–124.

Merrill, A.H. et al., 2005. Sphingolipidomics: High-throughput, structure-specific, and quantitative analysis of sphingolipids by liquid chromatography tandem mass spectrometry. Methods, 36(2), pp.207–224.

Michel, V. & Bakovic, M., 2007. Lipid rafts in health and disease. Biology of the cell / under the auspices of the European Cell Biology Organization, 99(3), pp.129–40.

Miljan, E.A. et al., 2002. Interaction of the extracellular domain of the epidermal growth factor receptor with gangliosides. The Journal of biological chemistry, 277(12), pp.10108–13.

Minkler, P.E. & Hoppel, C.L., 2010. Separation and characterization of cardiolipin molecular species by reverse-phase ion pair high-performance liquid chromatography-mass spectrometry. Journal of lipid research, 51(4), pp.856–65.

Mizutani, K. et al., 2003. Amyotrophic lateral sclerosis with IgM antibody against gangliosides GM2 and GD2. Internal medicine (Tokyo, Japan), 42(3), pp.277–80.

Monroe, E.B. et al., 2007. Measuring salty samples without adducts with MALDI MS. International Journal of Mass Spectrometry, 260(2-3), pp.237–242.

Muley, S.A. & Parry, G.J., 2012. Multifocal motor neuropathy. Journal of clinical neuroscience : official journal of the Neurosurgical Society of Australasia, 19(9), pp.1201–9.

Murphy, R.C., Fiedler, J. & Hevko, J., 2001. Analysis of nonvolatile lipids by mass spectrometry. Chemical reviews, 101(2), pp.479–526.

Murphy, S.A. & Nicolaou, A., 2013. lipidomics applications in health, disease and nutrition research. Molecular nutrition & food research, 57(8), pp.1336–46.

Muthing, J., 1998. TLC in Structure and Recognition Studies of Glycosphingolipids. In E. Hounsell, ed. Glycoanalysis Protocols. Totowa, New Jersey: Humana Press, pp. 183.

Nagai, Y., Momoi, T., Saito, M., Mitsuzawa, E. and Ohtani, S. 1976. Ganglioside syndrome, a new autoimmune neurologic disorder, experimentally induced with brain gangliosides. Neuroscience Letters, 2(2), 107-111.

Nakamura, K. et al., 2006. Structural Characterization of Neutral Glycosphingolipids by Thin-Layer Chromatography Coupled to Matrix-Assisted Laser Desorption/Ionization Quadrupole Ion Trap Time-of-Flight MS/MS. Analytical Chemistry, 78(16), pp.5736.

Nakatsuji, Y. & Miller, R., 2001. Selective Cell-Cycle Arrest and Induction of Apoptosis in Proliferating Neural Cells by Ganglioside GM3. Experimental Neurology, 168(2), pp.290–299.

Nemes, P., Woods, A.S. & Vertes, A., 2010. Simultaneous imaging of small metabolites and lipids in rat brain tissues at atmospheric pressure by laser ablation electrospray ionization mass spectrometry. Analytical chemistry, 82(3), pp.982–8.

Ngamukote, S. et al., 2007. Developmental changes of glycosphingolipids and expression of glycogenes in mouse brains. Journal of Neurochemistry, 103(6), pp.2327–2341.

Nicoll, G. et al., 2003. Ganglioside GD3 expression on target cells can modulate NK cell cytotoxicity via siglec-7-dependent and -independent mechanisms. European Journal of Immunology, 33(6), pp.1642–1648.

Niebroj-Dobosz, I. et al., 1999. Anti-neural antibodies in serum and cerebrospinal fluid of amyotrophic lateral sclerosis (ALS) patients. Acta neurologica Scandinavica, 100(4), pp.238–43.

Nimrichter, L. et al., 2008. E-selectin receptors on human leukocytes. Blood, 112(9), pp.3744–3752.

NINCDS, 1978. Criteria for diagnosis of Guillain-Barré syndrome. Annals of neurology, 3(6), pp.565–6.

Nobile-Orazio, E., 2001. Multifocal motor neuropathy. Journal of neuroimmunology, 115(1-2), pp.4–18.

Nohle, U. et al., 1985. Structural parameters and natural occurrence of 2-deoxy-2, 3-didehydro-N-glycoloyneuraminic acid. European Journal of Biochemistry, 152(2), pp.459–463.

Nojiri, H. et al., 1986. Ganglioside GM3: an acidic membrane component that increases during macrophage-like cell differentiation can induce monocytic differentiation of human myeloid and monocytoid leukemic cell lines HL-60 and U937. *Proceedings of the National Academy of Sciences of the United States of America*, 83(3), pp.782–6.

Norlén, L. et al., 1998. A new HPLC-based method for the quantitative analysis of inner stratum corneum lipids with special reference to the free fatty acid fraction. Archives of Dermatological Research, 290(9), pp.508–516.

Nygren, H. et al., 2011. Liquid chromatography-mass spectrometry (LC-MS)-based lipidomics for studies of body fluids and tissues. Methods in molecular biology (Clifton, N.J.), 708, pp.247–57.

O'Hanlon, G.M. et al., 1998. Mapping immunoreactive epitopes in the human peripheral nervous system using human monoclonal anti-GM1 ganglioside antibodies. Acta Neuropathologica, 95(6), pp.605–616.

Ogawa-Goto, K. et al., 1990. Different Ceramide Compositions of Gangliosides Between Human Motor and Sensory Nerves. Journal of Neurochemistry, 55(5), pp.1486–1493.

Ogawa-Goto, K. et al., 1993. Glycosphingolipids of Human Peripheral Nervous System Myelins Isolated from Cauda Equina. Journal of Neurochemistry, 61(4), pp.1398–1403.

Ogawa-Goto, K. et al., 1992. Myelin Gangliosides of Human Peripheral Nervous System: An Enrichment of GM1 in the Motor Nerve Myelin Isolated from Cauda Equina. Journal of Neurochemistry, 59(5), pp.1844–1849.

Ogawa-Goto, K. & Abe, T., 1998. Gangliosides and Glycosphingolipids of Peripheral Nervous System Myelins—a Minireview. Neurochemical Research, 23(3), pp.305–310.

Ohsawa, T., 1989. Changes of mouse brain gangliosides during aging from young adult until senescence. Mechanisms of Ageing and Development, 50(2), pp.169–177.

Ohta, Y., 1994. Binding affinities between human peripheral nerve GM1 and anti-GM1 antibodies. Teikyo Medical Journal, 17, pp.141–152.

Okada, M., Itoh, M., et al., 2002. b-series Ganglioside Deficiency Exhibits No Definite Changes in the Neurogenesis and the Sensitivity to Fas-mediated Apoptosis but Impairs Regeneration of the Lesioned Hypoglossal Nerve. Journal of Biological Chemistry , 277 (3), pp.1633–1636.

Okada, M., Itoh Mi, M., et al., 2002. b-series Ganglioside deficiency exhibits no definite changes in the neurogenesis and the sensitivity to Fas-mediated apoptosis but impairs regeneration of the lesioned hypoglossal nerve. The Journal of biological

chemistry, 277(3), pp.1633–6.

Pakiam, A.S. & Parry, G.J., 1998. Multifocal motor neuropathy without overt conduction block. Muscle & nerve, 21(2), pp.243–5.

Paller, A.S. et al., 1995. Ganglioside GT1b induces keratinocyte differentiation without activating protein kinase C. Experimental cell research, 217(1), pp.118–24.

Di Paolo, G. & De Camilli, P., 2006. Phosphoinositides in cell regulation and membrane dynamics. Nature, 443(7112), pp.651–7.

Parry, G.J. & Clarke, S., 1988. Multifocal acquired demyelinating neuropathy masquerading as motor neuron disease. Muscle & nerve, 11(2), pp.103–7.

Passarelli, M.K. & Winograd, N., 2011. Lipid imaging with time-of-flight secondary ion mass spectrometry (ToF-SIMS). Biochimica et biophysica acta, 1811(11), pp.976–90.

Pender, M.P. et al., 2003. Increased circulating T cell reactivity to GM3 and GQ1b gangliosides in primary progressive multiple sclerosis. Journal of clinical neuroscience : official journal of the Neurosurgical Society of Australasia, 10(1), pp.63–6.

Pestronk, A. et al., 1988. A treatable multifocal motor neuropathy with antibodies to GM1 ganglioside. Annals of neurology, 24(1), pp.73–8.

Pestronk, A. et al., 1990. Lower motor neuron syndromes defined by patterns of weakness, nerve conduction abnormalities, and high titers of antiglycolipid antibodies. Annals of neurology, 27(3), pp.316–26.

Pestronk, A. et al., 1989. Patterns of serum IgM antibodies to GM1 and GD1a gangliosides in amyotrophic lateral sclerosis. Annals of neurology, 25(1), pp.98–102.

Petkovic, M. et al., 2001. Detection of individual phospholipids in lipid mixtures by matrix-assisted laser desorption/ionization time-of-flight mass spectrometry: phosphatidylcholine prevents the detection of further species. Analytical biochemistry, 289(2), pp.202–16.

Petri, M., 2000. Epidemiology of the Antiphospholipid Antibody Syndrome. Journal of Autoimmunity, 15(2), pp.145–151.

Pluskal, T. et al., 2010. MZmine 2: modular framework for processing, visualizing, and analyzing mass spectrometry-based molecular profile data. BMC bioinformatics, 11(1), p.395.

Posse de Chaves, E. & Sipione, S., 2010. Sphingolipids and gangliosides of the nervous system in membrane function and dysfunction. FEBS letters, 584(9), pp.1748–59.

Powell, A.K. & Harvey, D.J., 1996. Stabilization of sialic acids in N-linked oligosaccharides and gangliosides for analysis by positive ion matrix-assisted laser desorption/ionization mass spectrometry. Rapid communications in mass spectrometry : RCM, 10(9), pp.1027–32.

Powell, H.C. et al., 1987. Relationship of adjuvants and swine influenza vaccine to experimental neuropathy in rabbits. Acta Neuropathologica, 73(1), pp.12–18.

Preti, A. et al., 1980. Occurrence of sialyltransferase activity in the synaptosomal membranes prepared from calf brain cortex. Journal of neurochemistry, 35(2), pp.281–96.

Prinetti, A. et al., 2007. Modulation of cell functions by glycosphingolipid metabolic remodeling in the plasma membrane. Journal of Neurochemistry, 103, pp.113–125.

Pulfer, M. & Murphy, R.C., 2003. Electrospray mass spectrometry of phospholipids. Mass spectrometry reviews, 22(5), pp.332–64.

Pyne, S. & Pyne, N., 2000. Sphingosine 1-phosphate signalling in mammalian cells. Journal of Biochemistry, 349(Pt 2), pp.385–402.

Pyo, H. et al., 1999. Gangliosides Activate Cultured Rat Brain Microglia. Journal of Biological Chemistry, 274(49), pp.34584–34589.

Rees, J.H., Gregson, N. a & Hughes, R. a, 1995. Anti-ganglioside GM1 antibodies in Guillain-Barré syndrome and their relationship to Campylobacter jejuni infection. Annals of neurology, 38(5), pp.809–16.

Rinaldi, S. et al., 2009. Analysis of lectin binding to glycolipid complexes using combinatorial glycoarrays. Glycobiology, 19(7), pp.789–796.

Sadatipour, B.T., Greer, J.M. & Pender, M.P., 1998. Increased circulating antiganglioside antibodies in primary and secondary progressive multiple sclerosis. Annals of neurology, 44(6), pp.980–3.

Saida, T. et al., 1981. Experimental allergic neuritis induced by galactocerebroside. Annals of Neurology, 9(S1), pp.87–101.

Saida, T. et al., 1979. Experimental allergic neuritis induced by sensitization with galactocerebroside. Science (New York, N.Y.), 204(4397), pp.1103–6.

Samuelsson, K. & Samuelsson, B., 1969. Gas-liquid chromatography-mass spectrometry of cerebrosides as trimethylsilyl ether derivatives. Biochemical and biophysical research communications, 37(1), pp.15–21.

Sandhoff, K. & Harzer, K., 2013. Gangliosides and gangliosidoses: principles of molecular and metabolic pathogenesis. The Journal of neuroscience : the official journal of the Society for Neuroscience, 33(25), pp.10195–208.

Sandhoff, K. & Kolter, T., 2003. Biosynthesis and degradation of mammalian glycosphingolipids. Philosophical transactions of the Royal Society of London. Series B, Biological sciences, 358(1433), pp.847–61.

Sandhoff, R. et al., 2002. Kidney sulfatides in mouse models of inherited glycosphingolipid disorders: determination by nano-electrospray ionisation tandem mass spectrometry. Journal of Biological Chemistry, 277(23), pp.20386–20398.

Scandroglio, F. et al., 2009. Thin layer chromatography of gangliosides. Glycoconjugate Journal, 26(8), pp.961–973.

Van Schaik, I.N. et al., 1995. Diagnostic value of GM1 antibodies in motor neuron disorders and neuropathies: a meta-analysis. Neurology, 45(8), pp.1570–7.

Scheltema, R.A. et al., 2011. PeakML/mzMatch: a file format, Java library, R library, and tool-chain for mass spectrometry data analysis. Analytical chemistry, 83(7), pp.2786–93.

Schengrund, C.-L., 2010. Lipid rafts: keys to neurodegeneration. Brain research bulletin, 82(1-2), pp.7–17.

Schiller, J. et al., 2007. MALDI-TOF MS in lipidomics. Frontiers in bioscience : a journal and virtual library, 12, pp.2568–79.

Schiller, J. et al., 2004. Matrix-assisted laser desorption and ionization time-of-flight (MALDI-TOF) mass spectrometry in lipid and phospholipid research. Progress in lipid research, 43(5), pp.449–88.

Schnaar, R., 2010. Brain gangliosides in axon-myelin stability and axon regeneration. Frontiers in Membrane Biochemistry, 584(9), pp.1741–1747.

Schnaar, R., 2004. Glycolipid-mediated cell-cell recognition in inflammation and nerve regeneration. Highlight Issue on Glycobiology Dedicated to the Memory of Victor Ginsburg, 426(2), pp.163–172.

Schneider, J.S. et al., 2010. GM1 ganglioside in Parkinson's disease: results of a five year open study. Journal of the neurological sciences, 292(1-2), pp.45–51.

Schwartz, S.A., Reyzer, M.L. & Caprioli, R.M., 2003. Direct tissue analysis using matrix-assisted laser desorption/ionization mass spectrometry: practical aspects of sample preparation. Journal of mass spectrometry : JMS, 38(7), pp.699–708.

Serb, A. et al., 2009. Top-down glycolipidomics: fragmentation analysis of ganglioside oligosaccharide core and ceramide moiety by chip-nanoelectrospray collision-induced dissociation MS2-MS6. Journal of mass spectrometry : JMS, 44(10), pp.1434–42.

Seybold, V. & Rahmann, H., 1985. Changes in developmental profiles of brain gangliosides during ontogeny of a teleost fish (Sarotherodon mossambicus, Cichlidae). Wilhelm Roux's Archives of Developmental Biology, 194(3), pp.166–172.

Seyfried, T. & Purna, M., 2010. Ganglioside GM3 is Antiangiongenic in Malignant Brain Cancer. Journal of Oncology, 2010(961243).

Sheikh, K.A., 1999. The distribution of ganglioside-like moieties in peripheral nerves. Brain, 122(3), pp.449–460.

Sherer, Y. et al., 2004. Autoantibody explosion in systemic lupus erythematosus: More than

100 different antibodies found in SLE patients. Seminars in Arthritis and Rheumatism, 34(2), pp.501–537.

Shrivas, K. et al., 2010. Ionic Matrix for Enhanced MALDI Imaging Mass Spectrometry for Identification of Phospholipids in Mouse Liver and Cerebellum Tissue Sections. Analytical chemistry, 82(21), pp.8800–8806.

Silversand, C. & Haux, C., 1997. Improved high-performance liquid chromatographic method for the separation and quantification of lipid classes: application to fish lipids. Journal of Chromatography B: Biomedical Sciences and Applications, 703(1-2), pp.7–14.

Simons, K. & Toomre, D., 2000. Lipid rafts and signal transduction. Nature reviews. Molecular cell biology, 1(1), pp.31–9.

Singer, S.J. & Nicolson, G.L., 1972. The fluid mosaic model of the structure of cell membranes. Science (New York, N.Y.), 175(4023), pp.720–31.

Smith, C.A. et al., 2006. XCMS: processing mass spectrometry data for metabolite profiling using nonlinear peak alignment, matching, and identification. Analytical chemistry, 78(3), pp.779–87.

Sonnino, S. et al., 2007. Gangliosides as components of lipid membrane domains. Glycobiology, 17(1), p.1R–13R.

Sonnino, S. & Prinetti, A., 2010. Sphingolipids as Signaling and Regulatory Molecules C. Chalfant & M. Del Poeta, eds., New York, NY: Springer New York.

Spiegel, S. & Milstien, S., 2003. Sphingosine-1-phosphate: an enigmatic signalling lipid. Nature reviews. Molecular cell biology, 4(5), pp.397–407.

Stoeckli, M. et al., 2005. MALDI MSI of compounds and metabolites in whole-body tissue sections. In 53rd ASMS Conference. San Antonion, TX.

Sturgill, E.R. et al., 2012. Biosynthesis of the major brain gangliosides GD1a and GT1b. Glycobiology, 22(10), pp.1289–301.

Sugiura, Y. et al., 2008. Imaging mass spectrometry technology and application on ganglioside study; visualization of age-dependent accumulation of C20-ganglioside molecular species in the mouse hippocampus. Y. Astier, ed. PloS one, 3(9), p.e3232.

Sullards, M.C. et al., 2007. Structure-specific, quantitative methods for analysis of sphingolipids by liquid chromatography-tandem mass spectrometry: "inside-out" sphingolipidomics. Methods in enzymology, 432(null), pp.83–115.

Sumner, A.J., 1981. The physiological basis for symptoms in Guillain-Barré syndrome. Annals of Neurology, 9(S1), pp.28–30.

Susuki, K. et al., 2007. Gangliosides contribute to stability of paranodal junctions and ion channel clusters in myelinated nerve fibers. Glia, 55(7), pp.746–757.

Suzuki, M., Yamakawa, T. & Suzuki, A., 1991. A micro method involving micro high-performance liquid chromatography-mass spectrometry for the structural characterization of neutral glycosphingolipids and monosialogangliosides. Journal of biochemistry, 109(4), pp.503–6.

Svennerholm, L., 1956. Composition of Gangliosides from Human Brain. Nature, 177(4507), pp.524–525.

Svennerholm, L., 1980. Ganglioside designation. Advances in experimental medicine and biology, 125, p.11.

Svennerholm, L. et al., 1994. Gangliosides and allied glycosphingolipids in human peripheral nerve and spinal cord. Biochimica et Biophysica Acta (BBA) - Lipids and Lipid Metabolism, 1214(2), pp.115–123.

Svennerholm, L. et al., 1989. Human brain gangliosides: developmental changes from early fetal stage to advanced age. Biochimica et biophysica acta, 1005(2), pp.109–17.

Sweeley, C. & Dawson, G., 1969. Determination of glycosphingolipid structures by mass spectrometry. Biochemical and Biophysical Research Communications, 37(1), pp.6.

Tajima, O. et al., 2009. Reduced motor and sensory functions and emotional response in GM3-only mice: emergence from early stage of life and exacerbation with aging. Behavioural brain research, 198(1), pp.74–82.

Takamiya, K., 1996. Mice with disrupted GM2/GD2 synthase gene lack complex gangliosides

but exhibit only subtle defects in their nervous system. Proceedings of the National Academy of Sciences, 93(20), pp.10662–10667.

Takamiya, K. et al., 1996. Mice with disrupted GM2/GD2 synthase gene lack complex gangliosides but exhibit only subtle defects in their nervous system. Proceedings of the National Academy of Sciences, 93(20), pp.10662–10667.

Tettamanti, G., 2004. Ganglioside/glycosphingolipid turnover: new concepts. Glycoconjugate journal, 20(5), pp.301–17.

Tettamanti, G. et al., 2003. Salvage pathways in glycosphingolipid metabolism. Biochimie, 85(3-4), pp.423–37.

Thomas, A. et al., 2012. Sublimation of new matrix candidates for high spatial resolution imaging mass spectrometry of lipids: enhanced information in both positive and negative polarities after 1,5-diaminonapthalene deposition. Analytical chemistry, 84(4), pp.2048–54.

Todeschini, A.R. et al., 2007. Ganglioside GM2-tetraspanin CD82 complex inhibits met and its cross-talk with integrins, providing a basis for control of cell motility through glycosynapse. The Journal of biological chemistry, 282(11), pp.8123–33.

Touboul, D. et al., 2007. MALDI-TOF and cluster-TOF-SIMS imaging of Fabry disease biomarkers. International Journal of Mass Spectrometry, 260, pp.158–165.

Touboul, D. et al., 2005. Lipid imaging by gold cluster time-of-flight secondary ion mass spectrometry: application to Duchenne muscular dystrophy. Journal of lipid research, 46(7), pp.1388–95.

Touboul, D., Laprévote, O. & Brunelle, A., 2011. Micrometric molecular histology of lipids by mass spectrometry imaging. Current opinion in chemical biology, 15(5), pp.725–32.

Tsui, Z.-C. et al., 2005. A method for profiling gangliosides in animal tissues using electrospray ionization-tandem mass spectrometry. Analytical biochemistry, 341(2), pp.251–8.

Tsuji, S. et al., 1988. Synthetic Sialyl Compounds as Well as Natural Gangliosides Induce Neuritogenesis in a Mouse Neuroblastoma Cell Line (Neuro2a). *Journal of Neurochemistry*, 50(2), pp.414–423.

Ueno, K., Ando, S. & Yu, R.K., 1978. Gangliosides of human, cat, and rabbit spinal cords and cord myelin. Journal of lipid research, 19(7), pp.863–71.

USP, 1990. USP General Test Chapter 621: Chromatography., Rockville, Maryland: United States Pharmacopeial Convention, Inc.

Valaperta, R. et al., 2006. Plasma membrane production of ceramide from ganglioside GM3 in human fibroblasts. FASEB journal : official publication of the Federation of American Societies for Experimental Biology, 20(8), pp.1227–9.

Valdes-Gonzalez, T. et al., 2011. New approach for glyco- and lipidomics – Molecular scanning of human brain gangliosides by TLC-Blot and MALDI-QIT-TOF MS. Journal of Neurochemistry, 116(5), pp.678–683.

Vanier, M.T. et al., 1971. Developmental profiles of gangliosides in human and rat brain. Journal of Neurochemistry, 18(4), pp.581–592.

Varki, A. & Schauer, R., 2009. Chapter 14 Sialic Acids. In A. Varki, R. Cummings, & J. Esko, eds. Essentials of Glycobiology. Cold Spring Harbor, NY: Cold Spring Harbor Laboratory Press.

Vriesendorp, F. et al., 1993. Serum antibodies to GM1, GD1b, peripheral nerve myelin, and Campylobacter jejuni in patients with Guillain-Barré syndrome and controls: correlation and prognosis. Annals of Neurology, 34(2), pp.130–135.

Vukelić, Z. et al., 2005. Screening and sequencing of complex sialylated and sulfated glycosphingolipid mixtures by negative ion electrospray Fourier transform ion cyclotron resonance mass spectrometry. Journal of the American Society for Mass Spectrometry, 16(4), pp.571–80.

Wakabayashi, M. et al., 2005. GM1 ganglioside-mediated accumulation of amyloid beta-protein on cell membranes. Biochemical and biophysical research communications, 328(4), pp.1019–23.

Waksman, B.H. & Adams, R.D., 1955. Allergic neuritis: an experimental disease of rabbits induced by the injection of peripheral nervous tissue and adjuvants. The Journal of experimental medicine, 102(2), pp.213–36.

Walkley, S.U., 2004. Secondary accumulation of gangliosides in lysosomal storage disorders. Seminars in cell & developmental biology, 15(4), pp.433–44.

Walter, F.K., 1919. Zur frage der lokalisation der polyneuritis. Zeitschrift für die gesamte Neurologie und Psychiatrie, 44(1), pp.150–178.

Walther, T.C. & Farese, R. V, 2012. Lipid droplets and cellular lipid metabolism. Annual review of biochemistry, 81, pp.687–714.

Wang, H., Post, S.N. & Woods, A., 2008. A minimalist approach to MALDI imaging of glycerophospholipids and sphingolipids in rat brain sections. Bioanalytical Mass Spectrometry: A special issue honoring Robert J. Cotter on the occasion of his 65th birthday, 278(2-3), pp.143–149.

Werner, I. & Odin, L., 1952. On the presence of sialic acid in certain glycoproteins and in gangliosides. Acta Societatis Medicorum Upsaliensis, 57(3-4), pp.230–41.

Whitfield, P.D. et al., 2001. Characterization of urinary sulfatides in metachromatic leukodystrophy using electrospray ionization-tandem mass spectrometry. Molecular genetics and metabolism, 73(1), pp.30–7.

Williams, M. & McCluer, R., 1980. The Use of Sep-Pak C18 Cartridges During the Isolation of Gangliosides. Journal of Neurochemistry, 35(1), pp.266–269.

Willison, H. & Yuki, N., 2002. Peripheral neuropathies and anti-glycolipid antibodies. Brain, 125(12), pp.2591–2625.

Wiseman, J.M. et al., 2005. Mass spectrometric profiling of intact biological tissue by using desorption electrospray ionization. Angewandte Chemie (International ed. in English), 44(43), pp.7094–7.

Wishart, D.S. et al., 2007. HMDB: the Human Metabolome Database. Nucleic acids research, 35(Database issue), pp.D521–6.

Yamaji, T., Teranishi, T. & Alphey, M., 2002. A small region of the natural killer cell receptor, Siglec-7, is responsible for its preferred binding to alpha 2,8-disialyl and branched alpha 2,6-sialyl residues. A comparison with Siglec-9. Journal of Biological ….

Yamashita, T. et al., 1999. A vital role for glycosphingolipid synthesis during development and differentiation. Proceedings of the National Academy of Sciences, 96(16), pp.9142.

Yamazaki, T. et al., 2008. Amyotrophic lateral sclerosis associated with IgG anti-GalNAc-GD1a antibodies. Clinical neurology and neurosurgery, 110(7), pp.722–4.

Yang, K. et al., 2009. Automated lipid identification and quantification by multidimensional mass spectrometry-based shotgun lipidomics. Analytical chemistry, 81(11), pp.4356.

Yao, D. et al., 2014. Neuronal Expression of GalNAc Transferase Is Sufficient to Prevent the Age-Related Neurodegenerative Phenotype of Complex Ganglioside-Deficient Mice. The Journal of neuroscience : the official journal of the Society for Neuroscience, 34(3), pp.880–91.

Yohe, H.C., Jacobson, R.I. & Yu, R.K., 1983. Ganglioside-basic protein interaction: protection of gangliosides against neuraminidase action. Journal of neuroscience research, 9(4), pp.401–12.

Yu, R. & Bieberich, E., 2001. Regulation of glycosyltransferases in ganglioside biosynthesis by phosphorylation and dephosphorylation. Molecular and Cellular Endocrinology, 177(1-2), pp.19–24.

Yu, R.K. et al., 2004. Regulation of ganglioside biosynthesis in the nervous system. Journal of lipid research, 45(5), pp.783–93.

Yuki, N., 1996. Acute paresis of extraocular muscles associated with IgG anti-GQ1b antibody. Annals of neurology, 39(5), pp.668–72.

Yuki, N. et al., 1993. An immunologic abnormality common to Bickerstaff's brain stem encephalitis and Fisher's syndrome. Journal of the Neurological Sciences, 118(1), pp.83–87.

Yuki, N. et al., 2001. Animal model of axonal Guillain-Barré syndrome induced by

sensitization with GM1 ganglioside. Annals of Neurology, 49(6), pp.712–720.

Yuki, N. et al., 2000. Clinical features and response to treatment in Guillain-Barré syndrome associated with antibodies to GM1b ganglioside. Annals of Neurology, 47(3), pp.314.

Yuki, N. & Hartung, H.-P., 2012. Guillain-Barré syndrome. The New England journal of medicine, 366(24), pp.2294–304.

Zaia, J., 2004. Mass spectrometry of oligosaccharides. Mass spectrometry reviews, 23(3), pp.161–227.

Zhou, M. et al., 2011. Mass spectrometry of intact V-type ATPases reveals bound lipids and the effects of nucleotide binding. Science (New York, N.Y.), 334(6054), pp.380–5.

Putative ID	Chain(s)	Ion	Exact m/z	Gradient 1 Rep 1 RT (min)	Gradient 1 Rep 2 RT (min)	Gradient 2 Rep 1 RT (min)	Gradient 2 Rep 2 RT (min)	Gradient 3 Rep 1 RT (min)	Gradient 3 Rep 2 RT (min)
Phosphoserine	36:1	[M-H]-	788.5447	20.67	20.68	NA	NA	26.09	26.09
Sulfatide	d18:1/18:0	[M-H]-	806.5457	19.95	19.96	44.14	44.13	23.11	23.15
Phosphoserine	40:6	[M-H]-	834.5290	20.29	20.3	40.39	42.77	25.06	25.08
Sulfatide	d18:1/24:1	[M-H]-	888.6240	20.96	21	47.52	47.54	28.6	28.62
Ganglioside GD1	d18:1/18:0	[M-2H]2-	917.4788	19.24	19.26	39.05	39.14	18.49	18.5
	d18:1/20:0	[M-2H]2-	931.4944	19.49	19.51	28.95	40.77	21.12	21.19
Ganglioside GT1	d18:1/18:0	[M-2H]2-	1063.027	19.24	19.19	35.82	35.99	15.46	15.48
	d18:1/20:0	[M-2H]2-	1077.0421	19.35	19.34	27.12	37.62	18.05	18.09
Ganglioside GM2	d18:1/18:0	[M-H]-	1382.816	19.95	19.96	44.22	44.36	22.19	22.23
	d18:1/20:0	[M-H]-	1410.847	20.34	20.35	36.83	NA	24.77	24.77
Ganglioside GM3	d18:1/18:0	[M-H]-	1179.737	19.98	19.99	44.39	44.46	22.65	22.67
	d18:1/20:0	[M-H]-	1207.768	20.34	20.38	31.01	NA	25.3	25.35
Ganglioside GM1	d18:1/18:0	[M-H]-	1544.869	19.9	19.94	43.25	43.31	21.67	21.71
	d18:1/20:0	[M-H]-	1572.9007	20.26	20.3	33.02	45.67	24.43	24.5
Ganglioside GQ1	d18:1/18:0	[M-2H]2-	1208.573	19.15	19.17	36.81	36.84	14.55	14.51
	d18:1/20:0	[M-2H]2-	1222.589	19.38	19.39	29.88	NA	17.36	17.41
t_{GQ1}-t_{PS} (min)				1.81	1.83	20.4	11.55	14.05	14.11

RT - Retention time

Raw retention data extracted for the major components of commercial ganglioside extract separated by reverse phase chromatography using three gradients; gradient 1 – ternary acetonitrile/isopropanol/ammonium formate; gradient 2 – acetonitrile/ammonium formate; and gradient 3 – isopropanol/ammonium formate.

226

Appendix 2; Retention Data from Separation and Analysis of Lipid Standards by HPLC-MSMS.

Raw mass lists of the 15-25 predominant peaks with normalised intensity >75,000, extracted from HPLC-MSMS separation and negative ion mode analysis of lipid standards. These were extracted by MZmine 2 open source software (Pluskal et al., 2010), using the parameters described in 4.2.3.4. Putative identifications were made using accurate mass and product ion spectra. Typical LC chromatograms for phospholipids, glycosphingolipids and simple sphingolipids are shown above raw mass lists corresponding to each category.
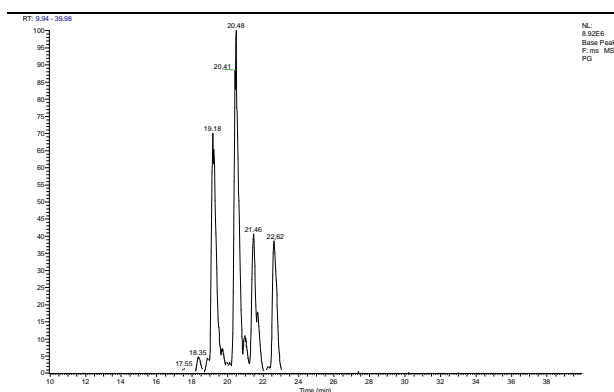
Base peak chromatogram of glycerophosphglycerol standard separation.

			Glycerophosphocholine			
Peak m/z	Retention Time (min)	Peak height	Ion/adduct	Molecular mass	Identification	Molecular formula
790.5176	20.46	4.3E+04	[M+Cl]-	755.5465	PC(34:3)	C42H78NO8P
766.5181	21.33	1.4E+05	[M+Cl]-	731.5465	PC(32:1)	C40H78NO8P
776.5464	21.33	7.9E+04	[M+FA-H]-	731.5465	PC(32:1)	C40H78NO8P
792.5345	22.06	6.0E+05	[M+Cl]-	757.5622	PC(34:2)	C42H80NO8P
802.5612	22.06	1.1E+05	[M+FA-H]-	757.5622	PC(34:2)	C42H80NO8P
816.5333	22.37	2.5E+05	[M+Cl]-	781.5622	PC(36:4)	C44H80NO8P
826.5618	22.37	1.5E+05	[M+FA-H]-	781.5622	PC(36:4)	C44H80NO8P
840.5331	22.37	1.4E+05	[M+Cl]-	805.5622	PC(38:6)	C46H80NO8P
850.5619	22.39	8.8E+04	[M+FA-H]-	805.5622	PC(38:6)	C46H80NO8P
768.5341	23.03	7.3E+04	[M+Cl]-	733.5622	PC(32:0)	C40H80NO8P
804.5775	23.45	8.7E+05	[M+FA-H]-	759.5778	PC(34:1)	C42H82NO8P
794.5496	23.47	1.3E+06	[M+Cl]-	759.5778	PC(34:1)	C42H82NO8P
744.5573	23.47	3.2E+05	[M-H]-	745.5621	PE(36:1)	C41H80NO8P
852.5074	23.47	8.5E+04	[M+FA-H]-	807.5050	PS(38:6)	C44H74NO10P
770.5731	24.42	7.7E+04	[M-H]-	771.5778	PE(38:2)	C43H82NO8P
854.5931	24.71	1.9E+05	[M+FA-H]-	809.5935	PC(38:4)	C46H84NO8P
794.5725	24.71	6.1E+04	[M-H]-	795.5778	PE(40:4)	C45H82NO8P
868.5645	24.73	4.5E+04	[M+Cl]-	833.5935	PC(40:6)	C48H84NO8P
844.5645	24.78	3.2E+05	[M+Cl]-	809.5935	PC(38:4)	C46H84NO8P
846.5800	25.49	6.4E+04	[M+Cl]-	811.6091	PC(38:3)	C46H86NO8P
832.6090	25.73	3.6E+05	[M+FA-H]-	787.6091	PC(36:1)	C44H86NO8P
822.5811	25.73	3.0E+05	[M+Cl]-	787.6091	PC(36:1)	C44H86NO8P

			Glycerophosphoethanolamine			
Peak m/z	Retention Time (min)	Peak height	Ion/adduct	Molecular mass	Identification	Molecular formula
719.4880	18.27	2.4E+05	[M-H]-	720.4941	PG(32:1)	C38H73O10P
660.4622	19.04	1.3E+05	[M-H]-	661.4683	PE(30:1)	C35H68NO8P
733.5038	19.38	7.9E+05	[M-H]-	734.5098	PG(33:1)	C39H75O10P
686.4778	19.70	1.3E+05	[M-H]-	687.4839	PE(32:2)	C37H70NO8P
721.5040	19.87	2.2E+05	[M-H]-	722.5097	PG(32:0)	C38H75O10P
747.5195	20.26	2.7E+05	[M-H]-	748.5254	PG(36:1)	C40H77O10P
662.4783	20.91	2.2E+05	[M-H]-	663.4839	PE(30:0)	C35H70NO8P
761.5351	21.40	6.2E+05	[M-H]-	762.5411	PG(35:1)	C41H79O10P
688.4933	21.51	1.4E+05	[M-H]-	689.4996	PE(32:1)	C37H72NO8P
676.4939	22.09	2.3E+05	[M-H]-	677.4995	PE(31:0)	C36H72NO8P

714.5094	22.17	2.1E+05	[M-H]-	715.5152	PE(34:2)	C39H74NO8P
760.4678	22.70	1.3E+05	[M+NaCl-H]-	703.5152	PE(23:1)	C38H74NO8P
702.5092	22.70	2.1E+05	[M-H]-	703.5152	PE(23:1)	C38H74NO8P
728.5244	23.12	4.8E+05	[M-H]-	729.5309	PE(35:2)	C40H76NO8P
690.5095	23.23	7.0E+05	[M-H]-	691.5152	PE(32:0)	C37H74NO8P
716.5252	23.67	1.1E+05	[M-H]-	717.5308	PE(34:1)	C39H76NO8P
742.5405	24.38	3.1E+05	[M-H]-	743.5465	PE(36:2)	C41H78NO8P
730.5406	24.86	1.0E+06	[M-H]-	731.5465	PE(35:1)	C40H78NO8P
756.5559	25.22	2.7E+05	[M-H]-	757.5622	PE(37:2)	C42H80NO8P
718.5406	25.49	1.0E+05	[M-H]-	719.5465	PE(34:0)	C39H78NO8P
744.5564	25.95	1.7E+05	[M-H]-	745.5621	PE(36:1)	C41H80NO8P
770.5722	26.37	1.2E+05	[M-H]-	771.5778	PC(35:2)	C43H82NO8P

Glycerophosphoglycerol

Peak m/z	Retention Time (min)	Peak height	Ion/adduct	Molecular mass	Identification	Molecular formula
719.4880	18.35	4.2E+05	[M-H]-	720.4941	PG (32:1)	C38H73O10P
745.5046	19.18	1.3E+05	[M-H]-	746.5098	PG (34:2)	C40H75O10P
1492.0162	19.18	3.1E+05	[2M-H]-	746.5098	PG (34:2)	C40H75O10P
803.4619	19.18	3.5E+05	[M+NaCl-H]-	746.5098	PG (34:2)	C40H75O10P
793.5034	19.53	5.3E+05	[M-H]-	794.5098	PG (38:6)	C44H75O10P
721.5039	19.94	3.0E+05	[M-H]-	722.5097	PG (32:0)	C38H75O10P
771.5190	20.11	2.7E+05	[M-H]-	772.5254	PG (36:3)	C42H77O10P
805.4777	20.48	4.4E+05	[M+NaCl-H]-	748.5254	PG (34:1)	C40H77O10P
1496.0482	20.48	7.8E+05	[2M-H]-	748.5254	PG (34:1)	C40H77O10P
747.5198	20.48	8.7E+06	[M-H]-	748.5254	PG (34:1)	C40H77O10P
795.5191	20.59	2.1E+05	[M-H]-	796.5254	PG (38:5)	C44H77O10P
773.5349	20.99	9.8E+05	[M-H]-	774.5410	PG (36:2)	C42H79O10P
1548.0787	21.46	1.0E+05	[2M-H]-	774.5410	PG (36:2)	C42H79O10P
831.4932	21.46	2.0E+05	[M+NaCl-H]-	774.5410	PG (36:2)	C42H79O10P
773.5350	21.46	3.6E+06	[M-H]-	774.5410	PG (36:2)	C42H79O10P
797.5347	21.69	1.6E+06	[M-H]-	798.5410	PG (38:4)	C44H79O10P
821.5347	21.74	1.9E+05	[M-H]-	822.5411	PG (40:6)	C46H79O10P
749.5350	22.12	1.1E+05	[M-H]-	750.5411	PG (34:0)	C40H79O10P
799.5503	22.27	1.7E+05	[M-H]-	800.5567	PG (38:3)	C44H81O10P
1552.1100	22.62	1.0E+05	[2M-H]-	776.5567	PG (36:1)	C42H81O10P
833.5092	22.62	1.9E+05	[M+NaCl-H]-	776.5567	PG (36:1)	C42H81O10P
775.5508	22.62	3.4E+06	[M-H]-	776.5567	PG (36:1)	C42H81O10P
823.5503	22.72	1.3E+05	[M-H]-	824.5567	PG (40:5)	C46H81O10P

Glycerophosphoserine

Peak m/z	Retention Time (min)	Peak height	Ion/adduct	Molecular mass	Identification	Molecular formula
786.5300	20.71	4.3E+05	[M-H]-	787.5363	PS(36:2)	C42H78NO10P
774.5300	21.35	2.7E+05	[M-H]-	775.5363	PS(35:1)	C41H78NO10P
834.5298	21.60	3.8E+05	[M-H]-	835.5363	PS(40:6)	C46H78NO10P
762.5303	21.97	6.0E+04	[M-H]-	763.5363	PS(34:0)	C40H78NO10P
788.5458	22.16	4.2E+05	[M-H]-	789.5520	PS(36:1)	C42H80NO10P
846.5044	22.19	6.5E+04	[M-Cl]-	811.5363	PS(38:4)	C44H78NO10P
810.5271	22.19	6.8E+04	[M-H]-	811.5363	PS(38:4)	C44H78NO10P
836.5454	22.45	6.4E+04	[M-H]-	837.5520	PS(40:5)	C46H80NO10P
838.5612	23.06	1.5E+05	[M-H]-	839.5676	PS(40:4)	C46H82NO10P
814.5614	23.38	2.0E+05	[M-H]-	815.5676	PS(38:2)	C44H82NO10P
816.5768	24.28	1.0E+05	[M-H]-	817.5833	PS(38:1)	C44H84NO10P
872.6393	28.59	6.6E+04	[M-H]-	873.6459	PS(42:1)	C48H92NO10P

Cardiolipin

Peak m/z	Retention Time (min)	Peak height	Ion/adduct	Molecular mass	Identification	Molecular formula
1185.7366	23.91	5.7E+05	[M-H]-	1186.7426	CL(54:6)	C63H112O16P2
592.3646	23.93	1.3E+05	[M-2H]2-	1186.7426	CL(54:6)	C63H112O16P2
1187.7509	24.50	1.8E+05	[M-H]-	1188.7582	CL(54:5)	C63H114O16P2

1419.9338	29.86	1.4E+05	[M-H]-	1421.9488	CL(70:9)	C81H140O17P2
1467.9307	30.12	1.6E+05	[M+Na-2H]-	1446.9566	CL(72:9)	C81H140O17P2
1445.9491	30.12	9.3E+05	[M-H]-	1446.9566	CL(72:9)	C81H140O17P2
722.4714	30.14	2.3E+05	[M-2H]2-	1446.9566	CL(72:9)	C81H140O17P2
1469.9435	30.78	7.1E+05	[M+Na-2H]-	1448.9722	CL(72:8)	C81H142O17P2
1435.9661	31.12	1.6E+05	[M-H]-	1436.9722	CL(71:7)	C80H142O17P2
1423.9644	31.17	3.9E+05	[M-H]-	1424.9722	CL(70:6)	C79H142O17P2
724.4863	31.29	2.9E+05	[M-2H]2-	1450.9879	CL(72:7)	C81H144O17P2
1449.9792	31.34	2.6E+06	[M-H]-	1450.9879	CL(72:7)	C81H144O17P2
1473.9774	31.97	1.9E+05	[M+Na-2H]-	1453.0035	CL(72:6)	C81H146O17P2
1451.9950	31.97	8.1E+05	[M-H]-	1453.0035	CL(72:6)	C81H146O17P2
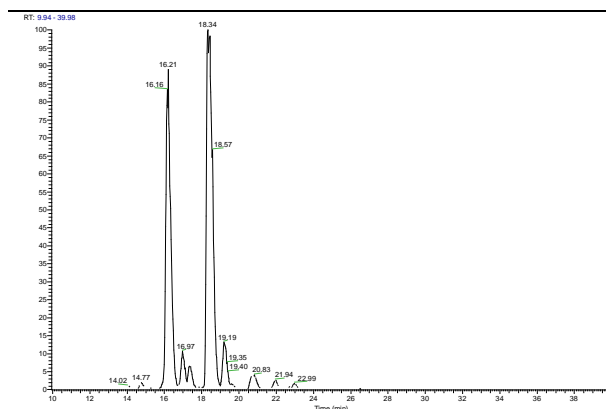
Base peak chromatogram of ganglioside GD1a standard separation.

asialoGM1

Peak m/z	Retention Time (min)	Peak height	Ion/adduct	Molecular mass	Identification	Molecular formula
1261.7195	18.96	1.6E+05	[M+Cl]-	1226.7499	GA1(d18:1/16:0)	C60H110N2O23
1287.7350	19.64	2.0E+05	[M+Cl]-	1252.7656	GA1(d18:1/18:1)	C62H112N2O23
1307.7614	20.15	1.0E+05	[M+Cl]-	1272.7918	GA1(t18:1/18:0)	C62H116N2O24
1299.7783	21.18	6.8E+05	[M+FA-H]-	1254.7812	GA1(d18:1/18:0)	C62H114N2O23
1289.7510	21.18	2.0E+06	[M+Cl]-	1254.7812	GA1(d18:1/18:0)	C62H114N2O23
1253.7736	21.26	1.1E+05	[M-H]-	1254.7812	GA1(d18:1/18:0)	C62H114N2O23
1301.7949	22.01	1.0E+05	[M+FA-H]-	1256.7969	GA1(d18:0/18:0)	C62H116N2O23
1291.7668	22.01	3.2E+05	[M+Cl]-	1256.7969	GA1(d18:0/18:0)	C62H116N2O24
1303.7666	22.38	1.0E+05	[M+Cl]-	1268.7969	GA1(d18:0/19:0)	C63H116N2O23
1327.8101	23.45	2.1E+05	[M+FA-H]-	1282.8125	GA1(d20:1/18:0)	C64H118N2O23
1317.7823	23.46	5.9E+05	[M+Cl]-	1282.8125	GA1(d20:1/18:0)	C64H118N2O23
1319.7976	24.17	1.7E+05	[M+Cl]-	1284.8282	GA1(d20:0/18:0)	C64H120N2O23

GM1

Peak m/z	Retention Time (min)	Peak height	Ion/adduct	Molecular mass	Identification	Molecular formula
789.9199	18.62	1.7E+06	[M-H+Cl]2-	1545.8767	GM1(d18:1/18:0)	C73H131N3O31
1544.8708	18.62	5.1E+06	[M-H]-	1545.8767	GM1(d18:1/18:0)	C73H131N3O31
1179.7378	19.25	1.3E+05	[M-H]-	1180.7445	GM3(d18:1/18:0)	C59H108N2O21
790.9277	19.39	1.6E+05	[M-H+Cl]2-	1547.8923	GM1(d18:0/18:0)	C73H133N3O31
1546.8860	19.43	3.9E+05	[M-H]-	1547.8923	GM1(d18:0/18:0)	C73H133N3O32
1558.8857	19.78	3.9E+05	[M-H]-	1559.8923	GM1(d18:1/19:0)	C74H133N3O31
796.9275	19.81	1.9E+05	[M-H+Cl]2-	1559.8923	GM1(d18:1/19:0)	C74H133N3O31
1572.9033	20.77	1.7E+06	[M-H]-	1573.9080	GM1(d20:1/18:0)	C75H135N3O31
803.9356	20.80	2.1E+06	[M-H+Cl]2-	1573.9080	GM1(d20:1/18:0)	C75H135N3O31
804.9431	21.58	3.0E+05	[M-H+Cl]2-	1575.9236	GM1(d20:0/18:0)	C75H137N3O31
1574.9164	21.58	7.1E+05	[M-H]-	1575.9236	GM1(d20:0/18:0)	C75H137N3O31
1586.9171	21.96	1.0E+05	[M-H]-	1587.9236	GM1 (d20:1/19:0)	C76H137N3O31
817.9512	22.98	1.3E+05	[M-H+Cl]2-	1601.9393	GM1(d20:1/20:0)	C77H139N3O31
1600.9335	23.03	2.2E+05	[M-H]-	1601.9393	GM1(d20:1/20:0)	C77H139N3O31
1614.9490	24.15	1.2E+05	[M-H]-	1615.9549	GM1(d20:1/21:0)	C78H141N3O31
1628.9642	25.09	1.1E+05	[M-H]-	1629.9706	GM1(d20:1/22:0)	C79H143N3O31

GM2

Peak m/z	Retention Time (min)	Peak height	Ion/adduct	Molecular mass	Identification	Molecular formula
1354.7861	16.66	1.1E+05	[M-H]-	1355.7925	GM2(d18:1/16:0)	C65H117N3O26
1382.8182	18.86	7.3E+06	[M-H]-	1383.8238	GM2(d18:1/18:0)	C67H121N3O26
708.8940	18.89	4.6E+05	[M-H+Cl]2-	1411.8551	GM2(d18:1/20:0)	C69H125N3O26
1384.8341	19.62	6.7E+05	[M-H]-	1385.8395	GM2(d18:0/18:0)	C67H123N3O26
1396.8333	20.00	5.1E+05	[M-H]-	1397.8395	GM2(d18:1/19:0)	C68H123N3O26
1410.8507	20.99	1.6E+05	[M-H]-	1411.8551	GM2(d20:1/18:0)	C69H125N3O26
722.9095	20.99	5.0E+05	[M-H+Cl]2-	1411.8551	GM2(d20:1/18:0)	C69H125N3O26
723.9172	21.73	1.5E+05	[M-H+Cl]2-	1413.8708	GM2(d20:0/18:0)	C69H127N3O26
1412.8644	21.73	1.2E+06	[M-H]-	1413.8708	GM2(d20:0/18:0)	C69H127N3O26
1438.8807	23.31	1.4E+05	[M-H]-	1439.8864	GM2(d20:1/20:0)	C71H129N3O26

GM3

Peak m/z	Retention Time (min)	Peak height	Ion/adduct	Molecular mass	Identification	Molecular formula
1151.7104	16.97	2.2E+06	[M-H]-	1152.7132	GM3(d18:1/16:0)	C57H104N2O21
1153.7258	17.74	2.8E+05	[M-H]-	1154.7288	GM3(d18:0/16:0)	C57H106N2O21
1179.7426	19.19	1.7E+06	[M-H]-	1180.7445	GM3(d18:1/18:0)	C59H108N2O21
1181.7577	19.97	2.1E+06	[M-H]-	1182.7601	GM3(d18:0/18:0)	C59H110N2O21
896.5908	20.09	3.2E+05	[M+Cl]-	861.6177	LacCer(d18:1/16:0)	C46H87NO13
1193.7568	20.40	6.1E+05	[M-H]-	1194.7601	GM3(d18:1/19:0)	C60H110N2O21
1207.7743	21.41	3.6E+05	[M-H]-	1208.7758	GM3(d20:1/18:0)	C61H112N2O21
1209.7881	22.07	5.0E+05	[M-H]-	1208.7758	GM3(d20:0/18:0)	C61H114N2O21
924.6223	22.50	1.3E+06	[M+Cl]-	889.6490	LacCer(d18:1/18:0)	C48H91NO13
934.6503	22.54	4.2E+05	[M+FA]-	889.6490	LacCer(d18:1/18:0)	C48H91NO13
1235.8046	23.64	2.0E+06	[M-H]-	1236.8071	GM3(d20:1/20:0)	C63H116N2O21
1237.8202	24.16	2.7E+05	[M-H]-	1238.8227	GM3(d20:0/20:0)	C63H118N2O21
1249.8203	24.60	6.7E+05	[M-H]-	1250.8227	GM3(d20:1/21:0)	C64H118N2O21
952.6535	24.67	5.6E+05	[M+Cl]-	917.6803	LacCer(d18:1/16:0)	C50H95NO13
1263.8358	25.52	1.3E+06	[M-H]-	1264.8384	GM3(d20:1/22:0)	C65H120N2O21
980.6846	26.85	3.1E+05	[M+Cl]-	945.7116	LacCer(d18:1/16:0)	C52H99NO13
1008.7160	28.79	3.4E+05	[M+Cl]-	973.7429	LacCer(d18:1/16:0)	C54H103NO13

GD1a

Peak m/z	Retention Time (min)	Peak height	Ion/adduct	Molecular mass	Identification	Molecular formula
917.4791	16.21	1.2E+07	[M-2H]2-	1836.9721	GD1(d18:1/18:0)	C84H148N4O39
935.4661	16.21	1.5E+06	[M-H+Cl]2-	1836.9721	GD1(d18:1/18:0)	C84H148N4O39
946.4567	16.21	1.1E+06	[M+Na-2H+Cl]2-	1836.9721	GD1(d18:1/18:0)	C84H148N4O39
918.4866	16.97	1.5E+06	[M-2H]2-	1838.9877	GD1(d18:0/18:0)	C84H150N4O39
924.4865	17.34	9.1E+05	[M-2H]2-	1850.9877	GD1(d18:1/19:0)	C85H150N4O39
960.4720	18.32	1.1E+06	[M+Na-2H+Cl]2-	1865.0034	GD1(d20:1/18:0)	C86H152N4O39
1864.5009	18.32	5.1E+05	[M-H]-	1865.0034	GD1(d20:1/18:0)	C86H152N4O39
931.4945	18.34	7.6E+06	[M-2H]2-	1865.0034	GD1(d20:1/18:0)	C86H152N4O39
949.4809	18.42	1.5E+06	[M-H+Cl]2-	1865.0034	GD1(d20:1/18:0)	C86H152N4O39
932.5008	19.19	1.8E+06	[M-2H]2-	1867.0190	GD1(d20:0/18:0)	C86H154N4O39
945.5098	20.73	5.4E+05	[M-2H]2-	1893.0347	GD1(d20:1/20:0)	C88H156N4O39
958.5165	20.83	5.7E+05	[M-2H]2-	1919.0503	GD1(d20:1/22:1)	C90H156N4O39

GD1b

Peak m/z	Retention Time (min)	Peak height	Ion/adduct	Molecular mass	Identification	Molecular formula
917.4791	15.58	6.1E+06	[M-2H]2-	1836.9721	GD1(d18:1/18:0)	C84H148N4O39
935.4667	15.58	2.8E+06	[M-H+Cl]2-	1836.9721	GD1(d18:1/18:0)	C84H148N4O39
946.4563	15.58	7.2E+05	[M+Na-2H+Cl]2-	1836.9721	GD1(d18:1/18:0)	C84H148N4O39
1835.9674	15.58	3.2E+05	[M-H]-	1836.9721	GD1(d18:1/18:0)	C84H148N4O39
936.9755	16.27	1.9E+05	[M-H+Cl]2-	1838.9877	GD1(d18:0/18:0)	C84H150N4O39

Peak m/z	Retention Time (min)	Peak height	Ion/adduct	Molecular mass	Identification	Molecular formula
918.4865	16.30	3.9E+05	[M-2H]2-	1838.9877	GD1(d18:0/18:0)	C84H150N4O39
924.4866	16.79	4.2E+05	[M-2H]2-	1850.9877	GD1(d18:1/19:0)	C85H150N4O39
942.4742	16.79	2.1E+05	[M-H+Cl]2-	1850.9877	GD1(d18:1/19:0)	C85H150N4O39
931.4949	17.83	5.2E+06	[M-2H]2-	1865.0034	GD1(d20:1/18:0)	C86H152N4O39
949.4818	17.83	4.4E+06	[M-H+Cl]2-	1865.0034	GD1(d20:1/18:0)	C86H152N4O39
960.9733	17.83	1.1E+06	[M+Na-2H+Cl]2-	1865.0034	GD1(d20:1/18:0)	C86H152N4O39
1863.9986	17.83	8.6E+05	[M-H]-	1865.0034	GD1(d20:1/18:0)	C86H152N4O39
932.5009	18.55	9.8E+05	[M-2H]2-	1867.0190	GD1(d20:0/18:0)	C86H154N4O39
961.4795	18.55	1.6E+05	[M+Na-2H+Cl]2-	1867.0190	GD1(d20:0/18:0)	C86H154N4O39
950.4891	18.60	5.0E+05	[M-H+Cl]2-	1867.0190	GD1(d20:0/18:0)	C86H154N4O39
938.5018	19.04	1.5E+05	[M-2H]2-	1879.0190	GD1(d20:1/19:0)	C87H154N4O39
963.4978	20.17	2.2E+05	[M-H+Cl]2-	1893.0347	GD1(d20:1/20:0)	C88H156N4O39
945.5099	20.20	3.7E+05	[M-2H]2-	1893.0347	GD1(d20:1/20:0)	C88H156N4O39
958.5175	20.37	1.8E+05	[M-2H]2-	1919.0503	GD1(d20:1/22:1)	C90H156N4O39
959.5255	22.51	1.3E+05	[M-2H]2-	1919.0503	GD1(d20:0/22:1)	C90H158N4O39

			GD3			
Peak m/z	Retention Time (min)	Peak height	Ion/adduct	Molecular mass	Identification	Molecular formula
1442.8018	14.04	4.5E+05	[M-H]-	1443.8086	GD3(d18:1/16:0)	C68H121N3O29
720.8973	14.06	6.0E+05	[M-2H]2-	1443.8086	GD3(d18:1/16:0)	C68H121N3O29
1470.8345	16.43	6.1E+05	[M-H]-	1471.8399	GD3(d18:1/18:0)	C70H125N3O29
734.9132	16.45	1.5E+06	[M-2H]2-	1471.8399	GD3(d18:1/18:0)	C70H125N3O29
735.9206	17.08	5.1E+05	[M-2H]2-	1473.8555	GD3(d18:0/18:0)	C70H127N3O29
1498.8639	18.71	4.9E+05	[M-H]-	1499.8712	GD3(d18:1/20:0)	C72H129N3O29
748.9283	18.71	9.7E+05	[M-2H]2-	1499.8712	GD3(d18:1/20:0)	C72H129N3O29
1179.7378	19.13	4.3E+05	[M-H]-	1180.7445	GM3(d18:1/18:0)	C59H108N2O21
748.9289	19.18	4.4E+05	[M-2H]2-	1499.8712	GD3(d18:1/20:0)	C72H129N3O29
749.9365	19.69	3.0E+05	[M-2H]2-	1501.8868	GD3(d18:0/20:0)	C72H131N3O29
1512.8805	20.38	2.6E+05	[M-H]-	1513.8868	GD3(d18:1/21:0)	C73H131N3O29
755.9363	20.38	6.6E+05	[M-2H]2-	1513.8868	GD3(d18:1/21:0)	C73H131N3O29
775.9509	21.13	3.2E+05	[M-2H]2-	1553.9181	GD3(d18:1/24:1)	C76H135N3O29
1526.8962	21.16	4.8E+05	[M-H]-	1527.9025	GD3(d18:1/22:0)	C74H133N3O29
762.9437	21.16	1.1E+06	[M-2H]2-	1527.9025	GD3(d18:1/22:0)	C74H133N3O29
769.9524	22.28	5.5E+05	[M-2H]2-	1541.9181	GD3(d18:1/23:0)	C75H135N3O29
1540.9115	22.28	5.8E+05	[M-H]-	1541.9181	GD3(d18:1/23:0)	C75H135N3O29
1554.9286	23.34	3.9E+05	[M-H]-	1555.9338	GD3(d18:1/24:0)	C76H137N3O29
776.9602	23.36	4.7E+05	[M-2H]2-	1555.9338	GD3(d18:1/24:0)	C76H137N3O29

			GT1b			
Peak m/z	Retention Time (min)	Peak height	Ion/adduct	Molecular mass	Identification	Molecular formula
1417.7097	13.71	3.0E+05	[2M-3H]3-	2128.0675	GT1(d18:1/18:0)	C95H165N5O47
1074.0184	13.74	7.1E+05	[M+Na-3H]2-	2128.0675	GT1(d18:1/18:0)	C95H165N5O47
1063.0308	13.74	4.1E+06	[M-2H]2-	2128.0675	GT1(d18:1/18:0)	C95H165N5O47
1064.0380	14.48	4.4E+05	[M-2H]2-	2130.0832	GT1(d18:0/18:0)	C95H167N5O47
1070.0375	15.02	5.8E+05	[M-2H]2-	2142.0832	GT1(d18:1/19:0)	C96H167N5O47
1086.0481	15.39	1.5E+05	[M-2H]2-	2174.1094	GT1(t18:0/20:0)	C97H171N5O48
1077.0458	15.94	8.3E+06	[M-2H]2-	2156.0988	GT1(20:1/18:0)	C97H169N5O47
1096.0194	15.96	1.7E+05	[M+K-3H]2-	2156.0988	GT1(20:1/18:0)	C97H169N5O47
1443.7230	15.96	1.9E+05	[2M+Na-4H]3-	2156.0988	GT1(20:1/18:0)	C97H169N5O47
1436.3971	15.99	8.6E+05	[2M-3H]3-	2156.0988	GT1(20:1/18:0)	C97H169N5O47
1088.0331	16.01	1.4E+06	[M+Na-3H]2-	2156.0988	GT1(20:1/18:0)	C97H169N5O47
1078.0531	16.80	1.3E+06	[M-2H]2-	2158.1145	GT1(d20:0/18:0)	C97H171N5O47
1089.0410	16.88	2.0E+05	[M+Na-3H]2-	2158.1145	GT1(d20:0/18:0)	C97H171N5O47
1084.0535	17.41	1.7E+05	[M-2H]2-	2170.1145	GT1(d20:1/19:0)	C98H171N5O47
931.4971	18.52	1.6E+05	[M-2H]2-	1865.0034	GD1(d20:1/18:0)	C86H152N4O39
1091.0615	18.60	1.7E+05	[M-2H]2-	2184.1301	GT1(d20:1/20:0)	C99H173N5O47
1098.0687	20.03	2.0E+05	[M-2H]2-	2198.1458	GT1(d20:1/21:0)	C100H175N5O47
1105.0764	21.22	1.2E+05	[M-2H]2-	2212.1614	GT1(d20:1/22:0)	C101H177N5O47

GQ1b

Peak m/z	Retention Time (min)	Peak height	Ion/adduct	Molecular mass	Identification	Molecular formula
1216.5748	13.31	1.7E+05	[M-2H]2-	2435.1578	GQ1(t18:1/18:0)	C106H182N6O56
1219.5668	13.33	3.1E+05	[M+Na-3H]2-	2435.1578	GQ1(t18:1/18:0)	C106H182N6O56
1208.5796	13.36	2.4E+06	[M-2H]2-	2419.1629	GQ1(d18:1/18:0)	C106H182N6O55
1063.0312	13.70	1.3E+05	[M-2H]2-	2128.0675	GT1(d18:1/18:0)	C95H165N5O47
1209.5869	14.41	2.4E+05	[M-2H]2-	2421.1786	GQ1(d18:0/18:0)	C106H184N6O55
1215.5863	14.76	3.3E+05	[M-2H]2-	2433.1786	GQ1(d18:1/19:0)	C107H184N6O55
1630.4634	15.57	1.6E+05	[2M-3H]3-	2447.1942	GQ1(d20:1/18:0)	C108H186N6O55
1241.5654	15.61	2.5E+05	[M+K-3H]2-	2447.1942	GQ1(d20:1/18:0)	C108H186N6O55
814.7271	15.64	1.0E+05	[M-3H]3-	2447.1942	GQ1(d20:1/18:0)	C108H186N6O55
1233.5818	15.64	6.8E+05	[M+Na-3H]2-	2447.1942	GQ1(d20:1/18:0)	C108H186N6O55
1222.5952	15.64	2.6E+06	[M-2H]2-	2447.1942	GQ1(d20:1/18:0)	C108H186N6O55
1077.0465	16.08	2.2E+05	[M-2H]2-	2156.0988	GT1(d20:1/18:0)	C97H169N5O47
1085.0439	16.08	2.1E+06	[M+Na-3H]2-	2172.0937	GT1(d20:1/18:0)	C97H169N5O47
1236.6101	19.23	1.0E+05	[M-2H]2-	2475.2255	GQ1(d20:1/20:0)	C110H190N6O55
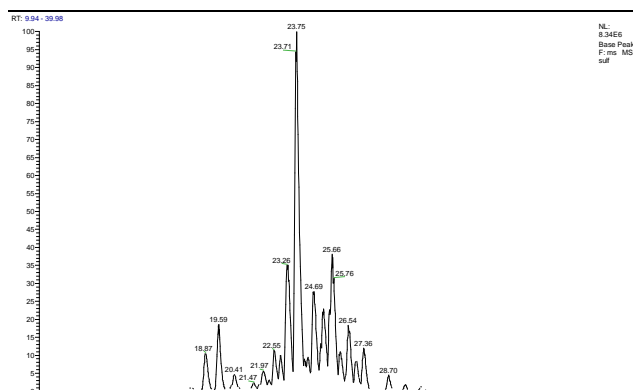
Base peak chromatogram of sulfatide standard separation.

Ceramide

Peak m/z	Retention Time (min)	Peak height	Ion/adduct	Molecular mass	Identification	Molecular formula
588.4771	21.59	1.4E+05	[M+Cl]-	553.5070	Cer(d18:1/16:0(2OH))	C34H67NO4
622.5421	23.52	1.3E+05	[M+CH3COO]-	563.5277	Cer(d18:1/18:1)	C36H69NO3
668.5474	23.53	1.1E+05	[M+FA-H]-	581.5383	Cer(d18:1/18:0(2OH))	C36H71NO4
616.5084	23.82	2.8E+06	[M+Cl]-	581.5383	Cer(d18:1/18:0(2OH))	C36H71NO4
580.5318	23.84	8.9E+05	[M-H]-	581.5383	Cer(d18:1/18:0(2OH))	C36H71NO4
618.5239	24.57	4.4E+05	[M+Cl]-	583.5540	Cer(d18:0/18:0(2OH))	C36H73NO4
582.5473	24.60	1.8E+05	[M-H]-	583.5540	Cer(d18:0/18:0(2OH))	C36H73NO4
630.5239	24.92	1.4E+05	[M+K-2H]-	593.5747	Cer(d18:1/18:0)	C38H75NO3
608.5629	26.00	1.2E+05	[M-H]-	609.5696	Cer(d20:1/18:0(2OH))	C38H75NO4
644.5396	26.00	3.2E+05	[M+Cl]-	609.5696	Cer(d20:1/18:0(2OH))	C38H75NO4
670.5551	26.25	1.2E+05	[M+Cl]-	635.5853	Cer(d18:1/24:1(2OH))	C40H77NO4
684.5707	27.11	2.3E+05	[M+K-2H]-	647.6216	Cer(d18:1/24:1)	C40H76NO3

Glycolylceramide

Peak m/z	Retention Time (min)	Peak height	Ion/adduct	Molecular mass	Identification	Molecular formula
762.5660	22.97	8.5E+05	[M+Cl]-	727.5962	GlcCer(d18:1/18:0)	C42H81NO8
854.6726	27.26	5.5E+05	[M+FA-H]-	809.6745	GlcCer(d18:1/24:1)	C48H91NO8
844.6448	27.29	2.1E+06	[M+Cl]-	809.6745	GlcCer(d18:1/24:1)	C48H91NO8
818.6288	27.31	7.6E+05	[M+Cl]-	783.6588	GlcCer(d20:1/20:0)	C46H89NO8
858.6603	28.17	7.0E+05	[M+Cl]-	823.6901	GlcCer(d18:1/25:1)	C48H91NO8CH2
832.6448	28.26	9.3E+05	[M+Cl]-	783.6588	GlcCer (d20:1/21:0)	C47H91NO8
872.6756	29.07	9.6E+05	[M+Cl]-	837.7058	GlcCer(d20:1/24:1)	C50H95NO8
856.6890	29.14	6.0E+05	[M+FA-H]-	811.6901	GlcCer (d18:1/24:0)	C48H93NO8
846.6605	29.17	3.6E+06	[M+Cl]-	811.6901	GlcCer(d18:1/24:0)	C48H93NO8
876.6708	29.50	7.4E+05	[M+Cl]-	841.7007	GlcCer(d18:1/26:0)	C49H95NO9

Peak m/z	Retention Time (min)	Peak height	Ion/adduct	Molecular mass	Identification	Molecular formula
860.6756	29.99	1.2E+06	[M+Cl]-	825.7058	GlcCer (d18:1/25:0)	C49H95NO8
874.6907	30.78	7.4E+05	[M+Cl]-	839.7214	GlcCer (d18:1/26:0)	C50H97NO8

Sulfatide						
Peak m/z	Retention Time (min)	Peak height	Ion/adduct	Molecular mass	Identification	Molecular formula
822.5415	18.87	8.8E+05	[M-H]-	823.5479	Sulf(d18:1/18:0(2OH))	C42H81NO12S
806.5467	19.56	1.5E+06	[M-H]-	807.5530	Sulf(d18:1/18:0)	C42H81NO11S
886.6079	22.55	9.4E+05	[M-H]-	887.6156	Sulf(d18:1/24:2)	C48H89NO11S
878.6047	23.26	4.0E+05	[M-H]-	879.6106	Sulf(d18:1/22:0(2OH))	C46H89NO12S
904.6194	23.30	2.8E+06	[M-H]-	905.6262	Sulf(d18:1/24:1(2OH))	C48H91NO12S
888.6253	23.75	8.2E+06	[M-H]-	889.6312	Sulf(d18:1/24:1)	C48H91NO11S
862.6097	23.80	5.9E+05	[M-H]-	863.6156	Sulf(d18:1/22:0)	C46H89NO11S
904.6185	24.08	3.2E+05	[M-H]-	905.6261	Sulf(d18:1/24:1(2OH))	C48H91NO12S
918.6346	24.18	7.4E+05	[M-H]-	919.6419	Sulf(d20:1/23:1(2OH))	C49H93NO12S
890.6400	24.36	7.7E+05	[M-H]-	891.6469	Sulf(d18:1/24:0)	C48H93NO11S
902.6403	24.69	2.3E+06	[M-H]-	903.6469	Sulf(d20:1/23:1)	C49H93NO11S
932.6503	25.06	1.1E+06	[M-H]-	917.6626	Sulf(d20:1/24:1(2OH))	C50H95NO12S
906.6355	25.20	1.8E+06	[M-H]-	907.6418	Sulf(d18:0/24:1(2OH))	C48H93NO12S
916.6555	25.52	1.9E+06	[M-H]-	917.6626	Sulf(d20:1/24:1)	C50H95NO11S
890.6410	25.66	3.2E+06	[M-H]-	891.6469	Sulf(d18:0/24:1)	C48H93NO11S
920.6508	26.10	9.0E+05	[M-H]-	921.6575	Sulf(d20:0/23:0(2OH))	C49H95NO12S
892.6564	26.19	4.0E+05	[M-H]-	893.6626	Sulf(d18:0/24:0)	C48H95NO11S
930.6714	26.40	3.7E+05	[M-H]-	931.6782	Sulf(d18:1/27:1)	C51H97NO11S
934.6661	26.96	7.0E+05	[M-H]-	935.6732	Sulf(d18:0/26:0(2OH))	C50H97NO12S
918.6715	27.36	9.8E+05	[M-H]-	919.6782	Sulf(d18:0/26:0)	C50H97NO11S

Sphingomyelin						
Peak m/z	Retention Time (min)	Peak height	Ion/adduct	Molecular mass	Identification	Molecular formula
715.5775	22.37	2.5E+05	[M-CH3]-	730.5989	SM(d18:1/20:0)	C41H83N2O6P
765.5704	22.37	6.4E+05	[M+Cl]-	730.5989	SM(d18:1/20:0)	C41H83N2O6P
775.5972	22.37	1.1E+06	[M+FA-H]-	730.5989	SM(d18:1/18:0)	C41H83N2O6P
767.5857	23.14	4.4E+05	[M+Cl]-	732.6145	SM(d18:1/20:0)	C41H83N2O6P
803.6292	24.79	2.4E+05	[M+FA-H]-	758.6302	SM(d18:1/20:0)	C43H87N2O6P
793.6008	24.79	4.0E+05	[M+Cl]-	758.6302	SM(d18:1/20:0)	C43H87N2O6P
829.6447	24.97	1.7E+05	[M+FA-H]-	784.6458	SM(d18:1/22:1)	C45H89N2O6P
819.6160	25.01	3.0E+05	[M+Cl]-	784.6458	SM(d18:1/22:1)	C45H89N2O6P
795.6162	25.53	2.2E+05	[M+Cl]-	760.6458	SM(d18:0/20:0)	C43H89N2O6P
833.6317	26.01	2.3E+05	[M+Cl]-	798.6615	SM(d18:2/23:0)	C46H91N2O6P
771.6396	26.95	1.6E+05	[M-CH3]-	786.6615	SM(d18:1/22:0)	C45H91N2O6P
831.6610	26.97	3.1E+05	[M+FA-H]-	786.6615	SM(d18:1/22:0)	C45H91N2O6P
821.6320	26.97	5.8E+05	[M+Cl]-	786.6615	SM(d18:1/22:0)	C45H91N2O6P
823.6473	27.67	2.5E+05	[M+Cl]-	788.6771	SM(d18:0/22:0)	C45H93N2O6P
861.6626	27.93	1.6E+05	[M+Cl]-	826.6928	SM(d18:2/25:0)	C48H95N2O6P
835.6472	28.22	2.9E+05	[M+Cl]-	800.6771	SM(d18:1/23:0)	C46H93N2O6P
845.6757	28.24	1.9E+05	[M+FA-H]-	800.6771	SM(d18:1/23:0)	C46H93N2O6P
875.6785	28.90	1.9E+05	[M+Cl]-	840.7084	SM(d18:1/26:1)	C49H97N2O6P
799.6711	29.03	2.1E+05	[M-CH3]-	814.6928	SM(d18:1/24:0)	C47H95N2O6P
859.6918	29.03	4.5E+05	[M+FA-H]-	814.6928	SM(d18:1/24:0)	C47H95N2O6P
849.6634	29.08	1.1E+06	[M+Cl]-	814.6928	SM(d18:1/24:0)	C47H95N2O6P
851.6779	29.77	2.1E+05	[M+Cl]-	816.7084	SM(d18:0/24:0)	C47H97N2O6P

ID	Peak m/z	Standard retention time (min)	peak intensity	retention time (min)	peak intensity	retention time (min)	peak intensity	retention time (min)	peak intensity	retention time (min)	peak intensity	retention time (min)	peak intensity	retention time (min)	peak intensity	retention time (min)	peak intensity	retention time (min)
									Repeat separations of Commercial Ganglioside Extract (CGE)									
GM1 d18:1/18:0	1544.8688	18.6	1.29E+06	18.37	1.28E+06	18.43	1.34E+06	18.57	1.24E+06	18.42	2.12E+06	18.41	1.66E+06	18.33	4.87E+06	18.35	6.28E+06	18.39
GM1 d20:1/18:0	1572.9001	20.8	8.11E+05	20.59	8.18E+05	20.61	8.06E+05	20.72	8.66E+05	20.56	1.20E+06	20.64	9.71E+05	20.53	3.08E+06	20.49	3.97E+05	20.57
GM1 d20:1/20:0	1600.9314	23.0	1.56E+04	22.81	1.73E+04	22.85	2.07E+04	22.97	2.23E+04	22.84	2.70E+04	22.86	1.92E+04	22.79	6.69E+04	22.71	9.81E+03	22.81
GM2 d18:1/18:0	1382.8160	18.9	2.91E+04	18.67	2.86E+04	18.73	3.03E+04	18.84	3.27E+04	18.74	4.62E+04	18.73	3.31E+04	18.68	1.18E+05	18.62	1.29E+04	18.72
GM2 d20:1/18:0	1410.8473	21.0	1.28E+04	20.86	1.39E+04	20.91	1.40E+04	20.99	1.31E+04	20.75	2.02E+04	20.86	1.54E+04	20.77	4.83E+04	20.75	7.22E+03	20.87
GM3 d18:1/18:0	1179.7366	19.2	7.55E+04	19.01	7.86E+04	19.02	7.57E+04	19.13	9.04E+04	18.95	1.35E+05	18.98	8.72E+04	18.94	3.05E+05	18.94	3.47E+04	19.01
GM3 d18:1/20:0	1207.7679	21.4	1.63E+04	21.13	1.62E+04	21.15	1.76E+04	21.26	1.90E+04	21.19	2.78E+04	21.17	1.79E+04	21.09	6.61E+04	21.08	8.08E+03	21.17
GD1a d18:1/18:0	917.4782	16.2	3.68E+06	16.01	3.96E+06	16.06	4.03E+06	16.2	4.79E+06	16.04	6.20E+06	16	4.86E+06	15.9	1.31E+07	15.9	2.02E+06	15.99
GD1a d18:1/19:0	924.4860	17.3	1.16E+05	17.19	1.08E+05	17.21	1.19E+05	17.33	1.38E+05	17.14	1.76E+05	17.18	1.31E+05	17.06	2.76E+05	17.04	4.84E+04	17.15
GD1a d20:1/18:0	931.4939	18.3	4.33E+06	18.27	4.45E+06	18.3	4.68E+06	18.37	5.19E+06	18.22	6.55E+06	18.21	5.56E+06	18.13	1.55E+07	18.1	2.32E+06	18.26
GD1b d18:1/18:0	917.4782	15.6	-	15.47	-	15.5	-	15.62	-	15.44	-	15.46	-	15.3	-	15.34	-	15.42
GD1b d18:1/19:0	924.4860	16.8	-	16.63	-	16.7	-	16.78	-	16.61	-	16.61	-	16.68	-	16.47	-	16.61
GD1b d20:1/18:0	931.4939	17.8	-	17.73	-	17.78	-	17.88	-	17.69	-	17.69	-	17.6	-	17.59	-	17.67
GD3 d18:1/18:0	734.9151	16.5	1.65E+04	16.35	1.78E+05	16.32	1.96E+05	16.43	2.09E+05	16.17	5.40E+05	16.13	1.76E+05	16.09	6.56E+05	16.29	8.77E+04	16.37
GD3 d20:1/18:0	748.9278	18.7	5.09E+04	18.57	5.49E+04	18.62	6.14E+04	18.74	5.95E+04	18.49	7.70E+04	18.41	5.51E+04	18.25	2.23E+05	18.64	2.94E+04	18.75
GD3 d18:1/24:1	775.9512	21.1	1.36E+04	20.98	1.69E+04	21	1.70E+04	21.09	1.51E+04	20.89	1.93E+04	20.91	1.46E+04	20.75	4.91E+04	21.06	7.16E+03	21.2
GT1b d18:1/18:0	1063.0265	13.7	2.28E+05	13.61	2.32E+05	13.68	2.63E+05	13.79	2.87E+05	13.53	3.82E+05	13.50	2.57E+05	13.30	8.11E+05	13.57	1.01E+05	13.65
GT1b d18:1/19:0	1070.0338	15.0	7.74E+03	14.82	8.85E+03	14.88	1.03E+04	14.97	1.11E+04	14.71	1.29E+04	14.61	9.92E+03	14.54	2.74E+04	14.75	5.57E+03	14.88
GT1b d20:1/18:0	1077.0416	15.9	5.78E+05	15.94	6.22E+05	15.96	6.51E+05	16.07	7.85E+05	15.81	9.88E+05	15.81	7.35E+05	15.60	2.20E+06	15.85	2.77E+05	16.05

Appendix 4; Mass Filters, Putative Identifications, and Intensities Applied and Extracted from HPTLC-MSI Separations of Ganglioside Brain Extracts.

putative identifications	Adduct	mass filter value	mass filter colour	wild type		GalNAcT knockout		GD3 knockout	
				filter 'hits'	ROI peak intensity	filter 'hits'	ROI peak intensity	filter 'hits'	ROI peak intensity
Sulfatide d18:1/18:0	[M-H]-	807	White	196	3.0	150	4.8	182	4.5
Phosphoinositol 38:3	[M-H]-	887	White	104	8.5	113	7.3	170	10.0
Sulfatide d18:1/24:1	[M-H]-	890	White	361	19.0	268	16.8	278	29.0
Sulfatide d18:1/24:1(2OH)	[M-H]-	905	White	262	5.0	198	6.0	213	7.5
GM3 d18:1/18:0	[M-H]-	1180	Red	107	6.0	220	30.8	356	31.3
GM3 d20:1/18:0	[M-H]-	1208	Red	137	1.5	199	5.0	262	9.8
GM2 d18:1/18:0	[M-H]-	1384	Pink	156	14.0	-	-	94	3.3
GM2 18:0/20:0	[M-H]-	1412	Pink	126	2.5	-	-	-	-
GD3 d18:1/18:0	[M-H2O-H]-	1453	Orange	70	5.0	239	34.8	-	-
GD3 d18:0/20:0	[M-H2O-H]-	1481	Orange	66	1.5	222	16.0	-	-
9OAc-GD3 d18:1/18:0	[M-H2O-H]-	1495	Turquoise	-	-	278	23.0	-	-
9OAc-GD3 d18:0/20:0	[M-H2O-H]-	1523	Turquoise	-	-	200	13.5	-	-
GM1 d18:0/18:0	[M-H]-	1546	Blue	339	31.5	-	-	394	29.5
GM1 d20:1/18:0	[M-H]-	1574	Blue	240	12.5	-	-	263	12.8
GD1b d18:1/18:0	[M-H_2O-H]-	1819	Cyan	190	19.0	-	-	-	-
GD1b d20:1/18:0	[M-H_2O-H]-	1848	Cyan	102	8.0	-	-	-	-
GD1a d18:1/18:0	[M+Na-2H]-	1859	Yellow	104	13.5	-	-	209	16.0
GD1a d20:1/18:0	[M+Na-2H]-	1887	Yellow	122	2.0	-	-	170	4.0
OAc-GD1a d18:1/18:0	[M+Na-2H]-	1899	Yellow	-	-	-	-	213	1.5
OAc-GD1a d20:1/18:0	[M+Na-2H]-	1927	Yellow	-	-	-	-	83	1.5
GT1b d18:1/18:0	[M+Na-H2O-2H]-	2132	Green	89	0.8	-	-	-	-

putative identifications	Adduct	mass filter value	mass filter colour	NFL rescue		PLP rescue		THY1 112 rescue		THY1 115 rescue	
				filter 'hits'	ROI peak intensity	filter 'hits'	ROI peak intensity	filter 'hits'	ROI peak intensity	filter 'hits'	ROI peak intensity
Sulfatide d18:1/18:0	[M-H]-	807	White	177	4.0	70	3.0	186	2.0	173	3.3
Phosphoinositol 38:3	[M-H]-	887	White	120	7.3	112	14.5	91	2.0	64	4.0
Sulfatide d18:1/24:1	[M-H]-	890	White	198	14.3	163	10.0	294	7.0	379	19.0
Sulfatide d18:1/24:1(2OH)	[M-H]-	905	White	170	6.8	102	4.0	153	5.0	171	4.5
GM3 d18:1/18:0	[M-H]-	1180	Red	183	39.0	212	37.5	112	12.0	153	22.0
GM3 d20:1/18:0	[M-H]-	1208	Red	132	6.8	156	4.5	94	2.0	143	3.8
GM2 d18:1/18:0	[M-H]-	1384	Pink	329	4.3	-	-	86	5.0	139	5.0
GM2 18:0/20:0	[M-H]-	1412	Pink	-	-	-	-	-	-	-	-
GD3 d18:1/18:0	[M-H2O-H]-	1453	Orange	387	28.0	348	28.5	204	15.0	352	19.0
GD3 d18:0/20:0	[M-H2O-H]-	1481	Orange	302	14.3	743	7.0	117	4.0	156	4.0
9OAc-GD3 d18:1/18:0	[M-H2O-H]-	1495	Turquoise	125	19.5	216	12.5	60	5.0	163	4.5
9OAc-GD3 d18:0/20:0	[M-H2O-H]-	1523	Turquoise	157	11.8	130	5.0	92	3.0	116	2.5
GM1 d18:0/18:0	[M-H]-	1546	Blue	167	25.8	122	13.5	236	29.0	268	31.3
GM1 d20:1/18:0	[M-H]-	1574	Blue	82	6.5	-	-	134	7.0	151	4.8
GD1b d18:1/18:0	[M-H_2O-H]-	1819	Cyan	77	3.8	-	-	146	4.5	109	2.5
GD1b d20:1/18:0	[M-H_2O-H]-	1848	Cyan	38	1.0	-	-	76	1.0	77	1.0
GD1a d18:1/18:0	[M+Na-2H]-	1859	Yellow	83	5.0	793	2.0	79	4.0	44	5.8
GD1a d20:1/18:0	[M+Na-2H]-	1887	Yellow	55	1.8	-	-	-	-	-	-
GT1b d18:1/18:0	[M+Na-H2O-2H]-	2132	Green								

peak m/z	headgroup ID	hydrocarbon	wild type dataset ID	wild type dataset distribution	knockout dataset ID	knockout dataset distribution	NFL dataset ID	NFL dataset distribution
701.5	PA	C36:1	x	root ganglion	x	universal	x	universal
726.6	HexCer	d18:1/18:0	x	white matter	x	white matter	x	white matter
728.6	HexCer	d18:0/18:0	x	white matter	x	white matter	x	white matter
742.6	HexCer	d18:1/18:0(2OH)	x	white matter	x	white matter	x	white matter
744.6	PE	C36:1	x	universal	x	universal	x	universal
747.5	PG	C34:1	x	grey matter	x	grey matter	x	grey matter
750.5	Sulfatide	d18:1/14:0	x	universal	x	universal	x	universal
754.6	HexCer	d18:1/20:0	x	white matter	x	white matter	x	white matter
756.6	HexCer	d18:0/20:0	x	white matter	x	white matter	x	white matter
766.5	PE	C38:4	x	grey matter	x	grey matter	x	grey matter
767.5	PG	36:5	x	white matter	x	white matter	x	white matter
770.6	HexCer	d18:1/20:0(2OH)	x	white matter	x	white matter	x	grey matter
774.6	PE	C38:0	x	grey matter	x	grey matter	x	universal
778.5	Sulfatide	d18:1/16:0	x	root ganglion	x	universal	x	white matter
781.5	PI	C30:0	x	white matter	x	white matter	x	universal
788.6	PS	C36:1	x	universal	x	universal	x	universal
790.5	PE	C40:6	x	grey matter	x	grey matter	x	grey matter
793.5	PG	C38:6	x	white matter	x	white matter	x	white matter
795.5	PG	C38:5	x	white matter	x	white matter	x	white matter
804.5	Sulfatide	d18:1/18:1	x	root ganglion	x	universal	x	universal
806.6	Sulfatide	d18:1/18:0	x	universal	x	universal	x	universal
816.6	PS	C38:1	x	white matter	x	white matter	x	white matter
819.5	PG	C40:7	x	white matter	x	white matter	x	white matter
821.6	PG	C40:6	x	white matter	x	white matter	x	white matter
832.6	LacCer	d18:1/14:0	x	root ganglion	x	universal	x	white matter
834.6	PS/Sulf/LacCer	C40:6/d18:1/20:0/(	x	universal	x	universal	x	universal
835.5	PI	C34:1	x	white matter	x	white matter	x	white matter
847.6	PG	C42:7	x	white matter	x	white matter	x	white matter
849.6	PG	C42:6	x	white matter	x	white matter	x	white matter
850.6	Sulfatide	d18:1/20:0(2OH)	x	white matter	x	white matter	x	white matter
857.5	PE	C36:4	x	grey matter	x	grey matter	x	grey matter
860.6	LacCer	d18:1/16:0	x	white matter	x	white matter	x	white matter
862.6	Sulfatide	d18:1/22:0	x	universal	x	universal	x	universal
864.6	PS	C42:5					x	white matter
872.6	PS	C42:1	x	root ganglion				
874.6	PE	C46:6	x	universal	x	white matter	x	universal
876.6	PE	C46:5	x	universal	x	universal	x	universal
878.6	PE/Sulf/PI	C46:4/d18:1/22:0(2	x	universal	x	universal	x	universal
885.6	PE	C38:4	x	grey matter	x	grey matter	x	grey matter
886.6	Sulfatide	d18:1/24:1	x	root ganglion	x	universal	x	universal
888.7	Sulfatide	d18:1/24:1	x	universal	x	universal	x	universal
890.6	Sulfatide	d18:1/24:0	x	universal	x	universal	x	universal
892.6	PS	C44:5	x	universal	x	universal	x	universal
902.7	Sulfatide	d18:1/24:2	x	universal	x	white matter	x	universal
904.6	Sulfatide	d18:1/24:1(2OH)	x	universal	x	universal	x	universal
906.7	Sulfatide	d18:1/24:0(2OH)	x	universal	x	universal	x	universal
914.7	LacCer	d18:1/20:2	x	root ganglion	x	universal	x	universal
916.7	LacCer	d18:1/20:0	x	white matter	x	white matter	x	white matter
918.7	LacCer	d18:0/20:0	x	root ganglion	x	white matter	x	universal
920.7	PI-Cer	d18:0/26:0	x	universal	x	universal	x	universal
930.6	PS	C44:4	x	root ganglion				
932.7	LacCer	d18:1/20:0(2OH)	x	root ganglion	x	white matter	x	universal
965.5	PIP	C38:4	x	white matter	x	white matter	x	universal
982.5	PIP	C34:1	x	grey matter	x	grey matter	x	white matter
1179.7	GM3	d18:1/18:0			x	dorsal horn	x	dorsal horn
1207.8	GM3	d18:1/20:0			x	grey matter	x	dorsal horn
1382.8	GM2	d18:1/18:0	x	grey matter			x	dorsal horn
1426.8	GalNAc(NeuGc)GalGlcCer	d18:1/20:0	x	grey matter	x	grey matter	x	grey matter
1428.0	CL	C70:4	x	grey matter	x	grey matter	x	dorsal horn
1430.0	CL	C70:2	x	grey matter	x	grey matter	x	grey matter
1450.0	CL	C72:7	x	grey matter	x	grey matter	x	grey matter
1454.9	GalNAc(NeuGc)GalGlcCer	d18:1/22:0	x	grey matter	x	grey matter	x	grey matter
1456.0	CL	C72:4	x	grey matter	x	grey matter	x	grey matter
1470.8	GD3	d18:1/18:0	x	grey matter	x	dorsal horn	x	dorsal horn
1476.0	CL	C74:8	x	grey matter	x	grey matter	x	grey matter
1478.0	CL	C74:7	x	grey matter	x	grey matter	x	grey matter
1494.0	CL	C76:13	x	grey matter	x	grey matter	x	grey matter
1498.0	CL	C76:11	x	grey matter	x	grey matter	x	grey matter
1500.0	CL	C76:10	x	grey matter	x	grey matter	x	grey matter
1502.0	CL	C76:9	x	grey matter	x	grey matter	x	grey matter
1522.0	CL	C78:13	x	grey matter	x	grey matter	x	grey matter
1523.9	CL	C78:12	x	grey matter	x	grey matter	x	grey matter
1544.87	GM1	d18:1/18:0	x	dorsal horn			x	dorsal horn
1572.9	GM1	d20:1/18:0	x	grey matter			x	grey matter
1792	FucFucHexHexGalNAcGalGalCer	d18:1/24:0	x	dorsal horn			x	dorsal horn

Appendix 6; Detection of Complex-Ganglioside Specific Fragments from SIMS Analysis of Lipid Standards in Positive and Negative Ion Mode.

Positive Ion Mode SIMS Data from Lipid Standards. (+/-) refers to the presence or absence of that secondary ion in the lipid standard. Yellow indicates the detection of a specific secondary ion in spectra from complex ganglioside standards. Red indicates the detection of a secondary ion in spectra from a non-complex ganglioside lipid standard, which ruled out use of that ion as a charactistic fragment of complex gangliosides. Blue highlights those secondary ions that were potentially identified as complex ganglioside-specific.

Secondary ion m/z

m/z	GM1	GM2	GM3	GA1	GD1a	GD1b	GD3	GT1b	Cer	GalC	SM	SS	Sulf	PC	PE	PG	PS
147	+	+	+	+	+	+	+	+	-	+	+	-	+	-	+	-	-
155	-	-	-	-	-	-	-	-	-	-	-	-	-	-	-	+	-
165	-	-	-	-	-	-	-	-	-	-	-	-	+	+	-	-	+
173	-	-	-	-	-	-	-	-	-	-	-	-	-	-	-	+	-
184	-	-	-	-	-	-	-	-	-	-	+	-	-	-	+	-	+
198	-	-	-	-	-	-	-	-	-	-	-	-	-	+	-	-	+
207	+	+	+	+	+	+	+	+	+	+	+	-	+	-	+	+	-
221	+	+	+	+	+	+	+	+	+	+	+	-	+	-	+	+	-
224	-	-	-	-	-	-	-	-	-	-	-	-	-	+	-	-	-
237	+	-	-	-	-	-	-	-	-	-	+	-	+	-	-	+	-
242	-	-	-	-	-	-	-	+	-	-	-	-	-	-	-	-	-
250	-	-	-	-	-	-	-	-	-	-	-	+	-	-	-	-	-
265	+	+	+	+	+	+	+	+	+	+	+	+	+	-	-	-	-
281	+		+	+	+	+	+	+	+	+	+	+	+	-	+	+	+
284	-	-	-	+	+	+	+	+	-	-	-	-	-	-	-	-	-
288	-	+	-	-	-	-	-	-	-	-	-	-	-	-	-	-	-
292	-	+	-	-	+	+	-	+	-	-	-	+	-	-	-	-	-
304	-	-	-	-	-	-	+	+	-	+	-	-	-	-	-	-	-
308	-	+	-	-	+	+	-	-	-	-	-	+	+	-	-	-	-
313	-	-	-	-	-	-	-	-	-	-	-	-	-	-	+	+	-
322	+	+	-	+	+	+	-	+	-	-	-	-	+	-	-	-	-
325	+	-	-	-	-	-	+	+	-	-	+	+	+	-	-	-	-
339	+	-	-	-	-	-	+	+	-	-	-	-	+	-	-	-	-
348	-	+	-	+	+	+	-	+	-	-	-	-	-	-	-	-	-
355	+	-	-	+	-	-	-	-	-	-	+	-	+	-	-	-	-
368	-	-	+	-	+	+	+	-	-	+	-	-	-	-	-	-	-
379	-	-	-	+	+	+	-	-	-	-	-	-	-	-	-	-	-
443	-	-	-	-	-	-	-	-	+	+	-	-	-	-	-	-	-
518	+	-	-	-	-	-	-	-	-	-	+	-	-	-	-	-	-
524	-	-	+	-	-	-	-	-	-	-	-	-	-	-	-	-	-
534	+	-	-	-	-	-	-	-	-	-	+	-	-	-	-	-	-
538	-	-	-	+	-	-	-	-	-	-	-	-	-	-	-	-	-
545	-	-	-	-	-	-	-	-	-	+	-	-	-	-	-	-	-
552	-	-	+	-	-	-	-	-	-	-	-	-	-	-	-	-	-
563	-	-	-	-	-	-	-	-	-	+	-	-	-	-	+	-	-
577	+	-	-	-	-	-	-	-	-	-	-	-	-	-	-	+	-
592	-	-	-	-	-	-	-	-	-	-	-	-	-	-	-	+	+
605	-	-	-	-	-	-	-	-	-	+	-	-	-	-	-	+	-
608	-	-	-	-	-	-	-	-	-	-	-	-	-	-	-	-	+
630	-	-	-	-	-	-	-	-	-	-	-	+	-	-	-	-	-
648	+	+	-	-	+	+	-	+	-	-	-	-	-	-	-	-	-
662	-	-	+	-	-	-	-	+	-	-	+	-	-	-	+	-	-
663	-	-	-	-	+	-	+	-	+	-	-	-	-	-	-	-	-
664	+	+	-	-	-	-	-	-	-	-	-	-	-	-	-	-	-
670	-	-	-	-	-	-	-	-	-	-	-	+	-	-	-	-	-
686	+	+	-	-	+	+	-	+	-	-	-	-	-	-	-	-	-
689	-	-	-	-	-	-	-	-	-	+	-	-	-	-	-	-	-
723	-	-	-	-	-	-	-	-	-	+	-	-	-	-	-	-	-
733	-	-	-	+	+	-	+	-	-	-	-	-	+	-	-	-	-
748	-	-	-	-	-	-	-	-	-	-	-	-	-	-	+	-	-
751	-	-	-	+	-	-	+	-	-	-	-	-	-	-	-	-	-
760	+	-	-	-	-	+	-	-	-	-	-	-	-	-	-	-	-
779	+	+	-	+	+	+	+	+	-	-	-	-	+	-	-	-	-
789	-	-	-	-	-	-	-	-	-	-	-	-	-	-	-	-	+
795	-	-	-	-	-	-	-	-	-	-	-	-	-	-	-	+	-
807	-	+	-	-	+	+	+	+	-	-	-	-	+	-	-	-	-
822	-	-	-	-	-	-	+	-	-	-	-	-	-	-	-	+	-
835	-	-	-	-	-	-	-	-	-	-	-	+	-	-	-	-	-
879	-	+	-	-	-	+	-	-	-	-	-	-	+	-	-	-	-
893	-	-	-	+	-	-	-	-	-	-	-	-	-	-	-	-	-
907	+	-	-	+	+	+	-	-	-	-	-	-	-	-	-	-	-
914	-	-	-	+	-	-	+	-	-	-	-	-	-	-	-	-	-
941	-	-	-	+	-	-	-	-	-	-	-	-	-	-	-	-	-
1017	-	-	+	-	-	-	-	-	-	-	-	-	-	-	-	-	-
1114	-	-	-	-	-	-	-	-	-	-	+	-	-	-	-	-	-
1143	-	+	-	-	-	-	-	-	-	-	-	-	-	-	-	-	-
1278	-	-	-	+	-	-	-	-	-	-	-	-	-	-	-	-	-
1381	-	-	-	-	-	-	-	-	-	-	-	-	-	-	-	-	+

Negative Ion Mode SIMS Data from Lipid Standards. (+/-) refers to the presence or absence of that secondary ion in the lipid standard. Green indicates the detection of a specific secondary ion in spectra from complex ganglioside standards. Red indicates the detection of a secondary ion in spectra from a non-complex ganglioside lipid standard, which ruled out use of that ion as a charactistic fragment of complex gangliosides. Blue highlights those secondary ions that were potentially identified as complex ganglioside-specific.